Synthesis of Fluorescent Phosphorus Ligands and their Applications in Medical Imaging and Catalysis

Jennifer Fairbairn Wallis

Engineering Doctorate in Biopharmaceutical Process Development

Supervisor of Research: Dr Lee J. Higham

Industry Sponsor: High Force Research

School of Chemical Engineering – Newcastle University

June 2018

Abstract

This thesis reports the synthesis of novel, air-stable, fluorescent phosphorus-containing compounds, based on a Bodipy backbone, and their applications in cell imaging and catalysis. The syntheses of all the novel target compounds reported in this thesis are via a primary phosphine, an under-utilised class of compound due to a hazardous reputation. Chapter 1 explores the stability of primary phosphines, how they can be made user-friendly and the ability to create a library of novel phosphorus compounds via the phosphorus-hydrogen bonds. The LJH group synthesised the first, air-stable, fluorescent primary phosphine and Chapter 2 explores a second generation of this type of ligand with an increased fluorescent quantum yield due to the addition of alkyne groups on the boron atom. Chapter 3 details the coordination chemistry of primary phosphines to group 6 and 8 transition metals. Interestingly, the addition of the metals had different effects on the photophysical properties, group 6 metal complexes retained high quantum yields, whereas group 8 metals quenched the fluorescence, possibly due to the heavy atom effect.

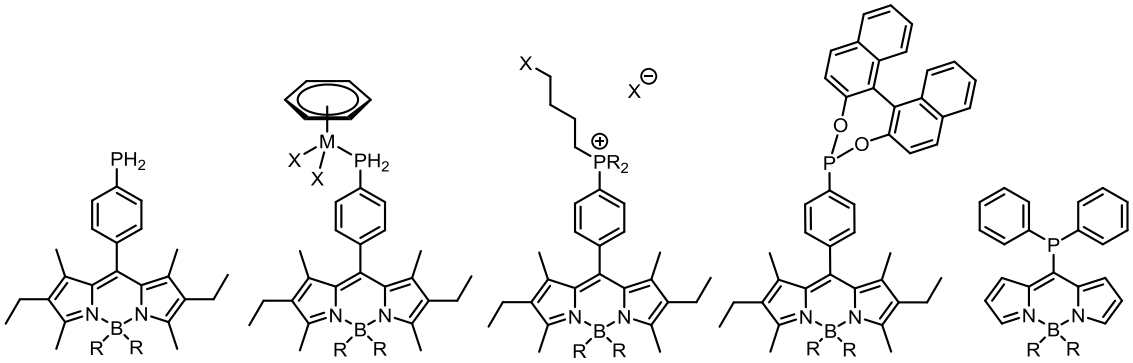

Chapter 4 discusses the synthesis of fluorescent phosphonium salts which have the potential to be used as trifunctional imaging agents. The three functions within the compounds include i) a fluorophore, to provide *in vitro* fluorescence imaging, ii) a positive charge on the phosphorus atom to introduce organelle specificity – in this case, to the mitochondria and iii) the inclusion of an ^{18}F radioisotope enables *in vivo* imaging techniques such as PET imaging. Chapter 5 shows further versatility of fluorescent primary phosphines where we report the synthesis of a novel, chiral, fluorescent phosphonite ligand that has been tested for its applications as a catalyst in asymmetric hydrogenation reactions of a benchmark substrate. The results showed full conversion and an enantiomeric excess (*ee*) of >99%. The final chapter discusses the importance of the aryl linker between the Bodipy core and the phosphorus atom. The compounds synthesised in this chapter show decreased fluorescence when the phosphorus atom is directly bound to the fluorophore and have potential applications as a switch.

List of Publications

L. H. Davies, J. F. Wallis, M. R. Probert and L. J. Higham, *Synthesis*, Efficient multigram synthesis of air-stable, fluorescent primary phosphines via palladium-catalyzed phosphonylation of aryl bromides, 2014, **46**, 2622-2628.

N. Fey, S. Papadouli, P. G. Pringle, A. Ficks, J. T. Fleming, L. J. Higham, J. F. Wallis, D. Carmichael, N. Mézailles and C. Müller, *Phosphorus, Sulfur, and Silicon and the Related Elements*, Setting P-Donor Ligands into Context: An Application of the Ligand Knowledge Base (LKB) Approach, 2015, **190**, 706-714.

S.Nigam, B. P. Burke, L. H. Davies, J. Domarkas, J. F. Wallis, P. G. Waddell, J. S. Waby, D. M. Benoit, A. Seymour, C. Cawthorne, L. J. Higham and S. J. Archibald, *Chem.Commun.*, Structurally optimised Bodipy derivatives for imaging of mitochondrial dysfunction in cancer and heart cells, 2016, **52**, 7114-7117.

L. H. Davies, J. F. Wallis, R. W. Harrington, P. G. Waddell & L. J. Higham, *J. Coord. Chem*., Air-stable fluorescent primary phosphine complexes of molybdenum and tungsten, 2016, **69**, 2069-2080.

Acknowledgements

First, I would like to sincerely thank my supervisor Dr Lee J. Higham, for giving me this opportunity and taking a chance on me! I have had the best time working with him and his research group over the last few years. I have been given the chance to attend several international and national conferences which have been quite an experience! Thank you for your patience and guidance throughout this EngD course.

I would like to thank the EPSRC for funding, as well as High Force Research who were my industrial sponsor. The team in the BBTC have been amazing throughout the years, so thank you for all of your help.

A special thank you to Dr Laura Davies who taught me everything I know about Bodipy and all of the special tricks required to synthesise them!

My time in the lab has been made significantly more entertaining and memorable by a number of people: the old school LJH group members: Dr Arne Ficks, Dr Manuel Abelairas-Edesa, Dr Connor Sibbald, Dr James Fleming, Dr Ana Cioran, the more recent LJH members: Charlotte Hepples, Antonio Sanchez-Cid and Graeme Bowling (not forgetting adopted member Dr Tommy Winstanley) and all of the other students within the Johnston Lab. A special mention to Manuel, (we were the original Boss-Monkey team and he introduced me to Estrella Galicia and Faustino I), James and Charlotte who have all assisted me with research in the lab, but have also created the best memories outside of the lab, and hope that we will continue to meet up at our annual beer and gin festivals throughout the year!

I could not have completed this work without the help of our fantastic crystallographer Dr Paul Waddell, and NMR experts Dr Corinne Wills and Prof. William Mcfarlane, they have undoubtedly helped me complete and understand this work.

Another special thank you to all of the academic research collaborators involved with this research, especially Prof Steve Archibald and Dr Amy Reeve who both helped out with cell studies.

I have been lucky enough to work with several Erasmus and Masters Students and I'd especially like to thank Francesca, Anna, Giorgia, Vince, Sophie, Tom and everyone else who contributed towards the Bodipy research!

Finally I'd like to thank my amazing Dad for always believing in me and helping me get to where I am today, even when I doubted myself he would always guide me and tell me I could do it - my Mam would be so proud of what I have achieved. My sisters Katie and Rachael and my boyfriend Chris have also been exceptionally patient during the last 5 years. I love you all!

Abbreviations

General:

β	Beta particle
B3LYP	Becke Parameter Lee-Yang-Parr
CT	Computed Tomography
DFT	Density Functional Theory
γ	Gamma ray
HOMO	Highest Occupied Molecular Orbital
HPLC	High-Performance Liquid Chromatography
LMCT	Ligand-to-Metal Charge Transfer
LUMO	Lowest Unoccupied Molecular Orbital
^{99m}	Metastable isotope
MLCT	Metal-to-Ligand Charge Transfer
MMCT	Metal-to Metal Charge Transfer
MRI	Magnetic Resonance Imaging
PET	Positron Emission Tomography
PeT	Photoinduced electron Transfer
RT	Room Temperature
SOMO	Singly Occupied Molecular Orbital
SPECT	Single Photon Emission Computed Tomography
TLC	Thin Layer Chromatography
$t_{1/2}$	Half-life

Chemicals:

Bodipy	4,4-difluoro-4-borata-3a-azonia-4a-aza-*s*-indacene
$CDCl_3$	Deuterated chloroform
DCM	Dichloromethane
DDQ	2,3-Dicyano-5,6-dichloroparabenzoquinone
DMSO	Dimethyl sulfoxide
DPPB	1,4-Bis-(diphenylphosphino)-butane
Et_2O	Diethyl ether

$HP(O)(OEt)_2$	Diethyl phosphite
$LiAlH_4$	Lithium aluminium hydride
$MgSO_4$	Magnesium sulphate
NEt_3	Triethylamine
$Pd(OAc)_2$	Palladium(II) acetate
$POBr_3$	Phosphoryl oxybromide
$POCl_3$	Phosphoryl oxychloride
TFA	Trifluoroacetic acid
THF	Tetrahydrofuran
TMSCl	Chlorotrimethylsilane

Units:

Å	Angstroms
cm	Centimetres
°	Degrees
°C	Degrees Celsius
eq	Equivalents
eV	Electron Volts
Hz	Hertz
h	Hours
L	Litres
mg	Milligrams
MHz	Megahertz
mmol	Millimolar
mins	Minutes
M	Molar
nm	Nanometres
ppm	Parts per million
s	Seconds

Experimental techniques terms:

APCI	Atmospheric-Pressure Chemical Ionisation
br	Broad
δ	Chemical shift
d	Doublet
ε	Molar Absorption Coefficient
EI	Electron Ionisation
ESI	Electrospray Ionisation
FTIR	Fourier Transform Infrared Spectroscopy
HRMS	High Resolution Mass Spectrometry
I	Nuclear Spin
J	Coupling Constant
LRMS	Low Resolution Mass Spectrometry
NIR	Near-Infrared
NSI	Nanospray Ionisation
m	Multiplet
NMR	Nuclear Magnetic Resonance
Φ_F	Quantum yield
q	Quartet
s	Singlet
t	Triplet

Table of Contents

Chapter 1: Background and Introduction

1 Background and Introduction

1.1 Organophosphorus Compounds

Organophosphorus compounds are phosphorus-containing organic molecules that have a range of applications in catalysis,[1] medicine,[2, 3] agriculture[4] and the plastics industry, where phosphorus is commonly used as a flame retardant.[5] Phosphorus is also found in natural products, such as a phosphate group – found in DNA, or as a C-P bond in compounds such as 2-aminoethylphosphonic acid and Fosfomycin, an effective antibiotic produced by certain Streptomyces species, both shown in Figure 1.1.[6, 7]

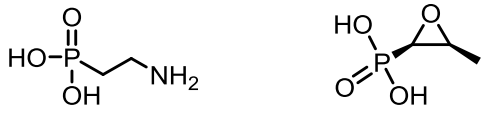

2-aminoethylphosphonic acid *Fosfomycin*

Figure 1.1 Natural products containing a C-P bond.

1.2 Phosphines

Of particular interest to this thesis are the phosphine compounds R_3P, and their derivatives, the phosphonium salts $[R_4P][X]$, their general structures are shown in Figure 1.2. The chemistry of phosphines is usually centred on the donation of the lone pair on the phosphorus atom to electrophilic centres.[8] Often, phosphines adopt a pyramidal structure, and if one assumes that the lone pair points out from the top of the pyramid, it is easy to understand that as the size of the substituents on the phosphorus atom increase, it is more difficult for the lone pair to bond with reagents.

In 1977, Tolman wrote a review which described the effects that steric hindrance has on phosphorus ligands in organometallic chemistry and homogeneous catalysis. He noted that prior to 1970 almost everything was rationalised in terms of electronic effects.[9]

1.2.1 Steric Parameters of Phosphorus Ligands

The Tolman cone angle θ_T is commonly used to describe the steric effects of phosphorus ligands. The steric parameter, when all three substituents are the same, was defined as the apex angle of a cylindrical cone, centred 2.28 Å away from the phosphorus atom and the edges of the cone just touching the Van der Waals radii of the outermost atoms, shown in Figure 1.2.

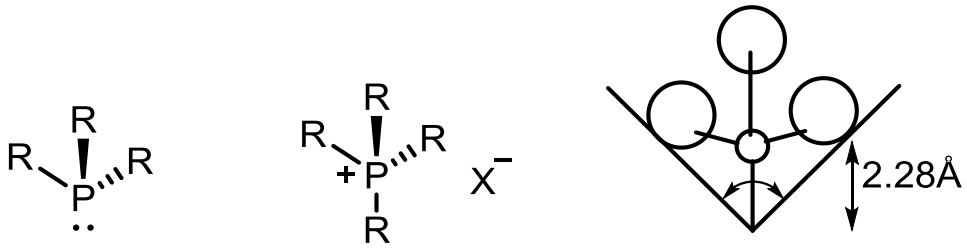

Figure 1.2 General structures of a phosphine and a phosphonium salt, and a schematic of the Tolman cone angle.

1.2.2 Electronic Parameters of Phosphorus Ligands

Tolman also used IR spectroscopy to determine the electronic parameter, ν, of phosphorus ligands, by determining the symmetric frequency of $[Ni(CO)_3L]$ complexes. The stretching frequency of the carbonyl vibration is dependent on the other ligands and the magnitude depends on the electronic nature of the complex. The phosphine ligand acts as a σ-donor which increases the electron density on the metal, the electron density is transferred through π-backbonding into the π* anti-bonding orbitals of the carbonyl group, which reduces the bond order of CO, as shown in Figure 1.3. Therefore, good net donor ligands are indicated by a shift of the CO stretching frequencies to lower wavenumbers, as they are lower in energy.[10]

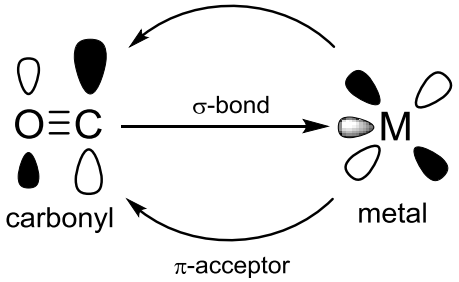

Figure 1.3 Back-bonding into the anti-bonding orbital of the carbonyl group.

In 2009 Gusev published a paper comparing the donor properties of a range of two-electron ligands. Where Tolman only used $[Ni(CO)_3L]$ complexes to identify CO stretching frequencies, Gusev also used $[IrCl(CO)_2L]$ and [IrCp(CO)L] complexes, as well as DFT calculations to find a relationship between the structural and experimental findings. After deducing that there were still complications when using the $[IrCl(CO)_2L]$ complex, due to two CO groups, he concluded that the [IrCp(CO)L] complex was the most advantageous due to the following factors: 1) low coordination number, therefore minimising any ligand repulsion, 2) only one CO ligand as opposed to two or three CO ligands reduced complications when analysing the IR spectra, 3) the CO ligand is at 90° angle to

the ligand L avoiding any interference due to the *trans* influence, as illustrated in Figure 1.4. There was found to be a high correlation between the observed IR stretching frequencies of the CO ligands and the DFT calculations for the [$Ni(CO)_3L$] and [IrCp(CO)L] complexes.[11]

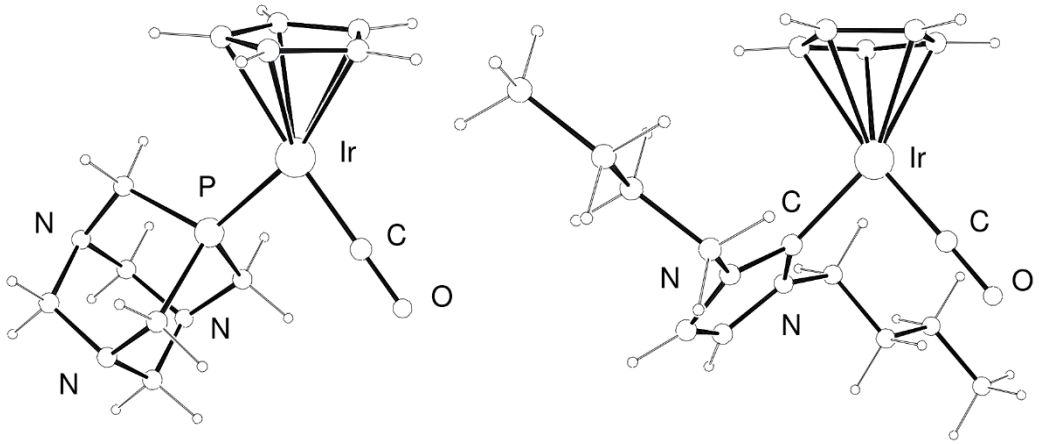

Figure 1.4 Structures of the [IrCp(CO)L] complexes, L = pta (1,3,5-triaza-7- phosphaadamantane) and biy (1,3-dibutylimidazolin-2-ylidene).[11]

1.2.3 Phosphine Ligands of Relevance

This introductory chapter started with organophosphorus compounds of biological interest and one of the research aims of the LJH research group is the development of phosphorus compounds with biological applications.

Phosphines are extremely versatile and can be used in several applications such as medicine; previous work within the Higham research group resulted in the synthesis of fluorescent rhenium complexes **2** and **3** from tridentate phosphorus compound **1a**, based on the fluorophore Bodipy, shown in Figure 1.5.[12] Tridentate phosphine **1a** was reacted with [$Re(CO)_5$][OTf] to produce tricarbonyl species **2** and [$ReCl(CO)_3(PPh_3)_2$] to form complex **3**. Rhenium and technetium are both in group 7 of the periodic table; however, technetium is radioactive. The two elements have similar chemistries; therefore, synthesising rhenium complexes as a cold standard for the radioactive technetium analogues would allow for comparisons between the two compounds to be made.

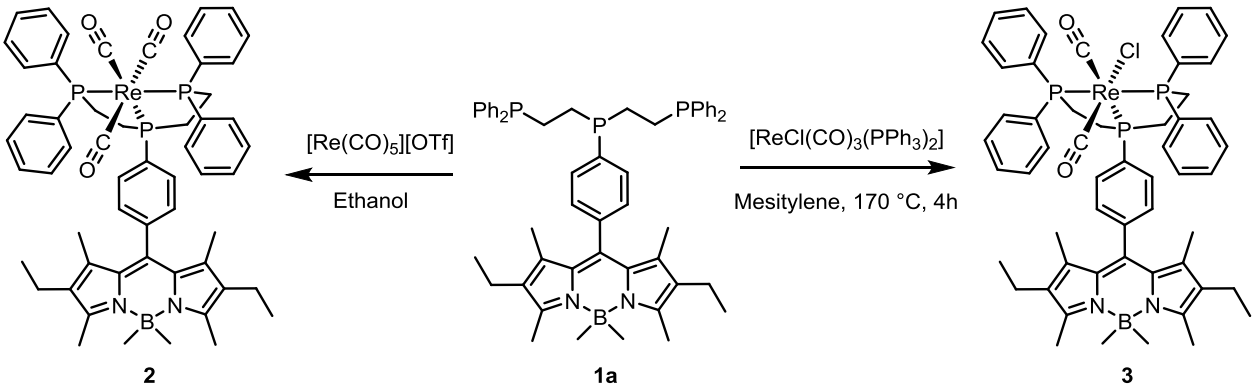

Figure 1.5 Synthesis of rhenium complexes 2 and 3 from tridentate phosphorus compound 1a to produce a cold standard for a SPECT imaging agent.

Both Bodipy-rhenium complexes **2** and **3** underwent a preliminary screening for cell testing in prostate carcinoma (PC-3) cells, shown in Figure 1.6. The two complexes displayed notable differences in the cell screening; compound **3** (top row) allowed for high resolution imaging and enabled visualisation of organelles without any apparent cytotoxic effects, whereas compound **2** (bottom row) caused some morphological changes to the cells. This enables the tricarbonyl complex to act in a therapeutic mode by promoting cell death. Complexes **2** and **3** both possessed negligible cytotoxicity at the concentrations required for SPECT (Single Photon Emission Computed Tomography) (Section 1.71) scanning and therefore both have the potential as imaging agents.

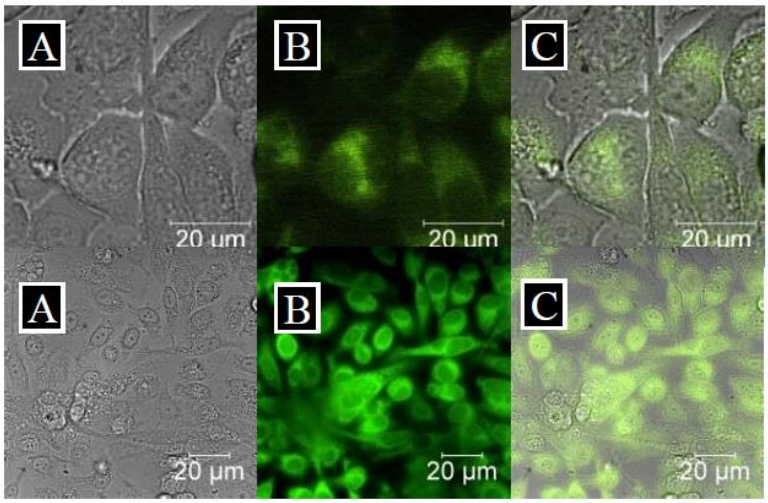

Figure 1.6 Imaging of PC-3 living cells with: top: *cis*-[ReCl(CO)$_2$(1a)], bottom: *fac*-[Re(CO)$_3$(1a)] (A) brightfield image, (B) green channel λex = 460-500 nm, long pass filtered at 510 nm, C) overlay of A and B.

The rhenium complexes constituted a cold standard for a corresponding technetium complex for use in SPECT imaging. Tridentate Bodipy compound **1a** was reacted with *fac*-[^{99m}Tc(CO)$_3$(OH$_2$)$_3$]$^+$ to form complex **4**. The crude reaction was monitored by HPLC which

displayed a single peak and matched well with triphos derivative **5** and the cold standard rhenium complex **2** as shown in Figure 1.7.

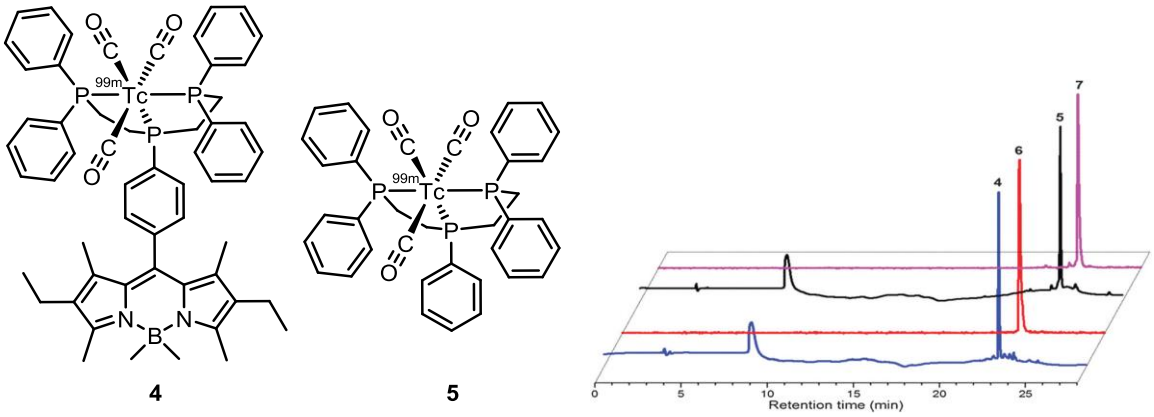

Figure 1.7, ^{99m}Tc Bodipy complex 4, Triphos control 5, and the HPLC chromatogram used for comparing the crude reactions of rhenium and technetium complexes showing analogous physical properties.

Technetium complex **4** was the first example of a phosphine-based, multi-functional imaging agent comprised of (i) a tridentate phosphine for kinetic stability, (ii) a fluorophore for *in vitro* imaging and (iii) a radioactive metal centre for *in vivo* imaging via SPECT.

1.2.4 Multifunctional Imaging Agents

The development of multimodal imaging agents, as opposed to single-modality imaging agents, is becoming increasingly popular due to the ability to overcome the current limitations of individual imaging techniques. One such limitation is the inability of radiopharmaceuticals to image the fate of the agents at a cellular level, which would increase the understanding of biological mechanisms and the localisation within a cell.[13] *In vitro* techniques such as fluorescence microscopy produce a higher spatial resolution than PET or SPECT radioimaging, (nm scale rather than mm), which would make it possible to follow mechanisms and processes at a subcellular level. Combination of the two imaging techniques would produce dual imaging agents that could provide a more detailed explanation of the events occurring within a cell.

Valliant synthesised a rhenium/technetium complex in 2004, based on a tridentate nitrogen ligand which is shown in Figure 1.8. It was synthesised as a multifunctional imaging agent consisting of (i) a radionuclide - ^{99m}Tc - for *in vivo* SPECT imaging, (ii) a quinoline fluorophore for fluorescence microscopy, an *in vitro* imaging technique, (iii) a tridentate nitrogen ligand to provide chelation stability of the metal and (iv) a peptide which can be used to guide radionuclides to a specific target receptor.[14]

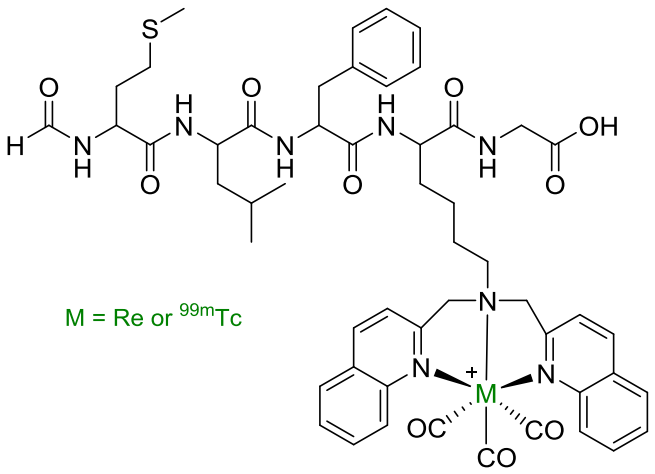

Figure 1.8 Valliant's multifunctional imaging agent.

Valliant used quinoline as a fluorophore in his complex; in the research that the Higham group are interested in, Bodipy is the fluorophore of choice, which will be discussed in detail in Section 1.5. There are other reports published in the literature showing the versatility of the Bodipy dye as a dual imaging agent. Li *et.al.* reported that the Bodipy structures shown in Figure 1.9 were used successfully as PET/fluorescent imaging probes after an efficient [^{19}F/^{18}F] exchange at the boron atom.[15, 16] Li commented that [^{18}F]-BAP-1 holds great potential for the diagnosis of Alzheimer's disease (AD), the cold analogue which contains ^{19}F has been developed for AD imaging by targeting cerebral β-amyloid plaques. By incorporating an ^{18}F radiolabel into the molecule, it makes it possible to correlate the images from the fluorescence imaging with images from SPECT scans to visualise the mode of action and the fate of radiopharmaceuticals within the body. [^{18}F]-V is an example of a trifunctional imaging agent, as well as the fluorescent core and the radiolabel for both *in vitro* and *in vivo* imaging techniques respectively, the positively charged ammonium group would guide the molecule to the myocardium, due to the attraction to the negatively charged mitochondrial matrix. [^{18}F]-V was tested as a heart imaging agent in mice models and successfully showed accumulation in the myocardium.[16] This multi-modal imaging agent is a foresight into the target compounds synthesised within this project.

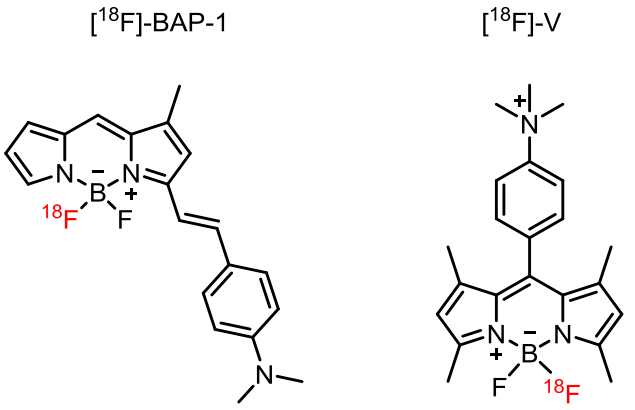

Figure 1.9 Bodipy compounds for potential use in AD diagnosis and cardiac imaging.

In 2016, Min *et. al.* published a review on radiolabelled tetraphenylphosphonium cation derivatives as myocardial imaging agents for PET, two examples of which are shown in Figure 1.10.[17] Triphenylphosphonium cations can penetrate cell and organelle membranes and accumulate in the mitochondria and heart cells due to the increased membrane potential as the positive charge is attracted to the negatively charged mitochondrial matrix. The authors noted that the alkyl-chain-conjugated triphenylphosphonium cations had improved characteristics through lipophilicity control.

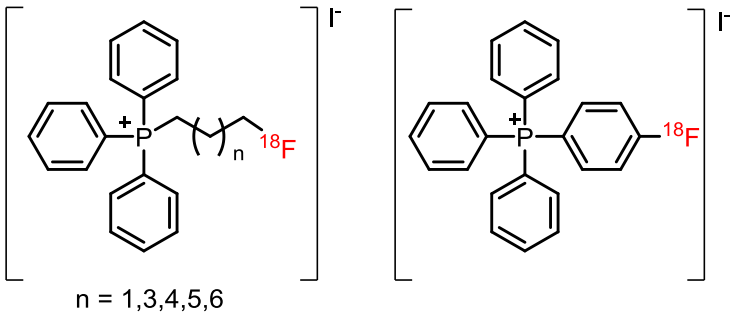

Figure 1.10 Radiolabelled phosphonium cations with applications in myocardial imaging.

The previous examples were of organophosphorus compounds used in imaging, this next section introduces phosphorus-containing therapeutics such as RAPTA-C, a ruthenium-based, anti-cancer drug, shown in Figure 1.11. Ruthenium complexes have shown great potential in treating cancers that have platinum drug resistance, as well as exhibiting fewer side effects and lower toxicity.[18] Dyson and co-workers have researched the anticancer properties of ruthenium half sandwich compounds coordinated to various arene ligands.[19] The pta ligand (1,3,5-triaza-7-phosphatricyclo[3.3.1.1]decane), is hydrophilic and promotes good aquatic solubility, which is important in therapeutic applications. The labile chloride ligands undergo aquation, (substitution for water), in a similar way to Cisplatin, which may be an important step for anticancer drug

activity. At physiological pH, the major species carries no charge and can diffuse through lipid membranes and move freely through cells. In some unhealthy cells, the pH is lower due to associated changes in metabolism, which can protonate the pta ligand, trapping the complex in the cell. Dyson *et.al* have completed studies that show protonated species induce DNA damage in cells more readily than un-protonated species.[20]

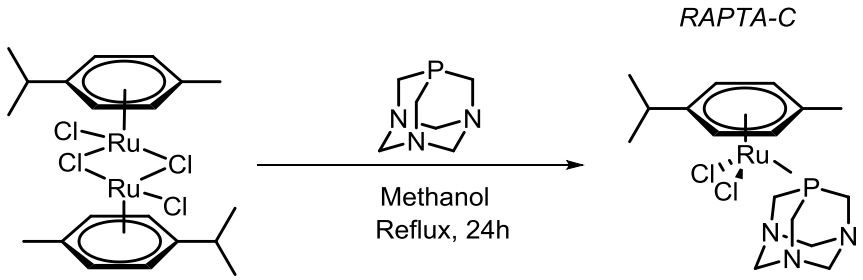

Figure 1.11 The synthesis of RAPTA-C from a ruthenium dimer [$RuCl_2$(*p*-cymene)] and pta (1,3,5-triaza-7-phosphatricyclo[3.3.1.1]decane).

Bodio and co-workers synthesised a Bodipy phosphine and the corresponding ruthenium (compound **6**, Fig. 1.12), gold and osmium complexes. All of the metal complexes were tested in human ovarian cancer cell lines A2780S and A2780cisR which were sensitive and are now resistant to Cisplatin. Bodio's complexes showed moderate cytotoxicity and a preference for accumulation in the cell membrane. The fluorescence properties of the complexes associated with the Bodipy ligand showed good emission and water solubility, which allowed for the monitoring of the compounds in cancer cells *in vitro*.[21]

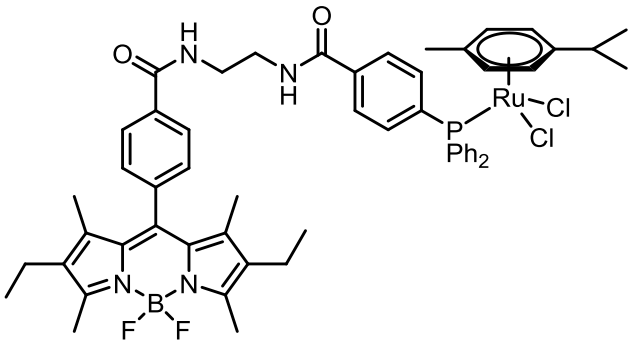

6

Figure 1.12 Bodio and co-workers synthesised ruthenium complex 6 as an imaging organometallic complex.

The examples described above have outlined various imaging techniques including fluorescence microscopy, SPECT and PET imaging, and the targeting of specific organelles within a cell. The primary target for this thesis is to develop a multi-modal compound that facilitates all of these

imaging techniques. The four functions that will be relevant to this project will now be discussed in detail: (i) primary phosphine synthesis, as a precursor to tridentate ligands that confer kinetic stability on resulting complexes, (ii) the fluorescent Bodipy core for *in vitro* imaging, (iii) incorporation of a radionuclide such as ^{18}F or ^{99m}Tc for PET and SPECT imaging, and (iv) a moiety that would allow for the direct targeting of an organelle, such as a phosphonium salt.

1.2.5 Primary Phosphines

An important class of compound for this thesis is the primary phosphine, which consists of two phosphorus-hydrogen bonds connected to an aryl or alkyl backbone. Working with primary phosphines is often assumed to be problematic due to their toxic and pyrophoric nature; however, the P–H bonds are highly reactive making them an excellent starting material for synthesising a range of functionalised phosphorus compounds.[22, 23] Figure 1.13 shows several types of reactions that can occur by starting with a primary phosphine.

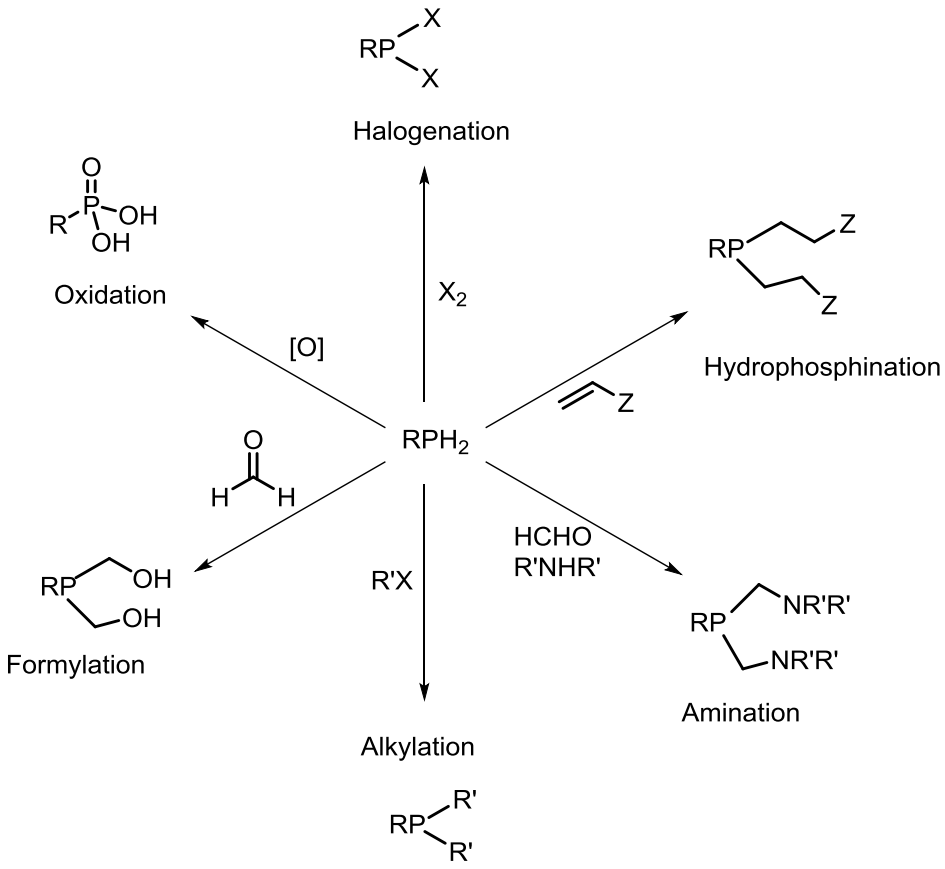

Figure 1.13 A range of reactions that can occur through a primary phosphine; R/R′ = alkyl or aryl group, X = halogen, Z = PR_2, NR_2.

The decomposition of primary phosphines occurs by an oxidation reaction with the formation of a strong P=O bond (544 kJ/mol) acting as the driving force.[24] Scheme 1.1 shows how primary phosphines are initially oxidised to phosphine oxides, before further oxidation which can result in phosphinic and phosphonic acid formation.[8]

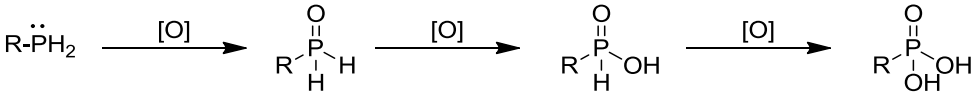

Scheme 1.1 A series of oxidation steps which are possible starting from a primary phosphine.

Despite this oxidation, it is possible to prepare certain primary phosphines which are "user-friendly", and within the past decade the number of air-stable examples in the literature has steadily increased, although there still remains fewer than twenty examples.[23] The stability of these compounds can be attributed to two main phenomena: steric effects and electronic effects.

It is essential to define the interpretation of "air-stable phosphines" within this research, and for the purpose of this thesis it is regarded as the measure of resistance of a primary phosphine to undergo oxidation by aerobic oxygen, and here we regard air-stable primary phosphines as those that display inertness to oxidation over several weeks. It is also worth noting that different authors have different definitions for "air-stable", making it difficult to directly compare examples within the literature.

1.2.5.1 Steric Protection

There are a number of primary phosphines in the literature that owe their stability, with respect to air-oxidation, to the steric bulk which surrounds the phosphorus, inhibiting the reaction with dioxygen. Three examples can be seen in Figure 1.14, phenylphosphine **7**, is a highly air-sensitive and pyrophoric liquid which undergoes oxidation rapidly. However, as you add substituents around the phosphorus atom such as the methyl groups in mesitylphosphine **8**, an increase in stability to air-oxidation is observed.[25] A further increase in stability is seen for **9**, supermesitylphosphine, which is described as odourless and air-stable.[26]

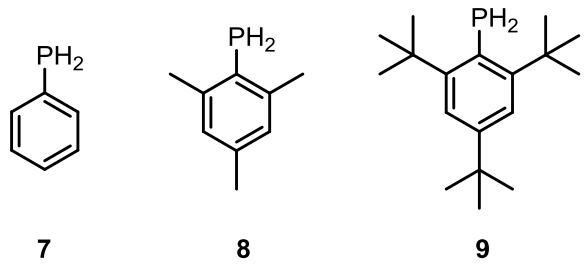

7 **8** **9**

Figure 1.14 Steric properties can help to protect primary phosphines from oxidation.

1.2.5.2 Unexplained Stability

There are several examples in the literature where steric hindrance cannot explain the stability towards air-oxidation. Figure 1.15 shows four examples; compounds **10** and **11** have been identified as air stable, the origin of which has been suggested as being due to negative hyperconjugation arising from the presence of the heteroatoms - however this is only a theory and has not been proven experimentally.[27] Henderson and co-workers postulated that the alkyl spacer between the ferrocene moiety and the phosphine was responsible for the air stability of compounds **13a** and **13b**, as compound **12** was found to be unstable in air, but no further explanation was provided.[28] A DFT-based model has been developed within the Higham group which may be able to offer an alternative explanation for the stability of these compounds, and is described next, in Section 1.2.5.3.

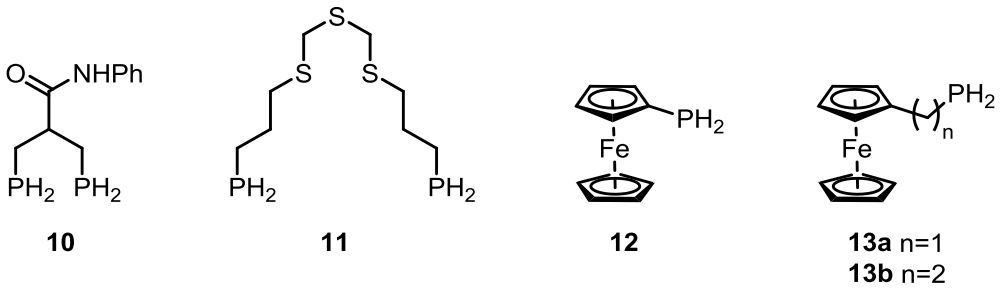

10 **11** **12** **13a** n=1 **13b** n=2

Figure 1.15 Examples of primary phosphines where steric effects are not responsible for their air-stability.

1.2.5.3 Electronic Effects

The aforementioned examples shown in Figure 1.15 demonstrate that an alternative explanation must be in operation here, rather than steric encumbrance. The Higham group has also synthesised several primary phosphines that are stable in air, and do not contain any steric encumbrance; therefore, it was necessary to consider the electronic nature of these compounds in some detail. Figure 1.16 shows two such examples, in this instance of chiral primary phosphines synthesised

within the research group for use as precursors to ligands with applications in transition metal catalysed asymmetric transformations, namely (*S*)-H-MOPH$_2$ **14** and (*R*)-MOPH$_2$ **15**.[29]

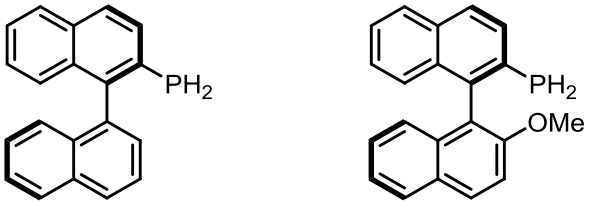

14 (*S*)-H-MOPH$_2$ **15** (*R*)-MOPH$_2$

Figure 1.16 Chiral primary phosphines 14 and 15 have significant π-conjugation and were found to be air-stable.

The LJH research group developed a computational model based on Density Functional Theory (DFT) calculations using the B3LYP function with a 6-31G* basis set in order to understand the relationship between phosphines and their stability in air.[30] The energies of the neutral primary phosphines and their radical cations were both calculated, as it is thought that the route to oxidation may occur via the radical cation; in 2005, Majima *et al*. described how the photoreaction of triarylphosphines resulted in their oxidation to the corresponding phosphine oxide. Laser flash photolysis and further analysis suggested that the radical cation of the triarylphosphine was initially formed, which eventually led to the formation of the oxide, see Figure 1.17.[31]

Figure 1.17 Proposed steps in the photolytic oxidation of a tertiary phosphine.

Initial findings showed one particular trend for the Highest Occupied Molecular Orbital (HOMO) in the neutral phosphines. It was found that the HOMO of the air-stable phosphines was situated on the backbone of the compound and away from the phosphorus atom as represented by compounds **11**, **13a** and **14** in Figure 1.18. The air-sensitive phosphines, such as phenylphosphine **7**, demonstrated that the phosphorus was incorporated into the HOMO.

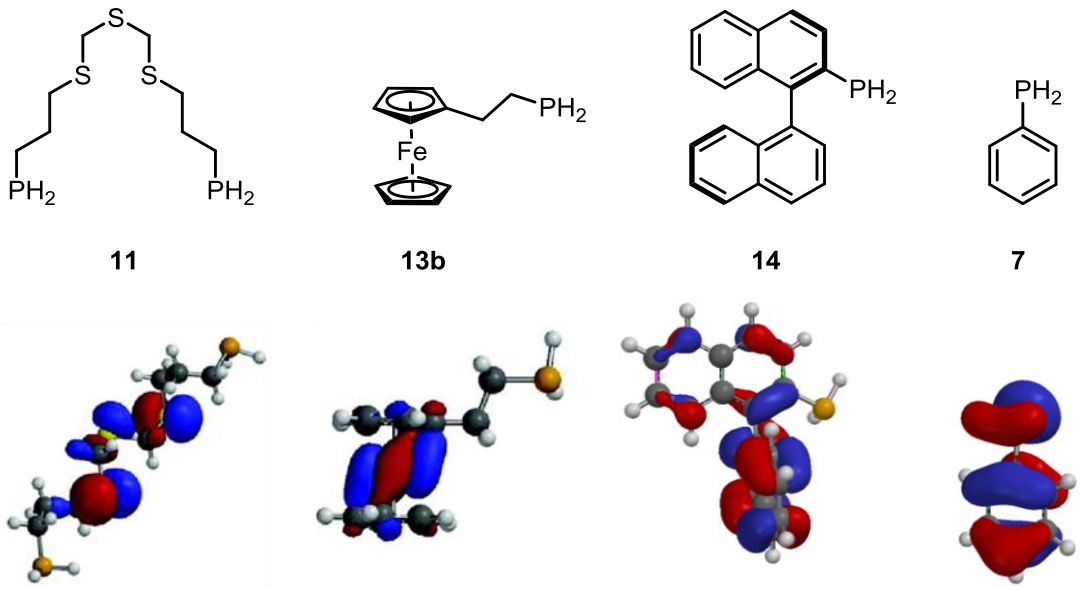

Figure 1.18 DFT calculations showing that the HOMO is delocalised away from the phosphorus atom on compounds which are experimentally found to be air-stable; note how compound 7 demonstrates phosphorus participation in the HOMO – this is a very air-sensitive compound.

However, the model showed that the HOMO for the tertiary phosphine, triphenylphosphine **16**, *does* contain the phosphorus atom – shown in Figure 1.19. As triphenylphosphine is an air-stable compound, the localisation of the phosphorus in the HOMO or not is unlikely to be able to explain the air-sensitivity of phosphines.

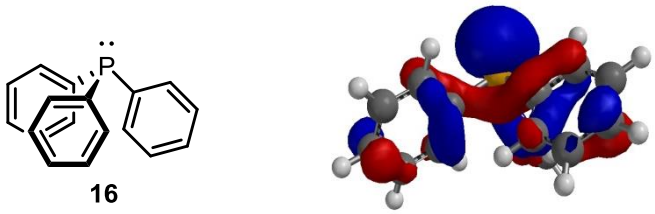

Figure 1.19 DFT calculations for triphenylphosphine showed that the phosphorus was incorporated into the HOMO. As PPh_3 is air-stable, this appears to rule out P atom participation in the HOMO (or not) as a rationale for air-stability.

Next, the corresponding radical cations of the aforementioned phosphines were studied and it was found that the phosphorus atom was incorporated into the Singly Occupied Molecular Orbital (SOMO) in all cases. More importantly, there also appeared to be a threshold SOMO energy value which correlated with resistance towards air-oxidation. When the energies of these SOMOs were plotted against their experimental air-stability, all of the primary phosphines with a SOMO energy below −10 eV were found to be experimentally air-stable, whereas those above this value are found to be air-sensitive. A graph showing these SOMO energies for a range of primary phosphines is

shown in Figure 1.20. Compounds **10**, **11**, **13a** and **14** all have SOMO energies below –10 eV and are predicted to be stable to air-oxidation - which was found experimentally to be true. Compounds **7**, **12**, **17**, **18** and **19** have SOMO energies above –10 eV and therefore are predicted to be unstable, which was also confirmed in laboratory testing.

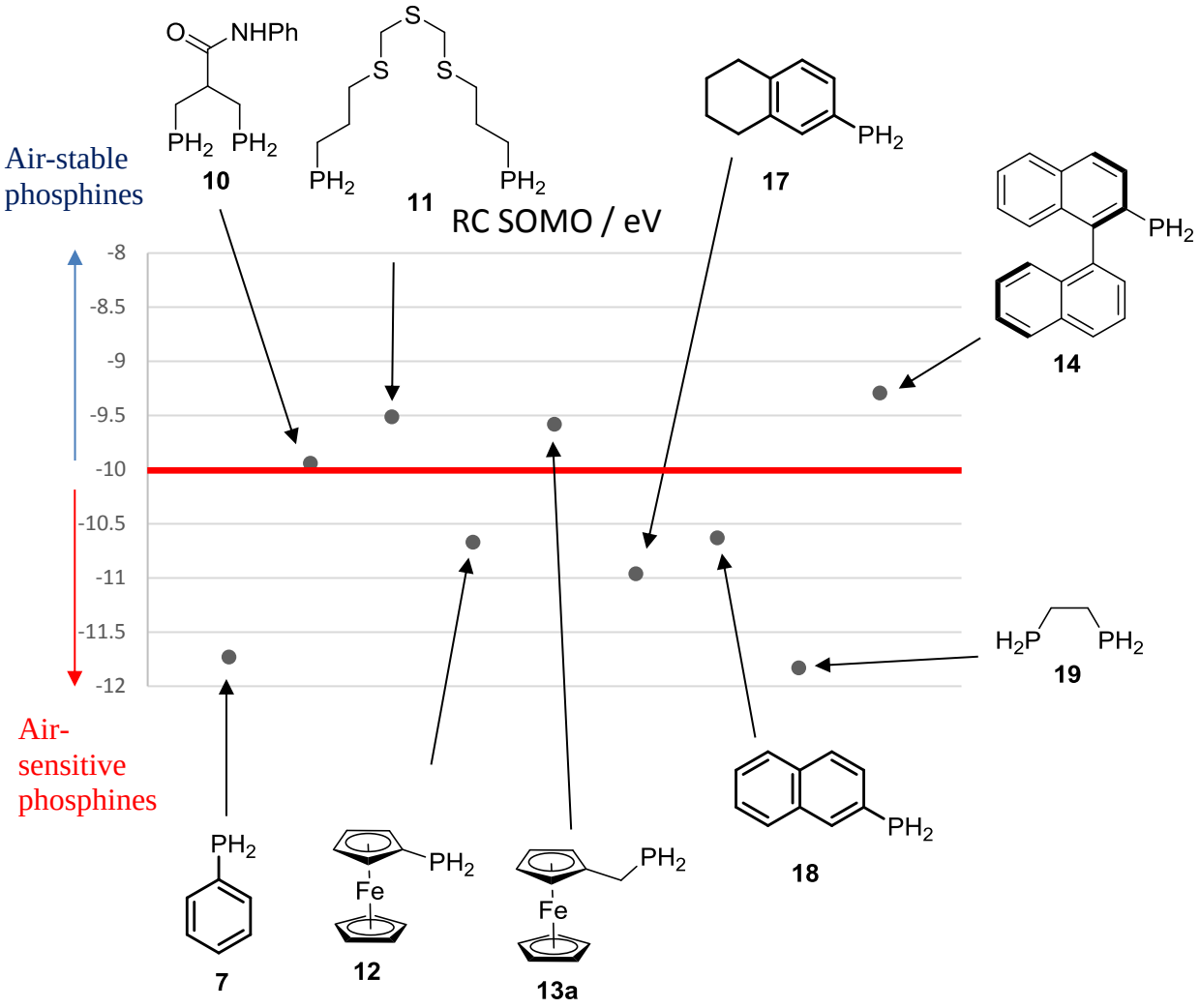

Figure 1.20 Plot showing the SOMO energies for a range of air-stable and air-sensitive primary phosphine radical cations, separated by an apparent threshold value of -10 eV.

One explanation for this phenomenon is that whilst increased π-conjugation in a molecule leads to higher energy orbitals, less or no conjugation will afford more stable ones. As such, a radical cation generated by the removal of an electron from a stable orbital will be more reactive, and enter into an irreversible oxidative chain reaction. The aforementioned work by Majima and Neta support this theory.[32, 33]Efforts to understand this proposed mechanism in better detail are underway.

Fluorophores also tend to be highly conjugated, and we were interested to ascertain if a primary phosphine with a Bodipy function, (highlighted in blue in Figure 1.21), would be air-stable. The

DFT-based computational model gave SOMO values of –8.82 eV for **20a** and –8.94 eV for **20b** and they are indeed air-stable. Compounds **20a**/**20b** are the first examples of air-stable, fluorescent primary phosphines and were synthesised within the Higham group in 2012.[34] In addition, primary phosphines **20a**/**20b** readily undergo hydrophosphination reactions to form tridentate compounds such as **1a**/**1b** ($BodP_3$), also shown in Figure 1.21, which remain highly fluorescent. The hydrophosphination of primary phosphines has been used as a means of generating tridentate phosphine ligands for coordinating a range of transition metals.[12]

The significance of the addition of a phosphorus atom on the photophysical properties of these compounds will be discussed in detail in the following section, because if the incorporation of the phosphorus atom causes fluorescence quenching, this will render them inapplicable as potential imaging agents.

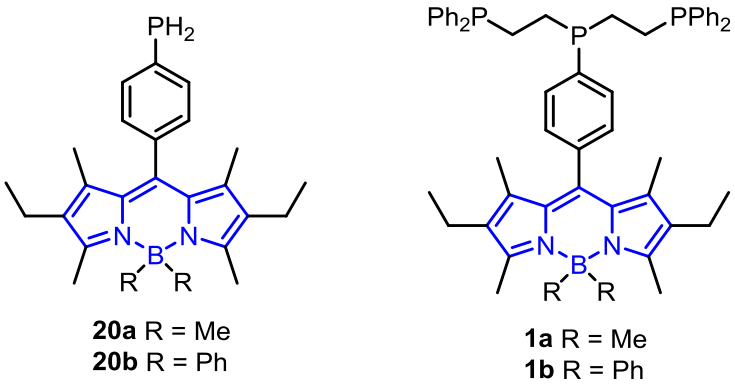

Figure 1.21 The first examples of an air-stable, fluorescent primary phosphine 20a/20b that can undergo a hydrophosphination reaction to give tridentate phosphines 1a/1b.

1.3 Luminescence

Luminescence is the emission of photons from an electronically excited species. There are many types of luminescence, including chemiluminescence (the emission of light due to chemical reactions), and photoluminescence (the emission of light due to the absorption of photons).[35]

1.3.1 Photoluminescence

Fluorescence is a type of photoluminescence and occurs when a photon relaxes from the singlet excited state to the singlet ground state (S_1-S_0), detailed in the Jablonski diagram shown in Figure 1.22.[36] There are also other pathways for de-excitation such as internal conversion and intersystem crossing, which may result in emission by phosphorescence, a spin-forbidden transition, where a photon relaxes from the triplet excited state to the singlet ground state (T_1-S_0).

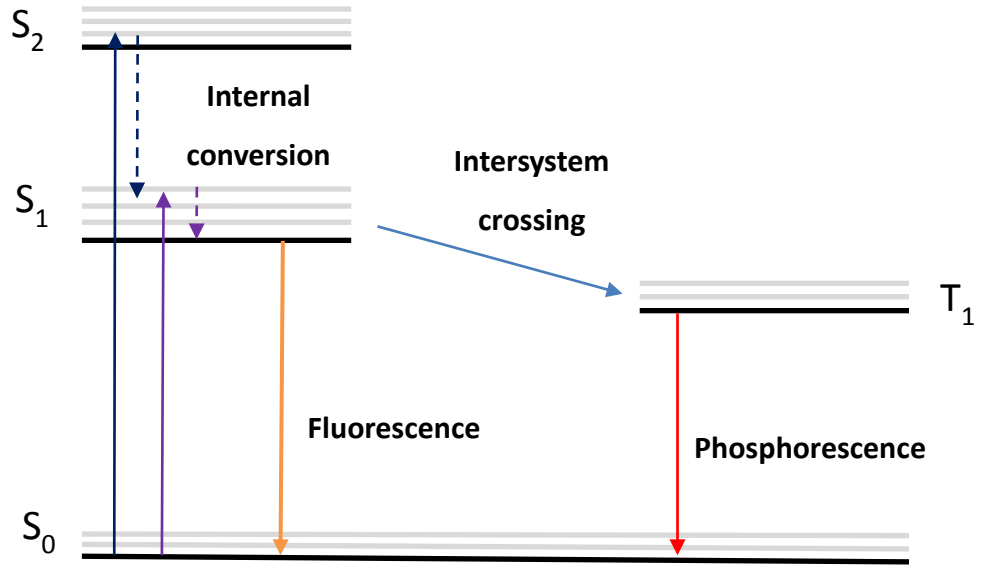

Figure 1.22 Schematic of a Jablonski Diagram outlining the important pathways of luminescence.

1.4 Fluorescent Dyes and Stains

Dyes and stains can be used to detect and visualise structures and processes within biology. Many of them contain a fluorescent component because they can be detected with incredible sensitivity, in principle to 'single molecule detection' levels of sensitivity.[35, 37] A fluorophore can repeatedly undergo the process of fluorescence, which means that a single fluorophore can generate a signal multiple times, making it a very sensitive technique for visualising biological samples. Fluorescent molecules are often used to visualise cells or tag part of a cell, there are many dyes and stains that can be purchased for these applications. Figure 1.23 shows three well known fluorophores, which can all be used for cell detection and live-cell imaging: Ethidium Bromide, Fluorescein and Bodipy.[38]

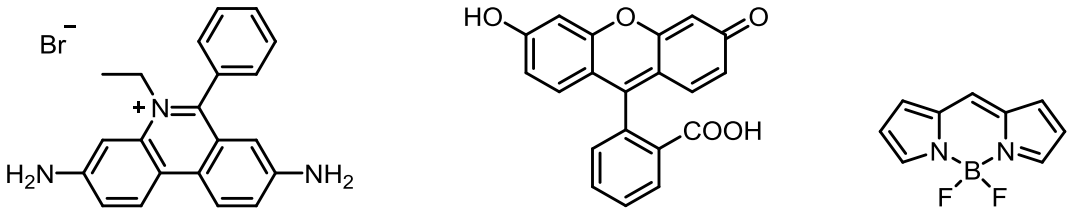

Ethidium Bromide *Fluorescein* *Bodipy*

Figure 1.23 Three well known fluorophores used for detection and imaging within cells: Ethidium Bromide, Fluorescein and Bodipy.

1.5 Bodipy

Bodipy (4,4-difluoro-4-borata-3a-azonia-4a-aza-*s*-indacene), shown in Figure 1.24, is one of the most versatile fluorophores available, due to it possessing many desirable properties, including (i) high quantum yields, (ii) a strong UV absorption profile and sharp fluorescence emission peak, (iii) high thermal and photochemical stability, (iv) negligible triplet state formation and (v) chemical robustness.[39, 40]

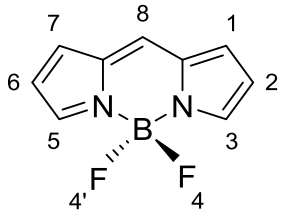

Figure 1.24 Bodipy (4,4-difluoro-4-borata-3a-azonia-4a-aza-*s*-indacene) core structure.

Figure 1.25 shows a typical Bodipy spectrum, where the absorption and emission maxima are characteristically around 500-530 nm; the Stokes shift is the energy gap between the maximum of the absorption and maximum of the fluorescence spectra. The Stokes shift is observed due to the loss of energy through non-radiative vibrational relaxations. For many fluorophores, a symmetrical absorption and emission spectra is observed, like a mirror image. This is due to the same transitions between S_0 and S_1 being the most favourable for both absorption and emission; however, there are exceptions to this rule that can alter a spectrum, such as S_0-S_2 transitions. These S_0-S_2 transitions have been noted for some Bodipy compounds and usually appear as a broad peak around 375 nm.

The fluorescence quantum yield (Φ) is an important tool for identifying the efficiency of a fluorophore to emit light. It is measured as the ratio between the number of photons emitted through fluorescence to the total number of absorbed photons - usually out of 1. Fluorophores with a quantum yield close to 1 are the best emitters, although several factors can influence the quantum yield of a fluorophore, including both temperature and solvent polarity.[39]

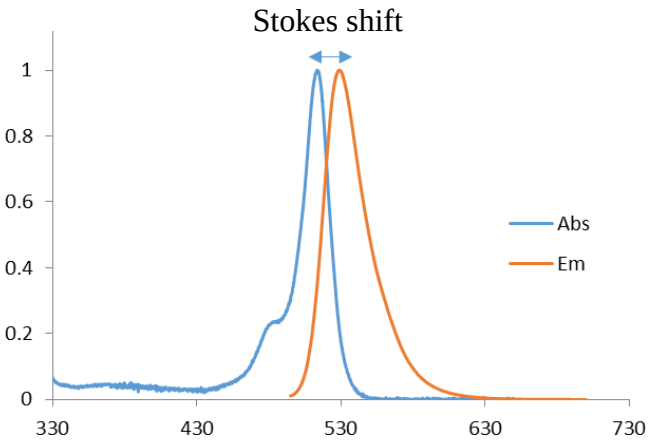

Figure 1.25 A typical Bodipy absorption and emission spectrum recorded in THF at room temperature.

The symmetrical Bodipy core is synthesised by a pyrrole condensation reaction. Two pyrrole units are bridged together by a highly electrophilic carbonyl, followed by an oxidation and finally the addition of boron trifluoride diethyl etherate to close the structure, as shown in Figure 1.26.[40]

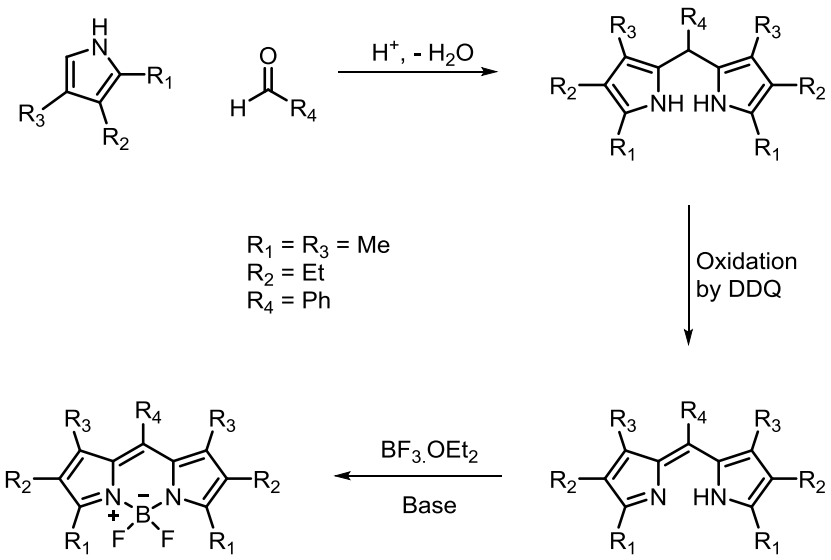

Figure 1.26 General synthesis of a symmetrical Bodipy system.

1.5.1 Modifications to the Bodipy Core

It is also possible to make unsymmetrical Bodipy compounds, such as **21** and **22**. The authors observed relatively small differences in terms of the absorption and emission maxima, and the quantum yields of these compounds compared well to symmetrical Bodipy systems (Fig. 1.27).[41] Comparison of compounds **21**-**24** generally showed a trend in red-shifted absorption and emission maxima as more substituents were introduced to the Bodipy core.

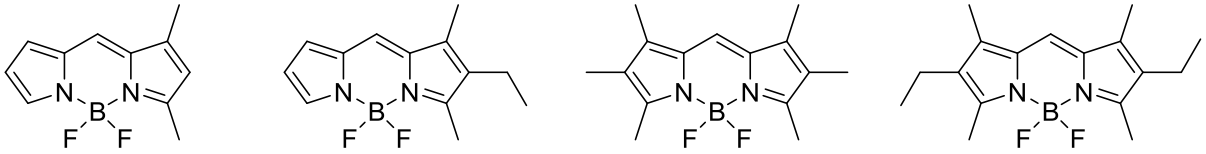

21
ϕ = 0.70
λ = 499 nm
λ = 509 nm

22
ϕ = 0.40
λ = 510 nm
λ = 520 nm

23
ϕ = 0.56
λ = 528 nm
λ = 535 nm

24
ϕ = 0.70
λ = 517 nm
λ = 546 nm

Figure 1.27 Unsymmetrical and symmetrical Bodipy compounds 21-24 (measurements recorded in ethanol).

A common position for the addition of further groups on to the Bodipy backbone is the *meso*-position at carbon 8 (Figure 1.24). It has been noted that the addition of alkyl and aryl groups at the 8-position have little effect on the absorption or emission wavelengths. However, further addition of substituents on the 1 and 7 positions has large effects on the quantum yield. The quantum yield of **25** is far less than the quantum yield of **26** (0.19 and 0.65 respectively). This has been attributed to the 1,7-substituents inhibiting free rotation about the phenyl group decreasing the loss of energy from the excited states by way of non-irradiative molecular motions.[39, 42] Similarly, the more substituted the aryl group on the *meso*-position, the higher the quantum yield - compare compounds **27** and **28** shown in Figure 1.28.

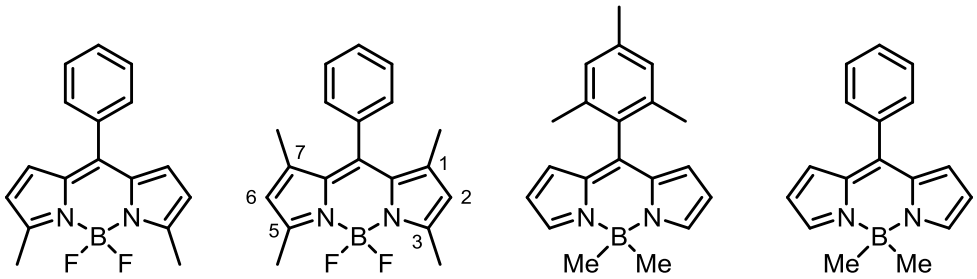

ϕ = 0.19
25

ϕ = 0.65
26

ϕ = 0.33
27

ϕ = 0.008
28

Figure 1.28 Substituted Bodipy cores have higher quantum yields which is attributed to the inhibition of free rotation about the phenyl group.

An *F*-Bodipy core with methyl groups on the 3 and 5 positions, such as compound **29** in Scheme 1.2, has been shown to be capable of undergoing chemical modifications due to the strong nucleophilic character of the methyl carbon atoms. The ability to extend the degree of π-conjugation at these 3 and 5 positions results in a bathochromic shift of the absorption and emission maxima.[40, 43] Both the mono- and di-substituted products can be obtained by varying the reaction times. The excitation wavelength of a fluorophore is important when they are being considered for imaging agents because fluorophores with a short wavelength (~500 nm, the blue/green region) have poor tissue penetration, and can be used for imaging cells and organelles

in vitro. The optimal excitation wavelengths are in the deep-red or near-infrared range (650-900 nm) as they have good tissue penetration and there is low autofluorescence, which limits the interference of background light with the images that are being produced.[44] Autofluorescence is the natural emission of light by biological structures, such as the mitochondria and can be problematic in fluorescence microscopy due to interference with the detection of a specific fluorescent signal.[45]

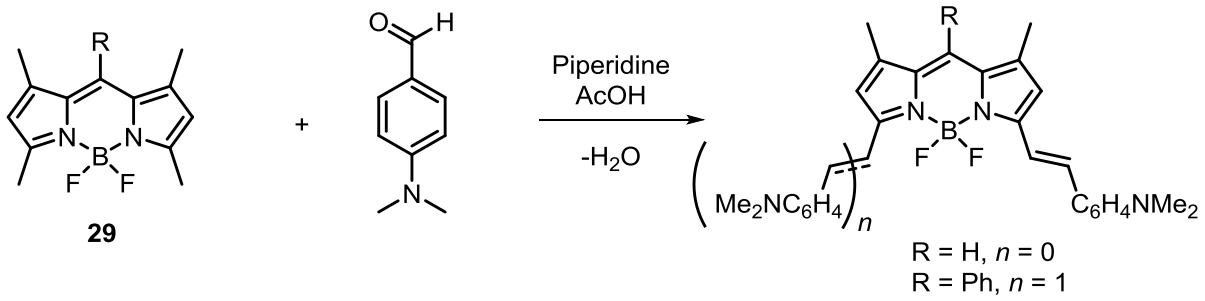

Scheme 1.2 Mono and di-substituted styryl-Bodipy derivatives achieved by condensation of 3,5-dimethyl Bodipys and aromatic aldehydes.

Mono- and di-substitution at these methyl groups can have an effect on the photophysical properties of a compound. An example, shown in Figure 1.29, compares the spectral data for the mono-substituted compound **30** and the di-substituted compound **31**. The study showed that the presence of the extra styryl group (compound **31**) gives a bathochromic shift in the UV absorbance of almost 100 nm and >50 nm in the emission spectrum. It was also noted that the quantum yields increased when the amine was protonated, due to Intramolecular Charge Transfer (ICT) in the excited state being disfavoured.[46]

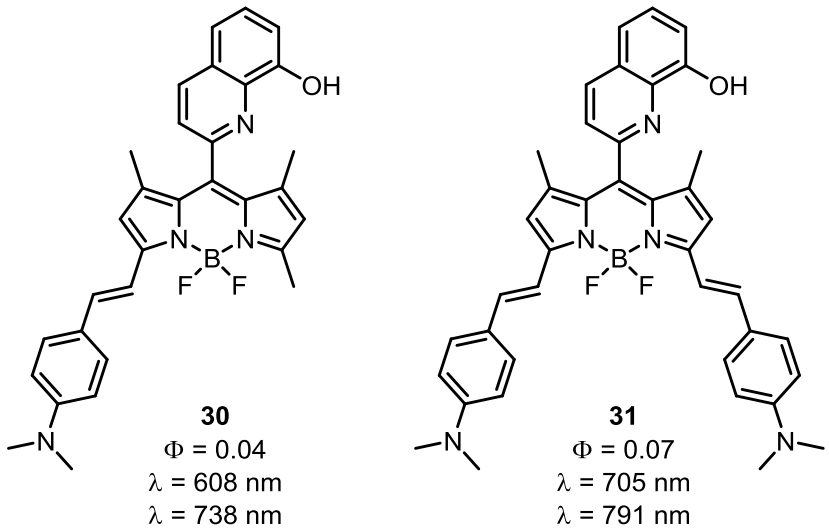

Figure 1.29 The spectral data of mono-substituted compound 30 and di-substituted compound 31, compared in methanol.

1.5.2 Preparation of *C*-Bodipys from *F*-Bodipys

The fluorines of the BF_2 group can be substituted for an alkyl or aryl group using lithium or Grignard reagents to form *C*-Bodipys. The addition of two equivalents of the reagent to precursor **32** produces the di-substituted product **33**. However, it is possible to control the substitution by using only one equivalent at low temperatures, in order to achieve mono-substituted Bodipy compounds such as compound **34** (Scheme 1.3).

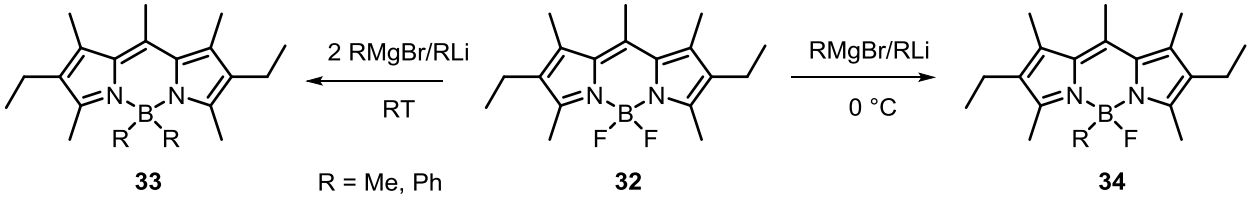

Scheme 1.3 Synthesis of C-Bodipys using Grignard reagents.

Synthesis of ethynyl (*E*-Bodipy) systems are also possible by the addition of ethynyl groups on to the boron atom. Compounds **35** and **36**, shown in Figure 1.30, were synthesised from 4-lithioethynyltoluene and 1-lithioethynylpyrene, respectively. Compound **36** was successfully conjugated to proteins, including bovine serum albumin and maintained a high fluorescence quantum yield.[47, 48]

The addition of ethynyl groups to the boron atom does not however bring them into conjugation with the Bodipy core, therefore similar absorption and emission maxima were observed as for the *C*-Bodipy systems.[47] The synthesis of ethynyl Bodipy structures will be discussed further in Chapter 2.

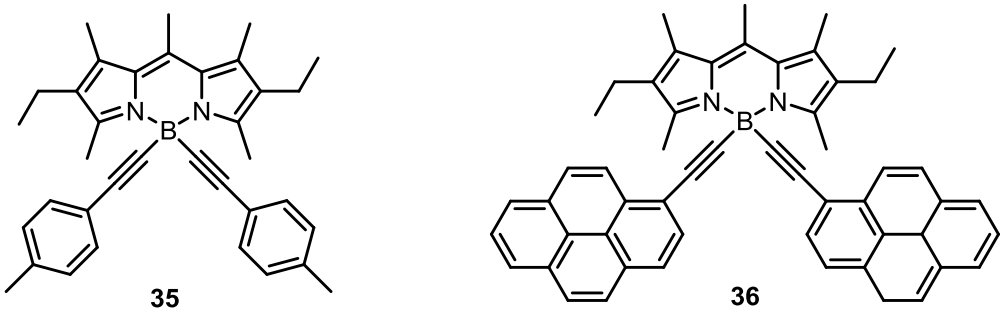

Figure 1.30 Synthesis of E-Bodipy systems by the incorporation of ethynyl groups onto the boron atom.

1.5.3 Photoinduced electron Transfer (PeT)

Photoinduced electron Transfer (PeT) is an excited state electron transfer process, and can sometimes lead to fluorescence quenching. There are various examples of Bodipy dyes being used as sensors to detect changes within a process, for example, a change in pH or the presence of metal ions, which can be indicated by an increase or decrease in fluorescence.[49, 50]

PeT occurs in a system containing an electron donor (D) and an acceptor (A), which when they are combined, form a D^+A^- species, which can then return to the ground state without photon emission. Both oxidative and reductive PeT processes are possible, shown schematically in Figure 1.31. The flow of electron donation is determined by the redox potentials of the fluorophore and the quencher.

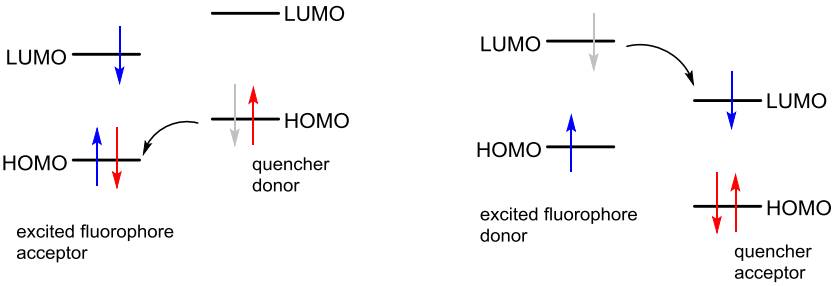

Figure 1.31 Adapted schematic of reductive PeT (left), where an electron is transferred from the HOMO of the quencher donor to the HOMO of the excited fluorophore acceptor and (right) oxidative PeT, where an electron is transferred from the LUMO excited fluorophore donor to the LUMO of the quencher acceptor.[35]

1.5.4 Fluorescence Quenchers

Fluorescence quenching refers to any process which diminishes the fluorescence intensity of a compound. There are several processes responsible for this, including excited state reactions, such as excimer formation, energy transfer and collisional quenching.

The formation of excimers (**exci**ted di**mers** formed by the collision of an excited molecule with an identical unexcited molecule) and exciplexes (**exci**ted com**plexes** formed by the collision of an excited molecule with a non-identical unexcited molecule) also decrease the fluorescence. The formation of excimers and exciplexes is a diffusion-controlled process and occurs more frequently in more highly concentrated solutions.[51]

Another form of quenching can be due to the presence of heavy atoms which promotes intersystem crossing, a non-radiative transition between two electronic states with different spin multiplicity *e.g.* S_1-T_1. This process is formally spin forbidden, although if the coupling between the orbital magnetic moment and the spin magnetic moment *i.e* spin-orbit coupling, is large enough, it can make this process possible. Heavy atoms often increase spin-orbit coupling, which in turn promotes intersystem crossing.[51] Another spin-forbidden process is phosphorescence, the emission of a

photon from an excited triplet state to the ground singlet state (T_1-S_0), shown in the Jablonski diagram in Figure 1.22.

This section has touched upon one important compound, **2** a tridentate phosphine-containing rhenium complex that was successfully used to image cancer cells, and subsequently led to the preparation of the technetium analogue **4**.[12] In the next section, examples of other fluorescent phosphorus-containing compounds are briefly discussed.

1.6 Phosphorus-containing Fluorescent Compounds

Fluorescent compounds containing nitrogen are common in applications such as near-infrared sensors and switches,[52, 53]intra-molecular charge transfer,[54] as OFF-ON fluorescent chemosensors and chemodosimeters for Cu^{2+} and Pb^{2+} complexes,[55] as pH indicators[56] and in the production of fluorescent carbon nanotubes.[57]

However, fluorescent molecules containing phosphorus are much less common, perhaps due to an assumption that a heavy atom could cause fluorescence quenching. Examples that are known in the literature usually refer to phosphonates, phosphine oxides and phosphonic acids.[4, 58]

Phosphonic acids and bisphosphonates have shown potential applications in bone imaging, due to their high affinity for calcium (II), which leads to accumulation of these compounds in areas with increased bone metabolism.[59, 60]

In 2013, Ishow and co-workers published their findings on fluorescent phosphonic and carboxylic acid nanoparticles. In particular the phosphonic acid derivatives, such as compounds **37a**/**37b** have been shown to chelate to metal oxide surfaces and form magnetofluorescent core-shell nanomaterials.[61] Yetimoğlu *et.al.* described how a fluorescent vinyl phosphonic acid had been synthesised as a sensor for Hg(II) detection in aqueous solution[62] and fluorescent phosphine oxides such as **38** act as efficient blue Thermally Activated Delayed Fluorescent (TADF) diodes, described by Huang *et al*.[63]

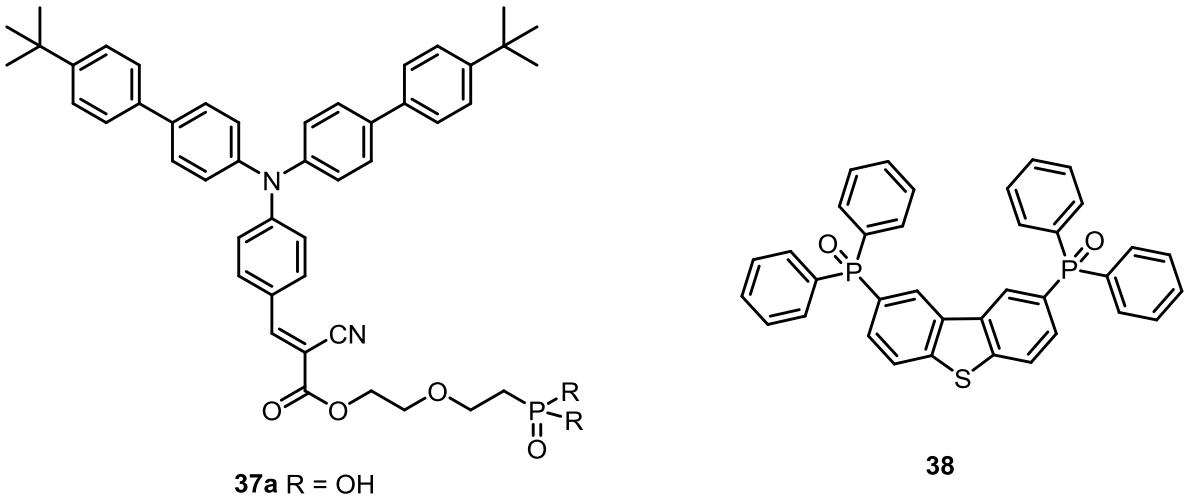

37a R = OH
37b R = OEt

38

Figure 1.32 Ishow's fluorescent phosphonic acid 37a, phosphonate 37b and Huang's phosphine oxide 38.

In 2015 Xiao and co-workers reported the synthesis of novel compounds PODIPY (phosphorus-dipyrromethene) **39** and aza-PODIPY (phosphorus-azadipyrromethene) **40**. They are related to the well-known Bodipy dyes, and have shown suitability for labelling living Hep-2 cells for imaging assays in the near-infrared region.[64] The photophysical data for the two compounds is shown in Figure 1.33, and although the absorption and emission maxima are in relative accordance with Bodipy dyes, the extinction coefficients are considerably lower (compare 34000 $M^{-1}cm^{-1}$ with 77000 $M^{-1}\,cm^{-1}$ (the extinction coefficient for compound **2**)).

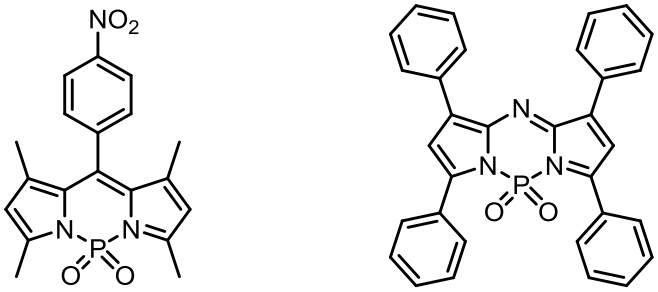

39
λ_{abs} = 510 nm
λ_{em} = 524 nm
ε = 34900 $M^{-1}cm^{-1}$

40
λ_{abs} = 625 nm
λ_{em} = 661 nm
ε = 33000 $M^{-1}cm^{-1}$

Figure 1.33 Novel PODIPY and aza-PODIPY compounds synthesised by Xiao.

An example of a fluorescent phosphine was described by Protasiewicz who synthesised a class of compound known as R_2-NBOPs (2,7-R_2-naphthobis(oxaphosphole)s) via the primary phosphine **41**, which are air and water stable and exhibit interesting blue fluorescence (Figure 1.34).[65]

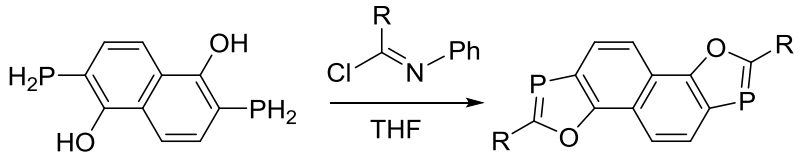

41 **42**

Figure 1.34 Protasiewicz et al. synthesised the di-primary phosphine 41 which was then converted into the fluorescent phospha-acene 42.

So far the versatility of primary phosphines and the role that fluorescence can play in imaging agents has been discussed. Another important feature in our multimodality imaging probe is the incorporation of a radiolabel, for example the addition of ^{99m}Tc to facilitate SPECT imaging, which was shown by the synthesis of complex **4**, illustrated in Figure 1.35.

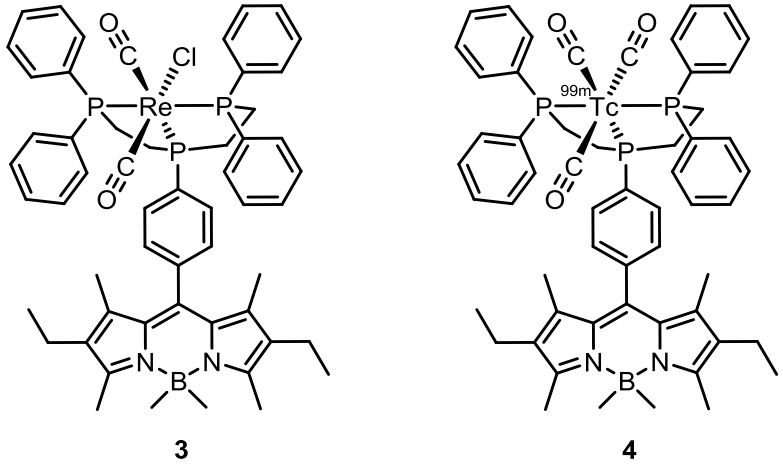

3 **4**

Figure 1.35 Re and Tc complexes of BodP_3 provide a cold and a hot fluorescent analogue of multimodal imaging agents.

1.7 Radioimaging

Radiopharmaceuticals are a type of compound that contain a radioactive label which can be used as a diagnostic or therapeutic agent. The two most commonly used techniques are Single Photon Emission Computed Tomography (SPECT) and Positron Emission Tomography (PET). The main difference between the two techniques is the type of radiotracer that is used, which is explained further in the following sections. SPECT and PET are often combined with other techniques such as Computed Tomography (CT) or Magnetic Resonance Imaging (MRI) to gain a better visualisation of *in vitro* processes.[13]

1.7.1 Single Photon Emission Computed Tomography (SPECT)

SPECT is a radio-imaging technique that is used to observe metabolic processes within the body.

The radionuclides that are introduced into the body emit a single γ-ray during decay, which is measured directly by a collimator.[66] The nuclides used in SPECT generally have a longer half-life than PET radionuclides, which together with the low cost of gamma cameras, makes a SPECT scan far cheaper and more easily available. However, the use of a collimator in SPECT results in low detection compared to PET, therefore between the two techniques, PET is more sensitive which means higher resolution.[13] The most commonly used SPECT radionuclides are shown in Table 1.1.[13]

Table 1.1 Commonly used SPECT radionuclides.

Nuclide	Half-life/h	Emission Type	Photon Emission Energies/MeV
^{123}I	13.2	Electron capture	0.16
^{99m}Tc	6	Isomeric transition	0.14
^{111}In	67.9	Electron capture	0.17/0.25
^{67}Ga	78.3	Electron capture	0.09/0.19/0.30
^{201}Tl	73.1	Electron capture	0.17

The most commonly used radionuclide in SPECT is ^{99m}Tc. It has ideal properties, which include a convenient half-life of 6 hours, and a relatively low cost of generation through the decay of the parent ^{99}Mo (half-life = 66 hours) using commercially available generator systems.[13] The ^{99}Mo/^{99m}Tc generators produce ^{99m}Tc in the form of [^{99m}Tc]-pertechnetate, in its highest oxidation state of +7. A popular technetium-based drug, ^{99m}Tc-Tetrofosmin (also known as Myoview), is synthesised from pertechnetate in a commercially available kit.[67] Myoview is a heart imaging agent based on the bidentate phosphorus ligand 1,2-bis[di(2-ethoxyethyl)phosphino]ethane, and has the structure shown in Figure 1.36. ^{99m}Tc is used in radiopharmaceuticals for imaging organs and metabolic processes in the body, including the lungs, liver, brain and kidneys.[68]

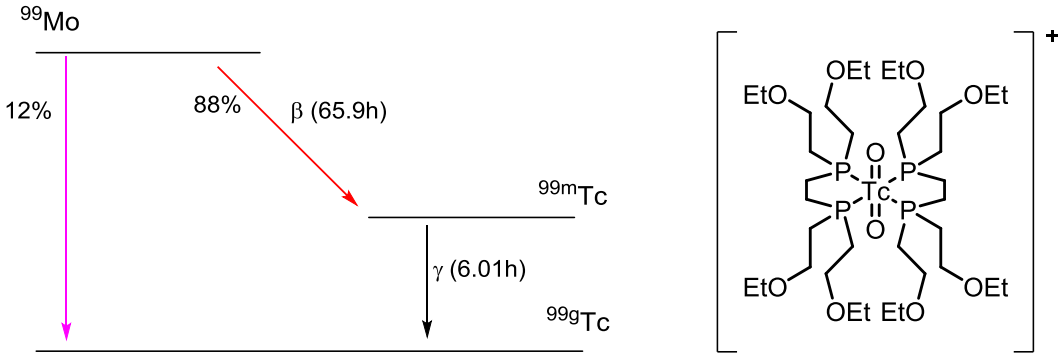

Figure 1.36 Schematic of ^{99}Mo decaying to ^{99m}Tc via β decay (left); ^{99m}Tc-Tetrafosmin which is commercially known as Myoview (right).

1.7.2 Positron Emission Tomography (PET)

In PET imaging, a positron-emitting radionuclide is introduced into the body, the positron is emitted from the nucleus and travels a short distance in the surrounding tissue before eventually colliding with an electron, causing a pair of γ-rays to be emitted at approximately 180° to one another. These γ-rays are detected by surrounding detectors, which records information about the positron annihilation. Once a large number of annihilation events have been recorded, the data can be reconstructed into an image, detailing information on the spatial distribution of radioactivity as a function of time, shown schematically in Figure 1.37.[13]

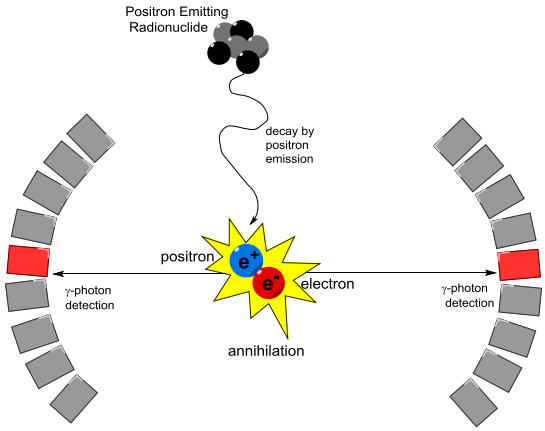

Figure 1.37 Adapted schematic of the principle behind PET imaging.[69]

There are a large number of radionuclides available for PET imaging - the most common are shown in Table 1.2.[13]

Table 1.2 Commonly used PET radionuclides.

Nuclide	Half-life / min	Emission type	Max. energy / MeV
^{11}C	20.3	β^+	0.97
^{18}F	110	β^+	0.64
^{64}Cu	762	β^+ / electron capture	0.66
^{68}Ga	68.1	β^+ / electron capture	1.90
^{76}Br	972	β^+ / electron capture	4.00
^{124}I	60192	β^+ / electron capture	2.14

One advantage of PET imaging over SPECT imaging is that the radiolabelled imaging agent is almost identical to its nonradioactive analogue. The most common radiolabel is ^{18}F due to its favourable half-life (110 mins), and although fluorine atoms are not common in biomolecules, it is relatively easy (in principle) to substitute a hydrogen or hydroxyl group with a fluorine atom and

retain the molecules original biological function, because fluorine and hydrogen are similar sized atoms so replacement between the two has limited effects, other than the difference in electronegativity. This may change the electronic properties of the compound, although there are examples where this change has proven advantageous.[70] The choice of radionuclide is very important - the half-life must be considered; some biological processes take longer than others and selecting a radionuclide with a half-life that is too short will result in no useful data being obtained. Secondly, as is evident in Table 1.2 above, radionuclides emit positrons at different energies, which effects the resolution of the PET image; ideally, the annihilation event will occur close to the origin of the positron, however, high energy positrons will travel further, resulting in annihilation events occurring remotely, thus increasing the uncertainty in its location and resulting in a lower resolution PET image.

1.7.3 Mitochondria Specific Compounds

The fourth and final aspect of the proposed multi-modal imaging agent studied in this thesis is the addition of a phosphonium cation to introduce mitochondria specific targeting.

Targeting the mitochondria has become a popular option for therapeutics due to the increasing knowledge of the link between mitochondrial dysfunction and several diseases such as a range of cancers,[71-73] Alzheimer's[74] and Parkinson's Disease.[75]

It is known that positively charged molecules are attracted to the negative charge within the mitochondrial matrix, therefore a phosphonium cation has been identified as a promising compound for specific targeting of the mitochondria (previously discussed in Section 1.2.4 and in more detail in Chapter 4).

So far, the four major functions of the target multi-modal imaging agent have been discussed – (i) primary phosphine synthesis, as a precursor to tridentate ligands that confer kinetic stability on resulting complexes, (ii) the fluorescent Bodipy core for *in vitro* imaging, (iii) incorporation of a radionuclide such as ^{18}F or ^{99m}Tc for PET/SPECT imaging, and (iv) a phosphonium salt, that would allow for the direct targeting of an organelle. The work presented in this thesis will exploit these advances and broaden the research into new territories.

The final sections of the introduction will briefly introduce the applications of phosphines in catalysis, in preparation for the penultimate chapter of this thesis where a novel, Bodipy-based,

fluorescent, chiral phosphonite has been synthesised for the first time and has been used successfully in an asymmetric hydrogenation reaction.

1.8 Phosphines in Catalysis

1.8.1 Asymmetric Catalysis

Asymmetric catalysis is an important method of synthesising chiral compounds with high enantioselectivity. An asymmetric catalyst favours the formation of one enantiomer over the other by lowering the transition state energy for the favoured enantiomer, making it kinetically more favourable to synthesise the lower energy route enantiomer.

Many of the building blocks in biological systems, such as sugars or amino acids, are produced exclusively as one single enantiomer.[76] There can be noticeable differences between two enantiomers, such as flavour. For example *l*-aspartame has a sweet taste and *d*-aspartame is tasteless;[77] another variance can be in the odour - for example carvone, a molecule found naturally in many essential oils; the (*R*)-(-) enantiomer has a distinctive spearmint smell but the (*S*)-(+) enantiomer smells like caraway seeds (Fig. 1.38).[78]

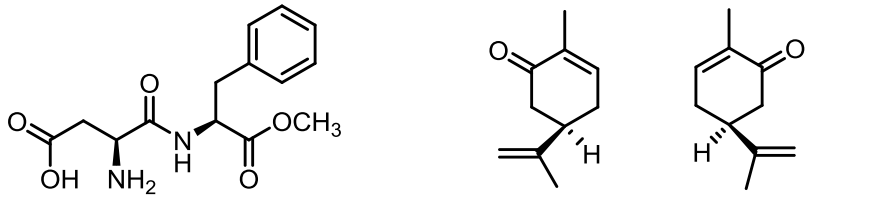

l-Aspartame *(R)-Carvone* *(S)-Carvone*

Figure 1.38 Different enantiomers can have varied tastes and odours, such as aspartame and carvone.

Chirality is also crucial in many pharmaceuticals, and there are several examples in the literature where only one enantiomer is effective. Citalopram for instance, is an anti-depressant drug which is sold as a racemic mixture, however, studies have shown that only the (*S*)-(+) enantiomer is responsible for the effectiveness of the drug.[79] Chirality is also essential for drug safety; *d*-penicillamine is used in chelation therapy and for the treatment of rheumatoid arthritis, whereas *l*-penicillamine is toxic and inhibits the action of pyridoxine, an essential B vitamin.[80] This reiterates the importance of catalysts that are able to selectively form one enantiomer over the other, and are therefore in high demand.

1.8.2 Asymmetric Hydrogenation

Asymmetric hydrogenation is the addition of two hydrogen atoms preferentially to one of two faces of an unsaturated substrate molecule, such as an alkene or ketone. The asymmetric hydrogenation of prochiral olefins is one of the most widely studied transformations in asymmetric catalysis. Figure 1.39 shows an example of asymmetric hydrogenation reported by Noyori and co-workers using a BINAP-Rh complex, which showed conversions up to 99% and with very high enantiomeric excesses, sometimes up to 99%.[81]

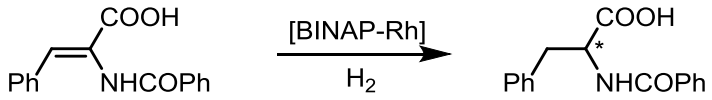

Figure 1.39 Asymmetric hydrogenation of α-(acylamino)acrylic acids with Rh-BINAP catalyst.

A chiral compound is one that is non-superimposable on its mirror image. The most common generator of asymmetry found in organic molecules is a chiral stereocentre, where a carbon atom has four different groups bonded to it. Another form is axial chirality, which is observed in atropisomeric biaryls, such as biphenyl or binaphthyl compounds, where rotation about the aryl-aryl bond is restricted, shown in Figure 1.40.

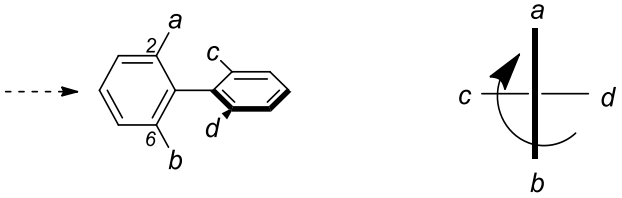

Figure 1.40 Viewing of the axis of chirality of a substituted biaryl - its configuration is assigned following the Cahn-Ingold-Prelog priority rules.

A major application of phosphines in catalysis was introduced in 1965 by Wilkinson and co-workers, who used [$RhCl(PPh_3)$] to catalyse the hydrogenation of alkenes.[82]

Monodentate phosphines dominated the catalysis industry for many years until the 1970s where the development of bidentate phosphines began, including major examples all shown in Figure 1.41, such as DIOP (2,3-*o*-isopropylidene-2,3-dihydroxy-1,4-bis-(diphenylphosphino)butane), BINAP (2,2'bis(diphenylphosphino)-1,1'-binaphthyl) and DuPhos (from the company name DuPont and the class of compound, phospholanes) which are all used in asymmetric reductions. BINAP in particular has had a significant impact on the industrial synthesis of compounds such as menthol which saw Noyori jointly win the 2001 Nobel Prize for his role in the development of the ligand.[81, 83, 84]

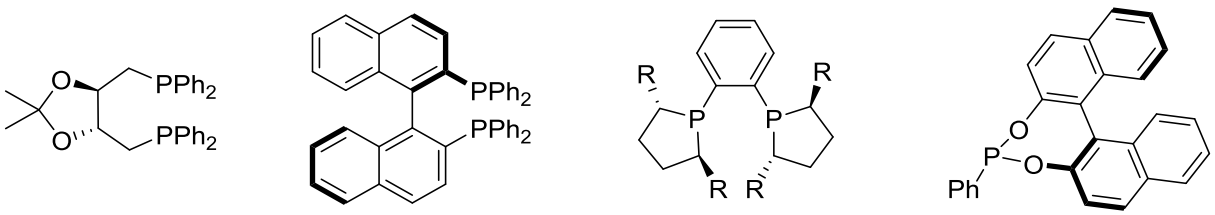

(*R*,*R*)-DIOP (*R*)-BINAP (*S*,*S*)-DuPhos (*S*)-Phosphonite

Figure 1.41 DIOP, BINAP, DuPhos and phosphonite ligands are all highly proven ligands in asymmetric catalysis.

The phosphonite ligand will be investigated in Chapter 5 of this thesis, where a novel fluorescent phosphonite has been synthesised and used in an asymmetric hydrogenation reaction with a benchmark substrate.

1.9 Aims of the project

Following this introductory section, this thesis describes the synthesis of the primary phosphines, as well as their coordination chemistry to transition metals. Chapters 4 and 5 concentrate on using these primary phosphines as important precursors to fluorescent phosphonium salts and fluorescent phosphonites for use in multi-modal imaging and catalysis. Finally, Chapter 6 explores the relationship between the aryl linker, separating the phosphorus moiety from the Bodipy core, and the photophysical properties of these derivatives.

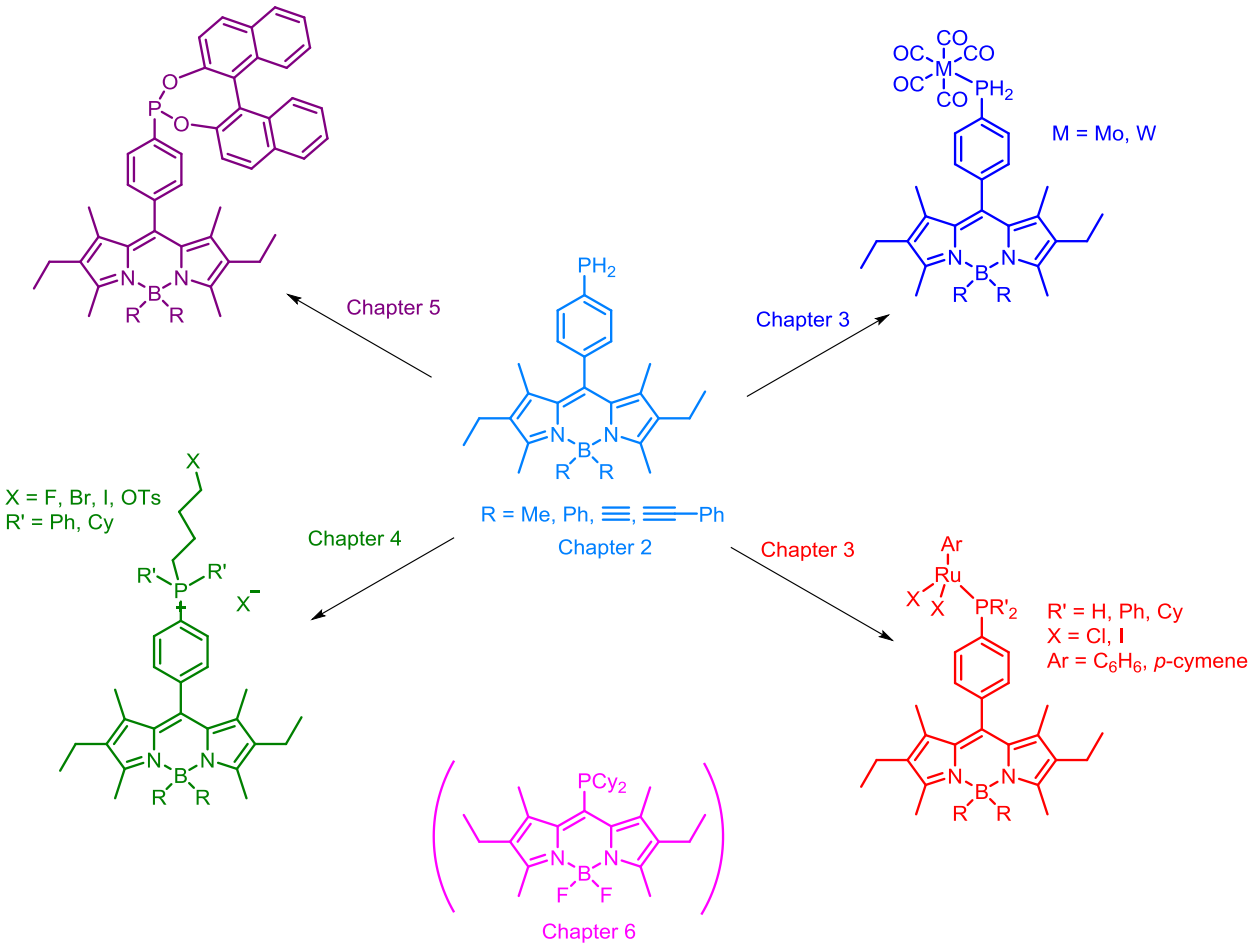

Chapter 2 discusses the synthesis of first and second generation primary phosphines, where the substituents attached to the boron atom were varied in order to synthesise highly fluorescent analogues.

Chapter 3 investigates the coordination chemistry of primary phosphines to group 6 and 8 transition metals. Primary phosphines are weaker donor ligands that their secondary and tertiary counterparts and therefore it is important to establish their ability to bind transition metals. Phosphine complexes of molybdenum carbonyls are often synthesised to elucidate the stereoelectronic nature of the

phosphines, due to a weakening of the CO triple bond. By varying the substituents on the phosphorus atom, the IR absorptions in the carbonyl region will be modified; better electron donors and/or poorer acceptors exhibit lower carbonyl stretching frequencies.
The coordination of four primary phosphines to a range of halo-bridged ruthenium(II) dimers was conducted and their photophysical properties were recorded to identify the effects that the coordination of transition metals has on the fluorescence of the phosphorus ligands. In order to make more direct comparisons to the ruthenium-phosphine pharmaceutical RAPTA-C, the coordination of ruthenium to tertiary phosphines was also briefly investigated.

Chapter 4 will investigate how primary phosphines can be used to prepare phosphonium salts of relevance to medical imaging. A major target is the synthesis of a multifunctional imaging probe, consisting of three functions: a phosphonium cation to allow for mitochondria-specific targeting within the cell, a Bodipy fluorophore for cell imaging via fluorescence microscopy, and the incorporation of an ^{18}F radionuclide for *in vivo* nuclear imaging.

The thesis will conclude with two short, ambitious accounts of new research avenues – Chapter 5 features a novel, fluorescent phosphonite which can afford an enantioselectivity of >99% for the asymmetric hydrogenation of benchmark substrate methyl (Z)-β-acetamidocinnamate (MAC), and Chapter 6, which will show the photophysical effects of the aryl linker in separating the phosphorus moiety from the Bodipy core, the photophysical properties will be examined to establish what effects the phosphorus group – when bound directly to the core – has on the photophysical properties of the derivatives.

Chapter 2: Synthesis of Air-stable, Fluorescent Primary Phosphines

L. H. Davies, J. F. Wallis, M. R. Probert and L. J. Higham, Efficient multigram synthesis of air-stable, fluorescent primary phosphines via palladium-catalyzed phosphonylation of aryl bromides, *Synthesis*, 2014, **46**, 2622-2628.

2 Air-stable, Fluorescent Primary Phosphines

Primary phosphines constitute a class of ligand which have been under-utilised due to their notorious reputation as highly air and moisture sensitive compounds.[22, 23, 85] As previously discussed in Section 1.2.2.3 it is possible for these compounds to be stabilised to air oxidation by the use of electronic effects, rather than steric protection.[30] This is achieved by incorporating a high level of π-conjugation within the compound. The Density Functional Theory (DFT) model developed by the Higham group concluded that primary phosphines that showed resistance to air oxidation contained either sufficient π-conjugation, steric bulk or heteroatoms.[30]

As previously discussed in the introduction, it is essential to define the meaning of "air-stable phosphines" in this thesis. And for the purposes of this research an "air-stable" phosphine is one which displays inertness towards oxidation over several weeks.

In 2006, Higham and co-workers synthesised the first air-stable, chiral primary phosphine (*R*)-$MOPH_2$, **15**, shown in Figure 2.1.[86] The discovery of this primary phosphine led to the development of the DFT model previously described.

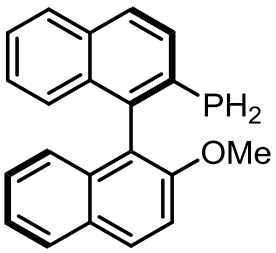

15 (*R*)-$MOPH_2$

Figure 2.1 The first air-stable, chiral primary phosphine.

In order to test the model's limitations, other highly conjugated backbones were sought. Fluorophores also tend to be highly conjugated systems therefore a primary phosphine containing a backbone based on the Bodipy core was modelled – and predicted to be air-stable.[34] This chapter will discuss the synthesis of a series of fluorescent primary phosphines based on the Bodipy fluorophore alongside their air stability studies and photophysical properties.

2.1 Synthesis of the First Generation of Fluorescent Primary Phosphines

The Higham group reported the original and improved syntheses of Bodipy primary phosphines **20a** and **20b** between 2012 and 2014.[34, 87] Both routes are shown in Figure 2.2 and will be briefly

discussed. The improved synthesis removed the problematic lowest-yielding step of the four-step synthesis, where an unwanted side product was formed.

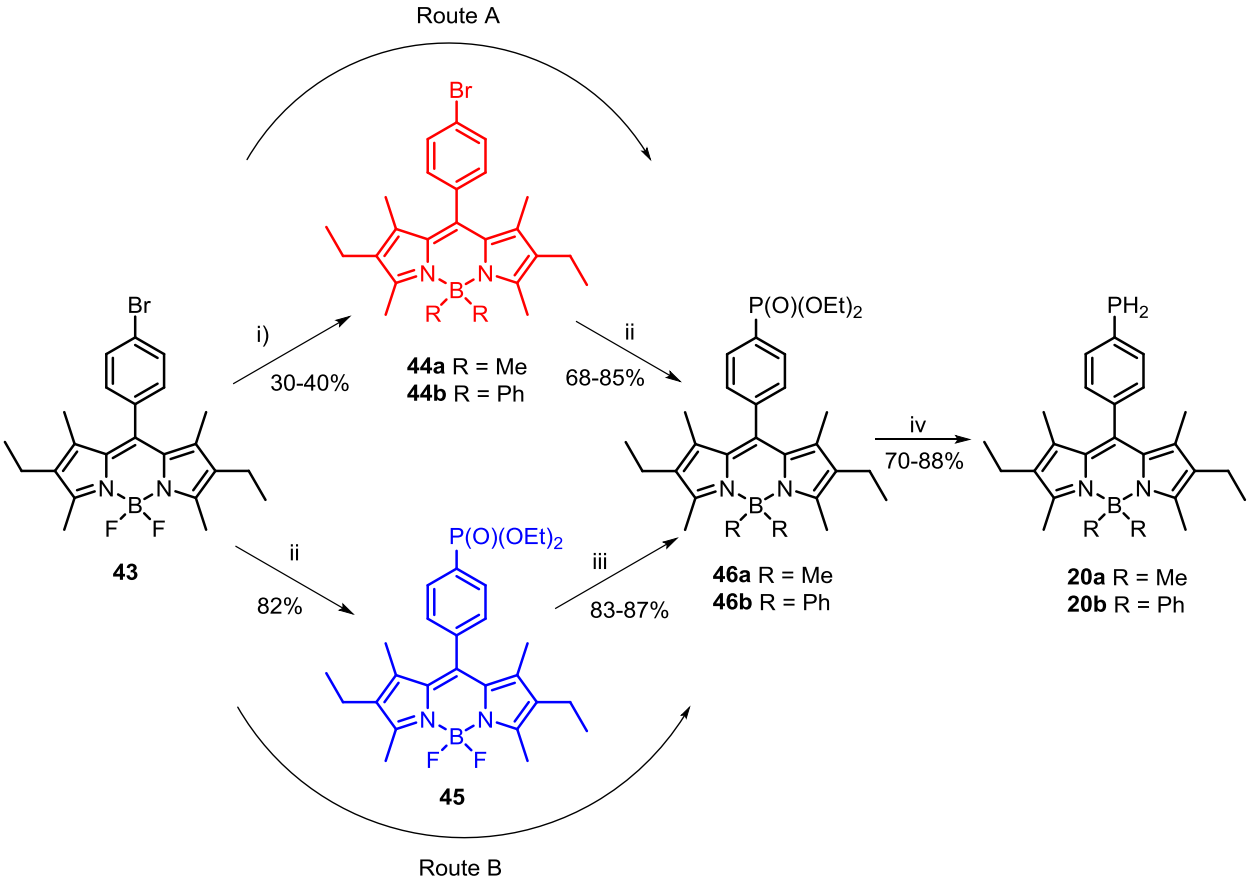

Figure 2.2 Original synthesis via the red route and the improved synthesis shown in the blue. i) 2 RLi, THF, RT ii) Pd(OAc)$_2$, DPPB, *i*Pr$_2$NEt, HP(O)(OEt)$_2$, DMSO, 90°C, iii) 2 RMgBr, THF, RT, iv) LiAlH$_4$/TMSCl, THF, –78°C to RT; R = Me or Ph.

The first step in both syntheses was a one-pot pyrrole condensation reaction between 3-ethyl-2,4-dimethyl-1-pyrrole and 4-bromobenzaldehyde to give **43** in a moderate yield of 55%, as illustrated in Scheme 2.1. The reaction was analysed by NMR spectroscopy, which confirmed the presence of the desired product. The $^{11}B\{^1H\}$ NMR spectrum showed a triplet at δ –0.2 ppm (J_{BF} = 31.8 Hz) and the $^{19}F\{^1H\}$ NMR spectrum showed a quartet at δ –145.6 ppm (equal intensity) with a coupling constant J_{FB} = 31.8 Hz. Since boron possesses two isotopes – ^{11}B (80%) and ^{10}B (20%), it is possible to detect coupling of both isotopes, in which case a quartet and a septet would be observed in the ^{19}F NMR spectrum. The dominant peaks would be the 1:1:1:1 quartet with the underlying seven line multiplet in between. In our case, the fluorine line widths are significantly broadened by the boron so that ^{10}B is not visible. The four lines of the quartet are not symmetrical because the ^{10}B peaks are actually shifted slightly to one side because of the isotope shift effect.

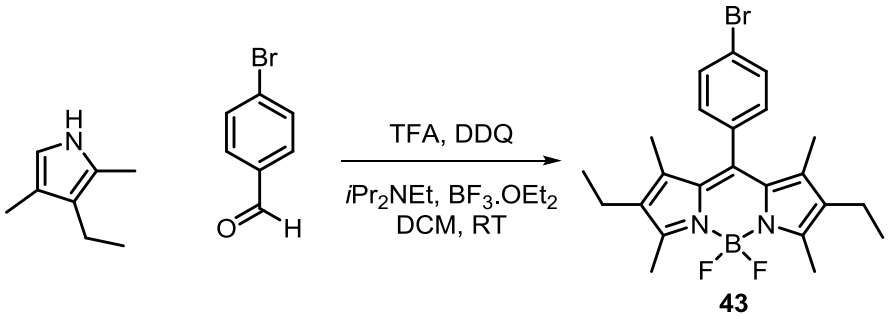

Scheme 2.1 Synthesis of the *F*-Bodipy aryl bromide 43.

Route A

In order to successfully synthesise primary phosphines **20a**/**20b**, the fluorine atoms had to be substituted for carbon-containing substituents. This is because previous work has shown that reducing the phosphonate **45**, where the fluorine atoms are still bound to the boron does not result in the desired primary phosphine but instead, the lithium aluminium hydride reducing agent attacks the BF_2 moiety and breaks open the Bodipy ring.[34]

The substitution of the fluorine atoms to form the methyl and phenyl derivatives was performed by stirring two equivalents of an organolithium reagent with Bodipy arylbromide **43** in anhydrous THF at room temperature for one hour. However, this step was low yielding (~30%) due to the formation of a side product, **47a** or **47b,** shown in Figure 2.3. The presence of polar side products was also noted when Ziessel and co-workers converted *F*-Bodipys into *C*-Bodipys – however they were not successfully isolated.[88]

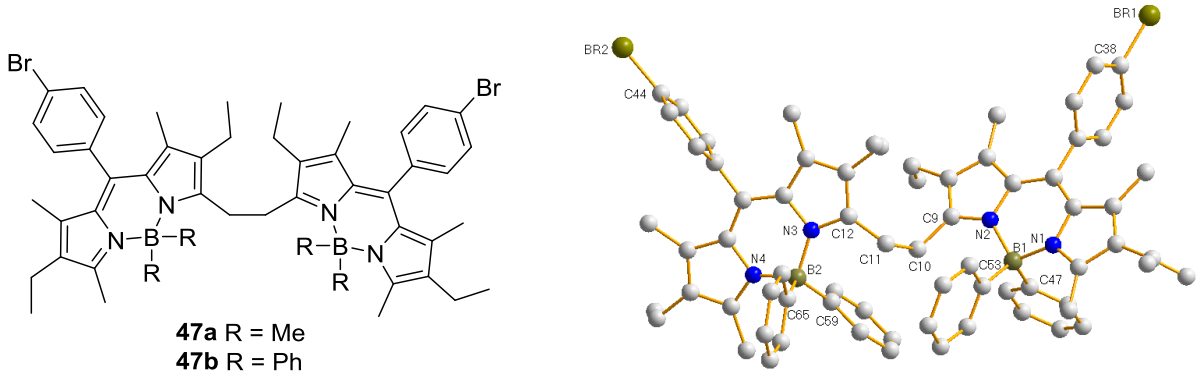

Figure 2.3 Side product and X-ray crystal structure of compound 47b. Crystals grown via slow diffusion using petrol:toluene. Selected bond distances [Å] and angles [°]: C10-C11 1.5610(4), Br1-C38 1.9022(3), Br2-C44 1.8964(3), all B-C bonds have an average distance of 1.62(4); C9-C10-C11 115.928(34), C47-B1-N1 107.663(22), N1-B1-N2 105.301(35), C47-B1-C53 117.366(2), C65-B2-C59 116.737(23), N3-B2-N4 105.058(30).

The side products were isolated in ~10% yield during the purification of the *C*-Bodipy compounds **44a** and **44b** by column chromatography and showed a connection of two units through the 3 and 5 carbon atoms. These methyl groups have previously been identified as acidic, and as described

in Section 1.51, the addition of substituents in these position has been reported.[43] The mechanism for the production of these side products is not known, although it is possible that it is a radical reaction.

The phosphonate was introduced *via* a palladium-catalysed cross-coupling reaction with diethyl phosphite in dimethyl sulfoxide at 90°C for three days. Introduction of the phosphonate group works efficiently with either the fluorine atoms or the methyl/phenyl groups on the boron atom; there was a marginally higher yield for the phosphonate coupling reaction with the fluorine atoms still present – therefore improving the yield of the reactions during the conversion of the *F*-Bodipys to the *C*-Bodipys was the important step.

Route B

Route B introduced the use of Grignard reagents rather than the organolithium reagents in attempts to minimise the formation of side products. Phosphonate **45** was reacted with two equivalents of methyl or phenylmagnesium bromide to form phosphonates **46a** and **46b** in higher yields (83-87% compared to 30-40%) and with no side products.

A common route to synthesising a primary phosphine is via a phosphonate, which are easily reduced using lithium aluminium hydride. In this case, a dual reducing agent was used – lithium aluminium hydride and chlorotrimethylsilane because Rajanbabu found that this mixture worked particularly well.[85, 89]

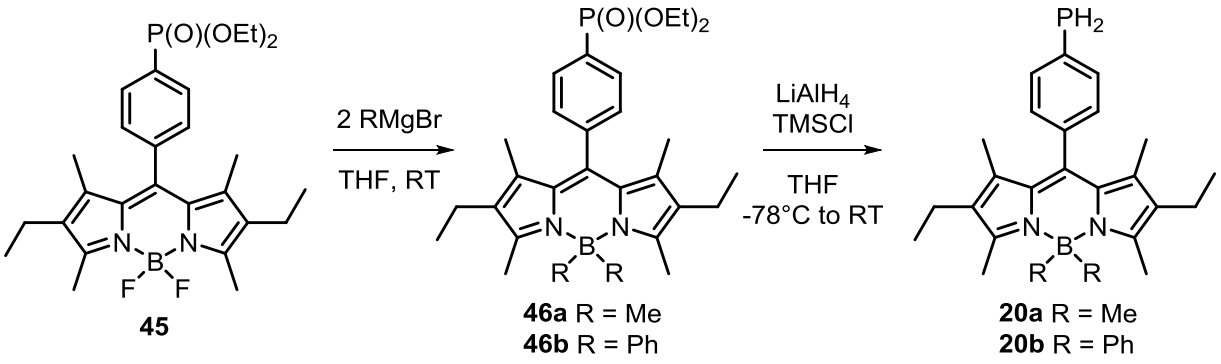

Scheme 2.2 Synthesis of aryl and alkyl phosphonates 46a/46b and reduction to primary phosphines 20a/20b.

2.2 Second Generation Air-stable, Highly Fluorescent Primary Phosphines

A second target for this project was to synthesise analogues of primary phosphines **20a** and **20b** that exhibited an increased fluorescence quantum yield. Within the literature, the addition of ethynyl groups to the boron atom has been shown to achieve this – two examples are compounds **35** and **36**, shown in Figure 2.4, they display high quantum yields of 0.95 and 0.94, respectively.

The compounds were synthesised by Ziessel *et. al.* in 2005 to determine the importance of the size of the Stokes' shift in an attempt to minimise fluorescence quenching during bioconjugation.[47]

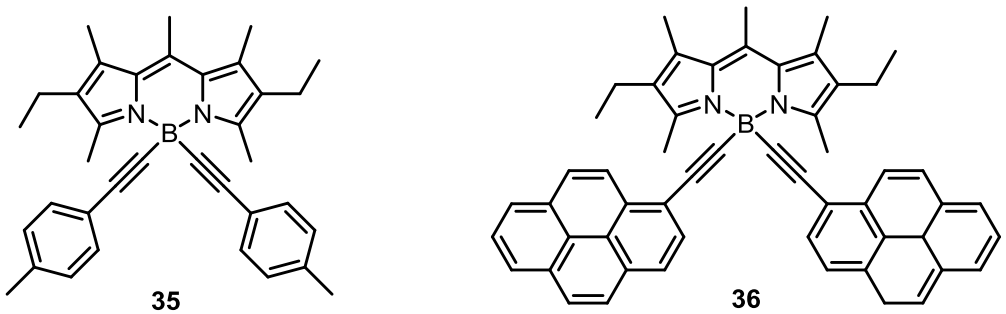

35
λ_{abs} = 516 nm
λ_{em} = 537 nm
Φ_F = 0.95

36
λ_{abs} = 516, 371 nm
λ_{em} = 535 nm
Φ_F = 0.94

Figure 2.4 Two examples of highly fluorescent ethynyl Bodipy dyes.

2.2.1 Synthesis of Novel Primary Phosphine 50

In order to introduce ethynyl groups on to the boron atom, Bodipy arylbromide **43** was reacted with two equivalents of ethynylmagnesium bromide at 75 °C in anhydrous THF under a nitrogen atmosphere for 16 hours (Scheme 2.3). The reaction was monitored by $^{11}B\{^1H\}$ NMR spectroscopy which showed a change from a triplet to a broad singlet, indicating the formation of a B-C bond. Analysis by $^{19}F\{^1H\}$ NMR spectroscopy also confirmed that there was no fluorine present. The presence of the ethynyl groups could also be observed in the ^1H NMR spectrum due to the new singlet peak at δ ~2.15 ppm, corresponding to the two terminal protons of the ethynyl groups. The product was purified by column chromatography on silica gel to give the novel Bodipy **48** in a good yield of 84%.

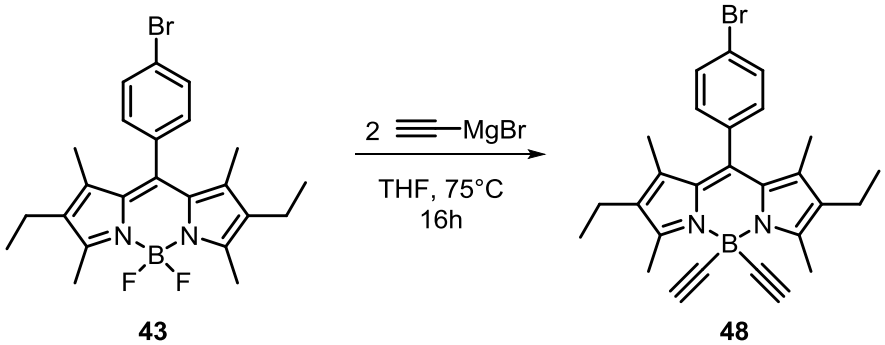

43 **48**

Scheme 2.3 Synthesis of the alkyne-Bodipy aryl bromide 48.

A crystal of **48** suitable for X-ray diffraction was obtained by slow diffusion of pentane into a deuterated chloroform solution of **48**; the molecular structure can be seen in Figure 2.5. This is the

first example of a Bodipy dye with an ethynyl group attached to the boron atom where no further substituents are present on the terminal end of the alkyne.

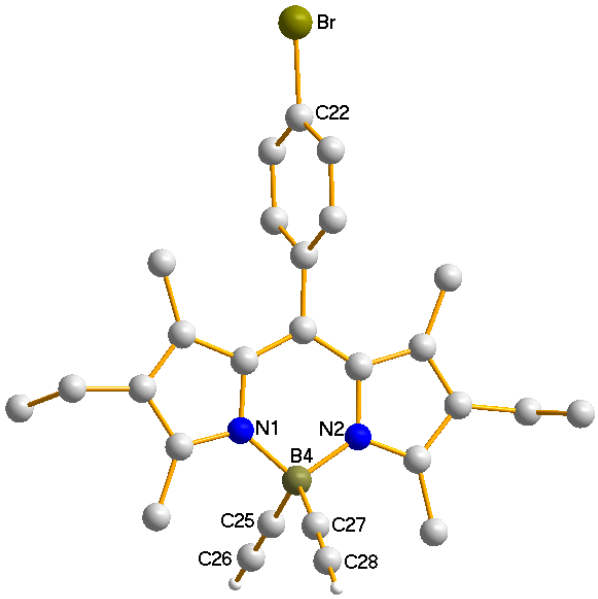

Figure 2.5 Molecular structure of 48. Selected bond distances [Å] and angles [°]: C25-B4 1.581(4), C27-B4 1.603(4), C22-Br 1.901(2), C25-C26 1.189(4), C27-C28 1.179(4); C25-B4-C27 111.5(2), N1-B4-N2 106.3(2), N1-B4-C25 108.5(2).

The B-C bond lengths of 1.581(4) and 1.603(4) Å and the alkyne C-C bond lengths of 1.179(4) and 1.189(4) Å respectively are all in agreement with literature references of similar structures.[47,90]

A palladium-catalysed cross-coupling reaction of ethynyl Bodipy **48** with diethyl phosphite in anhydrous dimethyl sulfoxide yielded novel phosphonate **49** after heating at 90°C for three days. It was important that the solvent was dry, as when the reaction was attempted with standard grade dimethyl sulfoxide, the desired product was not formed and starting material was still present. The reaction was monitored by $^{31}P\{^{1}H\}$ NMR spectroscopy and the formation of the phosphonate peak at δ 17.8 ppm was observed. The product was purified by column chromatography on silica gel to give phosphonate **49** as an orange solid in 55% yield.

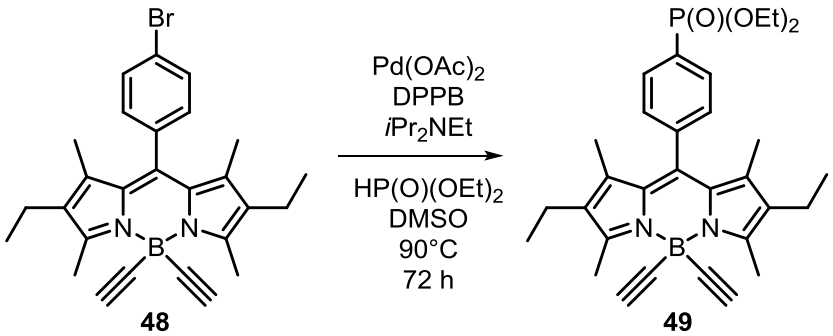

Scheme 2.4 Palladium-catalysed cross-coupling reaction to afford novel phosphonate 49.

A crystal of compound **49** suitable for X-ray diffraction was obtained by slow diffusion of pentane into a deuterated chloroform solution of **49**, and is shown in Figure 2.7. The reduction of phosphonate **49** to primary phosphine **50** was a quantitative reaction which was achieved using a dual reducing agent consisting of lithium aluminium hydride and chlorotrimethylsilane, as shown in Scheme 2.5.

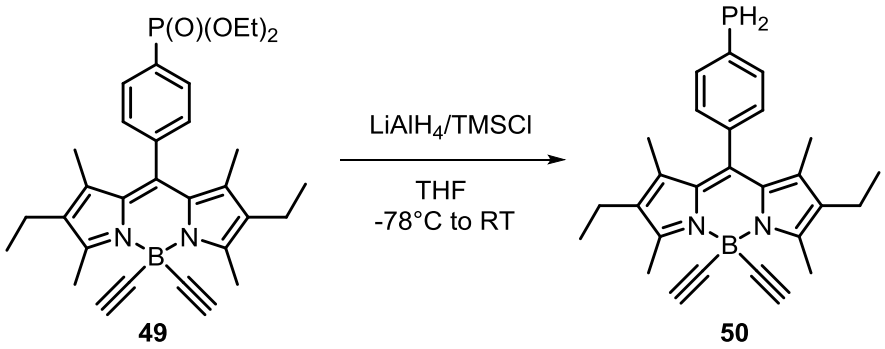

Scheme 2.5 Reduction of phosphonate 49 to novel primary phosphine 50.

The reaction was monitored by $^{31}P\{^{1}H\}$ NMR spectroscopy and showed a resonance at δ –121.6 ppm and no peak at δ 17.8, confirming that the phosphonate had been successfully reduced to the primary phosphine **50**. Analysis by $^{31}P–^{1}H$ NMR spectroscopy showed a triplet of triplets at δ –121.6 ppm, shown in Figure 2.6, due to the splitting of the signal by the two equivalent P–H protons and the two *ortho*-aryl protons on the phenyl ring attached to the Bodipy core. The coupling constants observed were typical for primary phosphines, ($^{1}J_{PH}$ = 203.1 Hz, $^{3}J_{PH}$ = 6.4 Hz).[8] Purification was performed using column chromatography on silica gel to afford primary phosphine **50** as a bright orange solid.

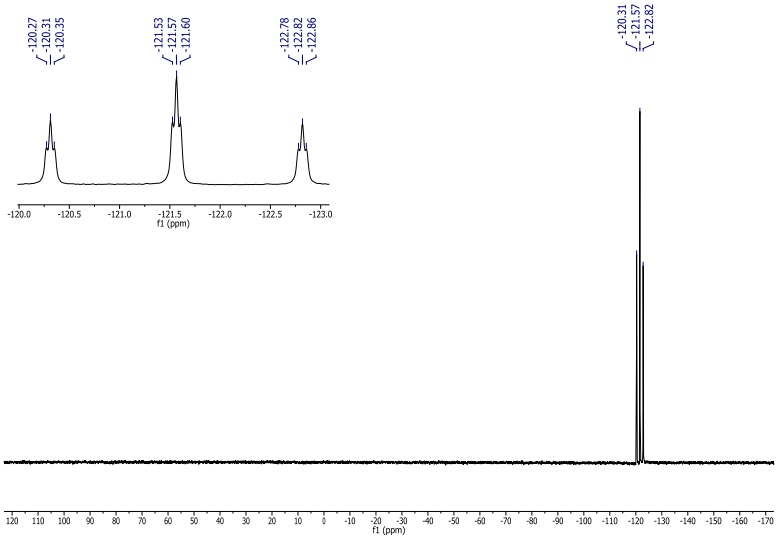

Figure 2.6 ^{31}P-^{1}H NMR spectrum of primary phosphine 50 showing a distinctive triplet of triplets.

After purification, a sample of primary phosphine **50** suitable for X-ray crystallographic analysis was obtained by slow diffusion of deuterated chloroform and pentane, as shown in Figure 2.7. The photophysical properties of all of these novel compounds will be discussed in Section 2.5.

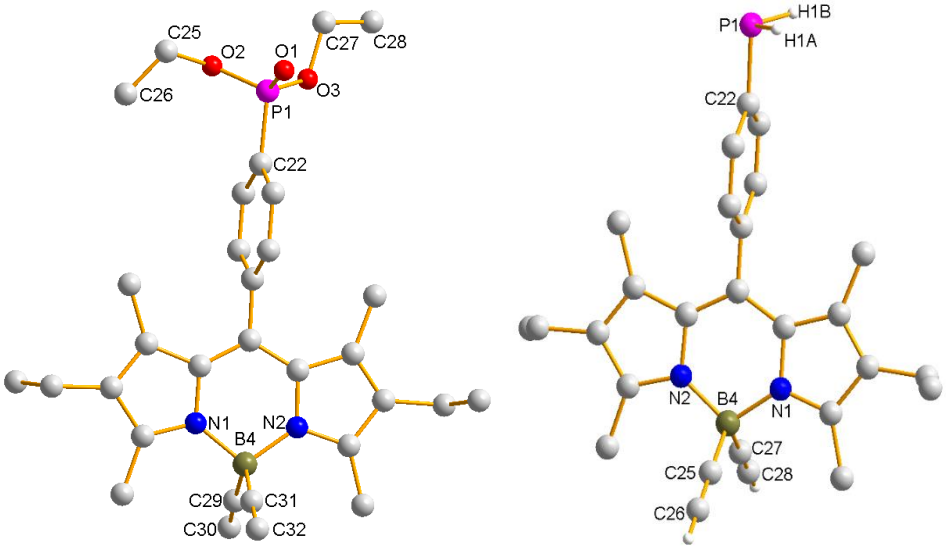

Figure 2.7: (Left) Molecular structure of novel phosphonate 49 obtained via slow diffusion of $CDCl_3$/pentane. Selected bond distances [Å] and angles [°]: P1-O1 1.4637(1), P1-O2 1.5732(1), P1-C22 1.7793(1), B4-C29 1.5729(1), C29-C30 1.1820(1); C22-P1-O1 111.745(3), P1-O3-C27 117.952(5), C32-C31-B4 179.357(5), C29-B4-C31 110.896(3). (Right) Molecular structure of novel primary phosphine 50. Selected bond distances [Å] and angles [°]: C25-B4 1.601(5), C27-B4 1.605(5), C22-P1 1.853(3); C25-B4-C27 111.7(3), N1-B4-N2 106.5(2), N1-B4-C27 109.7(3).

2.2.2 Extending the Ethynyl Chain

Within the literature there are examples of long-chained ethynyl groups bonded to the boron atom of a Bodipy core, rather than a simple alkyne group described above. This may be due to the accessibility of the required starting materials or may be due to the increased fluorescence quantum yields with longer chained substituents. Bard and co-workers synthesised **51** in 2011 and described the electrogenerated chemiluminescence (ECL) properties of three Bodipy derivatives, by varying the R groups on the 3 and 5 position of the Bodipy core.[91] Ziessel *et al*. synthesised compounds **52** and **53** between 2006 and 2008 (Figure 2.8), **52** exhibited a high quantum yield (0.89) and showed potential as a precursor for labelling biological materials. Whereas compound **53**, displayed a slight bathochromic shift with a quantum yield of 0.99 and is subsequently part of a library of novel compounds being used to investigate dendritic Bodipy scaffoldings for photon concentrators.[92, 93]

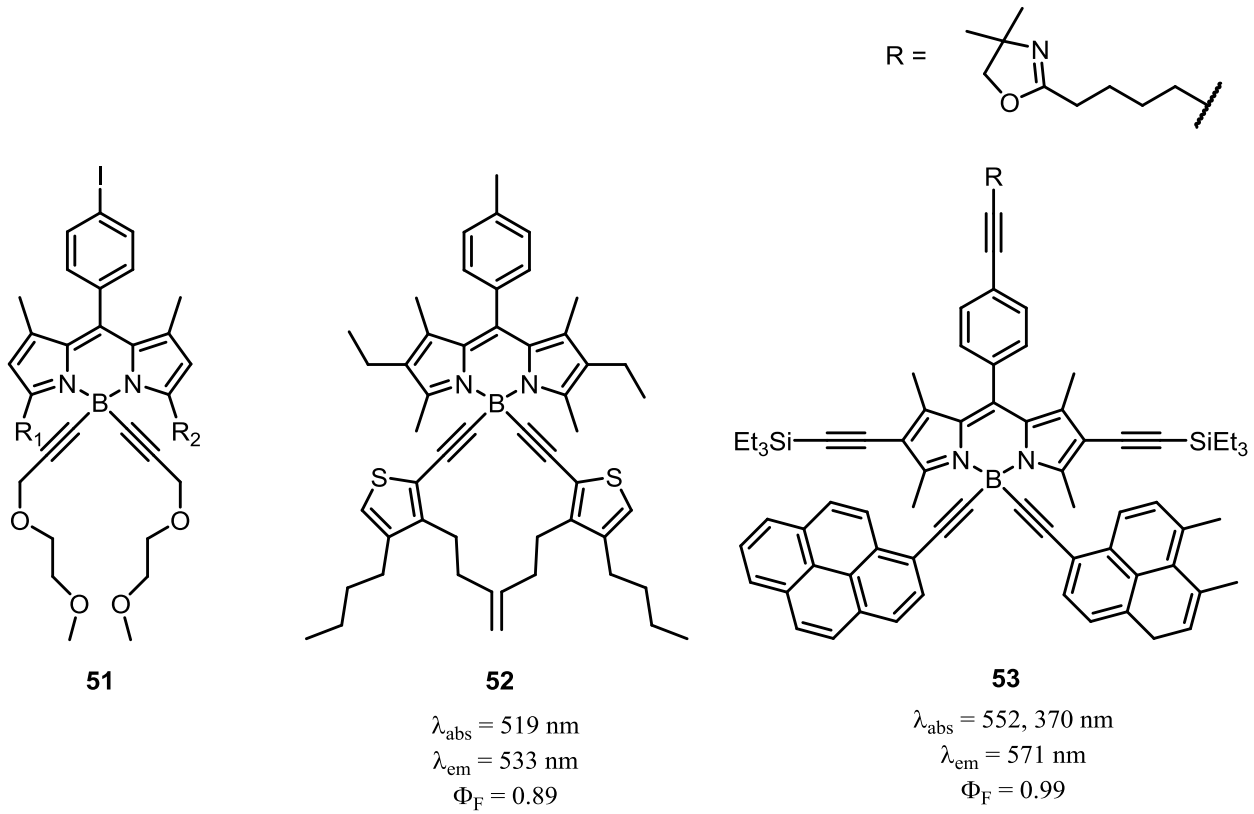

51

52

λ_{abs} = 519 nm
λ_{em} = 533 nm
Φ_F = 0.89

53

λ_{abs} = 552, 370 nm
λ_{em} = 571 nm
Φ_F = 0.99

Figure 2.8 Addition of alkyne-aryl groups on to the boron atom increase the fluorescence quantum yield.

2.2.3 Synthesis of Phenylethynyl Bodipy Derivatives

The next target was an extension of novel primary phosphine **50**. Compounds with extended ethynyl groups were attached to the boron atom and the photophysical properties were examined and compared to see if an increased fluorescence was observed.

Bodipy **54** can be synthesised via two routes, shown in Scheme 2.6. The first method involved the addition of two equivalents of phenylethynylmagnesium bromide to arylbromide **43**, stirred in THF at 75 °C for five days. The reaction was monitored by $^{11}B\{^1H\}$ NMR spectroscopy which showed the triplet, corresponding to the starting material, transform into a broad singlet at approximately δ −12.0 ppm. When all of the starting material had been converted to the desired product, the reaction was quenched with methanol and the solvent was removed *in vacuo*. The purple solid was purified using column chromatography on silica gel to give the desired product in 23% yield. The second route utilised the addition of *n*-butyllithium to phenylacetylene in THF at −78 °C, which gave the desired product overnight after the addition to compound **43**, and gave significantly higher yields (88%) after purification by column chromatography. Therefore, the second route is the more favourable method for synthesising compound **54**.

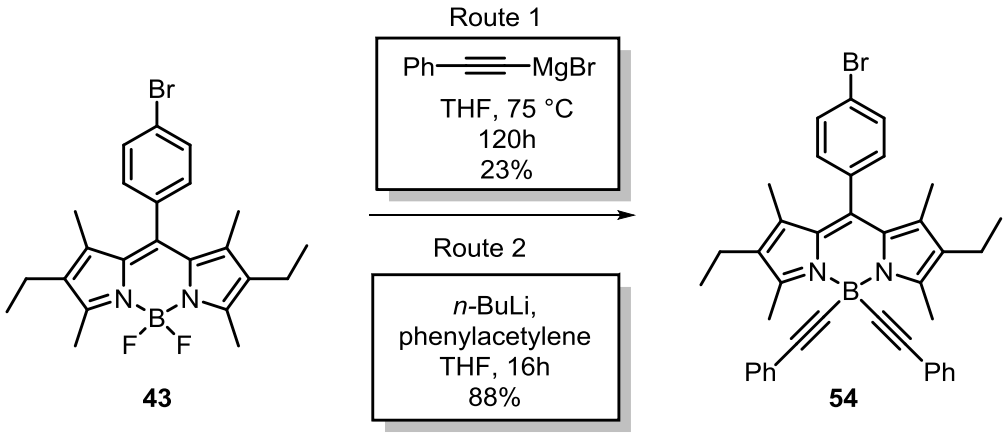

Scheme 2.6 Addition of phenylethynyl groups to the boron atom to yield compound 54.

The phosphonate group was added via a palladium-catalysed cross-coupling reaction using diethyl phosphite in anhydrous dimethyl sulfoxide at 90 °C for three days, illustrated in Scheme 2.7. The product was extracted with dichloromethane and washed with a large volume of water to remove the DMSO, and purified by column chromatography to give a red solid in a good yield of 73%. Analysis by $^{31}P\{^{1}H\}$ NMR spectroscopy showed a peak at δ 17.9 ppm which falls in the correct region for a phosphonate group.

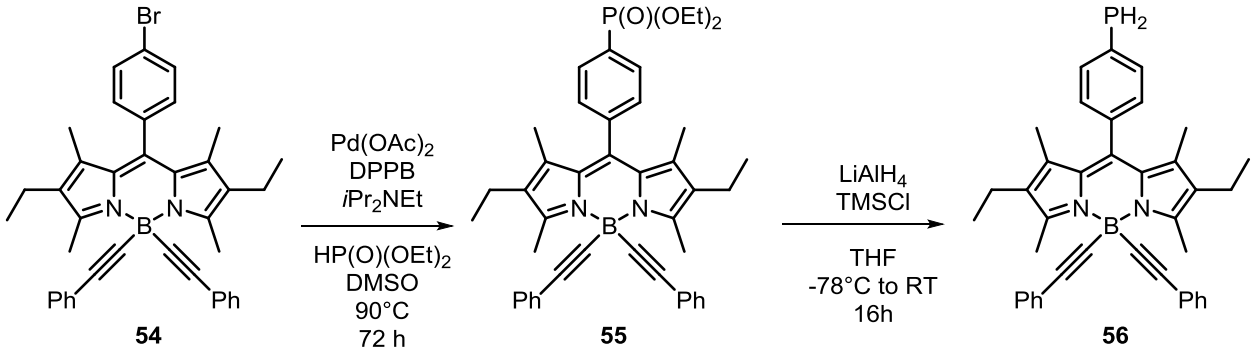

Scheme 2.7 A palladium-catalysed cross coupling reaction of 54 to the novel phosphonate 55, followed by a reduction to the novel primary phosphine 56.

Phosphonate **55** was reduced to novel primary phosphine **56** using the lithium aluminium hydride and chlorotrimethylsilane dual reducing agent (Scheme 2.7). The product was purified by column chromatography on silica gel to give the desired product as a red solid. Analysis by ^{31}P-^{1}H NMR spectroscopy showed a triplet of triplets at δ –122.3 ppm, with coupling constants of $^{1}J_{PH}$ = 202.9 Hz, $^{3}J_{PH}$ = 7.3 Hz, which again are typical values of a primary phosphine.[8]

2.3 Air Stability Studies of Primary Phosphines 50 and 56

The air-stability of the novel primary phosphines **50** and **56** has been examined both theoretically and experimentally. The synthesis of both compounds included purification by column

chromatography in air which is remarkable for this type of compound without the formation of a phosphine oxide. Air-stability studies that were performed on compounds **50** and **56** included $^{31}P\{^{1}H\}$ NMR spectroscopy studies and DFT calculations.

2.3.1 ^{31}P-^{1}H NMR Spectroscopy Studies

The air stability of novel primary phosphines **50** and **56** were measured using ^{31}P-^{1}H NMR spectroscopy. A neat sample of the phosphines and a sample dissolved in deuterated chloroform were exposed to the air, in a dark cupboard. Both samples showed no oxidation in neat form or in solution after three weeks, as shown in Figure 2.9.

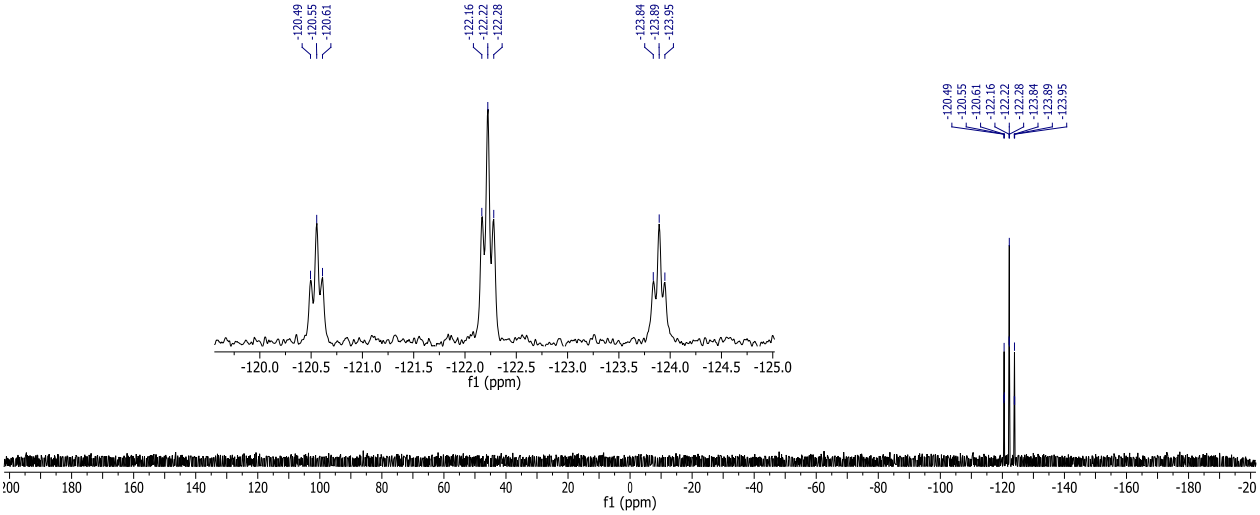

Figure 2.9 The $^{31}P\{^{1}H\}$ NMR spectrum of primary phosphine 50 after three weeks in air, in $CDCl_3$ showed no oxidation.

2.3.2 Spartan DFT Models

Identifying the reasons for the air-stability of primary phosphines was discussed previously in Section 1.2.2. One common contributor to air-stability is steric hindrance, however, in the cases of primary phosphines **20a**, **20b**, **50** and **56**, the PH_2 group is not subjected to this, and therefore, electronic factors must be considered as the controlling factor.

DFT calculations using a B3LYP functional with a 6-31G* basis set were employed to look at the electronic nature of the novel primary phosphines. The calculations identified where the HOMO was situated on the neutral compounds and it was determined that the localisation of the HOMO on the phosphorus atom resulted in air sensitivity. This theory is only applicable to primary phosphines, because tertiary arylphosphines, such as triphenylphosphine, which are well-known to be air-stable, exhibited a phosphorus-containing HOMO, implying incorrectly its instability in air.

The mechanism of phosphine oxidation has been postulated as being a radical reaction (Scheme 1.1, Section 1.2.8). Therefore, the radical cation SOMO energies of the primary phosphines were also calculated. The model suggested an air-stability threshold was observed at −10 eV, where air-stable phosphines had SOMO energies below this value. All four of the primary phosphines displayed SOMO energies of −8.94 eV, –8.82 eV, –8.96 eV and −8.17 eV, implying that they would be stable if they were synthesised experimentally. When all four of the primary phosphines are compared using the computational studies, it predicts that the phenylethynyl primary phosphine **56** will be most resistant to oxidation.

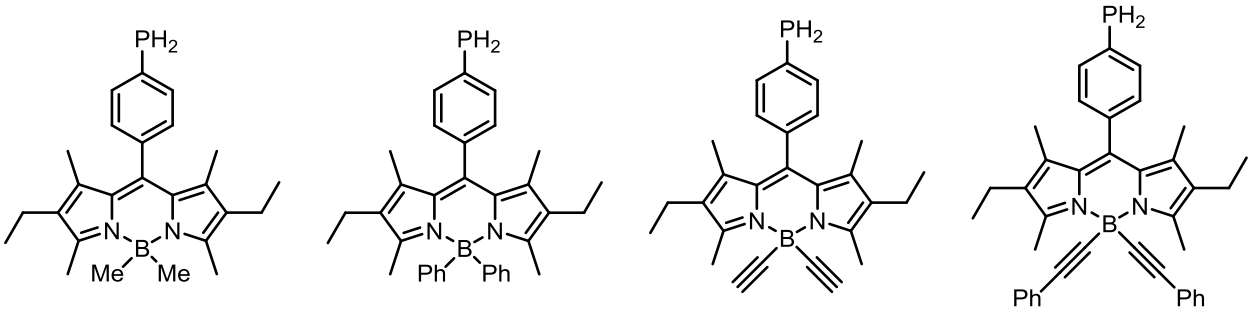

20a **20b** **50** **56**
–8.94 **–8.82** **–8.96** **–8.17**

Figure 2.10 Calculated SOMO energies in eV for radical cations of primary phosphines 20a, 20b, 50 and 56.

2.4 Photophysical Studies

Previous calculations were performed for first generation primary phosphines **20a**/**20b**, which both displayed no phosphorus-containing frontier orbitals for the neutral molecules until HOMO (-3) for **20a** and HOMO (-7) for **20b**. In both cases the energy difference between the HOMO and the orbital incorporating the phosphorus atom was 1.7 eV. This indicates that the reductive-PeT from the potential phosphorus donor may not be occurring, and the excited state is not quenched. This may be attributed to the phenyl spacer group between the Bodipy core and the phosphorus atom, which minimises the conjugation between the phosphorus lone pair and the Bodipy backbone.
It was important to understand the effects that the substituents had on the photophysical properties of the compounds described, and whether the addition of a phosphino group would quench the fluorescence of the Bodipy compounds via PeT.

The same calculations were conducted for novel primary phosphines **50** and **56**, which showed localisation of the HOMO on the Bodipy core until HOMO (-4) for **50**, illustrated in Figure 2.11 and HOMO (-8) for **56**, shown in Figure 2.12. The energy separation between the HOMO and these

orbitals were 1.4 and 1.6 eV respectively. As was the case for primary phosphines **20a** and **20b**, the model also predicts compounds **50** and **56** to be air-stable.

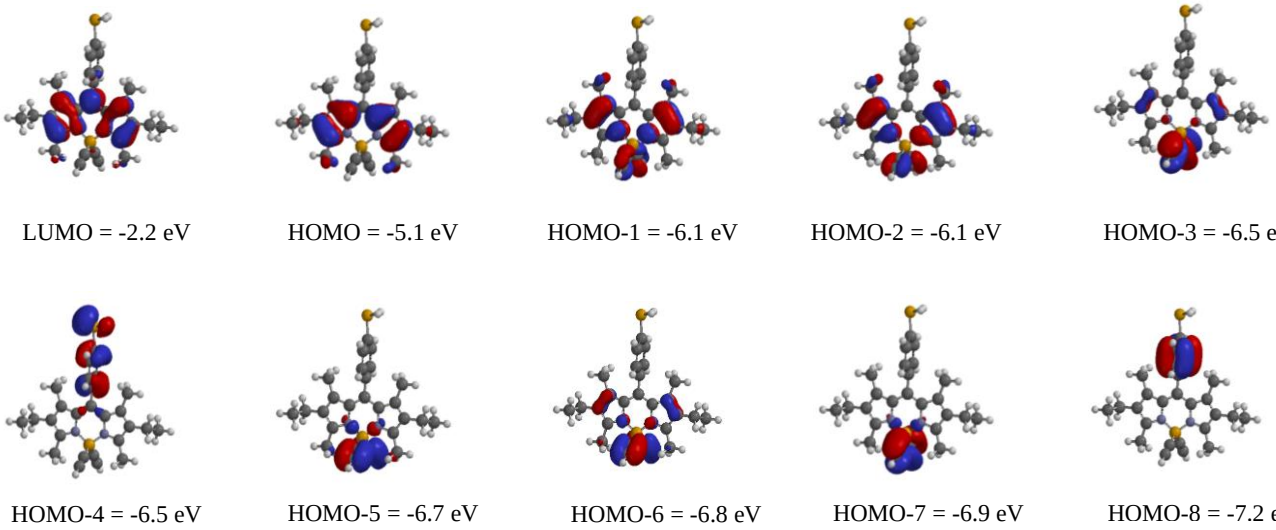

Figure 2.11 Calculated molecular orbital surfaces from LUMO to HOMO (-8) for primary phosphine 50.

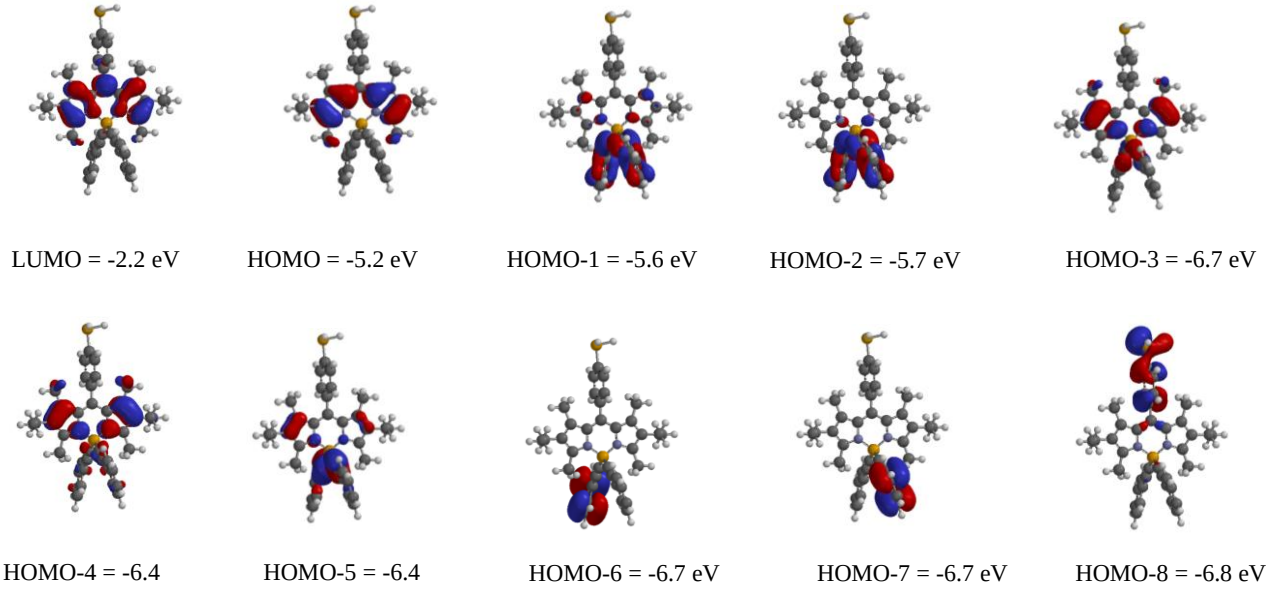

Figure 2.12 Calculated molecular orbital surfaces from LUMO to HOMO (-8) for primary phosphine 56.

Reference compounds **58-61** were synthesised in order to identify the effects that substituents, such as phosphorus, have on the photophysical effects when added to the 8-position. Photophysical data including absorption and emission maxima were collected for all of the compounds in anhydrous, degassed tetrahydrofuran and their quantum yields were measured with respect to compound **57**.

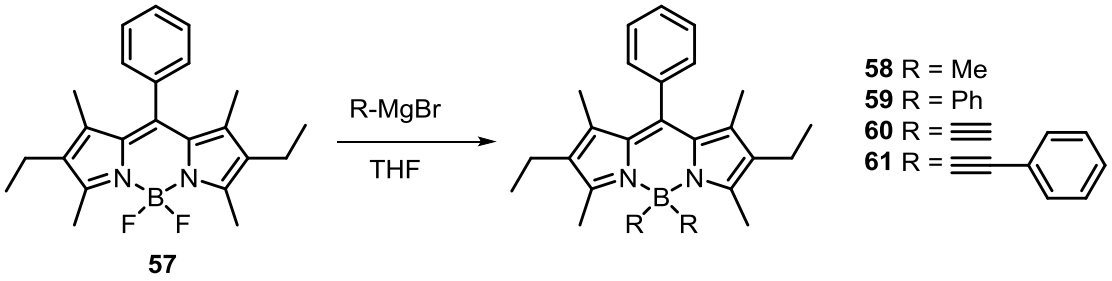

Figure 2.13 Reference compounds were synthesised with a proton where the bromo substituent would be.

Table 1.1 Photophysical data of first and second generation primary phosphines synthesised and described in this chapter.

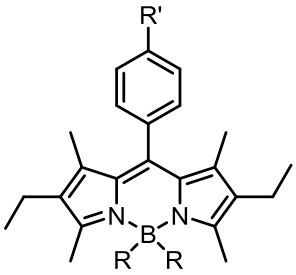

20a R = Me, R' = PH_2
20b R = Ph, R' = PH_2
43 R = F, R' = Br
44a R = Me, R' = Br
44b R = Ph, R' = Br
45 R = F, R' = $P(O)(OEt)_2$
46a R = Me, R' = $P(O)(OEt)_2$
46b R = Ph, R' = $P(O)(OEt)_2$
48 R = alkynyl, R' = Br
49 R = alkynyl, R' = $P(O)(OEt)_2$
50 R = alkynyl, R' = PH_2
54 R = phenylalkynyl, R' = Br
55 R = phenylalkynyl, R' = $P(O)(OEt)_2$
56 R = phenylalkynyl, R' = PH_2
57 R = F, R' = H
58 R = Me, R' = H
59 R = Ph, R' = H
60 R = alkynyl, R' = H
61 R = phenylalkynyl, R' = H

	λ_{abs} (nm)[a]	λ_{em} (nm)[a]	Φ[a,b]	ε ($M^{-1}cm^{-1}$)[a]
20a	512	526	0.33	79,000
20b	518	532	0.042	79,000
43	526	540	0.65	78,000
44a	514	524	0.36	87,000
44b	519	531	0.079	80,000
45	526	540	0.56	56,000
46a	513	527	0.29	91,000
46b	518	534	0.039	83,000
48	521	534	0.81	77,000
49	521	535	0.72	82,000
50	520	534	0.79	78,000
54	523	535	0.65	78,000
55	523	535	0.63	84,000
56	521	535	0.78	81,000
57	524	537	0.76	86,000
58	511	524	0.35	88,000
59	516	530	0.042	82,000
60	519	533	0.74	83,000
61	518	533	0.84	86,000

[a] Measured in dry, degassed tetrahydrofuran at room temperature, dyes were excited at 485 nm; [b] Fluorescence quantum yields were measured with respect to 4,4-difluoro-8-phenyl-1,3,5,7-tetramethyl-2,6-diethyl-4-bora-3a,4a-diaza-s-indacene 57. ε are quoted to 2 s.f.

2.4.1 Absorption and Emission Spectra

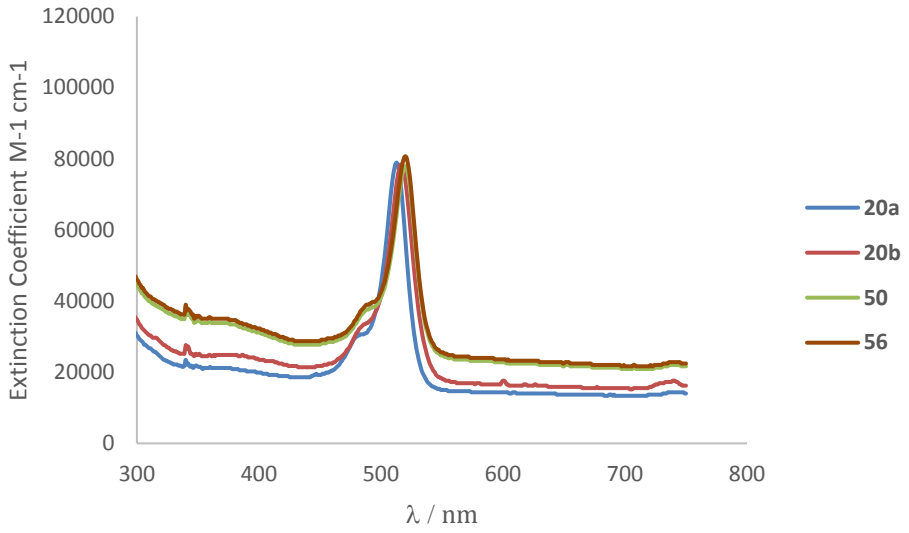

Figure 2.14 Absorption spectra for the primary phosphines 20a, 20b, 50 and 56, measured in dry, degassed tetrahydrofuran at room temperature.

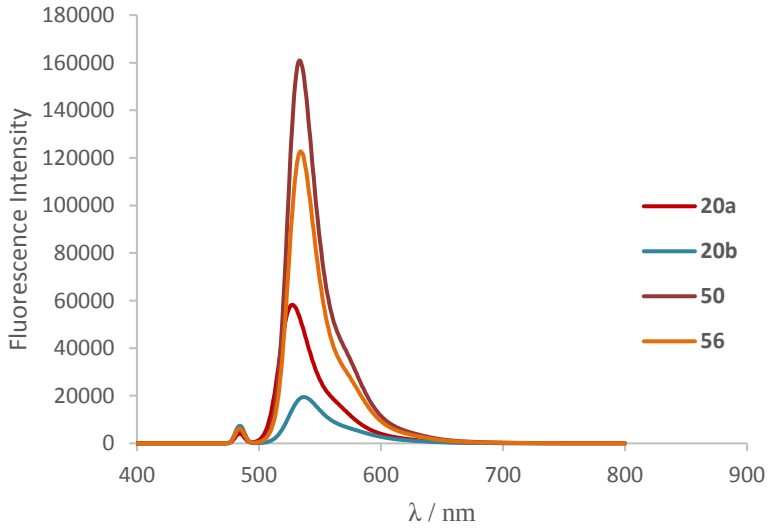

Figure 2.15 Emission spectra for the primary phosphines 20a, 20b, 50 and 56, measured in dry, degassed tetrahydrofuran at room temperature.

The absorption maxima for all of the Bodipy compounds described in this chapter are situated between 511 and 526 nm, corresponding to the S_0-S_1 (π-π^*) electronic transition associated with the Bodipy core. A broader less intense band seen at approximately 375 nm corresponds to the S_0-S_2 (π-π^*) transition of the boradiazaindacene unit. The emission maxima of the compounds are between 524 and 540 nm and the extinction coefficients range from 56,000 to 91,000 $M^{-1}cm^{-1}$, all of which are typical for Bodipy compounds published in the literature.[39]

As the four primary phosphines vary the substituent on the aryl group in the 8-position from a bromine atom to a phosphonate and finally a primary phosphine, the photophysical properties do not significantly change. The absorption and emission maxima are similar and the quantum yields are all comparable.

There is a slight hypsochromic shift in the absorption and emission spectra upon incorporation of the ethynyl substituents compared to the bromo difluoro precursor (3-5 nm), but the methyl and phenyl derivatives show a greater separation (7-16 nm). This may be observed due to the increased electron density around the boron atom – this is seen more for the methyl derivative due to the inductive effect being increased. When the substituents are varied on the boron atom, a change in the fluorescence quantum yield is observed; the addition of phenyl groups tends to produce low quantum yields, but as these groups are changed for methyl groups, the quantum yield is significantly increased. The new ethynyl derivatives have all shown to increase the quantum yield even further.

The incorporation of the $–PH_2$ moiety had little effect on the photophysical properties of novel primary phosphines **50** and **56** compared to their parent compounds **60** and **61** respectively, when a proton is in place of the phosphino group, indicating phosphorus groups can be added to these compounds without any significant change in their photophysical properties.

2.5 Summary

This chapter introduced the synthesis of the primary phosphines **20a** and **20b** and also describes an improved synthetic route. After this, the synthesis of the novel second generation primary phosphines **50** and **56** was described in a four-step synthetic procedure, which have shown remarkable air-stability – no oxidation of the primary phosphines was observed. This air-stability is in agreement with our DFT calculations, as both of the primary phosphines displayed SOMO values below the apparent threshold of –10 eV. The photophysical measurements concluded that the addition of the ethynyl groups to the boron atom significantly increased the fluorescence quantum yield compared to the alkyl and – especially – the aryl derivatives. The primary phosphines are an excellent starting point for synthesising a range of metal complexes which will be discussed in detail in Chapter 3.

2.6 Experimental

2.6.1 General Procedure

All air- and/or water-sensitive reactions were performed under a nitrogen atmosphere using standard Schlenk line techniques. Tetrahydrofuran was dried over sodium/benzophenone and deuterated chloroform was dried over phosphorus pentoxide; these solvents were distilled prior to use. Dimethyl sulfoxide was purchased from Fisher in an anhydrous state and was used as received. Most starting materials were purchased from Sigma Aldrich, Alfa Aesar or Fisher and were used as received. Column chromatography was performed on silica gel (40-63 μm, 60 Å) from Merck, thin-layer chromatography was carried out using Merck aluminium-based plates with silica gel and fluorescent indicator (254 nm). ^{1}H, $^{13}C\{^{1}H\}$, $^{19}F\{^{1}H\}$, $^{31}P\{^{1}H\}$ and $^{11}B\{^{1}H\}$ NMR spectra were recorded on a JEOL ECS-400 (^{1}H 399.78 MHz) or Bruker Avance III 300 (^{1}H 300.13 Hz) spectrometer at room temperature; ^{1}H and ^{13}C shifts are reported relative to tetramethylsilane, ^{31}P relative to 80% H_3PO_4, ^{11}B relative to $BF_3.Et_2O$ and ^{19}F relative to $CFCl_3$. Infrared spectra were recorded on a Varian 800 FT-IR spectrometer and mass spectrometry was carried out by the EPSRC NMSF, Swansea. DFT calculations were carried out on Spartan 14 using the B3LYP functional with a 6-31G* basis set, details of the xyz coordinates and SCF energies can be found in the appendix.

2.6.2 8-(4-Bromophenyl)-4,4-difluoro-1,3,5,7-tetramethyl-2,6-diethyl-4-bora-3a,4a-diaza-*s*-indacene (43)

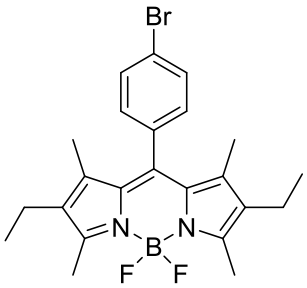

4-Bromobenzaldehyde (15.0 g, 81 mmol) was dissolved in anhydrous DCM (1500 mL) and 3-ethyl-2,4-dimethyl-1*H*-pyrrole (21.9 mL, 162 mmol) and TFA (0.025 mL) were added. The reaction mixture was stirred overnight under a nitrogen atmosphere at room temperature in a darkened flask. DDQ (20.2 g, 81 mmol) was added and the mixture was stirred for four hours. *i*-Pr_2NEt (84.7 mL, 486 mmol) and $BF_3.OEt_2$ (80.0 mL, 648 mmol) were added dropwise and the mixture was stirred at room temperature overnight. The volume was reduced by half and the mixture was washed with H_2O (3 x 150 mL) and brine (2 x 150 mL), then the organics were combined and dried with $MgSO_4$, filtered and the solvent removed *in vacuo* to yield a dark purple solid with a green tint. Purification using column chromatography on silica gel (toluene) afforded the dark purple product in a moderate yield (20.85 g, 56%).

^{1}H NMR (400 MHz, $CDCl_3$) δ 7.61 (d, $^3J_{HH}$ = 8.2 Hz, 2H), 7.16 (d, $^3J_{HH}$ = 8.2 Hz, 2H), 2.52 (s, 6H), 2.29 (q, $^3J_{HH}$ = 7.8 Hz, 4H), 1.30 (s, 6H), 0.96 (t, $^3J_{HH}$ = 7.8 Hz, 6H) ppm; **^{13}C{^{1}H} NMR** (100 MHz, $CDCl_3$) δ 154.2, 138.6, 138.2, 134.9, 133.1, 132.4, 130.6, 130.2, 123.1, 17.2, 14.7, 12.6, 12.0 ppm; **^{19}F{^{1}H} NMR** (376 MHz, $CDCl_3$) δ –145.6 [q (equal intensity),$^1J_{FB}$ = 31.8 Hz, 2F] ppm; **^{11}B{^{1}H} NMR** (128 MHz, $CDCl_3$) δ – 0.2 (t, $^1J_{FB}$ = 31.8 Hz, 1B) ppm; **IR** (neat) $\tilde{\nu}$: 2969, 2903 (C-H), 1532, 1475, 1403, 1318, 1255, 1185, 1066, 973, 754, 623 cm^{-1}; **HRMS** (ESI+) calcd. for $C_{26}H_{26}{}^{11}BBrF_2N_2$ [M]+ requires *m/z* 457.1368; found *m/z* 457.1368.

2.6.3 8-[(4-Diethylphosphonato)phenyl]-4,4-difluoro-1,3,5,7-tetramethyl-2,6-diethyl-4-bora-3a,4a-diaza-*s*-indacene (45)

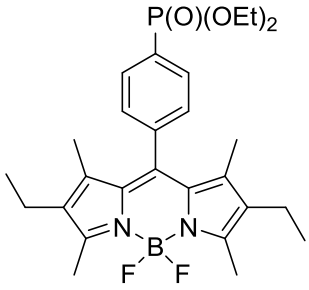

[Pd(OAc)$_2$] (1.02 g, 4.5 mmol), DPPB (1.94 g, 4.5 mmol) and arylbromide **43** (20.85 g, 45 mmol) were dissolved in anhydrous DMSO (800 mL) under a nitrogen atmosphere. *i*-Pr$_2$NEt (23.7 mL, 136.2 mmol) and diethyl phosphite (6.4 mL, 49.9 mmol) were added and the mixture was heated to 90 °C for 72 h. H_2O (500 mL) was added to the reaction mixture and the suspension was extracted with dichloromethane (600 mL). The organic layer was washed with H_2O (200 mL) and brine (200 mL), dried over $MgSO_4$, filtered and the solvent removed in vacuo to yield a dark pink / purple solid. Purification by column chromatography on silica gel (EtOAc:petrol, 3:2) gave the product in a moderate yield (15.0 g, 64%).

^{1}H NMR (400 MHz, $CDCl_3$) δ 7.91 (dd, $^3J_{HH}$ = 7.9 Hz, $^3J_{HP}$ = 12.9 Hz, 2H), 7.44 (dd, $^3J_{HH}$ = 8.0 Hz, $^4J_{HP}$ = 4.1 Hz, 2H), 4.28 (m, 4H), 2.44 (s, 6H), 2.28 (q, $^3J_{HH}$ = 8.3 Hz, 4H), 1.31 (t, $^3J_{HH}$ = 6.4 Hz, 6H), 1.21 (s, 6H), 0.97 (t, $^3J_{HH}$ = 7.6 Hz, 6H) ppm; **^{13}C{^{1}H} NMR** (100 MHz, $CDCl_3$) δ 154.3, 140.1, 138.4, 138.0, 133.1, 132.3 (d, J_{CP} = 10.5 Hz), 130.2, 129.7 (d, $^1J_{CP}$ = 121.7 Hz), 128.6 (d, J_{CP} = 15.3 Hz), 62.3 (d, $^2J_{CP}$ = 5.8 Hz), 17.0, 16.3 (d, $^3J_{CP}$ = 5.8 Hz), 14.6, 12.5, 11.7 ppm; **^{31}P{^{1}H} NMR** (162 MHz, $CDCl_3$) δ 18.3 ppm; **^{19}F{^{1}H} NMR** (376 MHz, $CDCl_3$) δ –145.6 (q (equal intensity), $^1J_{FB}$ = 32.0 Hz, 2F) ppm; **^{11}B{^{1}H} NMR** (128 MHz, $CDCl_3$) δ – 0.2 (t, $^1J_{FB}$ = 32.0 Hz, 1B) ppm; **IR** (neat) $\tilde{\nu}$: 2971, 2901, 1534, 1406, 1315, 1250, 1183, 1056, 975 cm^{-1}; **HRMS** (ESI$^+$) calcd. for $C_{27}H_{37}B_1F_2N_2P_1O_3$ $[M+H]^+$ requires *m/z* 516.2634; found *m/z* 516.2626.

2.6.4 8-(4-Diethylphosphonato)phenyl]-4,4-dimethyl-1,3,5,7-tetramethyl-2,6-diethyl-4-bora-3a,4a-diaza-s-indacene (46a)

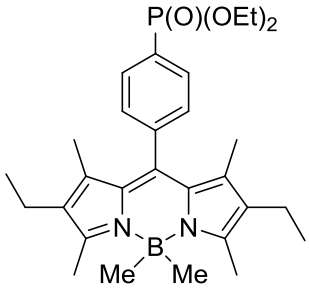

Phosphonate **45** (12.0 g, 23.2 mmol) was dissolved in anhydrous THF (300 mL). To this solution was added methylmagnesium bromide (15.5 mL, 46.5 mmol, 3.0 M solution in Et_2O) dropwise at room temperature. The mixture was left to stir until complete consumption of starting material was observed by TLC (~3 h). The reaction was quenched with MeOH (40 mL) and the solvent was evaporated to give a red solid, which was purified by column chromatography (EtOAc:petrol, 3:1) to give the product as a dark orange solid (9.81 g, 83%).

^{1}H NMR (400 MHz, $CDCl_3$) δ 7.89 (dd, $^3J_{HH}$ = 7.8 Hz, $^3J_{HP}$ = 13.1 Hz, 2H), 7.40 (dd, $^3J_{HH}$ = 7.8 Hz, $^4J_{HP}$ = 3.8 Hz, 2H), 4.09 (m, 4H), 2.44 (s, 6H), 2.27 (q, $^3J_{HH}$ = 7.3 Hz, 4H), 1.31 (t, $^3J_{HH}$ = 7.0 Hz, 6H), 1.19 (s, 6H), 0.93 (t, $^3J_{HH}$ = 7.4 Hz, 6H), 0.24 (s, 6H) ppm; **^{13}C{^{1}H} NMR** (100 MHz, $CDCl_3$) δ 150.8, 141.1(d, J_{CP} = 2.9 Hz), 138.5, 133.6, 132.4, 131.9 (d, J_{CP} = 10.5 Hz), 129.3 (d, J_{CP} = 10.5 Hz), 128.6 (d, $^1J_{CP}$ = 186.6 Hz), 128.4, 62.3 (d, $^2J_{CP}$ = 5.6 Hz), 17.5, 16.3 (d, $^3J_{CP}$ = 5.6 Hz), 14.4, 14.0, 11.7, 10.5 (br) ppm; **^{31}P{^{1}H} NMR** (162 MHz, $CDCl_3$) δ 18.7 ppm; **^{11}B{^{1}H} NMR** (128 MHz, $CDCl_3$) δ –1.9 (s, 1B) ppm; **IR** (neat) $\tilde{\nu}$: 2960, 2931, 1556, 1453, 1360, 1322, 1244, 1172, 1047, 1014, 945 cm^{-1}; **HRMS** (NSI^+) calcd. for $C_{29}H_{43}BN_2O_3P$ $[M+H]^+$ requires *m/z* 508.3135, found *m/z* 508.3129.

2.6.5 8-[(4-Diethylphosphonato)phenyl]-4,4-diphenyl-1,3,5,7-tetramethyl-2,6-diethyl-4-bora-3a,4a-diaza-s-indacene (46b)

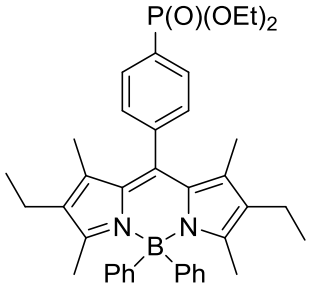

Phosphonate **45** (1.5 g, 2.9 mmol) was dissolved in anhydrous THF (50 mL). To this solution was added phenylmagnesium bromide (2.0 mL, 6.0 mmol, 3.0 M solution in Et_2O) dropwise at room

temperature. The mixture was left to stir until complete consumption of starting material was observed by TLC (1.5 h). The reaction was quenched with MeOH (40 mL) and the solvent was evaporated to give a dark red solid, which was purified by column chromatography (EtOAc : petrol, 2:1) to give the product as a dark red solid. (1.42 g, 87%).

^{1}H NMR (400 MHz, $CDCl_3$) δ 7.98 (dd, $^{3}J_{HH}$ = 7.8 Hz, $^{3}J_{HP}$ = 13.2 Hz, 2H), 7.53 (dd, $^{3}J_{HH}$ = 7.8 Hz, $^{4}J_{HP}$ = 4.0 Hz, 2H), 7.41 (m, 4H), 7.26-7.15 (m, 6H), 4.18 (m, 4H), 2.21 (q, $^{3}J_{HH}$ = 7.4 Hz, 4H), 1.79 (s, 6H), 1.35 (t, $^{3}J_{HH}$ = 7.2 Hz, 6H), 1.30 (s, 6H), 0.86 (t, $^{3}J_{HH}$ = 7.4 Hz, 6H) ppm; **^{13}C{^{1}H} NMR** (100 MHz, $CDCl_3$) δ 153.4, 150.1 (br), 141.3, 139.0, 134.8, 133.8, 133.1, 132.1 (d, J_{CP} = 10.4 Hz), 130.2, 129.1 (d, J_{CP} = 15.2 Hz), 128.8 (d, $^{1}J_{CP}$ = 187.9 Hz), 127.2, 125.5, 62.2 (d, $^{2}J_{CP}$ = 5.7 Hz), 17.3, 16.3 (d, $^{3}J_{CP}$ = 5.8 Hz), 14.7, 14.6, 12.1 ppm; **^{31}P{^{1}H} NMR** (162 MHz, $CDCl_3$) δ 18.7 ppm; **^{11}B{^{1}H} NMR** (128 MHz, $CDCl_3$) δ –1.1 (s, 1B) ppm; **IR** (neat) $\tilde{\nu}$: 2960, 1547, 1474, 1386, 1254, 1168, 1141, 1032, 970, 773 cm^{-1}; **HRMS** (NSI^{+}) calcd. for $C_{39}H_{47}BN_2O_3P$ $[M+H]^{+}$ requires *m/z* 632.3448, found *m/z* 632.3447.

2.6.6 8-[(4-Phosphino)phenyl]-4,4-dimethyl-1,3,5,7-tetramethyl-2,6-diethyl-4-bora-3a,4a-diaza-s-indacene (20a)

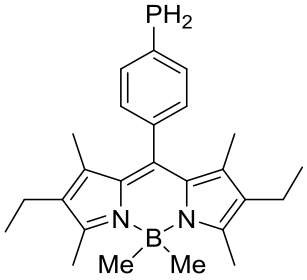

$LiAlH_4$ (57.8 mL, 57.8 mmol, 1.0 M solution in THF) was cooled to – 78 °C. TMSCl (7.35 mL, 57.8 mmol) was added and the mixture was warmed to room temperature over 45 minutes. The solution was cooled to –78 °C and phosphonate **46a** (9.81 g, 19.3 mmol) dissolved in anhydrous THF (900 mL) was added slowly. The solution was allowed to warm up to room temperature and stirred overnight. The mixture was concentrated *in vacuo* and slowly quenched with degassed H_2O (50 mL). The product was extracted with Et_2O (3 x 150 mL), dried over $MgSO_4$, filtered and the solvent was evaporated. The orange solid was purified by column chromatography on silica gel (chloroform:petrol, 1:4) to give the intended product (6.1 g, 79%).

^{1}H NMR (400 MHz, $CDCl_3$) δ 7.58 (m, 2H), 7.25 (m, 2H), 4.08 (d, $^{1}J_{HP}$ = 202.5 Hz, 2H), 2.43 (s, 6H), 2.33 (q, $^{3}J_{HH}$ = 7.6 Hz, 4H), 1.25 (s, 6H), 0.97 (t, $^{3}J_{HH}$ = 7.6 Hz, 6H), 0.26 (s, 6H) ppm; **^{13}C{^{1}H} NMR** ($CDCl_3$, 100 MHz) δ 150.7, 139.7, 137.2 134.9 (d, J_{CP} = 15.3 Hz), 133.7, 132.4,

128.9, 128.8 (d, J_{CP} = 5.7 Hz), 128.7, 17.4, 14.7, 14.3, 11.9, 10.4 (br) ppm; **^{31}P-^{1}H NMR** (400 MHz, $CDCl_3$) δ –121.6 (tt, $^{1}J_{PH}$ = 202.5 Hz, $^{3}J_{PH}$ = 7.4 Hz) ppm; **^{11}B{^{1}H} NMR** ($CDCl_3$, 128 MHz) δ –2.1 (s, 1B) ppm; **IR** (neat) $\tilde{\nu}$: 2958, 2925, 2361, 2341, 1551, 1470, 1531, 1167, 1143, 1110, 1060, 942 cm^{-1}; **HRMS** (NSI$^+$) calcd. for $C_{25}H_{35}BN_2P$ $[M+H]^+$ requires *m/z* 404.2662, found *m/z* 404.2665.

2.6.7 8-[(4-Phosphino)phenyl]-4,4-diphenyl-1,3,5,7-tetramethyl-2,6-diethyl-4-bora-3a,4a-diaza-s-indacene (20b)

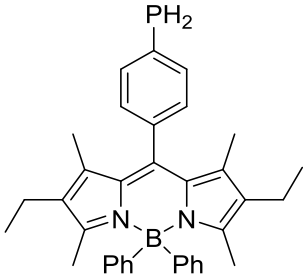

$LiAlH_4$ (6.73 mL, 6.73 mmol, 1.0 M solution in THF) was cooled to – 78 °C. TMSCl (0.85 mL, 6.73 mmol) was added and the mixture was warmed to room temperature over 45 minutes. The solution was cooled to –78 °C and phosphonate **46b** (1.42 g, 2.24 mmol) dissolved in anhydrous THF (150 mL) was added slowly. The solution was allowed to warm up to room temperature and stirred for 4 hours. The mixture was concentrated *in vacuo* and slowly quenched with degassed H_2O (20 mL). The product was extracted with Et_2O (3 x 50 mL), dried over $MgSO_4$, filtered and the solvent was evaporated. The orange solid was purified by column chromatography on silica gel, (dichloromethane:petrol, 1:2) to give the intended product. (0.90 g, 76%).

^{1}H NMR (400 MHz, $CDCl_3$) δ 7.63-7.58 (m, 2H), 7.40-7.37 (m, 4H), 7.28-7.16 (m, 8H), 4.11 (d, $^{1}J_{HP}$ = 202.5 Hz, 2H), 2.21 (q, $^{3}J_{HH}$ = 7.3 Hz, 4H), 1.76 (s, 6H), 1.31 (s, 6H), 0.90 (t, $^{3}J_{HH}$ = 7.3 Hz, 6H) ppm; **^{13}C{^{1}H} NMR** ($CDCl_3$, 100 MHz) δ 153.0, 150.3 (br), 139.9, 136.8, 135.1, 134.9 (d, J_{CP} = 15.3 Hz), 133.8, 132.8, 130.6, 129.0, 128.8 (d, J_{CP} = 5.6 Hz), 127.1, 125.4, 17.3, 14.7, 14.5, 12.1 ppm; **^{31}P-^{1}H NMR** (400 MHz, $CDCl_3$) δ –121.5 (tt, $^{1}J_{PH}$ = 202.5 Hz, $^{3}J_{PH}$ = 7.6 Hz) ppm; **^{11}B{^{1}H} NMR** ($CDCl_3$, 128 MHz) δ –1.1 (s, 1B) ppm; **IR** (neat) $\tilde{\nu}$: 2963, 2928, 2869, 2285, 1545, 1469, 1393, 1303, 1169, 1143, 962, 774 cm^{-1}; **HRMS** (APCI$^+$) calcd. for $C_{35}H_{39}BN_2P$ $[M+H]^+$ requires *m/z* 528.2975, found *m/z* 528.2970.

2.6.8 8-(4-Bromophenyl)-4,4-diethynyl-1,3,5,7-tetramethyl-2,6-diethyl-4-bora-3a,4a-diaza-s-indacene (48)

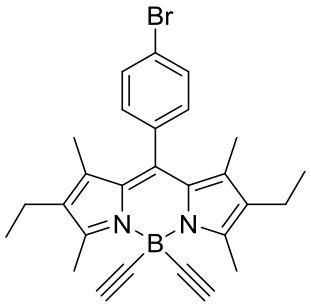

Arylbromide **43** (2.93 g, 6.38 mmol) was dissolved in anhydrous THF (60 mL) and ethynylmagnesium bromide (26.78 mL, 0.5M in THF, 13.89 mmol) was added dropwise. The reaction was heated to 76 °C overnight. The reaction was quenched with MeOH (10 mL) and the solvent was removed. The product was purified by column chromatography (toluene) to afford the desired product as a purple solid. (2.53 g, 84%).

^{1}H NMR (400 MHz, $CDCl_3$) δ 7.54 (d, $^{3}J_{HH}$ = 8.3 Hz, 2H), 7.12 (d, $^{3}J_{HH}$ = 8.3 Hz, 2H), 2.68 (s, 6H), 2.25 (q, $^{3}J_{HH}$ = 7.5 Hz, 4H), 2.15 (s, 2H), 1.23, (s, 6H), 0.92 (t, $^{3}J_{HH}$ = 7.5 Hz, 6H) ppm; **^{13}C{^{1}H} NMR** (100 MHz, $CDCl_3$) δ 153.6, 140.2, 136.6, 136.3, 132.9, 129.0, 128.9, 128.6, 128.5, 128.3, 82.9 (br), 17.4, 14.8, 14.0, 11.8 ppm; **^{11}B{^{1}H} NMR** (128 MHz, $CDCl_3$) δ –13.9 ppm; **IR** (neat) $\tilde{\nu}$: 3281, 2963, 2927, 2869, 2361, 2337, 2065, 1609, 1538, 1473, 1401, 1369, 1318, 1068, 977, 750 cm^{-1}; **HRMS** ($APCI^+$ SOLID) calcd. for $C_{27}H_{28}BBrN_2H$ $[M+H]^+$ requires *m/z* 470.1638, found *m/z* 470.1634.

2.6.9 8-[(4-Diethylphosphonate)phenyl]-4,4-diethynyl-1,3,5,7-tetramethyl-2,6-diethyl-4-bora-3a,4a-diaza-s-indacene (49)

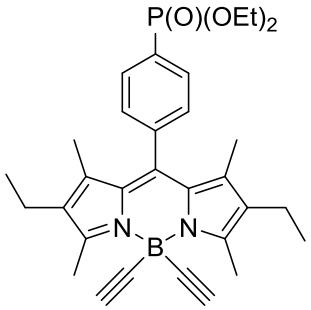

Arylbromide **48** (1.02 g, 2.16 mmol), $[Pd(OAc)_2]$ (0.048 g, 0.216 mmol) and DPPB (0.092 g, 0.216 mmol) were combined and dissolved in anhydrous DMSO (50 mL). *i*-Pr_2NEt (1.13 mL, 6.49 mmol)

and diethyl phosphite (0.31 mL, 2.38 mmol) were added and the reaction was heated to 90 °C for 72 h. The reaction mixture was cooled to room temperature and H_2O (40 mL) was added and the mixture was extracted with DCM (50 mL). The organics were washed with H_2O (30 mL), dried over $MgSO_4$, filtered and the solvent was removed. The dark red solid was purified by column chromatography on silica gel (ethyl acetate:petrol 3:1) to yield the desired product as a red solid (0.62 g, 55%).

^{1}H NMR (400 MHz, $CDCl_3$) δ 7.86 (dd, $^3J_{HH}$ = 8.1 Hz, $^3J_{HP}$ = 13.1 Hz, 2H), 7.38 (dd, $^3J_{HH}$ = 8.1 Hz, $^4J_{HP}$ = 3.9 Hz, 2H), 4.07 (m, 4H), 2.67 (s, 6H), 2.25 (q, $^3J_{HH}$ = 7.8 Hz, 4H), 2.15 (s, 2H), 1.26 (t, J_{HH} = 7.0 Hz, 6H), 1.17 (s, 6H), 0.91 (t, J = 7.5 Hz, 6H) ppm; **^{13}C{^{1}H} NMR**: δ 154.2, 140.6 (d, J = 3.3 Hz), 138.4, 136.2, 133.3, 132.2 (d, J = 10.0 Hz), 129.1, (d, J = 188.7 Hz), 128.8 (d, J = 15.0 Hz), 128.5, 83.0, 68.0, 62.4 (d, J = 5.6 Hz), 17.4, 16.4 (d, J = 6.1 Hz), 14.7, 14.0, 11.9 ppm; **^{31}P{^{1}H} NMR** (162 MHz, $CDCl_3$) δ 17.8 ppm; **^{11}B{^{1}H} NMR** (128 MHz, $CDCl_3$) δ –14.9 ppm; **HRMS** ($APCI^+$ SOLID) calcd. for $C_{31}H_{38}B_1N_2O_3P_1H$ $[M+H]^+$ requires *m/z* 528.2822, found *m/z* 528.2821.

2.6.10 8-[(4-Phosphino)phenyl]-4,4-diethynyl-1,3,5,7-tetramethyl-2,6-diethyl-4-bora-3a,4a-diaza-s-indacene (50)

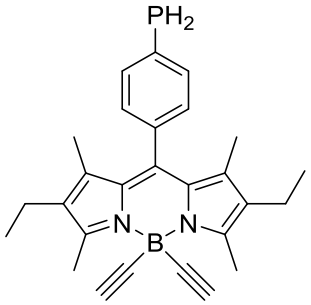

$LiAlH_4$ (2.55 mL, 1.0 M in THF, 2.55 mmol) was cooled to –78 °C. TMSCl (0.32 mL, 2.55 mmol) was added and the mixture was warmed to room temperature over 45 minutes. The solution was cooled to – 78 °C and phosphonate **49** (0.45 g, 0.88 mmol) in anhydrous THF (50 mL) was added slowly. The solution was allowed to warm to room temperature and stirred for four hours. The mixture was concentrated *in vacuo* and was slowly quenched with degassed water. The product was extracted with DCM (3 x 15 mL), dried over $MgSO_4$, filtered and the solvent was removed, producing an orange solid which was purified by column chromatography (chloroform:hexane 1:4) to yield an orange solid (0.280 g, 78%).

^{1}H NMR (400 MHz, $CDCl_3$) δ 7.59 (m, 2H), 7.23 (m, 2H), 4.08 (d, $^1J_{HP}$ = 202.9 Hz, 2H), 2.74 (s, 6H), 2.33 (q, $^3J_{HH}$ = 7.6 Hz, 4H), 2.23 (s, 2H), 1.27 (s, 6H), 0.98 (t, $^3J_{HH}$ = 7.6 Hz, 6H) ppm; **^{13}C NMR** (100 MHz, $CDCl_3$) δ 153.9, 139.5, 136.6, 136.2, 135.2 (d, J_{CP} = 9.1 Hz), 133.1, 129.4,

129.2, 128.9, 128.6 (d, J_{CP} = 5.8 Hz), 82.9, 17.4, 14.8, 14.1, 12.1 ppm; **^{31}P NMR** (162 MHz, $CDCl_3$) δ –121.6 (tt, $^{1}J_{PH}$ = 202.9 Hz, $^{3}J_{PH}$ = 6.7 Hz) ppm; **^{11}B NMR** (128 MHz, $CDCl_3$) δ –14.9 ppm; **IR** (neat) $\tilde{\nu}$: 3292, 2960, 2926, 2870, 2360, 2341, 2301, 2060, 1540, 1473, 1261, 1172, 1109, 1067, 964 cm^{-1}; **HRMS** ($APCI^+$ SOLID) calcd. for $C_{27}H_{31}B_1N_2P_1$ $[M+H]^+$ requires *m/z* 424.2349, found *m/z* 424.2345.

2.6.11 Preparation of 8-(4-Bromophenyl)-4,4-diethynylphenyl-1,3,5,7-tetramethyl-2,6-diethyl-4-bora-3a,4a-diaza-*s*-indacene (54)

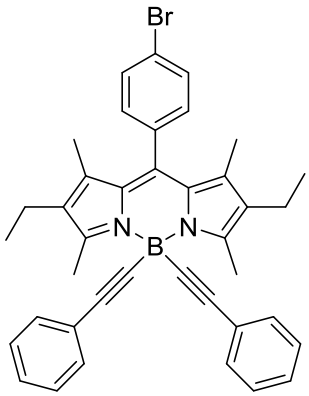

Phenylacetylene (0.24 mL, 2.18 mmol) was dissolved in anhydrous THF (6 mL) and cooled to –78°C, to this flask was added *n*-Butyllithium (1.5 mL, 2.4 mmol, 1.6M in hexane) and the solution was stirred for 15 minutes. In a separate flask arylbromide **43** (0.50 g, 1.09 mmol) was dissolved in anhydrous THF (15 mL), the phenylacetylene mixture was added dropwise to the Bodipy solution at – 78°C and the reaction mixture was stirred overnight at room temperature. The compound was purified by column chromatography on silica gel (dichloromethane:petrol, 2:1) to yield the desired product as an orange solid (0.60, 88%).

^{1}H NMR (700 MHz, $CDCl_3$) δ 7.53-7.04 (m, 14H), 2.78 (s, 6H), 2.26 (q, $^{3}J_{HH}$ = 7.6 Hz, 4H), 1.23 (s, 6H), 0.92 (t, $^{3}J_{HH}$ = 7.6 Hz, 6H) ppm; **^{13}C{^{1}H} NMR** (176 MHz, $CDCl_3$) δ 154.2, 136.1, 135.5, 133.1, 132.5, 132.3, 131.6, 130.5, 129.0, 128.5, 128.0, 127.1, 125.5, 95.3, 81.7, 17.5, 14.9, 14.1, 12.1 ppm; **^{11}B{^{1}H} NMR** (96 MHz, $CDCl_3$) δ –12.6 ppm; **HRMS** ($ASAP^+$ SOLID) calcd. for $C_{39}H_{37}BBrN_2$ $[M+H]^+$ requires m/z 622.2269, found m/z 622.2233.

2.6.12 Preparation of 8-[(4-Diethylphosphonate)phenyl]-4,4-diethynylphenyl-1,3,5,7-tetramethyl-2,6-diethyl-4-bora-3a,4a-diaza-*s*-indacene (55)

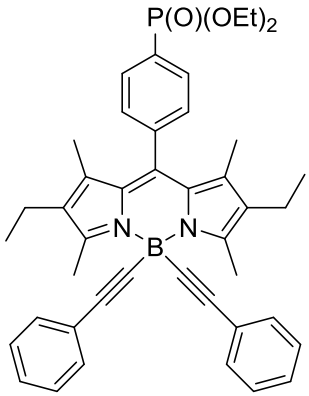

Arylbromide **54** (0.29 g, 0.47 mmol), $[Pd(OAc)_2]$ (0.011 g, 0.047 mmol) and DPPB (0.020 g, 0.047 mmol) were combined and dissolved in anhydrous DMSO (12 mL). After five minutes of stirring, *i*-Pr_2NEt (0.07 mL, 0.52 mmol) was added, followed by diethyl phosphite (0.25 mL, 1.41 mmol). The reaction mixture was heated to 90 °C for 48 hours under nitrogen. The mixture was extracted with DCM (3 x 25 mL) and washed with water (3 x 25 mL), dried over $MgSO_4$, filtered and the solvent was removed *in vacuo*. The resultant purple solid was purified by column chromatography on silica gel (ethyl acetate:petrol, 3:1) to give the product as a purple solid (0.235 g, 73%).

^{1}H NMR (300 MHz, $CDCl_3$) δ 7.85 (dd, $^3J_{HH}$ = 8.3 Hz, $^3J_{HP}$ = 13.1 Hz, 2H), 7.39 (dd, $^3J_{HH}$ = 8.3 Hz, $^4J_{HP}$ = 3.9 Hz, 2H), 7.33-7.30 (m, 4H), 7.16-7.08 (m, 6H), 4.07 (m, 4H), 2.78 (s, 6H), 2.26 (q, $^3J_{HH}$ = 7.5 Hz, 4H), 1.24 (t, J_{HH} = 7.1 Hz, 6H), 1.18 (s, 6H), 0.93 (t, *J* = 7.5 Hz, 6H) ppm; **^{13}C{^{1}H} NMR** (75 MHz, $CDCl_3$) δ 154.3, 140.8 (d, *J* = 3.3 Hz), 138.4, 135.9, 133.2, 132.2 (d, *J* = 10.2 Hz), 131.5, 129.0 (d, *J* = 188.8 Hz), 128.9 (d, *J* = 15.0 Hz), 128.6, 128.0, 127.0, 125.4, 119.4, 95.3, 62.3 (d, *J* = 5.5 Hz), 17.4, 16.3 (d, *J* = 6.0 Hz), 14.7, 14.0, 11.9 ppm; **^{31}P{^{1}H} NMR** (121 MHz, $CDCl_3$) δ 17.9 ppm; **^{11}B{^{1}H} NMR** (96 MHz, $CDCl_3$) δ –12.7 ppm.

2.6.13 Preparation of 8-[(4-Phosphino)phenyl]-4,4-diethynylphenyl-1,3,5,7-tetramethyl-2,6-diethyl-4-bora-3a,4a-diaza-*s*-indacene (56)

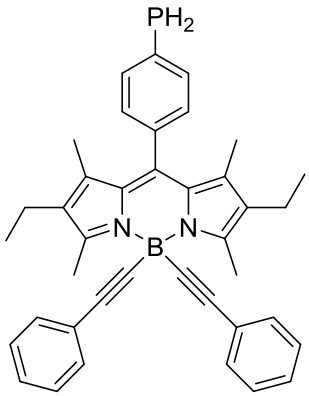

$LiAlH_4$ (1.01 mL, 1.0 M in THF, 1.01 mmol) was cooled to –78 °C, and TMSCl (0.13 mL, 2.55 mmol) was added; the mixture was warmed to room temperature over 45 minutes. The solution was cooled to –78 °C and phosphonate **55** (0.23 g, 0.34 mmol) in anhydrous THF (30 mL) was added dropwise. The solution was warmed to room temperature and stirred for four hours. The mixture was concentrated *in vacuo* and slowly quenched with degassed H_2O (10 mL). The product was extracted with DCM (3 x 15 mL), dried over $MgSO_4$, filtered and the solvent was removed, producing an orange solid which was purified by column chromatography on silica gel (chloroform:hexane 1:2) to yield a red solid (0.05 g, 78%).

^{1}H NMR (300 MHz, $CDCl_3$) δ 7.53 (m, 2H), 7.35-7.32 (m, 2H), 7.21-7.12 (m, 10H), 4.02 (d, $^1J_{HP}$ = 202.8 Hz, 2H), 2.79 (s, 6H), 2.30 (q, $^3J_{HH}$ = 7.6 Hz, 4H), 1.24 (s, 6H), 0.95 (t, $^3J_{HH}$ = 7.5 Hz, 6H) ppm; **^{13}C{^{1}H} NMR** (75 MHz, $CDCl_3$) δ 154.0, 139.5, 136.5, 136.3, 135.2, (d, J_{CP} = 16.3 Hz), 133.0, 131.7, 129.1, 128.8 (d, J_{CP} = 5.7 Hz), 128.1, 127.1, 125.7, 60.5, 41.5, 22.8, 17.6, 14.9, 14.1, 12.2 ppm; **^{31}P NMR** (121 MHz, $CDCl_3$) δ –122.3 (tt, $^1J_{PH}$ = 202.9 Hz, $^3J_{PH}$ = 7.0 Hz) ppm; **^{11}B{^{1}H} NMR** (96 MHz, $CDCl_3$) δ –12.5 ppm; **IR** (neat) $\tilde{\nu}$: 3292, 2960, 2925, 2360, 1541, 1473, 1314, 1171, 963, 691 cm^{-1}; **HRMS** (ASAP$^+$ SOLID) calcd. for $C_{39}H_{39}B_1N_2P_1$ $[M+H]^+$ requires m/z 576.2980, found m/z 576.2919.

2.6.14 Preparation of 8-Phenyl-4,4-diethynyl-1,3,5,7-tetramethyl-2,6-diethyl-4-bora-3a,4a-diaza-s-indacene (60)

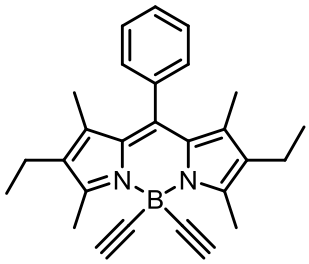

Compound **57** (0.25 g, 0.65 mmol) was dissolved in anhydrous THF (5 mL), and ethynylmagnesium bromide (2.76 mL, 05 M in THF, 1.38 mmol) was added dropwise. The mixture was heated to 76 °C overnight before being quenched with methanol (5 mL) and the solvent removed. The compound was purified by column chromatography on silica gel (petrol:toluene 1:4) to yield the desired product as a red solid (0.21 g, 82%).

^{1}H NMR (700 MHz, $CDCl_3$) δ 7.41-7.39 (m, 3H), 7.26-7.24 (m, 2H), 2.71 (s, 6H), 2.29 (q, $^{3}J_{HH}$ = 7.6 Hz, 4H), 2.19 (s, 2H), 1.22 (s, 6H), 0.95 (t, $^{3}J_{HH}$ = 7.6 Hz, 6H) ppm; **^{13}C{^{1}H} NMR** (176 MHz, $CDCl_3$) δ 153.6, 140.2, 136.6, 136.3, 132.9, 129.0, 128.9, 128.6, 128.5, 96.0, 82.9, 17.4, 14.8, 14.0, 11.8 ppm; **^{11}B{^{1}H} NMR** (96 MHz, $CDCl_3$) δ –14.8 ppm; **IR** (neat) $\tilde{\nu}$: 3273, 2965, 2929, 2871, 2057, 1540, 1474, 1315, 1173, 973, 718 cm^{-1}; **HRMS** ($ASAP^+$ SOLID) calcd. for $C_{27}H_{30}B_1N_2$ $[M+H]^+$ requires m/z 392.2533, found m/z 392.2530.

2.6.15 8-Phenyl-4,4-diethynylphenyl-1,3,5,7-tetramethyl-2,6-diethyl-4-bora-3a,4a-diaza-s-indacene (61)

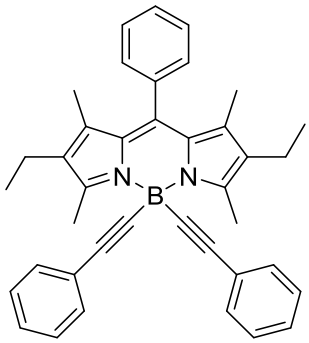

Compound **57** (0.50 g, 1.32 mmol) was dissolved in anhydrous THF (15 mL), and phenylethynylmagnesium bromide (2.76 mL, 1.0 M in THF, 2.76 mmol) was added dropwise. The mixture was heated to 76 °C for five days before being quenched with methanol (5 mL) and the solvent removed. The compound was purified by column chromatography on silica gel (dichloromethane:petrol, 2:1) to yield the desired product as a red solid (0.23, 33%).

^{1}H NMR (700 MHz, $CDCl_3$) δ 7.45-7.10 (m, 15H), 2.79 (s, 6H), 2.28 (q, $^{3}J_{HH}$ = 7.6 Hz, 4H), 1.21 (s, 6H), 0.94 (t, $^{3}J_{HH}$ = 7.6 Hz, 6H) ppm; **^{13}C{^{1}H} NMR** (176 MHz, $CDCl_3$) δ 153.8, 140.2, 136.6, 136.4, 132.8, 132.6, 131.7, 129.2, 129.0, 128.7, 128.1, 127.1, 125.7, 95.2, 81.7, 17.5, 14.9, 14.1, 11.9 ppm; **^{11}B{^{1}H} NMR** (96 MHz, $CDCl_3$) δ –12.5 ppm; **IR** (neat) $\tilde{\nu}$: 3059, 2961, 2927, 2869, 2178, 1611, 1538, 1474, 1315, 1171, 963, 715, 689 cm^{-1}; **HRMS** ($ASAP^+$ SOLID) calcd. for $C_{39}H_{38}BN_2$ $[M+H]^+$ requires m/z 544.3164, found m/z 544.3129.

Chapter 3: Coordination Chemistry of Bodipy Primary Phosphines

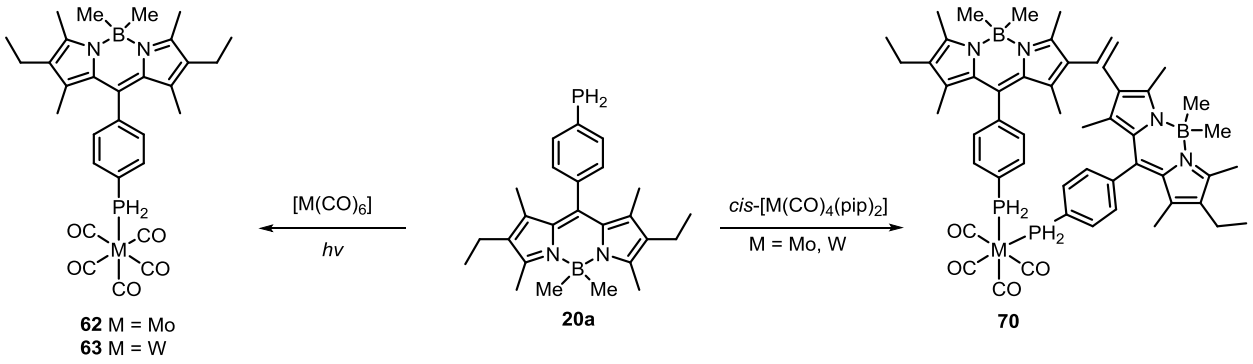

62 M = Mo
63 M = W

20a

70

L. H. Davies, J. F. Wallis, R. W. Harrington, P. G. Waddell & L. J. Higham, *J. Coord. Chem*., Air-stable fluorescent primary phosphine complexes of molybdenum and tungsten. 2016, **69**, 2069-2080.

3 Coordination Chemistry of Primary Phosphines

This chapter describes the synthesis of a library of fluorescent transition metal phosphine complexes. The primary phosphines **20a**, **20b**, **50** and **56** whose synthesis was described in Chapter 2, were coordinated to group 6 and 8 transition metals and their photophysical properties were examined.

3.1 Introduction

There have been extensive coordination studies of tertiary and secondary phosphines to transition metals, however, the equivalent studies of primary phosphines is relatively limited.[22, 23] This may be due to the anticipated difficulty of working with primary phosphines, due to their reputation as spontaneously flammable compounds. In addition, the electronic and steric properties of primary phosphines are different to secondary and tertiary phosphines - due to the presence of the two hydrogen atoms on the phosphorus, the lone-pair orbital has more s-character associated with it, resulting in a weaker donor ligand with regard to transition metal binding ability.

3.2 Fluorescent Transition Metal Phosphine Complexes

Metals are typically thought of as fluorescence quenchers, due to the heavy atom effect, which promotes intersystem crossing to the triplet state and leads to non-radiative decay to the ground state. The presence of the phenyl spacer group in the ligands described in Chapter 2, appears to segregate the phosphino group from the Bodipy, and quenching of the fluorescence is not observed. In this section, the effect of the photophysical behaviour of these compounds when coordinated to transition metals was of interest, as to whether quenching would be observed.

3.2.1 Synthesis of Group 6 [M(CO)$_5$L] complexes (M=Mo, W)

Molybdenum carbonyl complexes of phosphines are usually synthesised in order to gain insight into the electronic nature of a given phosphine, due to the change in the IR absorptions in the carbonyl region. This is dependent on the substituents attached to the phosphorus; better electron donors/poorer acceptors give rise to lower carbonyl stretching frequencies.[28, 94]

Hey-Hawkins *et al.* reported the synthesis and X-ray crystal structure of a primary ferrocenylphosphine tungsten(II) complex in 2002 that showed a distorted capped octahedral structure. Hey-Hawkins has since published other molybdenum and tungsten primary ferrocenylphosphine complexes.[95-97] Figure 3.1 shows a ferrocenylphosphine tungsten complex which was used in the hydrophosphination of a range of alkenes. It was found that the alkenes

bearing a strong electron withdrawing group, such as acrylonitrile had faster reaction times than alkenes containing weaker electron withdrawing groups, such as methyl acrylate.[95]

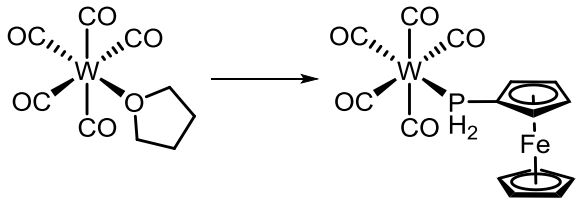

Figure 3.1 A ferrocenylphosphine tungsten complex synthesised by Hey-Hawkins and used in hydrophosphination reactions of alkenes.

The synthesis of the first and second generation primary phosphines (**20a**, **20b**, **50** and **56**) was described in Chapter 2 – this section describes the synthesis of the group 6 complexes formed from those primary phosphines and a comparison of their photophysical properties will then be discussed.

The molybdenum and tungsten primary phosphine complexes were synthesised starting from the metal hexacarbonyl in a photochemical reaction using UV irradiation. The appropriate metal hexacarbonyl, $[Mo(CO)_6]$ and $[W(CO)_6]$, was dissolved in anhydrous tetrahydrofuran and irradiated with UV light in a quartz vessel under a stream of nitrogen for one hour. The primary phosphine was dissolved in anhydrous tetrahydrofuran and added to the quartz vessel, and the reaction mixture was stirred for a further thirty minutes which led to the mono-substituted complexes $[M(CO)_5(\mathbf{20a})]$, $[M(CO)_5(\mathbf{20b})]$, $[M(CO)_5(\mathbf{50})]$ and $[M(CO)_5(\mathbf{56})]$ (M = Mo and W), illustrated in Scheme 3.1.

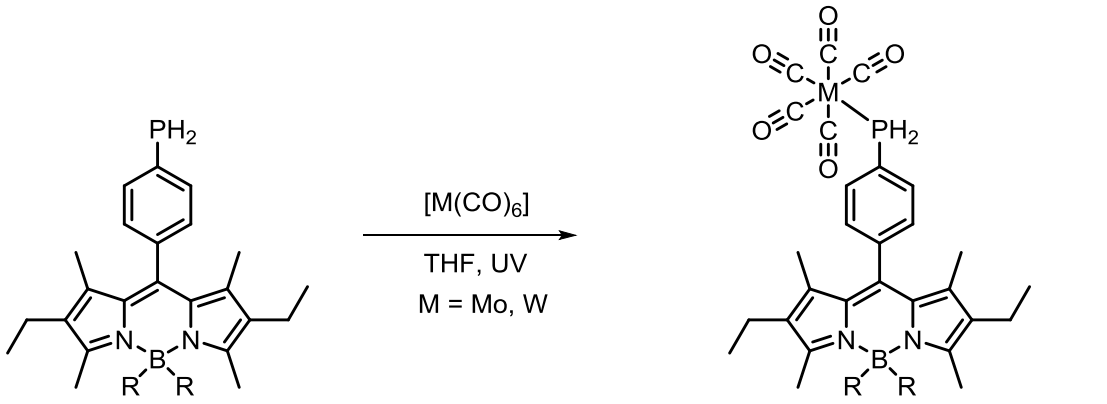

20a R = Me
20b R = Ph
50 R = C≡CH
56 R = C≡C–Ph

62 $[Mo(CO)_5(\mathbf{20a})]$ **66** $[Mo(CO)_5(\mathbf{50})]$
63 $[W(CO)_5(\mathbf{20a})]$ **67** $[W(CO)_5(\mathbf{50})]$
64 $[Mo(CO)_5(\mathbf{20b})]$ **68** $[Mo(CO)_5(\mathbf{56})]$
65 $[W(CO)_5(\mathbf{20b})]$ **69** $[W(CO)_5(\mathbf{56})]$

Scheme 3.1 Primary phosphines 20a, 20b, 50 and 56 were reacted with $[Mo(CO)_6]$ and $[W(CO)_6]$ to produce the primary phosphine metal complexes shown.

Analysis of the four mono-substituted molybdenum complexes by $^{31}P\{^{1}H\}$ NMR spectroscopy gave downfield peaks of approximately δ –64 ppm relative to the primary phosphine peak (~ δ −122 ppm) and coupling constants of $^{1}J_{PH}$ = 326 Hz. The chemical shift compares well to examples in the literature, such as $[Mo(CO)_5(FcCH_2PH_2)]$ (Fc = ferrocene) which was reported by Henderson and gives a signal in the $^{31}P\{^{1}H\}$ NMR spectrum at δ –63.2 ppm and shows a phosphorus–hydrogen coupling constant of $^{1}J_{PH}$ = 315 Hz.[28] Hey-Hawkins *et al.* published a $[Mo(CO)_5(FcPH_2)]$ derivative which showed a comparable $^{1}J_{PH}$ coupling constant of 328.0 Hz and a chemical shift of δ −81.5 ppm on the $^{31}P\{^{1}H\}$ NMR spectrum .[95]

The tungsten complexes also showed downfield shifts close to δ –85 ppm and coupling constants of $^{1}J_{PH}$ = 340 Hz. ^{183}W satellite peaks were also visible on the $^{31}P\{^{1}H\}$ NMR spectra that showed $^{1}J_{PW}$ coupling constants of approximately 223 Hz. These data are comparable to that measured for $[W(CO)_5(PhPH_2)]$ published by McFarlane in 1976, who gave values of δ –90.2 ppm, $^{1}J_{PH}$ = 343.5 Hz and $^{1}J_{PW}$ = 220 Hz.[98] The characteristic NMR and IR data for all of the molybdenum and tungsten complexes have been compiled into Table 3.1.

A crystalline sample of **63** was analysed by X-ray crystallography and the solid state structure was determined as shown in Figure 3.2. The W1–P1 of 2.4957(0) Å is in agreement with published examples.[99]

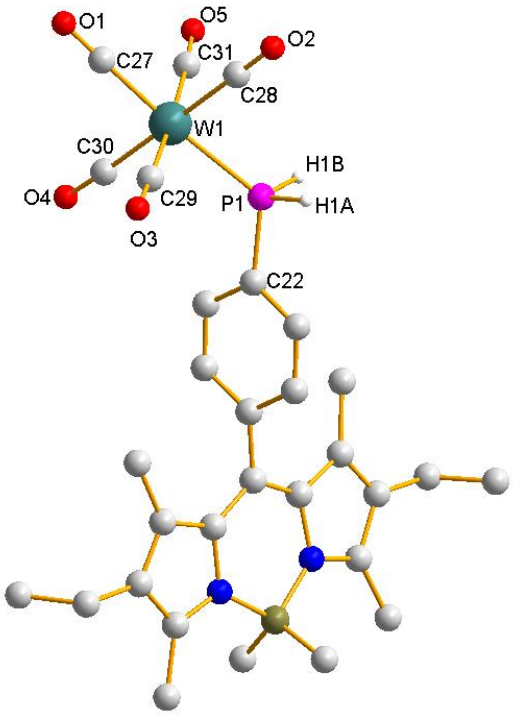

Figure 3.2 Molecular structure of 63. Crystals grown via slow diffusion of chloroform:pentane. Selected bond lengths [Å] and angles [°]: W1-P1 2.4957(0), P1-C22 1.8194(0), W1-C27 2.010(4), W1-C28 2.048(4), W1-C29 2.019(5), W1-C30 2.035(5), W1-C31 2.041(5), C-O average 1.14(0); C22-P1-W1 125.21(1), C22-P1-H1A 99.12(1), W1-C28-O2 179.09(0), H1B-P1-H1a 95.50(1).

A side-product formed in these reactions was the di-substituted complex where two primary phosphine units had coordinated to the metal centre. Previously within the Higham research group, these di-substituted group 6 complexes were intentionally synthesised *via* the route shown in Scheme 3.2. The metal hexacarbonyl is reacted with two equivalents of piperidine which replaces two carbonyl groups, and when $[M(CO)_4(piperidine)_2]$ is reacted with two equivalents of a primary phosphine in refluxing dichloromethane, two ligands are coordinated to the metal centre to form complexes *cis*–$[M(CO)_4(RPH_2)_2]$. The di-substituted molybdenum complex **70** gave a triplet of multiplets in the ^{31}P-^{1}H NMR spectrum at δ –51.6 ppm and a $^{1}J_{PH}$ coupling constant of 316.5 Hz. The di-substituted tungsten complex **71** also showed a triplet of multiplets in the ^{31}P-^{1}H NMR spectrum at δ –76.9 ppm and a $^{1}J_{PH}$ coupling constant of 388.9 Hz, a tungsten satellite peak was also observed with a coupling constant of $^{1}J_{PW}$ = 217.4 Hz. Details of the synthesis can be found in the experimental section.[100]

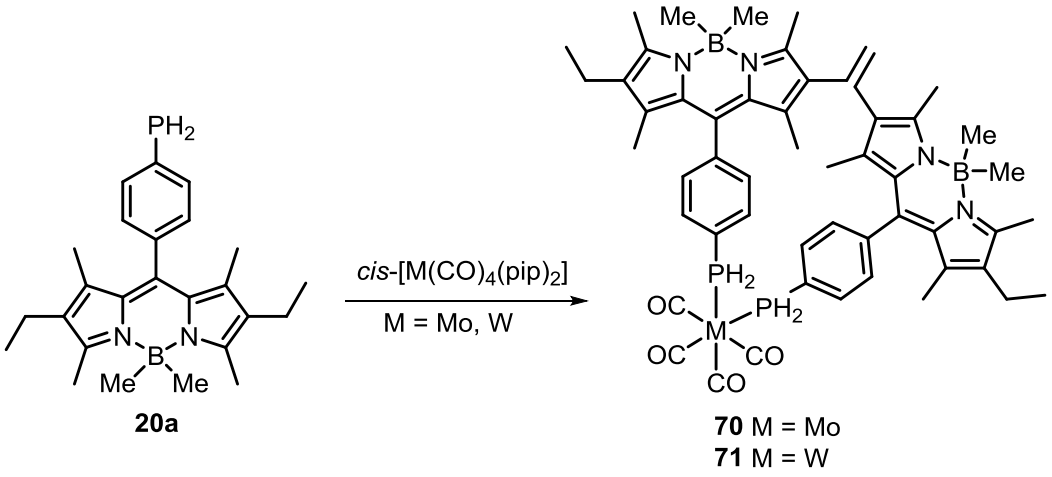

Scheme 3.2 Synthesis of group 6 di-substituted complexes [M(CO)$_4$(20a)$_2$].

3.2.2 IR and NMR Spectroscopic Characterisation

The carbonyl groups bound to the metal show distinctive peaks in the IR spectrum. In the case of the pentacarbonyl complexes synthesised within this series, three carbonyl stretching frequencies can be observed; bonds corresponding to the A_1 (*cis/equatorial*), A_1 (*trans/axial*) and E absorbance's are in accordance with the C_{4v} point group - to which they have been assigned.[99, 101, 102] Table 3.1 shows the IR and NMR data for compounds **62**-**69**, alongside two literature examples which have been added for comparison. Hey-Hawkins *et. al*. researched transition metal ferrocenylphosphine complexes that could subsequently be used in hydrophosphination reactions.[95] Goerlich and co-workers synthesised a range of 1-adamantylphosphine complexes by reacting 1-adamantylphosphine with molybdenum and tungsten carbonyl compounds.[102]

Table 3.1 Selected IR and NMR data for monodentate group 6 transition metal-phosphine complexes.

Compound	ν(CO)A$_1$ *Eq* cm^{-1}	ν(CO)A$_1$ *Ax* cm^{-1}	ν(CO), E cm^{-1}	^{31}P δ, ppm	$^1J_{P\text{-}H}$, Hz	$^1J_{P\text{-}W}$, Hz	δ ($^2J_{P\text{-}C}$) CO *trans*	δ ($^2J_{P\text{-}C}$) CO *cis*
62	2076	1992	1929	−63.5	326.7	-	208.8 (24.2)	204.7 (9.8)
63	2077	1973	1902	−85.7	340.6	222.9	198.3 (23.1)	195.5 (7.2)
64	2077	1945	1917	−64.2	330.5	-	208.4 (24.2)	203.5 (8.9)
65	2076	1969	1921	−85.7	342.5	223.3	198.2 (22.8)	194.3 (7.1)
66	2076	1994	1928	−64.0	328.3	-	207.7 (24.1)	203.5 (9.2)
67	2075	1972	1914	−85.6	342.1	223.7	198.0 (22.6)	195.3 (7.0)
68	2077	1989	1924	−64.7	327.9	-	208.2 (24.3)	204.4 (9.2)
69	2075	1974	1915	−85.7	342.2	222.4	198.3 (22.9)	194.3 (6.9)
Mo(CO)$_5$FcPH$_2$[a]	2074	1950	1933	81.5	328.0	-	208.8 (23.7)	205.0 (9.2)
W(CO)$_5$FcPH$_2$[a]	2073	1935	1906	101.8	341.5	221.0	198.1 (22.2)	195.9 (7.1)
Mo(CO)$_5$(1-AdPH$_2$)[b]	2074	1987	1952	28.5	308.2	-	208.3 (21.9)	205.4 (8.9)
W(CO)$_5$(1-AdPH$_2$)[b]	2075	1980	1945	47.6	321.0	212.5	196.9 (21.8)	196.9 (6.9)

IR recorded neat; NMR in *d*-chloroform, Fc = ferrocene, 1-Ad = 1-adamantyl. [a] IR in nujol. [b] IR in hexane.

3.2.3 Photophysical Studies

After successfully synthesising a range of group 6 metal phosphine complexes, it was important to determine and understand their photophysical properties. It was imperative to know how the coordination of metals affected the quantum yield in the resultant complex and whether the presence of the heavy atoms quenched the fluorescence of the free ligand. The photophysical data were collected for the primary phosphines and their transition metal complexes in anhydrous, degassed tetrahydrofuran at room temperature, and are shown in Table 3.2.

Table 3.2 Photophysical properties of primary phosphines 20a, 20b, 50 and 56 and their novel group 6 metal complexes 62-69.

	λ_{abs} (nm)[a]	λ_{em} (nm)[a]	Φ[a,b]	ε ($M^{-1}cm^{-1}$)[a]
20a	512	526	0.33	79,000
[Mo(CO)$_5$(20a)] (62)	512	527	0.25	72,000
[W(CO)$_5$(20a)] (63)	512	527	0.20	73,000
20b	518	532	0.042	79,000
[Mo(CO)$_5$(20b)] (64)	519	534	0.055	75,000
[W(CO)$_5$(20b)] (65)	519	535	0.059	75,000
50	520	534	0.79	78,000
[Mo(CO)$_5$(50)] (66)	521	534	0.53	77,000
[W(CO)$_5$(50)] (67)	520	534	0.45	75,000
56	521	535	0.78	81,000
[Mo(CO)$_5$(56)] (68)	521	535	0.59	77,000
[W(CO)$_5$(56)] (69)	522	536	0.60	78,000

[a] Measured in dry, degassed tetrahydrofuran at room temperature, dyes were excited at 485 nm; [b] Fluorescence quantum yields were measured with respect to 4,4-difluoro-8-phenyl-1,3,5,7-tetramethyl-2,6-diethyl-4-bora-3a,4a-diaza-s-indacene **57**. ε given to 2 s.f.

The absorption maxima for the parent primary phosphines ranged from 512 nm for **20a** to 521 nm for **56**, and upon complexation to the molybdenum and tungsten carbonyl complexes varied by 1-2 nm. As the substituents on the boron atom are changed from methyl to phenyl to ethynyl and phenylethynyl, a small bathochromic shift is observed.

In general, a decrease in the fluorescence quantum yield is observed, (except for primary phosphine **20b**) but the complexes remain highly fluorescent. Figures 3.3 and 3.4 show the absorption and emission spectra for the four tungsten complexes **63**, **65**, **67** and **69**. The spectra for the molybdenum complexes can be found in the appendix.

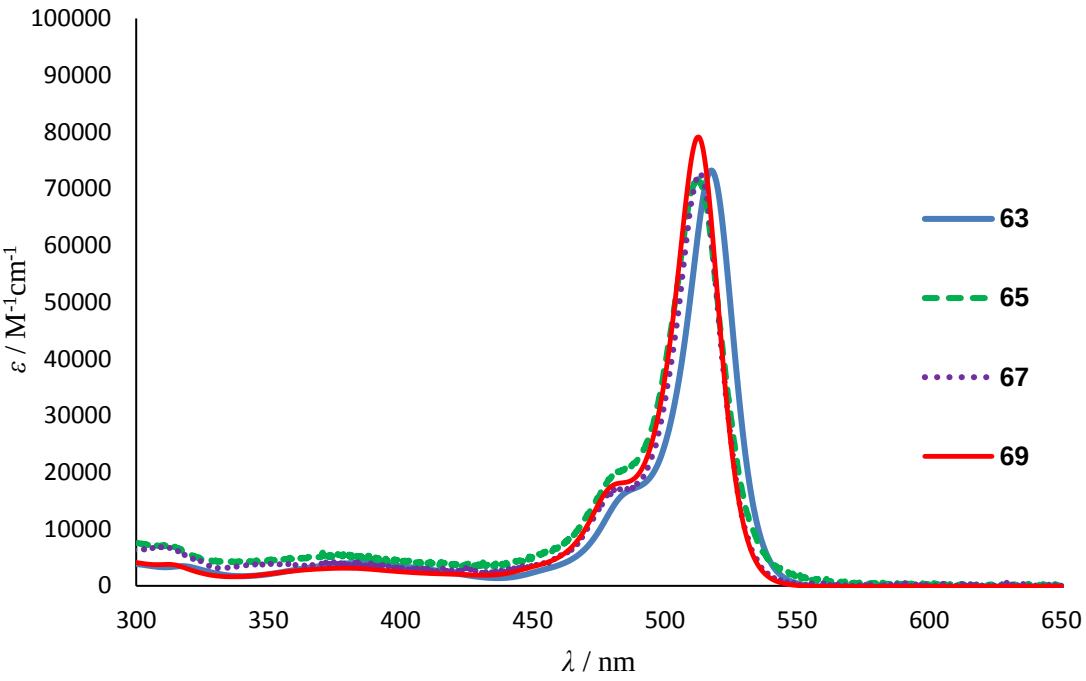

Figure 3.3 Absorption spectra for tungsten complexes 63, 65, 67 and 69, measured in dry, degassed tetrahydrofuran at room temperature.

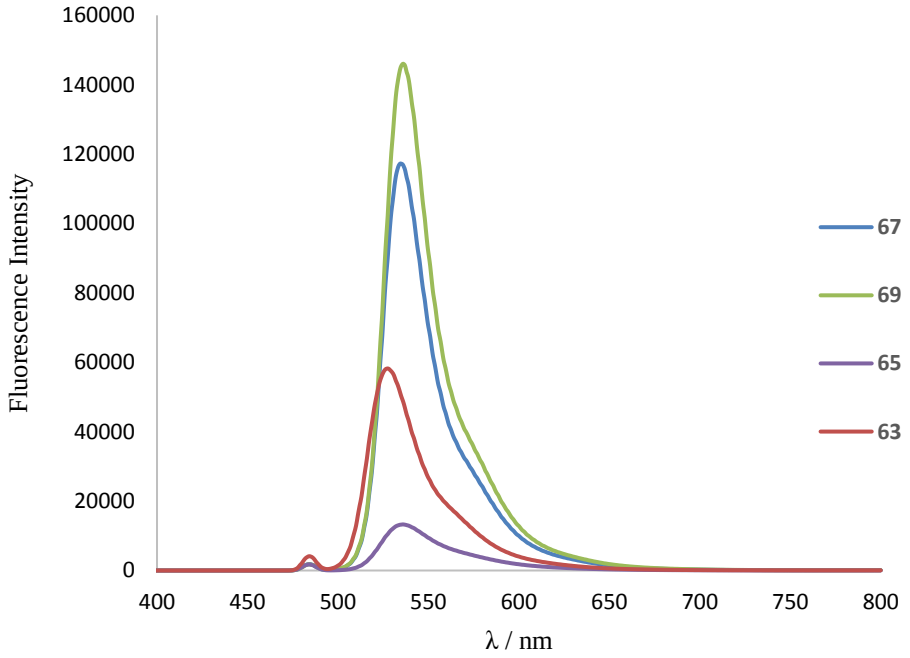

Figure 3.4 Emission spectra for tungsten complexes 63, 65, 67 and 69, measured in dry, degassed tetrahydrofuran at room temperature.

This research has identified that the coordination of primary phosphines **20a**, **20b**, **50** and **56** to group 6 metals, molybdenum and tungsten pentacarbonyl complexes, does not appear to

significantly quench the fluorescence quantum yield of these novel complexes. This means that these complexes may have potential applications as imaging agents.

3.3 Synthesis of [RuX_2(arene)(RPH_2)] Complexes

Having established that the coordination of primary phosphines **20a**, **20b**, **50** and **56** to group 6 metals does not appear to cause quenching, the next target was bio-relevant group 8 metal ruthenium. The introductory section discussed the importance of RAPTA-C as a ruthenium anti-cancer drug, it would therefore be interesting to synthesise a fluorescent ruthenium complex in order to monitor the mode of action within cells *in vitro*. Therefore, primary phosphines **20a**, **20b**, **50** and **56** were reacted with four ruthenium dimers, $[RuCl_2(C_6H_6)]_2$, $[RuCl_2(p\text{-cymene})]_2$, $[RuI_2(C_6H_6)]_2$ and $[RuI_2(p\text{-cymene})]_2$ to form a library of novel ruthenium phosphine complexes. Their photophysical properties were analysed and a number of X-ray crystal structures were obtained.

3.3.1 Ruthenium Complexes in Medicine

Ruthenium has shown promise in pharmacological applications due to its ability to access many different oxidation states. There has been much interest in ruthenium complexes as anticancer agents, due to their effective behaviour towards cancerous cells, without toxic side effects, unlike their platinum analogues. Cisplatin was the first platinum-containing anti-cancer drug to be synthesised and since its success, several more platinum containing drugs have been produced, shown in Figure 3.5.[103]

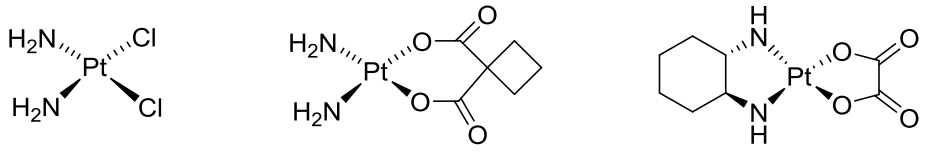

Figure 3.5 Platinum containing pharmaceuticals Cisplatin, Carboplatin and Oxaliplatin.

Carboplatin and Oxaliplatin are direct analogues of Cisplatin, and their modes of action are all known; the chloride or dicarboxylate ligands generate a *bis*-aqua species when undergoing hydrolysis within a cell, which binds irreversibly to DNA through two guanine bases, forming a "kink" which stops the cell from replicating and leads to apoptosis.[104] Platinum compounds have shown great promise in chemotherapeutics, however, they also come with several side effects, such as nerve damage, nausea and hair loss. Ruthenium compounds have been found to show fewer and less severe side effects. Two examples are NAMI-A and KP1019, shown in Figure 3.6. These drugs

are both structurally similar to each other, although they exhibit different anticancer activities. Whilst KP1019 is active against primary cancers – the main tumour, NAMI-A is effective against secondary tumour cells - cells from the main tumour that may have migrated around the body via the bloodstream and into a different organ.[18]

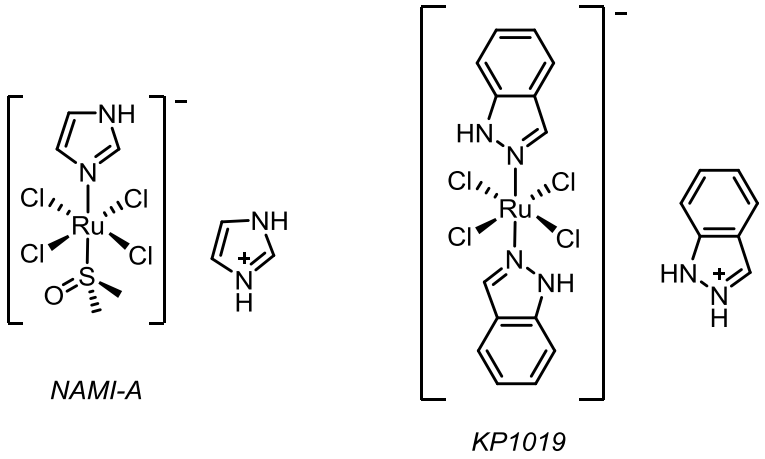

Figure 3.6 NAMI-A and KP1019 are two ruthenium based anti-cancer drugs that have been entered into clinical trials.

3.3.2 Ruthenium Phosphine Complexes

There have been several ruthenium phosphine complexes published with potential therapeutic properties.[105-109] In Sections 1.2.4 and 3.3.1, the importance of ruthenium in medicine was discussed, and RAPTA-C was highlighted as an anti-cancer drug currently in clinical trials (Fig 3.7). The next section will discuss the coordination chemistry of fluorescent primary phosphines to several ruthenium dimers. The photophysical properties of these novel complexes will also be measured in order to identify what effects are observed.

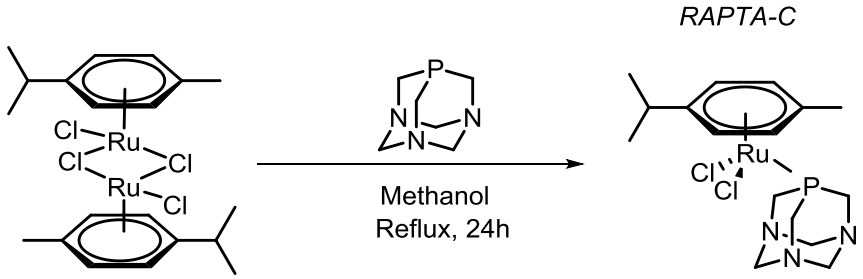

Figure 3.7 Synthesis of RAPTA-C, an anti-cancer drug in clinical trials.

3.3.3 Synthesis of Novel Fluorescent Ruthenium Complexes

Primary phosphines **20a**, **20b**, **50** and **56** were reacted with benzene and *p*-cymene ruthenium(II) dimer complexes, containing an iodo or chloro bridge, to form novel complexes **72-87** as shown in

Scheme 3.3. The weak bridge of the ruthenium dimer can be broken by a stronger donor such as a phosphine, to generate an 18-electron species.

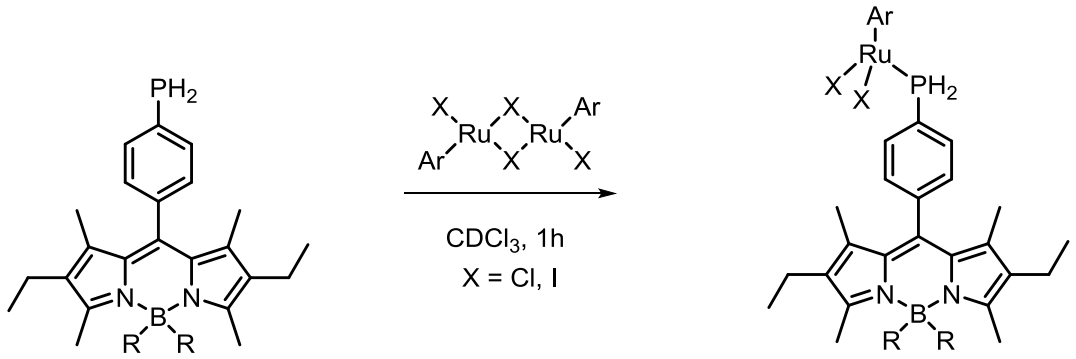

20a R = Me
20b R = Ph
50 R = C≡CH
56 R = C≡C–Ph

72 [$RuCl_2(C_6H_6)$(**20a**)]
73 [$RuCl_2$(*p*-cymene)(**20a**)]
74 [$RuI_2(C_6H_6)$(**20a**)]
75 [RuI_2(*p*-cymene)(**20a**)]
76 [$RuCl_2(C_6H_6)$(**20b**)]
77 [$RuCl_2$(*p*-cymene)(**20b**)]
78 [$RuI_2(C_6H_6)$(**20b**)]
79 [RuI_2(*p*-cymene)(**20b**)]
80 [$RuCl_2(C_6H_6)$(**50**)]
81 [$RuCl_2$(*p*-cymene)(**50**)]
82 [$RuI_2(C_6H_6)$(**50**)]
83 [RuI_2(*p*-cymene)(**50**)]
84[$RuCl_2(C_6H_6)$(**56**)]
85 [$RuCl_2$(*p*-cymene)(**56**)]
86 [$RuI_2(C_6H_6)$(**56**)]
87 [RuI_2(*p*-cymene)(**56**)]

Scheme 3.3 Primary phosphines can be reacted with ruthenium (II) dimers to give the novel complexes shown.

Two equivalents of primary phosphine **20a**, **20b**, **50** and **56** were reacted with one equivalent of a ruthenium dimer in deuterated chloroform at room temperature for one hour. The solution was analysed by $^{31}P\{^{1}H\}$ NMR spectroscopy which showed a single product peak and no starting material peak (δ −121 ppm), in the ^{31}P-^{1}H NMR spectra a triplet of triplets was observed, with coupling constants consistent with the presence of a primary phosphine ($^{1}J_{PH}$ = 398.1 Hz, $^{3}J_{PH}$ = 11.0 Hz).[8] Table 3.3 shows the phosphorus chemical shifts observed for each complex alongside the phosphorus-hydrogen coupling constants. The iodo-bridged ruthenium dimers tended to give a downfield shift of approximately δ −50 ppm, whereas the chloro-bridged dimers appeared further downfield at between δ −30 and −32 ppm.

Table 3.3 Phosphorus chemical shifts and phosphorus-hydrogen couplings for the ruthenium complexes 72-87 in deuterated chloroform.

Compound	^{31}P δ, ppm	$^{1}J_{PH}$, Hz	$^{3}J_{PH}$, Hz
[$RuCl_2(C_6H_6)$(**20a**)] **72**	−31.3	397.2	10.7
[$RuCl_2$(*p*-cymene)(**20a**)] **73**	−29.5	390.8	11.5
[$RuI_2(C_6H_6)$(**20a**)] **74**	−49.8	398.3	11.5
[RuI_2(*p*-cymene)(**20a**)] **75**	−43.7	392.2	10.9
[$RuCl_2(C_6H_6)$(**20b**)] **76**	−31.4	395.8	10.9
[$RuCl_2$(*p*-cymene)(**20b**)] **77**	−30.2	390.0	11.1
[$RuI_2(C_6H_6)$(**20b**)] **78**	−50.2	398.5	11.2
[RuI_2(*p*-cymene)(**20b**)] **79**	−43.9	391.8	11.2
[$RuCl_2(C_6H_6)$(**50**)] **80**	−32.4	398.3	11.9
[$RuCl_2$(*p*-cymene)(**50**)] **81**	−30.3	390.4	11.4
[$RuI_2(C_6H_6)$(**50**)] **82**	−50.1	398.1	11.6
[RuI_2(*p*-cymene)(**50**)] **83**	−43.9	390.8	11.4
[$RuCl_2(C_6H_6)$(**56**)] **84**	−32.2	398.0	11.9
[$RuCl_2$(*p*-cymene)(**56**)] **85**	−30.5	391.2	11.6
[$RuI_2(C_6H_6)$(**56**)] **86**	−49.6	398.4	11.2
[RuI_2(*p*-cymene)(**56**)] **87**	−44.6	391.4	11.5

Complexes **72**, **74** and **75** were crystallised by adding a layer of pentane over a deuterated chloroform solution of the relevant complex, which formed crystals suitable for analysis by X-ray diffraction, as shown in Figures 3.8, 3.9 and 3.10.

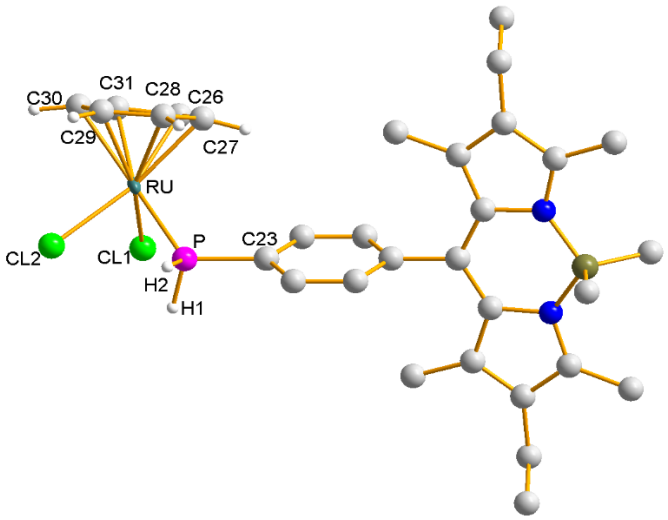

Figure 3.8 X-Ray crystal structure of 72. Crystals grown via slow diffusion of $CDCl_3$:pentane. Selected bond distances [Å] and angles [°]: P-C23 1.8218(1), Ru-P 2.2944(1), Ru-Cl1 2.3879(1), Ru-Cl2 2.4226(1), P-H1 1.25(5), P-H2 1.26(5), aromatic carbon atoms show an average distance of 2.19(6); Cl1-Ru-Cl2 87.820(4), Ru-P-C23 121.189(4), Cl1-Ru-P 83.369(3), Cl2-Ru-P 78.61(5).

The Ru−P bond length of 2.2944(1) Å and the Ru−Cl bond lengths of 2.3879(1) and 2.4226(1) Å respectively, are in agreement with other similar reported examples.[110]

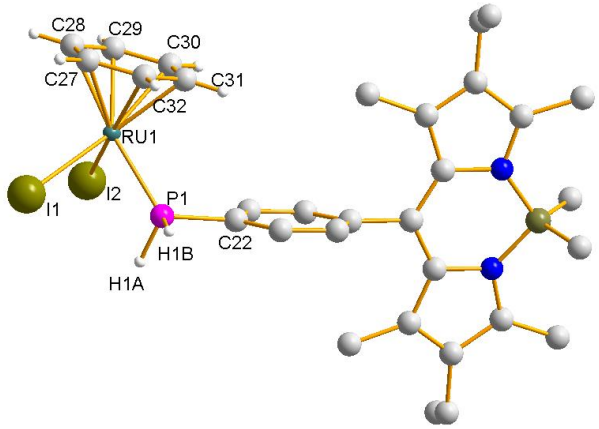

Figure 3.9 X-Ray crystal structures of 74. Crystals grown in $CDCl_3$. Selected bond distances [Å] and angles [°]: P1-C22 1.8203(0), P1-H1 1.275(0), P1-Ru1 2.2912(0), Ru-I1 2.7021(0), Ru1-I2 2.7054(0), Ru-aromatic C average distance 2.20(0); C22-P1-Ru1 118.182(1), P1-Ru1-I1 81.902(1), H1A-P1-H1B 100.695(1).

The Ru−P bond length of 2.2912(0) Å and Ru−I bond lengths of 2.7021(0) and 2.7054(0) Å are also in agreement with reported examples.[111]

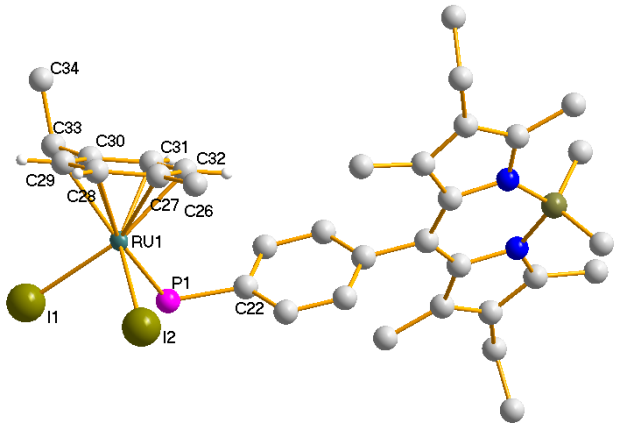

Figure 3.10 Molecular structure of 75. Crystals grown in $CDCl_3$. Selected bond distances [Å] and angles [°]: C22-P1 1.8103(1), P1-Ru1 2.2918(1), Ru1-I1 2.7220(1), Ru1-I2 2.7138(1), Ru1-aromatic C average distance 2.24(1); C22-P1-Ru1 115.206(2), I1-Ru1-I2 89.788(2), I1-Ru1-P1 81.642(2), I2-Ru-P1 84.0253(2).

The Ru−P bond length of 2.2918(1) Å and Ru−I bond lengths of 2.7220(1) and 2.7138(1) Å are also in agreement with other published examples.[110, 111]

When primary phosphine **20b** was reacted with the $[RuCl_2(p\text{-cymene})]_2$ dimer, along with the intended product **77**, a side product was also formed where a phenyl group on the boron atom had been replaced by an OH group (compound **77a**, Figure 3.11).

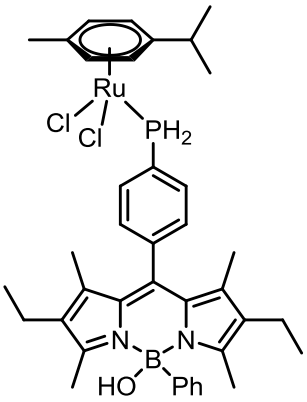

77a

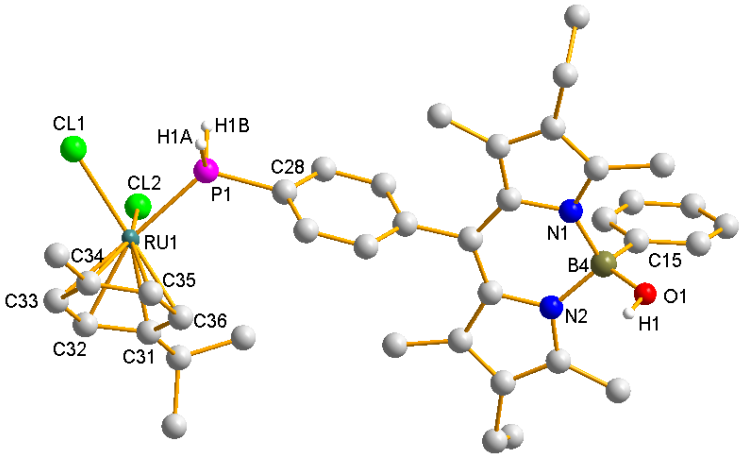

Figure 3.11 ChemDraw structure and X-ray crystal structure of 77a. Crystals grown in $CDCl_3$. Selected bond distances [Å] and angles [°]: P1-C28 1.818(2), Ru1-P1 2.3066(6), B4-O1 1.430(3), B4-C15 1.617(4), Ru-Cl 2.41(6); O1-B4-C15 110.27(19), C28-P1-Ru1 122.48(7), Cl1-Ru1-Cl2 86.44(2).

It was not immediately obvious how this substitution had occurred, as the carbon-boron bond is quite robust in our hands. However, it is possible to use the OH as a good leaving group and substitute it for a different group. The addition of a radiolabel such as ^{18}F would enable the compound to be used in PET imaging; there are examples in the literature where this substitution has in fact been exploited, as shown in Figure 3.12.[112] In this way, it is possible to create a multi-

modal imaging agent – the Bodipy function facilitates *in vitro* cell imaging and the ^{18}F PET label allows for *in vivo* clinical imaging of a patient.

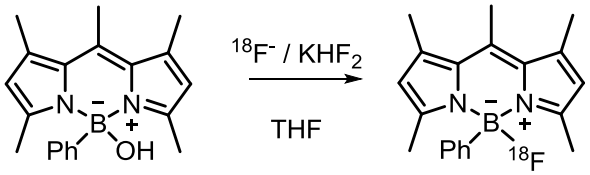

Figure 3.12 An example from the literature where an OH group has been replaced by an ^{18}F radiolabel.

3.3.4 Photophysical Properties of [RuX$_2$(arene)(RPH$_2$)] Complexes

The photophysical properties of the novel ruthenium phosphine complexes were recorded in anhydrous tetrahydrofuran at room temperature. The absorption and emission maxima, quantum yield and extinction coefficients were identified and can be found in Table 3.4.

Table 3.4 Photophysical properties of [RuX$_2$(arene)(RPH$_2$)] complexes (X = I, Cl)

	λ_{abs} (nm)[a]	λ_{em} (nm)[a]	Φ[a,b]	ε ($M^{-1}cm^{-1}$)[a]
20a	512	526	0.33	79,000
[RuCl$_2$(C$_6$H$_6$)(**20a**)] (**72**)	512	527	0.09	74,000
[RuCl$_2$(*p*-cymene)(**20a**)] (**73**)	512	527	0.09	77,000
[RuI$_2$(C$_6$H$_6$)(**20a**)] (**74**)	512	528	0.06	74,000
[RuI$_2$(*p*-cymene)(**20a**)] (**75**)	512	527	0.02	72,000
20b	518	532	0.042	79,000
[RuCl$_2$(C$_6$H$_6$)(**20b**)] (**76**)	518	534	0.017	73,000
[RuCl$_2$(*p*-cymene)(**20b**)] (**77**)	518	534	0.011	73,000
[RuI$_2$(C$_6$H$_6$)(**20b**)] (**78**)	519	534	0.007	72,000
[RuI$_2$(*p*-cymene)(**20b**)] (**79**)	519	534	0.005	75,000
50	520	534	0.79	78,000
[RuCl$_2$(C$_6$H$_6$)(**50**)] (**80**)	520	534	0.36	79,000
[RuCl$_2$(*p*-cymene)(**50**)] (**81**)	521	534	0.14	78,000
[RuI$_2$(C$_6$H$_6$)(**50**)] (**82**)	521	534	0.27	77,000
[RuI$_2$(*p*-cymene)(**50**)] (**83**)	521	534	0.31	74,000
56	521	535	0.78	81,000
[RuCl$_2$(C$_6$H$_6$)(**56**)] (**84**)	521	535	0.40	79,000
[RuCl$_2$(*p*-cymene)(**56**)] (**85**)	521	535	0.38	79,000
[RuI$_2$(C$_6$H$_6$)(**56**)] (**86**)	521	535	0.32	77,000
[RuI$_2$(*p*-cymene)(**56**)] (**87**)	521	535	0.29	78,000

[a] Measured in dry, degassed tetrahydrofuran at room temperature, dyes were excited at 485 nm; [b] Fluorescence quantum yields were measured with respect to 4,4-difluoro-8-phenyl-1,3,5,7-tetramethyl-2,6-diethyl-4-bora-3a,4a-diaza-s-indacene **57**. **ε** quoted to 2 s.f.

Table 3.4 shows the photophysical properties of the free primary phosphines compared to their ruthenium complexes. Primary phosphine **20a** – which has methyl groups attached to the boron atom, has shown a dramatic decrease in the fluorescent quantum yield upon coordination to the

ruthenium dimers. The absorption and emission maxima and the extinction coefficients have all remained similar to the free primary phosphine. The same relationship can be seen between primary phosphine **20b** and its ruthenium complexes – the phenyl substituents on the boron atom have already significantly lowered the quantum yield, and upon complexation, the quantum yield is decreased further. Primary phosphines **50** and **56** contain ethynyl-type substituents on the boron atom and the free primary phosphines have a much higher quantum yield; however, the same relationship is observed and the quantum yields are also decreased upon complexation to the ruthenium dimers.

3.4 DFT Calculations on the $[M(CO)_5(RPH_2)]$ and $[RuX_2(arene)(RPH_2)]$ complexes (M = Mo, W)

It was important to investigate why the ruthenium complexes exhibited a reduced quantum yield, whereas the group 6 metals did not. DFT computational studies were performed on the synthesised ruthenium, molybdenum and tungsten complexes. All of the modelled group 6 and 8 complexes showed a Bodipy-based HOMO, however, the ruthenium complexes contained a metal-based LUMO whereas the group 6 complexes had a Bodipy-based LUMO. Figures 3.13, 3.14 and 3.15 show complexes **62**, **63** and **72** illustrating the different nature of the HOMO and LUMO orbital distributions. Other ruthenium complexes including complexes **73-79** were also modelled and can be seen in the appendix where the same orbital distribution is observed.

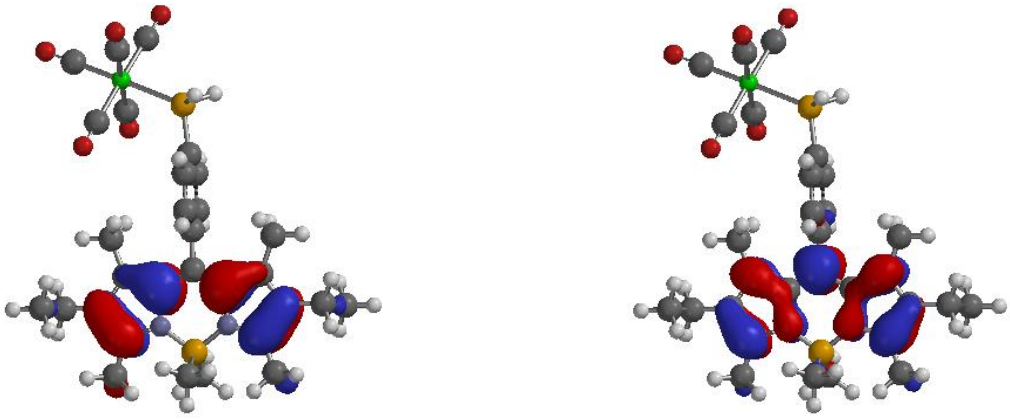

HOMO -5.2 eV LUMO -2.2 eV

Figure 3.13 Molybdenum complex $[Mo(CO)_5(20a)]$ (62) showing the HOMO and LUMO distribution for complex 62.

Figure 3.13 shows the molybdenum complex **62** where the HOMO and LUMO are both visible on the Bodipy core, the phosphorus atom is not incorporated into the HOMO until HOMO (-3). The same is observed for the tungsten complex **63**, the phosphorus is not incorporated into the HOMO until HOMO (-3).

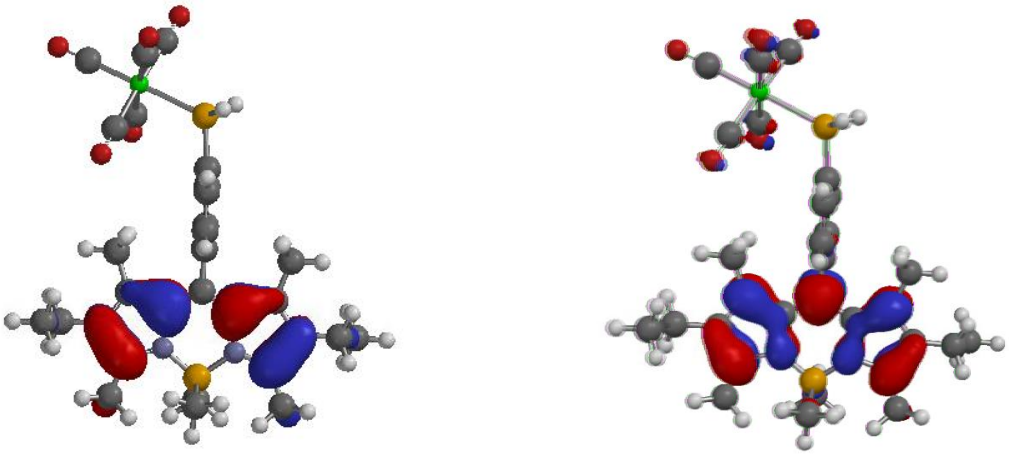

HOMO -5.3 eV LUMO -2.2 eV

Figure 3.14 Tungsten complex [$W(CO)_5$(20a)] (63) with the HOMO and LUMO orbitals shown.

The ruthenium complexes however, exhibit a metal-based LUMO rather than a Bodipy-based LUMO and show more quenched fluorescence than the group 6 complexes. This may suggest that the ruthenium metal orbitals are involved in the fluorescence process, possibly in a LMCT process, which may identify why a bigger increase in fluorescence quenching is observed for them.

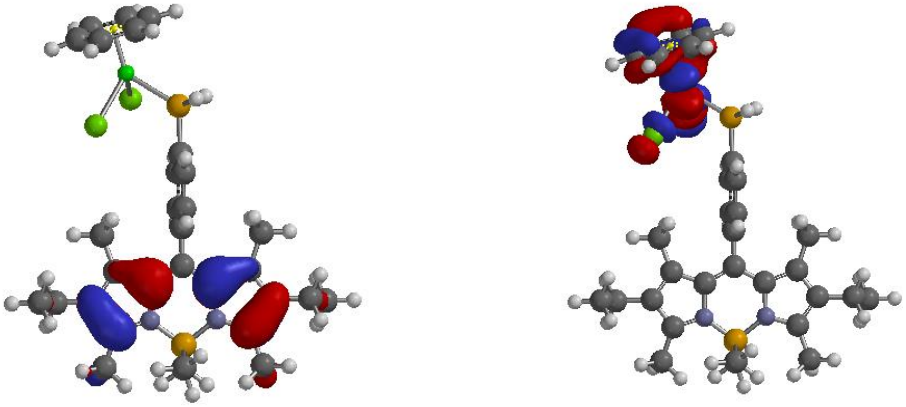

HOMO -5.2 eV LUMO -2.8 eV

Figure 3.15 Ruthenium complex [$RuCl_2(C_6H_6)$(20a)] (72) with the HOMO and LUMO orbitals depicted.

3.5 Tertiary Phosphine-Ruthenium Complexes

Despite the large degree of fluorescent quenching observed on binding to ruthenium, some of the resultant complexes did remain fluorescent. This led us to investigate the possibility of synthesising a fluorescent ruthenium-phosphine complex – similar to RAPTA-C but with a different tertiary phosphine.

RAPTA-C, shown in Scheme 3.4, was formed by the reaction of dichloro(*p*-cymene) ruthenium(II) dimer and pta (1,3,5-triaza-7-phosphatricyclo[3.3.1.1]decane) in refluxing methanol (see Section 1.2.4). RAPTA-C has shown promising properties as an anti-cancer drug, and it would be interesting to synthesise a fluorescent analogue to facilitate *in vitro* imaging and help elucidate the mode of action.[19]

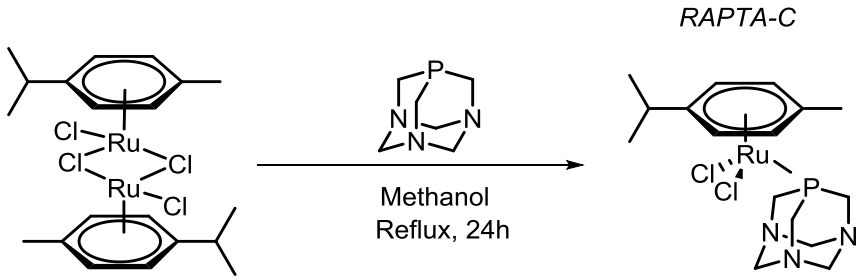

Scheme 3.4 Synthesis of the ruthenium-phosphine complex RAPTA-C.

The RAPTA-C structure includes a tertiary phosphine bound to a ruthenium metal centre; therefore, it was proposed to synthesise a fluorescent version of RAPTA-C by coordinating the Bodipy-based tertiary phosphines **89a** and **89b** to the $[RuI_2(p\text{-cymene})]_2$ and $[RuCl_2(C_6H_6)]_2$ dimers. This approach is similar to that published by Bodio and co-workers, who developed a phosphine that had an extended linker between the Bodipy core and the diphenylphosphino moiety, which was then coordinated to ruthenium (Figure 3.16).[21] Therefore, it would be interesting to synthesise an alternative compound where the diphenylphosphino group was attached to the Bodipy core with a shorter linker, and see how this affects the fluorescence of the compound.

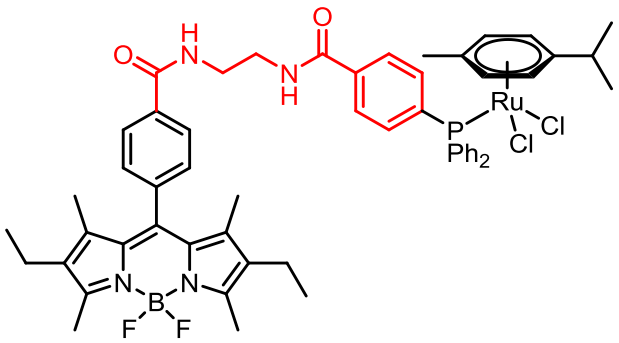

Figure 3.16 Bodio and co-workers developed a Bodipy-based phosphine and coordinated it to ruthenium.

3.5.1 Synthesis of Fluorescent Tertiary Phosphines 89a and 89b.

The synthesis of the tertiary phosphines **89a** and **89b** will be discussed in detail in Chapter 4; Scheme 3.5 shows the reaction conditions that were used. Phosphorus pentachloride was dissolved in anhydrous toluene and primary phosphine **20a** was added, the reaction was stirred at room temperature for one hour. The solution was analysed by $^{31}P\{^{1}H\}$ NMR spectroscopy, which identified the presence of dichlorophosphine **88** (δ 159.7 ppm). The orange solid was dissolved in anhydrous THF and two equivalents of dicyclohexylmagnesium chloride/ phenylmagnesium bromide were added, which formed tertiary phosphines **89a** and **89b**.

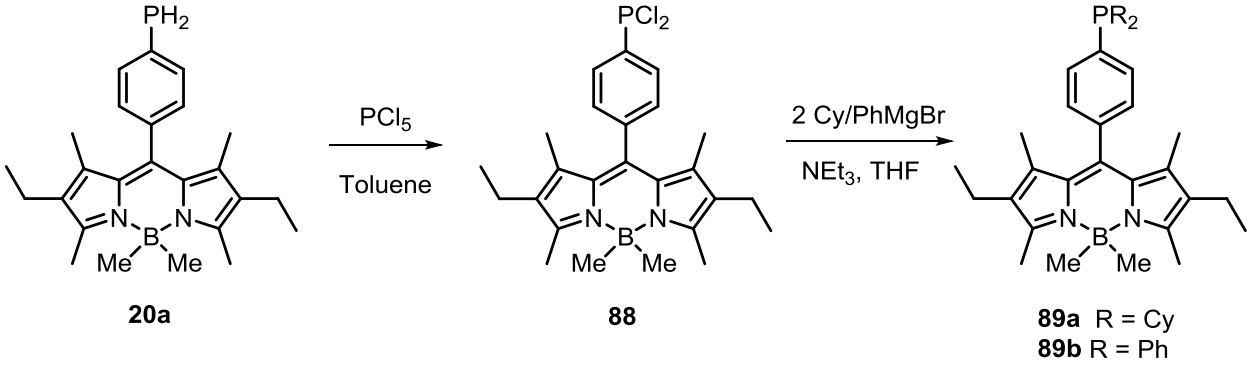

Scheme 3.5 Synthesis of the tertiary phosphines 89a and 89b from primary phosphine 20a.

Tertiary phosphines **89a** and **89b** were then reacted with the ruthenium(II) dimer precursors in the same manner as primary phosphine **20a** was, analysis by $^{31}P\{^{1}H\}$ NMR spectroscopy identified that the product peak had shifted downfield – implying complexation with ruthenium.

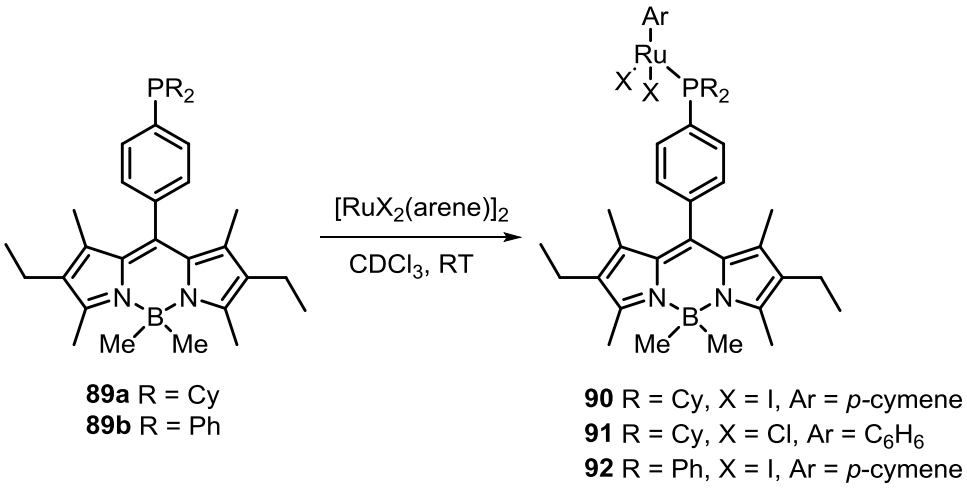

Scheme 3.6 Tertiary phosphines were reacted with ruthenium dimers to give novel complexes 90-92.

In general, the coordination of ruthenium to tertiary phosphines **89a** and **89b** causes a decrease in the fluorescence quantum yield, however, the complexes do still remain moderately fluorescent and could be useful for *in vitro* imaging. The Stokes' shift appears to increase in the complexes (19-23 nm) compared to the free tertiary phosphines (14 nm).

The future work for these compounds will include sending the complexes with the most interesting photophysical properties, such as 92, to Dyson and co-workers in Zurich to see how they compare to RAPTA-C complexes when tested *in vitro*. It would also be interesting to explore further the relationship between primary and tertiary phosphine complexes and the resulting photophysical complexes.

Table 3.5 Photophysical properties for tertiary phosphines 89a and 89b and their ruthenium phosphine complexes 90, 91 and 92.

	$\lambda_{abs\ (nm)}$	$\lambda_{em\ (nm)}$	Φ_F
Bod-PCy$_2$ 89a	512	526	0.44
Bod-PPh$_2$ 89b	513	527	0.29
[RuI$_2$(89a)(*p*-cymene)] 90	511	531	0.16
[RuCl$_2$(89a)(C$_6$H$_6$)] 91	513	531	0.19
[RuI$_2$(89b)(*p*-cymene)] 92	510	533	0.04

Measured in dry, degassed tetrahydrofuran at room temperature, dyes were excited at 485 nm; Fluorescence quantum yields were measured with respect to 4,4-difluoro-8-phenyl-1,3,5,7-tetramethyl-2,6-diethyl-4-bora-3a,4a-diaza-s-indacene **57**.

3.6 Summary

This chapter has explored the coordination of novel Bodipy primary phosphines with group 6 and 8 transition metals, for both a fundamental insight into their reactivity and coordination chemistry, but also to probe their photophysical properties and establish whether they can be used as *in vitro* imaging agents. The four primary phosphines were reacted with molybdenum and tungsten hexacarbonyl to form $[M(CO)_5(RPH_2)]$ complexes. We have demonstrated that the air-stability of these primary phosphines does not hinder their reactivity in transition metal coordination chemistry. All of the novel complexes were characterised by IR and NMR spectroscopy and one tungsten complex (**63**) was also successfully analysed by X-ray crystallography. The group 6 complexes retained high quantum yields with respect to the free primary phosphine ligands, with only a relatively slight decrease observed. The extinction coefficients were only slightly decreased by the metal coordination and the absorption and emission maxima were only marginally altered by 1-2 nm.

Primary phosphines **20a**, **20b**, **50** and **56** were also reacted with four ruthenium(II) dimers, $[RuCl_2(C_6H_6)]_2$, $[RuCl_2(p\text{-cymene})]_2$, $[RuI_2(C_6H_6)]_2$ and $[RuI_2(p\text{-cymene})]_2$ to form a library of novel ruthenium phosphine complexes. The compounds were analysed by NMR spectroscopy and several complexes were characterised by X-ray crystallography. In these cases, the complexation caused a significant decrease in the fluorescence quantum yields compared to the uncomplexed primary phosphines. The absorption and emission maxima remained similar to the free primary phosphine whereas the extinction coefficients gave slightly lower values than the free phosphine.

DFT calculations were performed in order to try and understand why the ruthenium complexes quench the fluorescence more than the molybdenum and tungsten complexes. The molybdenum and tungsten complexes displayed a Bodipy-based HOMO and LUMO whereas the ruthenium complexes exhibited a Bodipy-based HOMO and a metal-based LUMO. This would suggest that the ruthenium metal orbitals are involved in the fluorescence process, possibly in a MLCT process, which may identify why a bigger increase in fluorescence quenching is observed for them.

Tertiary phosphines **89a** and **89b** were also coordinated to ruthenium dimers $[RuI_2(p\text{-cymene})]_2$ and $[RuCl_2(C_6H_6)]_2$ to form fluorescent ruthenium-phosphine complexes, which could be tested in cells for anti-cancer properties and be compared to RAPTA-C. These tertiary phosphines are of key importance in Chapter 4 where the synthesis of a range of phosphonium salts is discussed, for applications in mitochondrial imaging.

3.7 Experimental

3.7.1 General procedure

All air- and/or water-sensitive reactions were performed under a nitrogen atmosphere using standard Schlenk line techniques. Tetrahydrofuran and toluene were dried over sodium/benzophenone and sodium, respectively, and dichloromethane was dried over calcium hydride – these solvents were distilled prior to use. Solvents used for column chromatography were not anhydrous. All starting materials were purchased from Aldrich, Acros Organics, Alfa Aesar, or Strem and used as received. The ruthenium complexes and $[Mo(CO)_6]$ and $[W(CO)_6]$ were used as received, other than $[RuI_2(C_6H_6)]_2$ which was synthesised following the published literature procedure.[113] Flash chromatography was performed on silica gel from Fluorochem (silica gel, 40–63 u, 60 A). Thin-layer chromatography was carried out on Fisher aluminium-based plates with silica gel and fluorescent indicator (254 nm). ^{1}H, $^{13}C\{^{1}H\}$, $^{31}P\{^{1}H\}$, ^{31}P-^{1}H, and $^{11}B\{^{1}H\}$ NMR spectra were recorded on a JEOL Lambda 500 (^{1}H 500.16 MHz), JEOL ECS-400 (^{1}H 399.78 MHz), or Bruker Avance III 300 (^{1}H 300.13 Hz) spectrometer at room temperature (21 °C); ^{1}H and ^{13}C shifts are reported relative to tetramethylsilane, ^{31}P relative to 80% H_3PO_4, ^{11}B relative to $BF_3.Et_2O$ and ^{19}F relative to $CFCl_3$. Infrared spectra were recorded on a Varian 800 FT-IR spectrometer and mass spectrometry was carried out by the EPSRC NMSF, Swansea. DFT calculations were carried out on Spartan 14 using the B3LYP functional with a 6-31G* basis set, details of the xyz coordinates and SCF energies can be found in the appendix.

3.7.2 $[Mo(CO)_5(20a)]$ (62)

A solution of $[Mo(CO)_6]$ (0.066 g, 0.25 mmol) in anhydrous THF (15 mL) was irradiated with UV light in a quartz vessel under a stream of nitrogen at room temperature for one hour. Primary phosphine **20a** (0.100 g, 0.25 mmol) in anhydrous THF (15 mL) was added and the mixture was stirred for a further thirty minutes. The solvent was removed and the red product was purified by column chromatography (hexane:chloroform, 4:1), to yield the intended product as an orange solid (0.041 g, 26%).

^{1}H NMR (300 MHz, $CDCl_3$) δ 7.66 (m, 2H), 7.42 (m, 2H), 5.56 (d, $^{1}J_{HP}$ = 326.7 Hz, 2H), 2.45 (s, 6H), 2.31 (q, J = 7.5 Hz, 4H), 1.25 (s, 6H), 0.99 (t, J = 7.5 Hz, 6H), 0.28 (s, 6H) ppm; **$^{13}C\{^{1}H\}$ NMR** (75 MHz, $CDCl_3$) δ 208.8 (d, $^{2}J_{CP}$ = 24.2 Hz), 204.7 (d, $^{2}J_{CP}$ = 9.8 Hz), 151.2, 139.9, 138.7, 133.6, 132.9, 132.7 (d, J_{CP} = 11.7 Hz), 130.0 (d, J_{CP} = 10.6 Hz), 128.8, 126.8 (d, $^{1}J_{CP}$ = 42.3 Hz),

17.6, 14.8, 14.5, 12.1, 10.4 (br) ppm; **^{31}P-^{1}H NMR** (121 MHz, $CDCl_3$) δ −63.5 (tt, $^{1}J_{PH}$ = 326.7 Hz, $^{3}J_{PH}$ = 11.8 Hz) ppm; **^{11}B{^{1}H} NMR** (96 MHz, $CDCl_3$) δ −2.2 ppm; **IR** (neat) $\tilde{\nu}$: 2962, 2929, 2868, 2076, 1992, 1929 cm^{-1}; **HRMS** ($APCI^+$) calcd. for $C_{30}H_{35}B_1N_2P_1O_5Mo_1$ $[M + H]^+$ requires *m/z* 636.1476, found 636.1493.

3.7.3 [W(CO)$_5$(20a)] (63)

A solution of $[W(CO)_6]$ (0.050 g, 0.14 mmol) in anhydrous THF (15 mL) was irradiated with UV light in a quartz vessel under a stream of nitrogen at room temperature for one hour. Primary phosphine **20a** (0.057 g, 0.14 mmol) in anhydrous THF (15 mL) was added and the mixture was stirred for a further thirty minutes. The solvent was evaporated and purified by column chromatography (hexane:chloroform, 4:1) which yielded a red solid (0.018 g, 18%).

^{1}H NMR (300 MHz, $CDCl_3$) δ 7.67 (m, 2H), 7.46 (m, 2H), 5.91 (d, $^{1}J_{HP}$ = 340.3 Hz, 2H), 2.46 (s, 6H), 2.32 (q, J = 7.6 Hz, 4H), 1.25 (s, 6H), 0.99 (t, J = 7.6 Hz, 6H), 0.29 (s, 6H) ppm; **^{13}C{^{1}H} NMR** (75 MHz, $CDCl_3$) δ 198.3 (d, $^{2}J_{CP}$ = 23.1 Hz), 195.5 (d, $^{2}J_{CP}$ = 7.2 Hz), 151.3, 140.2, 138.5, 133.6, 132.9, 132.8 (d, J_{CP} = 11.3 Hz), 130.1 (d, J_{CP} = 10.5 Hz), 128.8, 126.1 (d, $^{1}J_{CP}$ = 47.3 Hz), 17.6, 14.8, 14.5, 12.2, 10.5 (br) ppm; **^{31}P-^{1}H NMR** (121 MHz, $CDCl_3$) δ −85.7 (tt, $^{1}J_{PH}$ = 340.6 Hz, $^{3}J_{PH}$ = 12.1 Hz, $^{1}J_{PW}$ = 222.9 Hz) ppm; **^{11}B{^{1}H} NMR** (96 MHz, $CDCl_3$) δ −1.6 ppm; **IR** (neat) $\tilde{\nu}$: 2958, 2926, 2869, 2077, 1973, 1902 cm^{-1}; **HRMS** ($APCI^+$) calcd. for $C_{30}H_{35}N_2O_5P_1{}^{10}B_1{}^{182}W_1$ $(M + H)^+$ requires *m/z* 726.1890, found 726.1902.

3.7.4 [Mo(CO)$_5$(20b)] (64)

A solution of $[Mo(CO)_6]$ (0.015 g, 0.056 mmol) in anhydrous THF (8 mL) was irradiated with UV light in a quartz vessel under a stream of nitrogen at room temperature for 45 minutes. A solution of **20b** (0.030 g, 0.056 mmol) in THF (8 mL) was added and the reaction was stirred for a further 30 minutes. The solvent was removed and the orange solid was purified by column chromatography (petrol:chloroform, 4:1) to yield the product as an orange solid (8 mg, 19%).

^{1}H NMR (300 MHz, $CDCl_3$) δ 7.63-7.58 (m, 2H), 7.40-7.37 (m, 4H), 7.28-7.16 (m, 8H), 4.11 (d, $^{1}J_{HP}$ = 202.5 Hz, 2H), 2.21 (q, $^{3}J_{HH}$ = 7.3 Hz, 4H), 1.76 (s, 6H), 1.31 (s, 6H), 0.90 (t, $^{3}J_{HH}$ = 7.3 Hz, 6H) ppm; **^{13}C{^{1}H} NMR** (75 MHz, $CDCl_3$) δ 208.4 (d, $^{2}J_{CP}$ = 24.2 Hz), 203.5 (d, $^{2}J_{CP}$ = 8.9 Hz), 153.0, 150.3, 139.9, 136.8, 135.1, 134.9 (d, J_{CP} = 15.3 Hz), 133.8, 132.8, 130.6, 129.0, 128.8 (d, J_{CP} = 5.6 Hz), 127.1, 125.4, 17.3, 14.7, 14.5, 12.1 ppm; **^{31}P-^{1}H NMR** (121 MHz, $CDCl_3$) δ –64.2

(tt, $^{1}J_{PH}$ = 330.5 Hz, $^{3}J_{PH}$ = 11.7 Hz) ppm; **^{11}B{^{1}H} NMR** (96 MHz, $CDCl_3$) δ 1.7 ppm; **IR** (neat) $\tilde{\nu}$: 2961, 2923, 2858, 2077, 1945, 1917 cm^{-1}.

3.7.5 [W(CO)$_5$(20b)] (65)

A solution of [$W(CO)_6$] (0.020 g, 0.056 mmol) in anhydrous THF (8 mL) was irradiated with UV light in a quartz vessel under a stream of nitrogen at room temperature for 30 minutes. A solution of **20b** (0.030 g, 0.056 mmol) in THF (8 mL) was added and the reaction was stirred for a further 30 minutes. The solvent was removed and the orange solid was purified by column chromatography (petrol:chloroform, 4:1) to yield the product as an orange solid (18 mg, 38 %).

^{1}H NMR (300 MHz, $CDCl_3$) δ 7.63-7.58 (m, 2H), 7.40-7.37 (m, 4H), 7.28-7.16 (m, 8H), 4.11 (d, $^{1}J_{HP}$ = 202.5 Hz, 2H), 2.21 (q, $^{3}J_{HH}$ = 7.3 Hz, 4H), 1.76 (s, 6H), 1.31 (s, 6H), 0.90 (t, $^{3}J_{HH}$ = 7.3 Hz, 6H) ppm; **^{13}C{^{1}H} NMR** (75 MHz, $CDCl_3$) δ 198.2 (d, $^{2}J_{CP}$ = 22.8 Hz), 194.3 (d, $^{2}J_{CP}$ =7.1 Hz), 153.0, 150.3, 139.9, 136.8, 135.1, 134.9 (d, J_{CP} = 15.3 Hz), 133.8, 132.8, 130.6, 129.0, 128.8 (d, J_{CP} = 5.6 Hz), 127.1, 125.4, 17.3, 14.7, 14.5, 12.1 ppm; **^{31}P-^{1}H NMR** (121 MHz, $CDCl_3$) δ –85.7 (tt, $^{1}J_{PH}$ = 342.5 Hz, $^{3}J_{PH}$ = 12.3 Hz, $^{1}J_{PW}$ = 223.3 Hz) ppm; **^{11}B{^{1}H} NMR** (96 MHz, $CDCl_3$) δ 1.7 ppm; **IR** (neat) $\tilde{\nu}$: 2962, 2910, 2360, 2076, 1969, 1921 cm^{-1}.

3.7.6 [Mo(CO)$_5$(50)] (66)

A solution of [$Mo(CO)_6$] (0.025 g, 0.094 mmol) in anhydrous THF (10 mL) was irradiated with UV light in a quartz vessel under a stream of nitrogen at room temperature for 45 minutes. A solution of **50** (0.040 g, 0.094 mmol) in THF (10 mL) was added and the reaction was stirred for a further 30 minutes. The solvent was removed and the orange solid was purified by column chromatography (petrol:chloroform, 4:1) to yield the product as an orange solid (11 mg, 16%).

^{1}H NMR (300 MHz, $CDCl_3$) δ 7.66 (m, 2H), 7.40 (m, 2H), 5.54 (d, $^{1}J_{HP}$ = 327.3 Hz, 2H), 2.74 (s, 6H), 2.33 (q, J = 7.5 Hz, 4H), 2.23 (s, 2H), 1.25 (s, 6H), 0.97 (t, J = 7.5 Hz, 6H) ppm; **^{13}C{^{1}H} NMR** (75 MHz, $CDCl_3$) δ 207.7 (d, $^{2}J_{CP}$ = 24.1 Hz), 203.5 (d, $^{2}J_{CP}$ = 8.9 Hz), 154.3, 139.6, 136.3, 136.2, 133.4, 133.3, 132.8 (d, J_{CP} = 11.8 Hz), 129.7 (d, J_{CP} = 10.5 Hz), 128.7, 103.9, 98.4, 17.4, 14.8, 14.1, 12.0 ppm; **^{31}P-^{1}H NMR** (121 MHz, $CDCl_3$) δ −64.0 (tt, $^{1}J_{PH}$ = 327.1 Hz, $^{3}J_{PH}$ = 12.4 Hz) ppm; **^{11}B{^{1}H} NMR** (96 MHz, $CDCl_3$) δ −13.9 ppm; **IR** (neat) $\tilde{\nu}$: 3295, 2962, 2925, 2854, 2360, 2076, 1994, 1928, 699 cm^{-1}.

3.7.7 [W(CO)$_5$(50)] (67)

A solution of [W(CO)$_6$] (0.042 g, 0.118 mmol) in anhydrous THF (15 mL) was irradiated with UV light in a quartz vessel under a stream of nitrogen at room temperature for 45 minutes. A solution of **50** (0.050 g, 0.118 mmol) in THF (15 mL) was added and the reaction was stirred for a further 30 minutes. The solvent was removed and the orange solid was purified by column chromatography (petrol:chloroform, 4:1) to yield the product as an orange solid (15 mg, 20%).

^{1}H NMR (300 MHz, $CDCl_3$) δ 7.65 (m, 2H), 7.44 (m, 2H), 5.89 (d, $^1J_{HP}$ = 339.4 Hz, 2H), 2.75(s, 6H), 2.32 (q, J = 7.8 Hz, 4H), 2.23 (s, 2H), 1.25 (s, 6H), 0.99 (t, J = 7.5 Hz, 6H) ppm; **^{13}C{^{1}H} NMR** (75 MHz, $CDCl_3$) δ 198.0 (d, $^2J_{CP}$ = 22.6 Hz), 195.3 (d, $^2J_{CP}$ = 7.0 Hz), 154.4, 139.1, 138.1, 136.3, 133.5, 132.8 (d, J_{CP} = 11.4 Hz), 129.8 (d, J_{CP} = 10.3 Hz), 128.8, 126.5, 100.1, 83.1, 17.4, 14.8, 14.1, 12.1 ppm; **^{31}P-^{1}H NMR** (121 MHz, $CDCl_3$) δ −85.6 (tt, $^1J_{PH}$ = 342.1 Hz, $^3J_{PH}$ = 12.7 Hz, $^1J_{PW}$ = 223.10 Hz) ppm; **^{11}B{^{1}H} NMR** (96 MHz, $CDCl_3$) δ −13.9 ppm; **IR** (neat) $\tilde{\nu}$: 3295, 2958, 2854, 2924, 2360, 2075, 1972, 1914, 698 cm^{-1}.

3.7.8 [Mo(CO)$_5$(56)] (68)

A solution of [Mo(CO)$_6$] (0.027 g, 0.047 mmol) in anhydrous THF (10 mL) was irradiated with UV light in a quartz vessel under a stream of nitrogen at room temperature for 45 minutes. A solution of **56** (0.013 g, 0.047 mmol) in THF (10 mL) was added and the reaction was stirred for a further 30 minutes. The solvent was removed and the orange solid was purified by column chromatography (petrol:chloroform, 4:1) to yield the product as an orange solid (12 mg, 31%).

^{1}H NMR (300 MHz, $CDCl_3$) δ 7.53 (m, 2H), 7.35-7.32 (m, 2H), 7.21-7.12 (m, 10H), 4.08 (d, $^1J_{HP}$ = 202.8 Hz, 2H), 2.79 (s, 6H), 2.30 (q, $^3J_{HH}$ = 7.6 Hz, 4H), 1.24 (s, 6H), 0.95 (t, $^3J_{HH}$ = 7.5 Hz, 6H) ppm; **^{13}C{^{1}H} NMR** (75 MHz, $CDCl_3$) δ 208.2 (d, J_{CP} = 24.2 Hz), 204.4 (d, J_{CP} = 9.2 Hz), 154.0, 139.5, 136.5, 136.3, 135.2, (d, J_{CP} = 16.3 Hz), 133.0, 131.7, 129.1, 128.8 (d, J_{CP} = 5.7 Hz), 128.1, 127.1, 125.7, 60.5, 41.5, 22.8, 17.6, 14.9, 14.1, 12.2 ppm; **^{31}P-^{1}H NMR** (121 MHz, $CDCl_3$) δ –64.7 (tt, $^1J_{PH}$ = 327.9 Hz, $^3J_{PH}$ = 11.8 Hz) ppm; **^{11}B{^{1}H} NMR** (96 MHz, $CDCl_3$) δ –12.5 ppm; **IR** (neat) $\tilde{\nu}$: 3574, 2962, 2930, 2845, 2358, 2077, 1989, 1924 cm^{-1}.

3.7.9 [W(CO)$_5$(56)] (69)

A solution of [W(CO)$_6$] (0.018 g, 0.052 mmol) in anhydrous THF (8 mL) was irradiated with UV light in a quartz vessel under a stream of nitrogen at room temperature for 30 minutes. A solution of **56** (0.030 g, 0.052 mmol) in THF (8 mL) was added and the reaction was stirred for a further 30

minutes. The solvent was removed and the orange solid was purified by column chromatography (petrol:chloroform, 4:1) to yield the product as an orange solid (13 mg, 28%).

^{1}H NMR (300 MHz, $CDCl_3$) δ 7.53 (m, 2H), 7.35-7.32 (m, 2H), 7.21-7.12 (m, 10H), 4.12 (d, $^{1}J_{HP}$ = 342.3 Hz, 2H), 2.79 (s, 6H), 2.30 (q, $^{3}J_{HH}$ = 7.6 Hz, 4H), 1.24 (s, 6H), 0.95 (t, $^{3}J_{HH}$ = 7.5 Hz, 6H) ppm; **^{13}C{^{1}H} NMR** (75 MHz, $CDCl_3$) δ 198.3 (d, $^{2}J_{CP}$ = 22.9 Hz), 194.3 (d, $^{2}J_{CP}$ = 6.9 Hz), 154.5, 139.3, 138.9, 136.0, 133.2, 132.8 (d, J_{CP} = 11.6 Hz), 131.6, 129.8 (d, J_{CP} = 10.8 Hz), 128.9, 128.1, 127.1, 125.5, 104.0, 103.2, 100.1, 17.5, 14.9, 14.1, 12.1 ppm; **^{31}P-^{1}H NMR** (121 MHz, $CDCl_3$) δ –85.7 (tt, $^{1}J_{PH}$ = 342.3 Hz, $^{3}J_{PH}$ = 12.4 Hz, $^{1}J_{PW}$ = 222.8 Hz) ppm; **^{11}B{^{1}H} NMR** (96 MHz, $CDCl_3$) δ –12.6 ppm; **IR** (neat) $\tilde{\nu}$: 3648, 2960, 2922, 2852, 2360, 2075, 1974, 1915 cm^{-1}.

3.7.10 [Mo(CO)$_4$(20a)$_2$] (70)

cis-[$Mo(CO)_4(pip)_2$] (0.070 g, 0.19 mmol) and 8-((4-phosphino)phenyl)-4,4-dimethyl-1,3,5,7-tetramethyl-2,6-diethyl-4-bora-3a,4a-diaza-s-indacene (0.150 g, 0.37 mmol) were dissolved in anhydrous dichloromethane (6 mL) under nitrogen. The reaction was refluxed for two hours and analysed by $^{31}P\{^{1}H\}$ NMR spectroscopy. The complex was purified by column chromatography on silica gel (petroleum ether/dichloromethane 3:1, R_f = 0.4) to yield an orange solid (0.120 g, 63%). A sample suitable for X-ray crystallographic analysis was obtained from chloroform/pentane. **^{1}H NMR** (400 MHz, $CDCl_3$) δ 7.64 (dd, $^{3}J_{HH}$ = 7.8 Hz, $^{3}J_{HP}$ = 11.5 Hz, 4H), 7.26 (dd, $^{3}J_{HH}$ = 7.8 Hz, $^{4}J_{HP}$ = 1.4 Hz, 4H), 5.50 (dd, $^{1}J_{HP}$ = 318.9 Hz, $^{3}J_{HP}$ = 8.7 Hz, 4H), 2.44 (s, 12H), 2.29 (q, $^{3}J_{HH}$ = 7.8 Hz, 8H), 1.22 (s, 12H), 0.96 (t, $^{3}J_{HH}$ = 7.8 Hz, 12H), 0.26 (s, 12H) ppm; **^{13}C{^{1}H} NMR** (100 MHz, $CDCl_3$) δ 213.2 (m, CO), 207.8 (*pseudo* t, $^{2}J_{CP}$ = 9.6 Hz, CO), 151.1, 139.5, 138.8, 133.5, 132.9 (*pseudo* t, J_{CP} = 4.8 Hz), 132.8, 129.8 (*pseudo* t, J_{CP} = 4.8 Hz), 128.8, 127.2 (m), 17.5, 14.7, 14.4, 12.1, 10.4 (br) ppm; **^{31}P-^{1}H NMR** (202 MHz, $CDCl_3$) δ −56.1 (m) ppm; **^{11}B{^{1}H} NMR** (128 MHz, $CDCl_3$) δ −1.8 ppm; **IR** (neat): $\tilde{\nu}$ = 2360 (w, PH), 2332 (w, PH), 2029 (s, CO), 1947 (s, CO), 1919 (s, CO), 1896 (s) (CO) cm^{-1}; **HRMS** (ESI^{+}) calcd for $C_{54}H_{69}B_2N_4P_2O_4Mo_1$ $[M+H]^{+}$ requires m/z 1012.4084, found *m/z* 1012.4078 (0.6 ppm).

3.7.11 [W(CO)$_4$(20a)$_2$] (71)

cis-[$W(CO)_4(pip)_2$] (0.057 g, 0.126 mmol) and 8-((4-phosphino)phenyl)-4,4-dimethyl-1,3,5,7-tetramethyl-2,6-diethyl-4-bora-3a,4a-diaza-s-indacene (0.100 g, 0.247 mmol) were dissolved in anhydrous toluene (5 mL) under nitrogen. The reaction was heated to 75°C for 20 hours and the

solvent was evaporated. The complex was purified by column chromatography on silica gel (petroleum ether/dichloromethane 5:1, R_f = 0.2) to yield an orange solid (0.092 g, 67%). **^{1}H NMR** (400 MHz, $CDCl_3$) δ 7.64 (dd, $^3J_{HH}$ = 7.9 Hz, $^3J_{HP}$ = 11.8 Hz, 4H), 7.42 (dd, $^3J_{HH}$ = 7.9 Hz, $^4J_{HP}$ = 1.6 Hz, 4H), 5.79 (d, $^1J_{HP}$ = 388.9 Hz, 4H), 2.44 (s, 12H), 2.29 (q, $^3J_{HH}$ = 7.6 Hz, 8H), 1.24 (s, 12H), 0.96 (t, $^3J_{HH}$ = 7.6 Hz, 12H), 0.26 (s, 12H) ppm; **^{13}C{^{1}H} NMR** (100 MHz, $CDCl_3$) δ 203.5 (m, CO), 199.3 (*pseudo* t, $^2J_{CP}$ = 7.3 Hz, CO), 151.2, 139.7, 138.6, 133.4, 132.9 (*pseudo* t, J_{CP} = 5.7 Hz), 132.7, 129.8 (*pseudo* t, J_{CP} = 4.3 Hz), 128.7, 126.9, 17.4, 14.7, 14.3, 12.0, 10.4 (br) ppm; **^{31}P-^{1}H NMR** (202 MHz, $CDCl_3$) δ −76.9 (m) ppm; **^{31}P{^{1}H} NMR** (202 MHz, $CDCl_3$) δ −76.9 ($^1J_{PW}$ = 217.4 Hz) ppm; **^{11}B{^{1}H} NMR** (128 MHz, $CDCl_3$) δ −2.0 ppm; **IR** (neat): $\tilde{\nu}$ = 2961 (w), 2926 (w), 2870 (w), 2359 (w, PH), 2341 (w, PH), 2026 (s, CO), 1940 (s, CO), 1912 (s, CO), 1888 (s, CO), 1549 (s), 1454 (m), 1404 (m), 1360 (m), 1319 (s), 1262 (m), 1171 (s), 1145 (s), 1112 (m), 1020 (m), 981 (m), 944 (s), 884 (s), 795 (s) cm^{-1}; **HRMS** (ESI$^+$) calcd for $C_{54}H_{68}B_2N_4P_2O_4W_1$ $[M]^+$ requires m/z 1102.4507, found *m*/*z* 1102.4486 (1.9 ppm).

3.7.12 [RuCl$_2$(η^6-C$_6$H$_6$)(20a)] (72)

20a (0.050 g, 0.12 mmol) and dichloro(benzene)ruthenium(II) dimer (0.030 g, 0.06 mmol) were dissolved in $CDCl_3$ (3 mL) and stirred under nitrogen for one hour to yield an orange solid (0.078 g, 99%). A sample suitable for X-ray crystallographic analysis was obtained from chloroform/hexane. **^{1}H NMR** (500 MHz, $CDCl_3$) δ 7.98 (dd, $^3J_{HH}$ = 7.8 Hz, $^3J_{HP}$ = 11.8 Hz, 2H), 7.48 (dd, $^3J_{HH}$ = 7.8 Hz, $^4J_{HP}$ = 1.4 Hz, 2H), 5.87 (d, $^1J_{HP}$ = 397.2 Hz, 2H), 5.58 (s, 6H), 2.45 (s, 6H), 2.30 (q, $^3J_{HH}$ =7.7 Hz, 4H), 1.28 (s, 6H), 0.97 (t, $^3J_{HH}$ = 7.7 Hz, 6H), 0.27 (s, 6H) ppm; **^{13}C{^{1}H} NMR** (100 MHz, $CDCl_3$) δ 151.4, 141.1, 138.3, 133.0 (d, J_{CP} = 5.8 Hz), 132.8 (d, J_{CP} = 8.4 Hz), 130.1 (d, J_{CP} = 11.4 Hz), 128.6, 128.1, 127.1, 88.0 (d, J_{CP} = 3.8 Hz), 17.5, 14.8, 14.5, 12.1, 10.4 (br) ppm; **^{31}P-^{1}H NMR** (162 MHz, $CDCl_3$) δ −31.3 (tt, $^1J_{PH}$ = 397.2 Hz, $^3J_{PH}$ = 10.7 Hz) ppm; **^{11}B{^{1}H} NMR** (128 MHz, $CDCl_3$) δ −1.8 (s) ppm; **IR** (neat) $\tilde{\nu}$: 2963, 2928, 2870, 2359 (w, PH), 2343 (w, PH), 1549, 1435, 1360, 1317, 1262, 1172, 1145, 1111, 1021, 981, 944, 877, 795 cm^{-1}; **HRMS** (ESI$^+$) calcd. for $C_{31}H_{40}B_1N_2P_1Cl_2RuNa$ $[M+Na]^+$ requires m/z 677.1348, found *m*/*z* 677.1381.

3.7.13 [RuCl$_2$(*p*-cymene)(20a)] (73)

20a (0.060 g, 0.15 mmol) and dichloro(*p*-cymene)ruthenium(II) dimer (0.046 g, 0.075 mmol) were dissolved in $CDCl_3$ (3 mL) and stirred at room temperature under nitrogen for one hour. The solvent

was removed to give an orange solid (0.098 g, 93%). **^{1}H NMR** (500 MHz, $CDCl_3$) δ 7.95 (m, 2H), 7.48 (m, 2H), 5.76 (d, $^{1}J_{HP}$ = 390.1 Hz, 2H), 5.38 ($^{3}J_{HH}$ = 5.9 Hz, 2H), 5.21 ($^{3}J_{HH}$ = 5.9 Hz, 2H), 2.78 (m, 1H), 2.46 (s, 6H), 2.30 (q, $^{3}J_{HH}$ = 7.4 Hz, 4H), 2.14 (s, 3H), 1.29 (s, 6H), 1.25 (d, $^{3}J_{HH}$ = 6.9 Hz, 6H), 0.99 (t, *J* = 7.4 Hz, 6H), 0.28 (s, 6H) ppm; **^{13}C{^{1}H} NMR** (100 MHz, $CDCl_3$) δ 151.4, 140.9, 138.4, 133.1 (d, J_{CP} = 8.5 Hz), 132.9 (d, J_{CP} = 8.5 Hz), 130.0 (d, J_{CP} = 10.1 Hz), 128.7, 127.8, 127.4, 106.4, 100.9, 87.1 (d, $^{2}J_{CP}$ = 4.9 Hz), 86.4 (d, $^{2}J_{CP}$ = 4.2 Hz), 31.1, 22.3, 18.7, 17.5, 14.8, 14.5, 12.2, 10.5 (br) ppm; **^{31}P-^{1}H NMR** (162 MHz, $CDCl_3$) δ −29.5 (tt, $^{1}J_{PH}$ = 390.8 Hz, $^{3}J_{PH}$ = 11.5 Hz) ppm; **^{11}B{^{1}H} NMR** (128 MHz, $CDCl_3$) δ −1.5 (s) ppm.

3.7.14 [$RuI_2(\eta^6\text{-}C_6H_6)$(20a)] (74)

20a (0.050 g, 0.12 mmol) and diiodo(benzene)ruthenium(II) dimer (0.053 g, 0.062 mmol) were dissolved in anhydrous DCM (3 mL) and stirred at 60°C under nitrogen for two hours. The solvent was removed to give an orange solid (0.088 g, 93%). **^{1}H NMR** (300 MHz, $CDCl_3$) δ 8.01 (m, 2H), 7.48 (m, 2H), 7.07 (d, $^{1}J_{HP}$ = 398.3 Hz, 2H), 5.66 (s, 6H), 2.46 (s, 6H), 2.32 (q, *J* = 7.6 Hz, 4H), 1.30 (s, 6H), 0.99 (t, *J* = 7.6 Hz, 6H), 0.29 (s, 6H) ppm; **^{13}C{^{1}H} NMR** (100 MHz, $CDCl_3$) δ 151.4, 141.0, 138.4, 133.1 (d, J_{CP} = 2.4 Hz), 132.7 (d, J_{CP} = 8.6 Hz), 131.3, 130.7, 130.1 (d, J_{CP} = 10.0 Hz), 128.7, 88.9 (d, $^{2}J_{CP}$ = 4.0 Hz), 17.6, 14.8, 14.5, 12.2, 10.6 (br) ppm; **^{31}P-^{1}H NMR** (121 MHz, $CDCl_3$) δ −49.8 (tt, $^{1}J_{PH}$ = 398.3 Hz, $^{3}J_{PH}$ = 11.4 Hz) ppm; **^{11}B{^{1}H} NMR** (96 MHz, $CDCl_3$) δ 0.6 (s) ppm; **HRMS** (NSI^+) calcd. for $C_{32}H_{43}B_1I_2N_2P_1Ru_1O_1$ $[M + OCH_3]^+$ requires m/z 862.0402, found *m*/*z* 862.0402.

3.7.15 [RuI_2(*p*-cymene)(20a)] (75)

20a (0.050 g, 0.12 mmol) and diiodo(*p*-cymene)ruthenium(II) dimer (0.060 g, 0.062 mmol) were dissolved in $CDCl_3$ (3 mL) and stirred under nitrogen for one hour, the solvent was removed to give an orange solid (0.12 g, 95%). A sample suitable for X-ray crystallographic analysis was obtained via slow diffusion of pentane/chloroform. **^{1}H NMR** (500 MHz, $CDCl_3$) δ 7.99 (m, 2H), 7.45 (m, 2H), 6.54 (d, $^{1}J_{HP}$ = 392.2 Hz, 2H), 5.40 (d, $^{3}J_{HH}$ = 5.9 Hz, 2H), 5.23 (d, $^{3}J_{HH}$ = 5.9 Hz, 2H), 2.99 (m, 1H), 2.46 (s, 6H), 2.36 (s, 3H), 2.30 (q, $^{3}J_{HH}$ =7.6 Hz, 4H), 1.28 (s, 6H), 1.25 (d, $^{3}J_{HH}$ =7.6 Hz, 6H), 0.98 (t, *J* = 7.6 Hz, 6H), 0.27 (s, 6H) ppm; **^{13}C{^{1}H} NMR** (100 MHz, $CDCl_3$) δ 151.3, 140.8, 138.5, 133.3 (d, J_{CP} = 8.1 Hz), 131.1 (d, J_{CP} = 11.5 Hz), 131.0, 130.7, 129.8 (d, J_{CP} = 9.7 Hz), 128.7, 109.6 (d, J_{CP} = 3.3 Hz), 101.6 (d, J_{CP} = 3.3 Hz), 87.8 (d, J_{CP} = 3.6 Hz), 86.9 (d, J_{CP} = 3.6 Hz), 32.0, 22.8, 20.2, 17.5, 14.8, 14.4, 12.2, 10.4 (br) ppm; **^{31}P-^{1}H NMR** (162 MHz, $CDCl_3$) δ −43.7 (tt, $^{1}J_{PH}$ = 392.2 Hz, $^{3}J_{PH}$ = 10.9) ppm; **^{11}B{^{1}H} NMR** (128 MHz, $CDCl_3$) δ −1.8 (s) ppm;

IR (neat) $\tilde{\nu}$: 2962, 2930, 2867, 2359, 2341, 1550, 1453, 1364, 1320, 1262, 1171, 1144, 1111, 1024, 981, 944, 887, 796 cm^{-1}; **HRMS** (ESI^+) calcd. for $C_{35}H_{48}B_1N_2P_1I_2Ru_1$ $[M]^+$ requires m/z 889.0898, found *m*/*z* 889.0930.

3.7.16 [$RuCl_2(\eta^6\text{-}C_6H_6)$(20b)] (76)

20b (0.050 g, 0.095 mmol) and dichloro(benzene)ruthenium(II) dimer (0.030 g, 0.060 mmol) were dissolved in $CDCl_3$ (3 mL) and stirred under nitrogen for one hour. The solvent was removed which gave an orange solid (0.070 g, 95%). **^{1}H NMR** (500 MHz, $CDCl_3$) δ 8.04 (m, 2H), 7.52 (m, 2H), 7.38 (m, 4H), 7.16-7.26 (m, 6H), 5.95 (d, $^1J_{HP}$ = 395.8 Hz, 2H), 5.63 (s, 6H), 2.20 (q, $^3J_{HH}$ = 7.4 Hz, 4H), 1.77 (s, 6H), 1.35 (s, 6H), 0.89 (t, $^3J_{HH}$ = 7.4 Hz, 6H) ppm; **^{13}C{^{1}H} NMR** (100 MHz, $CDCl_3$) δ 153.8, 150.1 (br), 140.7, 138.7, 134.6, 133.9, 133.4, 133.0 (d, J_{CP} = 8.6 Hz), 130.4, 130.2 (d, J_{CP} = 10.0 Hz), 127.9, 127.4, 125.7, 88.1, 17.5, 14.9, 14.4, 12.4 ppm; **^{31}P-^{1}H NMR** (162 MHz, $CDCl_3$) δ −31.4 (tt, $^1J_{PH}$ = 395.8 Hz, $^3J_{PH}$ = 10.9 Hz) ppm; **^{11}B{^{1}H} NMR** (128 MHz, $CDCl_3$) δ −0.9 (s) ppm; **IR** (neat) $\tilde{\nu}$: 2962, 2926, 2870, 2358 (w, PH), 2340 (w, PH), 1546, 1472, 1433, 1396, 1360, 1304, 1263, 1172, 1143, 1111, 1061, 1016, 973, 881, 772 cm^{-1}; **HRMS** (ESI^+) calcd. for $C_{41}H_{44}B_1N_2P_1Cl_2Ru_1Na$ $[M+Na]^+$ requires m/z 802.1743, found *m*/*z* 802.1758.

3.7.17 [$RuCl_2(\eta^6$-*p*-cymene)(20b)] (77)

20b (0.050 g, 0.095 mmol) and dichloro(*p*-cymene)ruthenium(II) dimer (0.028 g, 0.047 mmol) were dissolved in $CDCl_3$ (3 mL) and stirred at room temperature under nitrogen for one hour. The solvent was removed to give an orange solid (0.098 g, 93%). **^{1}H NMR** (300 MHz, $CDCl_3$) δ 7.99 (m, 2H), 7.61 (m, 1H), 7.49 (m, 1H), 7.25-7.06 (m, 6H), 5.77 (d, $^1J_{HP}$ = 390.0 Hz, 2H), 5.39 ($^3J_{HH}$ = 5.5 Hz, 2H), 5.23 ($^3J_{HH}$ = 6.2 Hz, 2H), 2.79 (m, 1H), 2.27 (q, $^3J_{HH}$ = 7.8 Hz, 4H), 2.22 (s, 6H), 2.16 (s, 3H), 1.37 (s, 6H), 1.27 (d, $^3J_{HH}$ = 6.6 Hz, 6H), 0.92 (t, J = 7.4 Hz, 6H) ppm; **^{13}C{^{1}H} NMR** (75 MHz, $CDCl_3$) δ 154.7, 152.5, 140.2, 138.8, 134.1, 133.3, 133.1, 132.5, 130.0 (d, J_{CP} = 10.0 Hz), 129.7 (d, J_{CP} = 10.0 Hz), 129.2, 127.3, 125.5, 106.4, 101.1, 87.1 (d, $^2J_{CP}$ = 4.9 Hz), 86.4 (d, $^2J_{CP}$ = 4.1 Hz), 31.1, 22.4, 17.4, 14.8, 15.0, 13.0, 12.1 ppm; **^{31}P-^{1}H NMR** (121 MHz, $CDCl_3$) δ−30.2 (tt, $^1J_{PH}$ = 390.0 Hz, $^3J_{PH}$ = 11.1 Hz) ppm; **^{11}B{^{1}H} NMR** (96 MHz, $CDCl_3$) δ −1.8 (s) ppm.

3.7.18 [$RuI_2(\eta^6\text{-}C_6H_6)$(20b)] (78)

20b (0.050 g, 0.095 mmol) and diiodo(benzene)ruthenium(II) dimer (0.040 g, 0.047 mmol) were dissolved in anhydrous DCM (3 mL) and stirred at 60°C under nitrogen for two hours. The solvent

was removed to give an orange solid (0.098 g, 93%). **^{1}H NMR** (300 MHz, $CDCl_3$) δ 8.06 (m, 2H), 7.57 (m, 4H), 7.44 (m, 2H), 7.24-7.10 (m, 6H), 7.06 (d, $^{1}J_{HP}$ = 398.5 Hz, 2H), 5.68 (s, 6H), 2.23 (s, 6H), 2.20 (q, $^{3}J_{HH}$ = 7.4 Hz, 4H), 1.35 (s, 6H), 0.90 (t, $^{3}J_{HH}$ = 7.4 Hz, 6H) ppm; **^{13}C{^{1}H} NMR** (100 MHz, $CDCl_3$) δ 153.8, 150.1 (br), 140.7, 138.7, 134.6, 133.9, 133.4, 133.0 (d, J_{CP} = 8.6 Hz), 130.4, 130.2 (d, J_{CP} = 10.0 Hz), 127.9, 127.4, 125.7, 88.1, 17.5, 14.9, 14.4, 12.4 ppm; **^{31}P-^{1}H NMR** (121 MHz, $CDCl_3$) δ −50.2 (tt, $^{1}J_{PH}$ = 398.5 Hz, $^{3}J_{PH}$ = 11.2 Hz) ppm; **^{11}B{^{1}H} NMR** (96 MHz, $CDCl_3$) δ 0.6 (s) ppm**.**

3.7.19 [RuI_2(*p*-cymene)(20b)] (79)

20b (0.050 g, 0.12 mmol) and diiodo(p-cymene)ruthenium(II) dimer (0.060 g, 0.062 mmol) were dissolved in $CDCl_3$ (3 mL) and stirred under nitrogen for one hour. The solvent was removed to give an orange solid (0.118 g, 97%). **^{1}H NMR** (500 MHz, $CDCl_3$) δ 8.01 (dd, $^{3}J_{HH}$ = 7.8 Hz, $^{3}J_{HP}$ = 11.3 Hz, 2H), 7.47 (dd, $^{3}J_{HH}$ = 7.8 Hz, $^{4}J_{HP}$ = 1.4 Hz, 2H), 7.37 (m, 4H), 7.26-7.16 (m, 6H), 6.94 (d, $^{1}J_{HP}$ = 391.8 Hz, 2H), 5.40 (d, $^{3}J_{HH}$ = 5.7 Hz, 2H), 5.23 (d, $^{3}J_{HH}$ = 5.7 Hz, 2H), 2.99 (m, 1H), 2.37 (s, 3H), 2.22 (q, *J* =7.8 Hz, 4H), 1.76 (s, 6H), 1.33 (s, 6H), 1.26 (d, $^{3}J_{HH}$ = 6.9 Hz, 6H), 0.90 (t, *J* = 7.02 Hz, 6H) ppm;**^{13}C{^{1}H} NMR** (100 MHz, $CDCl_3$) δ 158.3, 140.5, 138.7, 134.6, 133.9, 133.4 (d, J_{CP} = 5.7 Hz), 131.4, 130.9, 130.4, 129.9 (d, J_{CP} = 9.6 Hz), 127.3, 125.7, 109.6 (d, $^{2}J_{CP}$ = 3.0 Hz), 101.7 (d, J_{CP} = 3.0 Hz), 87.8 (d, J_{CP} = 3.0 Hz), 86.9 (d, J_{CP} = 3.0 Hz), 32.0, 22.8, 20.2, 17.5, 14.8, 14.7, 12.4 ppm; **^{31}P-^{1}H NMR** (162 MHz, $CDCl_3$) δ −43.9 (tt, $^{1}J_{PH}$ = 391.8 Hz, $^{3}J_{PH}$ = 11.2 Hz) ppm; **^{11}B{^{1}H} NMR** (128 MHz, $CDCl_3$) δ −1.0 (s) ppm; **IR** (neat) $\tilde{\nu}$: 2964, 2927, 2870, 2356 (w, PH), 2342 (w, PH), 1545, 1472, 1433, 1386, 1360, 1304, 1263, 1172, 1143, 1112, 1061, 1016, 973, 888, 859, 772 cm^{-1}; **HRMS** (ESI^+) calcd. for $C_{45}H_{52}B_1N_2P_1I_2Ru_1$ $[M]^+$ requires m/z 1013.1213, found *m*/*z* 1013.1194.

3.7.20 [$RuCl_2$(η^6-C_6H_6)(50)] (80)

50 (0.050 g, 0.12 mmol) and dichloro(benzene)ruthenium(II) dimer (0.029 g, 0.059 mmol) were dissolved in $CDCl_3$ (3 mL) and stirred at room temperature under nitrogen for 45 minutes. The solvent was removed to give the desired product as an orange solid (0.070 g, 95%). **^{1}H NMR** (300 MHz, $CDCl_3$) δ 7.99 (m, 2H), 7.49 (m, 2H), 5.87 (d, $^{1}J_{HP}$ = 397.9 Hz, 2H), 5.59 (s, 6H), 2.77 (s, 6H), 2.31 (q, *J* = 7.8 Hz, 4H), 2.26 (s, 2H), 1.25 (s, 6H), 0.99 (t, J_{HH} = 7.5 Hz, 6H) ppm; **^{13}C{^{1}H} NMR** (75 MHz, $CDCl_3$) δ 154.5, 135.7, 135.5, 132.9, 129.8, 129.6, 128.5, 128.3, 127.4, 124.9, 98.2, 88.0 (d, J_{CP} = 3.8 Hz), 29.7, 17.5, 14.9, 14.2, 12.2 ppm; **^{31}P-^{1}H NMR** (121 MHz, $CDCl_3$) δ −32.4 (tt, $^{1}J_{PH}$ = 398.3 Hz, $^{3}J_{PH}$ = 11.9 Hz) ppm; **^{11}B{^{1}H} NMR** (96 MHz, $CDCl_3$) δ −13.9 (s) ppm;

3.7.21 [$RuCl_2$(*p*-cymene)(50)] (81)

50 (0.033 g, 0.078 mmol) and dichloro(*p*-cymene)ruthenium(II) dimer (0.024 g, 0.039 mmol) were combined in anhydrous DCM (4 mL) and stirred for one hour. The solvent was removed to give a red solid (0.074, 97%). **^{1}H NMR** (300 MHz, $CDCl_3$) δ 7.96 (m, 2H), 7.45 (m, 2H), 5.74 (d, $^1J_{HP}$ = 390.7 Hz, 2H), 5.39 (d, $^3J_{HH}$ = 5.9 Hz, 2H), 5.22 (d, $^3J_{HH}$ = 5.9 Hz, 2H), 2.91 (m, 1H), 2.76 (s, 6H), 2.33 (q, $^3J_{HH}$ = 7.6 Hz, 4H), 2.24 (s, 2H), 2.13 (s, 3H), 1.30 (s, 6H), 1.24 (d, $^3J_{HH}$ = 7.0 Hz, 6H), 0.99 (t, *J* = 7.6 Hz, 6H) ppm; **^{13}C{^{1}H} NMR** (75 MHz, $CDCl_3$) δ 154.5, 139.8, 138.1, 135.9, 133.5, 133.2 (d, J_{CP} = 8.3 Hz), 129.7 (d, J_{CP} = 9.7 Hz), 128.6, 127.7, 106.6, 87.1(d, *J* = 5.1 Hz), 86.5 (d, *J* = 4.4 Hz), 81.4, 80.6, 31.1, 22.4, 18.7, 17.5, 14.8, 14.4, 12.2 ppm; **^{31}P-^{1}H NMR** (121 MHz, $CDCl_3$) δ −30.3 (tt, $^1J_{PH}$ = 390.4 Hz, $^3J_{PH}$ = 11.4 Hz) ppm; **^{11}B{^{1}H} NMR** (96 MHz, $CDCl_3$) δ −13.8 (s) ppm**.**

3.7.22 [$RuI_2(\eta^6\text{-}C_6H_6)$(50)] (82)

50 (0.025 g, 0.24 mmol) and diiodo(η^6-C_6H_6)ruthenium(II) dimer (0.025 g, 0.012 mmol) were dissolved in $CDCl_3$ (3 mL) and stirred at room temperature under nitrogen for 45 minutes. The solvent was removed to give the desired product as an orange solid (0.070 g, 95%). **^{1}H NMR** (300 MHz, $CDCl_3$) δ 7.99 (m, 2H), 7.49 (m, 2H), 5.87 (d, $^1J_{HP}$ = 397.9 Hz, 2H), 5.59 (s, 6H), 2.77 (s, 6H), 2.31 (q, *J* = 7.8 Hz, 4H), 2.26 (s, 2H), 1.25 (s, 6H), 0.99 (t, J_{HH} = 7.5 Hz, 6H) ppm; **^{13}C{^{1}H} NMR** (75 MHz, $CDCl_3$) δ 154.5, 135.7, 135.5, 132.9, 129.8, 129.6, 128.5, 128.3, 127.4, 124.9, 98.2, 88.2 (d, J_{CP} = 3.8 Hz), 29.7, 17.5, 14.9, 14.2, 12.2 ppm; **^{31}P-^{1}H NMR** (121 MHz, $CDCl_3$) δ −50.1 (tt, $^1J_{PH}$ = 398.1 Hz, $^3J_{PH}$ = 11.6 Hz) ppm; **^{11}B{^{1}H} NMR** (96 MHz, $CDCl_3$) δ −13.9 (s) ppm;

3.7.23 [RuI_2(*p*-cymene)(50)] (83)

50 (0.040 g, 0.094 mmol) and diiodo(p-cymene)ruthenium(II) dimer (0.046 g, 0.047 mmol) were dissolved in $CDCl_3$ (3 mL) and stirred under nitrogen for one hour. The solvent was removed to give an orange solid (0.118 g, 97%). **^{1}H NMR** ($CDCl_3$, 500 MHz) δ 8.01 (m, 2H), 7.47 (m, 2H), 7.37 (m, 4H), 7.26-7.16 (m, 6H), 6.94 (d, $^1J_{HP}$ = 391.8 Hz, 2H), 5.40 (d, $^3J_{HH}$ = 5.7 Hz, 2H), 5.23 (d, $^3J_{HH}$ = 5.7 Hz, 2H), 2.99 (m, 1H), 2.37 (s, 3H), 2.22 (q, *J* =7.8 Hz, 4H), 1.76 (s, 6H), 1.33 (s, 6H), 1.26 (d, $^3J_{HH}$ = 6.9 Hz, 6H), 0.90 (t, *J* = 7.02 Hz, 6H) ppm;**^{13}C{^{1}H} NMR** ($CDCl_3$, 100 MHz) δ 158.3, 140.5, 138.7, 134.6, 133.9, 133.4 (d, J_{CP} = 5.7 Hz), 131.4, 130.9, 130.4, 129.9 (d, J_{CP} = 9.6 Hz), 127.3, 125.7, 109.6 (d, $^2J_{CP}$ = 3.0 Hz), 101.7 (d, $^2J_{CP}$ = 3.0 Hz), 87.8, 86.9, 32.2, 22.8,

20.2, 17.6, 14.9, 14.7, 12.2 ppm; **^{31}P-^{1}H NMR** (162 MHz, $CDCl_3$) δ −43.9 (tt, $^{1}J_{PH}$ = 390.8 Hz, $^{3}J_{PH}$ = 11.4 Hz) ppm; **^{11}B{^{1}H} NMR** (128 MHz, $CDCl_3$) δ −13.7 (s) ppm.

3.7.24 [$RuCl_2(\eta^6\text{-}C_6H_6)$(56)] (84)

56 (0.025 g, 0.043 mmol) and dichloro(benzene)ruthenium(II) dimer (0.011 g, 0.022 mmol) were dissolved in $CDCl_3$ (2 mL) and stirred at room temperature under nitrogen for 45 minutes. The solvent was removed to give the desired product. **^{1}H NMR** (300 MHz, $CDCl_3$) δ 7.99 (m, 2H), 7.52 (m, 2H), 7.43-7.39 (m, 4H), 7.25-7.20 (m, 6H), 5.87 (d, $^{1}J_{HP}$ = 397.6 Hz, 2H), 5.59 (s, 6H), 2.88 (s, 6H), 2.37 (q, $^{3}J_{HH}$ = 7.5 Hz, 4H), 1.34 (s, 6H), 1.03 (t, $^{3}J_{HH}$ = 7.5 Hz, 6H) ppm; **^{13}C{^{1}H} NMR** (75 MHz, $CDCl_3$) δ 154.6, 140.3, 135.4, 133.4, 132.9, 132.1, 131.5, 129.8 (d, J_{CP} = 11.6 Hz), 128.6, 128.3, 128.0, 127.1, 125.5, 125.4, 87.9, 83.7, 17.4, 14.8, 14.1, 12.1 ppm; **^{31}P-^{1}H NMR** (162 MHz, $CDCl_3$) δ −32.2 (tt, $^{1}J_{PH}$ = 398.0 Hz, $^{3}J_{PH}$ = 11.9 Hz) ppm; **^{11}B{^{1}H} NMR** (128 MHz, $CDCl_3$) δ −12.6 (s) ppm.

3.7.25 [$RuCl_2(\eta^6$-*p*-cymene)(56)] (85)

56 (0.025 g, 0.043 mmol) and dichloro(benzene)ruthenium(II) dimer (0.013 g, 0.022 mmol) were dissolved in $CDCl_3$ (2 mL) and stirred at room temperature under nitrogen for 45 minutes. The solvent was removed to give the desired product. **^{1}H NMR** (300 MHz, $CDCl_3$) δ 7.96 (m, 2H), 7.50 (m, 2H), 7.43-7.40 (m, 4H), 7.28-7.22 (m, 6H), 5.75 (d, $^{1}J_{HP}$ = 389.9 Hz, 2H), 5.38 (d, J_{HH} = 6.0 Hz, 2H), 5.21 (d, J_{HH} = 6.0 Hz, 2H), 2.88 (s, 6H), 2.80 (m, 1H), 2.39 (q, $^{3}J_{HH}$ = 7.8 Hz, 4H), 2.15 (s, 3H), 1.34 (s, 6H), 1.27 (s, 3H), 1.24 (s, 3H), 1.03 (t, J = 7.5 Hz, 6H) ppm**; ^{13}C{^{1}H} NMR** δ 154.7, 140.1, 138.1, 135.6, 133.4, 132.2 (d, J_{CP} = 8.2 Hz), 131.6, 129.9 (d, J_{CP} = 10.4 Hz), 128.8, 128.1, 127.7, 127.2, 125.5, 106.5, 101.0, 87.1, 86.5, 81.4, 80.7, 31.1, 22.4, 18.7, 17.6, 14.9, 14.2, 12.3 ppm; **^{31}P-^{1}H NMR** (121 MHz, $CDCl_3$) δ −30.5 (tt, $^{1}J_{PH}$ = 391.2 Hz, $^{3}J_{PH}$ = 11.6 Hz) ppm; **^{11}B{^{1}H} NMR** (96 MHz, $CDCl_3$) δ −12.7 (s) ppm;

3.7.26 [$RuI_2(\eta^6\text{-}C_6H_6)$(56)] (86)

56 (0.025 g, 0.043 mmol) and dichloro(benzene)ruthenium(II) dimer (0.019 g, 0.022 mmol) were dissolved in $CDCl_3$ (3 mL) and stirred at room temperature under nitrogen for 45 minutes. The solvent was removed to give the desired product. **^{1}H NMR** (300 MHz, $CDCl_3$) δ 7.99 (m, 2H), 7.52 (m, 2H), 7.43-7.39 (m, 4H), 7.25-7.20 (m, 6H), 5.87 (d, $^{1}J_{HP}$ = 397.6 Hz, 2H), 5.59 (s, 6H), 2.88

(s, 6H), 2.37 (q, $^{3}J_{HH}$ = 7.5 Hz, 4H), 1.34 (s, 6H), 1.03 (t, $^{3}J_{HH}$ = 7.5 Hz, 6H) ppm; **^{13}C{^{1}H} NMR** (75 MHz, $CDCl_3$) δ 154.6, 140.3, 135.4, 133.4, 132.9, 132.1, 131.5, 129.8 (d, J_{CP} = 11.6 Hz), 128.6, 128.3, 128.0, 127.1, 125.5, 125.4, 87.9, 83.7, 17.4, 14.8, 14.1, 12.1 ppm; **^{31}P-^{1}H NMR** (162 MHz, $CDCl_3$) δ −49.6 (tt, $^{1}J_{PH}$ = 398.4 Hz, $^{3}J_{PH}$ = 11.2 Hz) ppm; **^{11}B{^{1}H} NMR** (128 MHz, $CDCl_3$) δ −12.6 (s) ppm.

3.7.27 [RuI$_2$(η^6-*p*-cymene)(56)] (87)

56 (0.025 g, 0.043 mmol) and dichloro(benzene)ruthenium(II) dimer (0.022 g, 0.022 mmol) were dissolved in $CDCl_3$ (2 mL) and stirred at room temperature under nitrogen for 45 minutes. The solvent was removed to give the desired product. **^{1}H NMR** (300 MHz, $CDCl_3$) δ 8.00 (m, 2H), 7.49 (m, 2H), 7.43-7.39 (m, 4H), 7.34-7.22 (m, 6H), 6.94 (d, $^{1}J_{HP}$ = 392.1 Hz, 2H), 5.42 (d, J_{HH} = 5.9 Hz, 2H), 5.23 (d, J_{HH} = 5.9 Hz, 2H), 3.00 (m, 1H), 2.88 (s, 6H), 2.38 (q, $^{3}J_{HH}$ = 7.6 Hz, 4H), 2.37 (s, 3H), 1.34 (s, 6H), 1.29 (s, 3H), 1.27 (s, 3H), 1.03 (t, $^{3}J_{HH}$ = 7.4 Hz, 6H) ppm; **^{13}C{^{1}H} NMR** (100 MHz, $CDCl_3$) δ 154.7, 140.0, 138.1, 136.0, 135.6, 133.6, 133.5, 133.4, 132.3, 131.7, 129.6 (d, J_{CP} =10.3 Hz), 128.8 (d, J_{CP} =7.7 Hz), 128.4, 128.1, 127.2, 125.5, 87.7, 86.9, 82.2, 32.1, 22.9, 20.2, 17.6, 14.9, 14.2, 12.3 ppm; **^{31}P-^{1}H NMR** (121 MHz, $CDCl_3$) δ −44.6 (tt, $^{1}J_{PH}$ = 391.4 Hz, $^{3}J_{PH}$ = 11.5 Hz) ppm; **^{11}B{^{1}H} NMR** (96 MHz, $CDCl_3$) δ −12.6 (s) ppm;

Chapter 4: Towards a Trifunctional Mitochondrial Imaging Agent

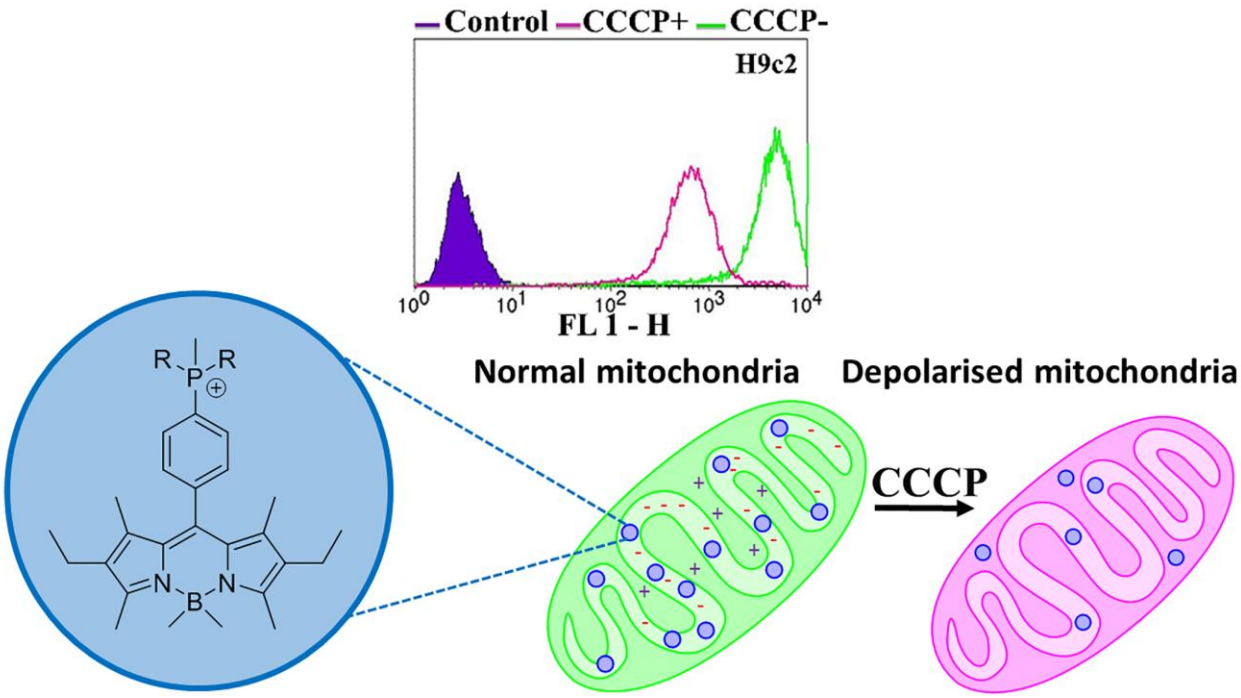

S.Nigam, B. P. Burke, L. H. Davies, J. Domarkas, J. F. Wallis, P. G. Waddell, J. S. Waby, D. M. Benoit, A. Seymour, C. Cawthorne, L. J. Higham and S. J. Archibald, *Chem. Commun.*, Structurally optimised Bodipy derivatives for imaging of mitochondrial dysfunction in cancer and heart cells, 2016, **52**, 7114-7117.

4 Towards a Trifunctional Mitochondrial Imaging Agent

This chapter describes the synthesis of fluorescent phosphonium salts which have the potential to be used as trifunctional imaging agents consisting of three features: i) a positive charge on the phosphorus atom to introduce organelle specificity, in this case to the mitochondria, ii) a fluorophore, to provide *in vitro* imaging and iii) the inclusion of an ^{18}F radionuclide to enable *in vivo* imaging techniques such as PET imaging. The work in this chapter was jointly performed between the Higham research group at Newcastle University and the Archibald research group at Hull University.[114]

4.1 Targeting the Mitochondria

Mitochondria are essential for most eukaryotic cells to function as they provide energy for the necessary activities in the form of ATP (adenosine triphosphate) *via* the oxidative phosphorylation pathway. This pathway releases free radicals as a side product and therefore the mitochondria are subjected to oxidative damage at a faster rate than the rest of the cell.[115] Mitochondrial dysfunction has been extensively studied and has found to be associated with several conditions including ischemia-reperfusion injury[116], Alzheimer's disease[74], a range of cancers[71-73] and Parkinson's disease.[75]

The mitochondrial membrane potential (MMP) is a key factor in conditions such as ischemic heart failure and cancer.[117] Loss of MMP is an early characteristic of apoptosis caused by myocardial ischemia and due to this change, the accumulation of MMP dependent compounds can increase by almost tenfold in cancerous and ischaemic heart cells. [17,118]

Lipophilic cations such as phosphonium salts are able to penetrate and accumulate within the mitochondrial matrix, and by attaching a bioactive molecule to the cation, it is possible for accumulation of the active molecule within the matrix, which could potentially open up a range of therapeutic options.[119, 120]

4.1.1 Phosphonium Cations

Neamati and co-workers synthesised compounds containing a triphenylphosphine moiety (Fig 4.1) which showed remarkable activity in a range of cancer cell lines, as well as in a mouse model of human breast cancer. The authors suggested that the mode of action was due to mitochondrial localisation causing decreased oxygen consumption, increased superoxide production and attenuated growth factor signalling.[121]

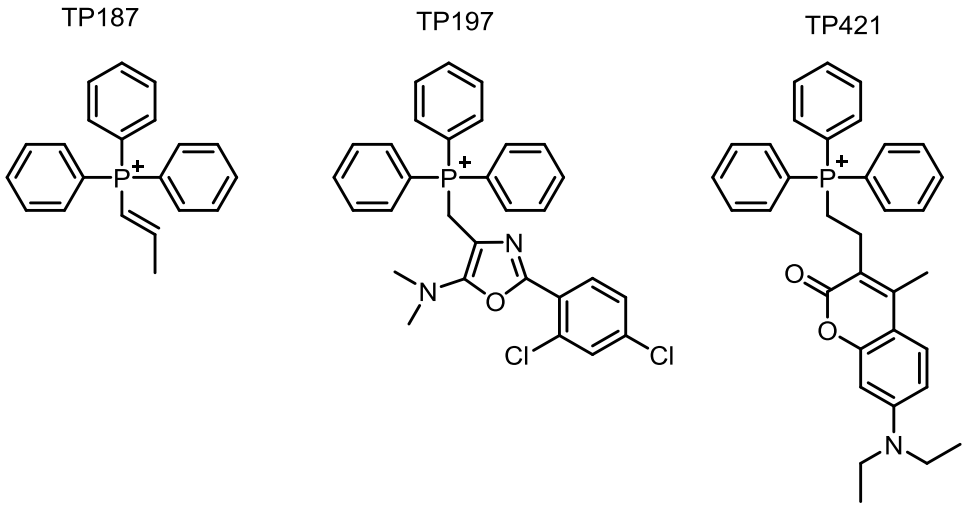

Figure 4.1 TP compounds synthesised by Neamati that show promising results for a range of cancer cell lines.

Figure 4.2 shows a series of mitochondria-targeting antioxidants synthesised by Murphy *et. al.* which are comprised of a triphenylphosphonium cation attached to the antioxidant chroman moiety of vitamin E via an alkyl linker. When the length of the linker was varied, the hydrophobicity of the compound was altered, the authors reported that a 10-carbon alkyl chain length gave the maximum antioxidant efficacy for this series of compounds.[115] The enhanced hydrophobicity that comes with a longer chain length, favours the accumulation of these compounds in mitochondria and preliminary biological data has demonstrated that they show greater efficacy in preventing mitochondrial oxidative damage than non-targeted compounds. This series of compounds describes an example of mitochondria-targeting phosphonium cations that protect the mitochondrial DNA from oxidative damage and therefore decrease the risk of diseases such as cancer and Alzheimer's.[115]

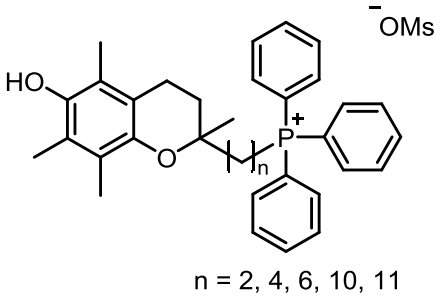

Figure 4.2 Triphenylphosphine salt synthesised by Murphy to target mitochondria, and protect mitochondrial DNA from oxidative damage.

Another example shown in Figure 4.3 identifies a series of triphenylphosphonium cations of a diterpenoid which were synthesised and tested in an *in vivo* phenyotypic sea urchin embryo. The results suggested that the cations induced mitotic spindle defects and mitotic arrest, presumably due to interactions with the mitochondrial DNA.[122] This research details an example of a

triphenylphosphonium cation being used to attack diseased cells and by inducing mitotic arrest, will stop cell division, which is suggested as a promising starting point for possible anticancer agents. Antimitotic drugs within the treatment of cancer are highly validated chemotherapy agents.[123] They work by inhibiting the polymerisation dynamics of microtubules (microtubules are formed during interphase and are essential for correct chromosome segregation and cell division undergoing mitosis).[124]

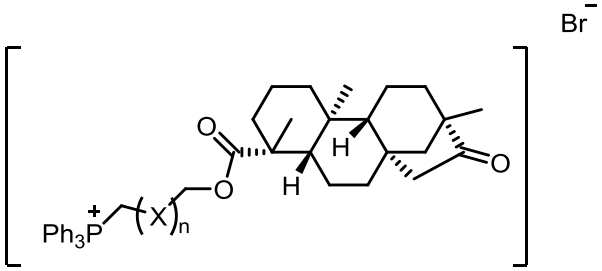

Figure 4.3 Phosphonium cations based on isosteviol derivatives were tested for antimitotic activity in a sea urchin embryo model.

4.2 Multifunctional Imaging Agents

The advantage of combining two or three imaging techniques within one probe permits a better understanding of what happens within a cell and the fate of a radiopharmaceutical inside the body. The use of Bodipy dyes as multifunctional imaging agents has increased in recent years. The addition of the positron emitting radioisotope, fluorine-18, to these compounds would result in a PET/optical imaging agent. ^{18}F-Positron emission tomography (PET) is a powerful technique which provides *in vivo* information on radiolabelled biomolecules. However, there are two major limitations to this technique 1) ^{18}F radionuclide has a half-life of 110 minutes, and therefore needs to be incorporated into the molecules as quickly as possible and 2) PET imaging has relatively low spatial resolution (1-2 mm).

The incorporation of an ^{18}F radiolabel into a triphenylphosphonium cation has been reported several times.[125-129] This enables mitochondria specific targeting combined with PET imaging within one probe. Figure 4.4 shows examples of compounds that have been effectively used in myocardial PET imaging. However, these compounds are not fluorescent, therefore they cannot be used in optical imaging which contrasts with the compounds prepared in this thesis.

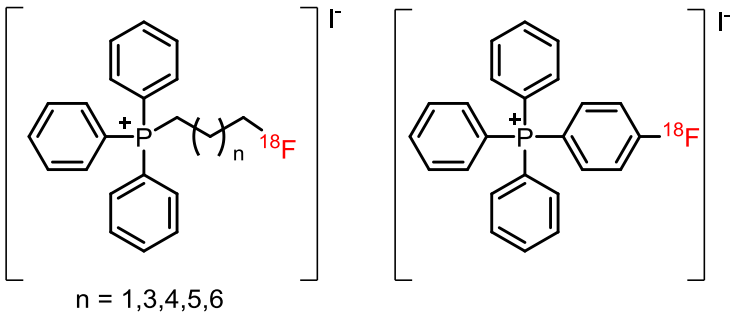

Figure 4.4 Examples of ^{18}F-radiolabelled triphenylphosphonium cations used in myocardial imaging.

4.3 Synthesis of Tertiary Phosphines 89a and 89b.

An important aim of this thesis is to combine a number of imaging techniques that have been discussed above: (i) *in vitro* imaging, (ii) *in vivo* imaging and (iii) mitochondria specific targeting all in a single molecular probe. As described above, there are several published examples of triphenylphosphonium salts currently being used in selective mitochondrial imaging. Our initial approach was to synthesise a fluorescent version of triphenylphosphine based on a Bodipy fluorophore, capable of dual imaging. The phosphonium salt would allow for selective mitochondrial imaging, and the Bodipy fluorophore for fluorescence microscopy.

4.3.1 Route 1

The tertiary phosphines **89a** and **89b** can be synthesised in two ways; the first route is from the primary phosphine, shown in Scheme 4.1. Phosphorus pentachloride was dissolved in anhydrous toluene and primary phosphine **20a** was added. After one hour at room temperature, the solvent was removed and the orange solid was analysed by $^{31}P\{^{1}H\}$ NMR spectroscopy, where no starting material was apparent and only a peak at δ 159.7 ppm was observed, corresponding to the dichlorophosphine **88**. The solid was dissolved in anhydrous THF and phenylmagnesium bromide or dicyclohexylmagnesium chloride were added. The reaction was stirred at room temperature for 16h. After purification by column chromatography, analysis by $^{31}P\{^{1}H\}$ NMR spectroscopy determined that the desired product had been synthesised (δ 2.9 ppm for **89a** and δ –5.5 ppm for **89b**). The advantage of using this route is the large number of organolithium and Grignard reagents available compared to the chloro-phosphine starting material required in route 2.

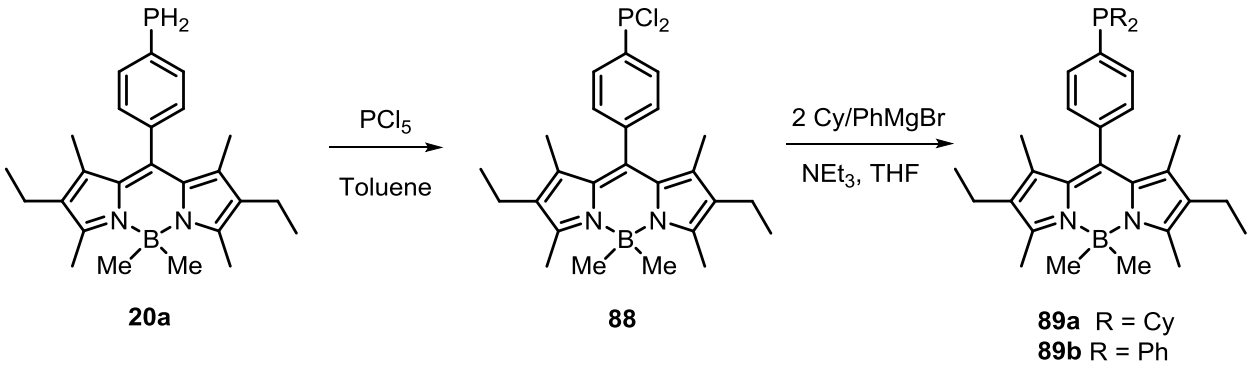

Scheme 4.1 First method for the synthesis of tertiary phosphines 89a and 89b.

4.3.2 Route 2

The second route for the synthesis of tertiary phosphines **89a** and **89b** is shown in Scheme 4.2. Arylbromide **44a** was reacted with *n*-butyllithium at –78°C in anhydrous diethyl ether followed by the addition of chlorodicyclohexyl- or chlorodiphenylphosphine. The reaction was monitored by $^{31}P\{^{1}H\}$ NMR spectroscopy and the product peaks were observed at δ 2.9 ppm for **89a** and δ –5.5 ppm for **89b**. Both compounds were purified by column chromatography on silica gel to give the desired products as orange solids.

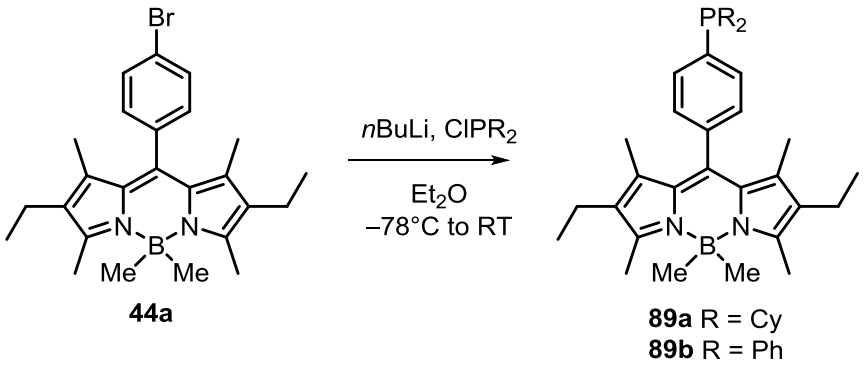

Scheme 4.2 Synthesis of tertiary phosphines 89a and 89b.

A crystal of **89b** was obtained *via* slow diffusion of DCM/pentane and analysed by X-ray diffraction, the molecular structure is shown in Figure 4.5. The three C–P bond lengths of 1.8312(19), 1.836(2) and 1.833(2) Å and the C–P–C bond angles of 100.95(9), 102.14(8) and 103.58(9)° are typical for tertiary phosphines and are a good comparison to triphenylphosphine.[130]

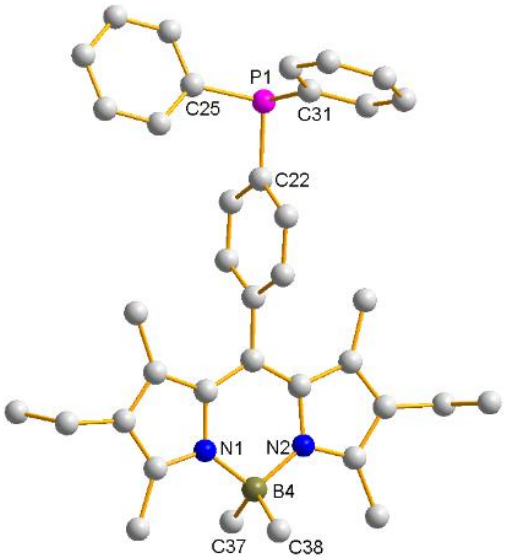

Figure 4.5 Molecular structure of 89b obtained by slow diffusion with dichloromethane/pentane. Hydrogen atoms have been omitted for clarity. Selected bond distances [Å] and angles [°]: C22-P1 1.8312(19), P1-C25 1.836(2), P1-C31 1.833(2), C37-B4 1.626(3), C38-B4 1.623(3) ; C22-P1-C25 100.95(9), C22-P1-C31 102.14(8), N1-B4-N2 105.14(14).

4.4 Phosphonium Salt Synthesis

In order to form a mitochondria-specific imaging agent, the phosphines needed to be transformed into the corresponding phosphonium cations. Phosphonium salts **93a** and **93b** were synthesised by reacting compounds **89a** and **89b** with methyl trifluoromethanesulfonate in DCM for two hours at room temperature, **93a** precipitated out of the solution as an orange solid whereas **93b** required purification by column chromatography (chloroform:methanol, 10:0.3) to give the desired product (Fig 4.6).[114]

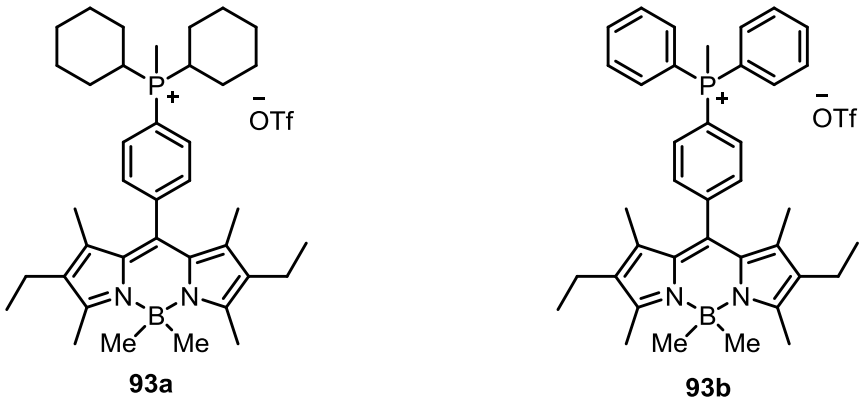

Figure 4.6 Structures of phosphonium derivatives 93a and 93b.

Compounds **93a** and **93b** were sent to Hull University, to the research group of Professor Steve Archibald who performed mitochondrial uptake studies. Compounds **93a** and **93b** were tested using confocal microscopy in human breast cancer cells (MCF-7) and rat cardiomyocytes (H9c2)

shown in Figure 4.7. Mitotracker deep red was used as a reference due to its sufficiently different photophysical properties to allow independent detection, (MDR emission wavelength is at 665 nm and Bodipy compounds at 532 nm).

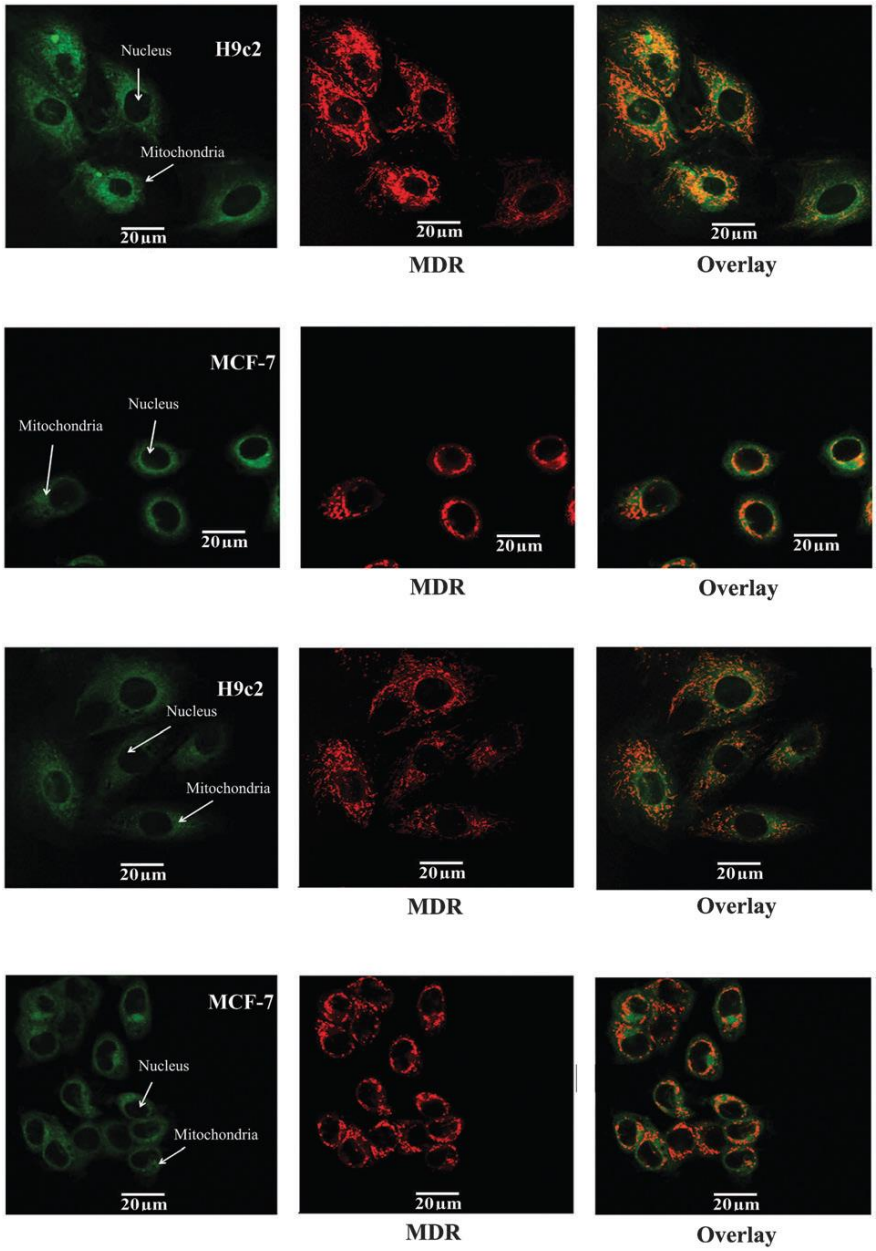

Figure 4.7 Confocal microscopy of 93a (top two rows) and 93b (bottom two rowa) in MCF-7 and H9c2 cell lines (left), mitotracker deep red (MDR) (centre) amd overlaid mitochondrial localisation (right).

Figure 4.7 confirms mitochondrial localisation of both of the Bodipy phosphonium salts **93a** and **93b** in H9c2 and MCF-7 cells; the overlay shows the green Bodipy compounds localise in the same area as the red MDR reference dye. Both compounds **93a** and **93b** showed a good localisation in the rat cardiomyocyte (H9c2) cells, however, in the human breast cancer cell line (MCF-7),

compound **93a** showed an increased uptake of 37% over the diphenyl derivative **93b**, indicating that it has a significantly greater potential as an imaging agent.

Since the MMP plays a key role in cardiac failure and cancer, the development of imaging agents that show MMP-dependant uptake provide an ideal tool to probe mitochondrial function, there are several derivatives based on rhodamine that are commonly used.[131] The MMP specific uptake of compounds **93a** and **93b** was measured using flow cytometry in the presence of carbonyl cyanide *m*-chlorophenylhydrazone (CCCP), a protonophore which eliminates the MMP (Fig 4.8).[132, 133] Both tracers showed a decrease in mean fluorescent intensity (MFI) upon CCCP induced MMP depolarisation in both cell lines. The dicyclohexyl derivative showed a 70% decrease in both the MCF-7 and H9c2 cells, and the diphenyl derivative showed a 38% and 58% decrease respectively.

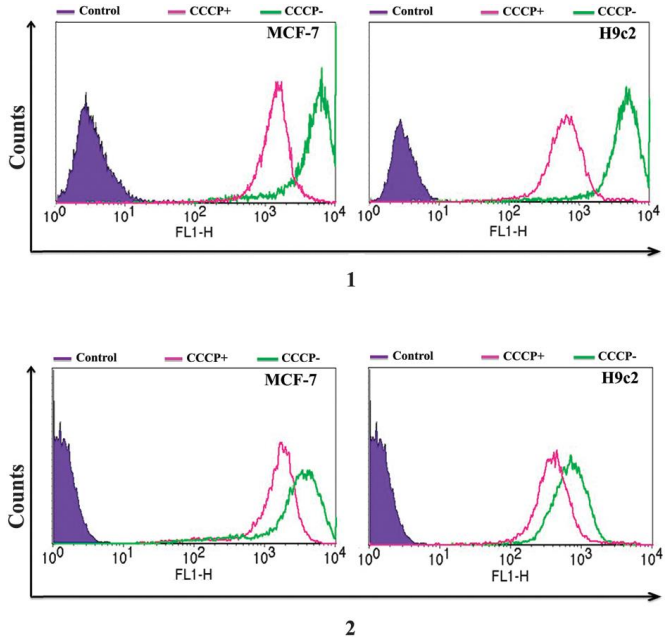

Figure 4.8 Flow cytometry studies of 93a (top) and 93b (bottom) in MCF-7 (*l*) and H9c2 (*r*) cells without (green) and with(pink) CCCP present to assess MMP uptake.

It was apparent that the dicyclohexyl derivative **93a** showed an increase in MMP-dependent, mitochondrial specific uptake. This was investigated further using DFT calculations to determine the distribution of the electron density of the phosphonium salt (Fig 4.9), which concluded that the charge is located on the phosphorus atom for the dicyclohexyl compound but for the diphenyl analogue it is delocalised on the aromatic rings. The lipophilicity (logP) of the two compounds was measured (**93a** (3.19) and **93b** (2.80)) and a significant variance was observed, which is possibly responsible for the difference in activity between the two compounds.

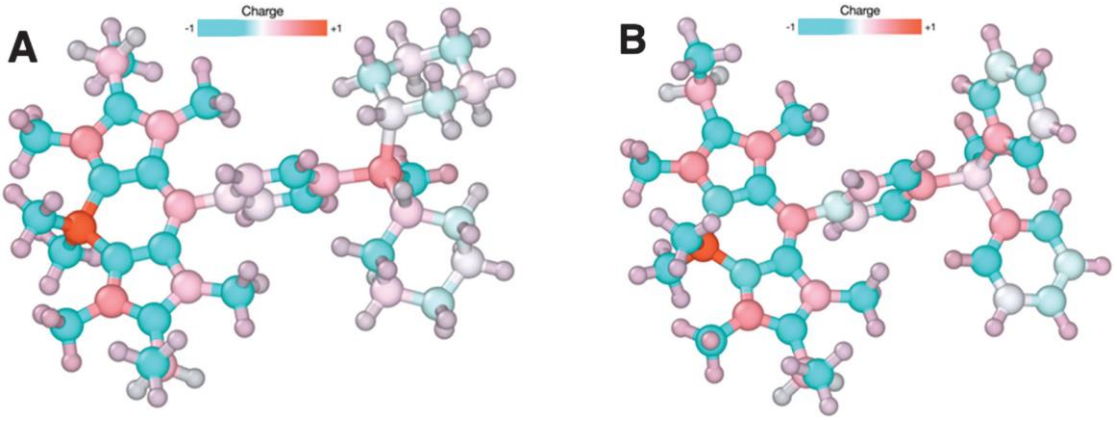

Figure 4.9 The electron density distribution for 93a and 93b was computed which illustrated that the charge is located on the phosphorus atom for 93a and on the aromatic rings for 93b.

4.5 Transforming the Fluorescent Phosphonium Salt into a PET Probe

Our approach to synthesising a multifunctional imaging agent containing a radionuclide was achieved by substituting the methyl trifluoromethanesulfonate reagent for a range of dihaloalkanes, such as 1-bromo-4-fluorobutane. These compounds would constitute a cold standard for a potential radiolabelled compound in the future.

^{18}F would be the most popular radionuclide of choice as it has an ideal half-life (110 minutes), however, ^{131}I is also currently being used in the treatment of thyroid cancer as the thyroid cells absorb iodine, and works by shrinking or destroying all or part of the thyroid.[134]

The addition of the dihaloalkane reagents has only been attempted with the dicyclohexylphosphine derivative so far, as this compound displayed more promising results as an imaging agent.

The novel phosphonium salts were initially synthesised by combining $BodPCy_2$ **89a** and the relevant dihaloalkane in anhydrous DCM. The reaction was stirred until complete consumption of the starting materials was confirmed by $^{31}P\{^1H\}$ NMR spectroscopy, which varied between 16-72 hours. Although these reaction conditions showed successful synthesis of the product when analysed by $^{31}P\{^1H\}$ NMR spectroscopy (~δ 34.0 ppm), there was always a second peak present corresponding to the phosphine oxide (~δ 42 ppm). The reactions were subsequently conducted in anhydrous toluene at 110 °C, which resulted in faster reaction times and cleaner products. In all cases, there was no starting material remaining after 16 hours and only small quantities of oxide remained (Figure 4.10, structure **89ab**).

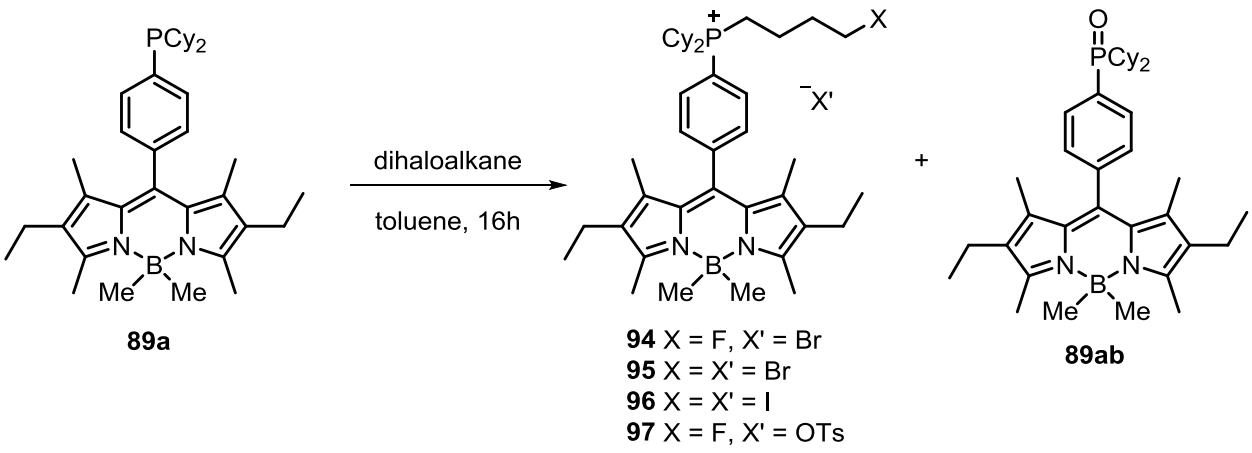

Figure 4.10 General synthesis of novel phosphonium salts 94-97 and phosphine oxide side product 89ab.

Crystals of compounds **94** and **95** suitable for X-ray analysis were obtained by slow diffusion of $CDCl_3$/pentane (**94**) and DCM/pentane (**95**) as shown in Figures 4.11 and 4.12. The F-C bond length of 1.316(19) Å and Br-C bond length of 2.00(2) Å are in agreement with examples reported in the literature.[87, 135]

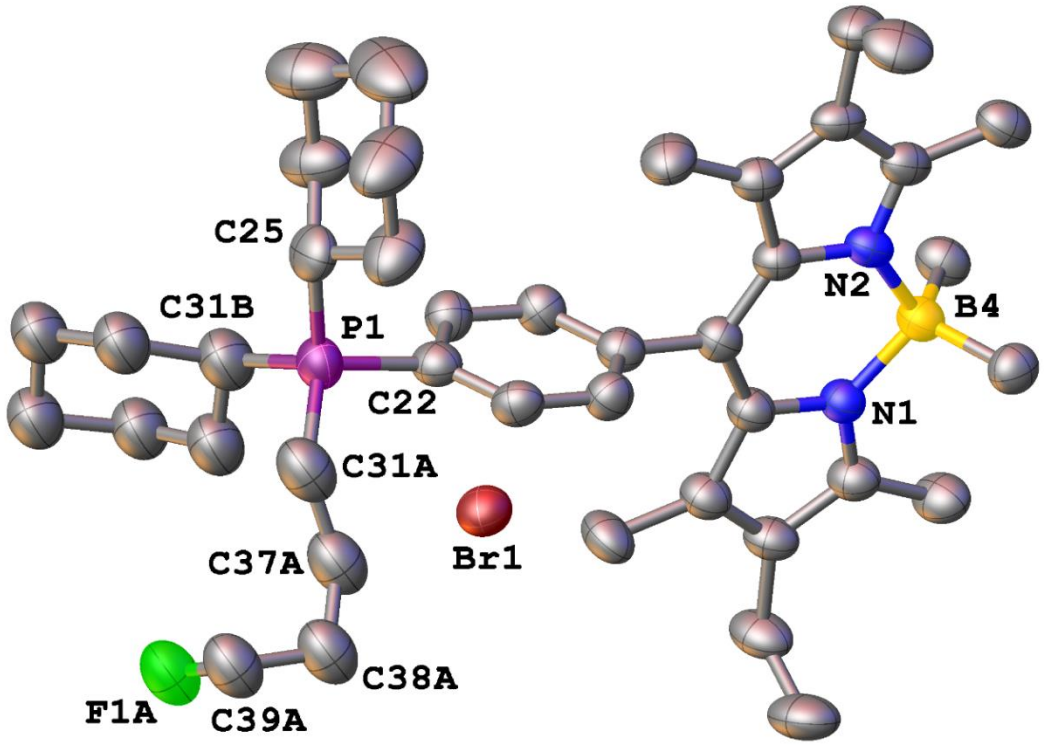

Figure 4.11 Molecular structures of 94 was obtained by slow diffusion with $CDCl_3$/pentane. Hydrogen atoms have been omitted for clarity. Selected bond distances [Å] and angles [°]: C22-P1 1.7952, P1-C31A 1.7998, P1-C31B 1.8051, P1-C25 1.8210, C39A-F1A 1.316(19); C22-P1-C31B 109.2(3), C31B-P1-C31A 110.5(3), C31B-P1-C25 109.7(3), F1A-C39A-C38A 119.0(2).

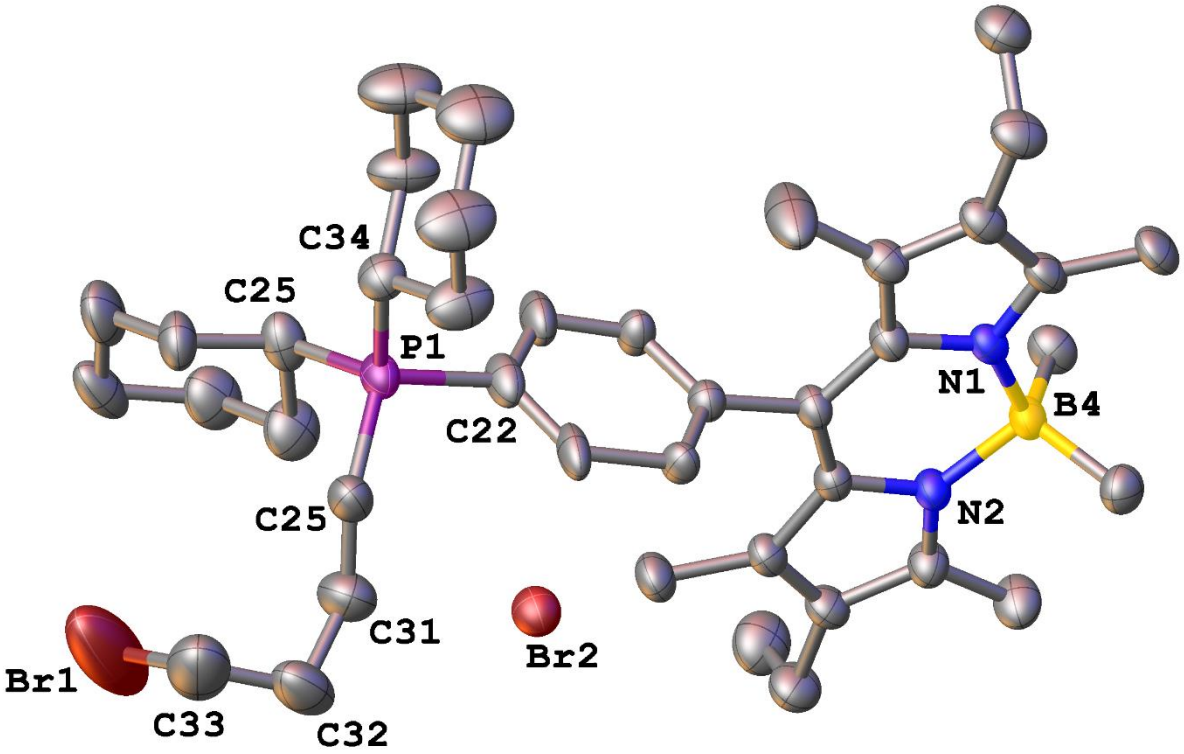

Figure 4.12 Molecular structures of 95 was obtained by slow diffusion with DCM/pentane Selected bond distances [Å] and angles [°]: C22-P1 1.795(5), P1-C25 1.806(5), P1-C34 1.826(6), C33-Br1 2.00(2); C22-P1-C25 109.87(18), C25-P1-C25 110.6(3), C25-P1-C34 109.0(2), Br1-C33-C32 105.0(14).

Compound **94** was also extensively analysed by NMR spectroscopy; Figure 4.13 shows the ^{1}H, $^{1}H\{^{31}P\}$ and $^{1}H\{^{19}F\}$ NMR spectra, which made it possible to deduce which peaks corresponded to the protons adjacent to the fluorine atom, due to the splitting patterns observed. The proton NMR spectrum at the top showed the aromatic protons around 7.7-8.0 ppm, the peaks highlighted in the box corresponded to protons on the alkyl chain attached to the phosphorus atom, but it was not immediately obvious which protons were adjacent to the fluorine or the phosphorus atom. Therefore the $^{1}H\{^{31}P\}$ and $^{1}H\{^{19}F\}$ NMR spectra were recorded which helped to identify which nucleus was splitting the protons into a doublet of triplets. It can be observed in the $^{1}H\{^{31}P\}$ spectrum, the doublet of triplets is still visible, whereas in the $^{1}H\{^{19}F\}$ spectrum it is a single triplet. This indicates that the fluorine atom is responsible for the splitting of the protons in this instance. The remainder of the spectra correlated well, signifying that the fluorine and phosphorus atoms are not visibly splitting any other protons.

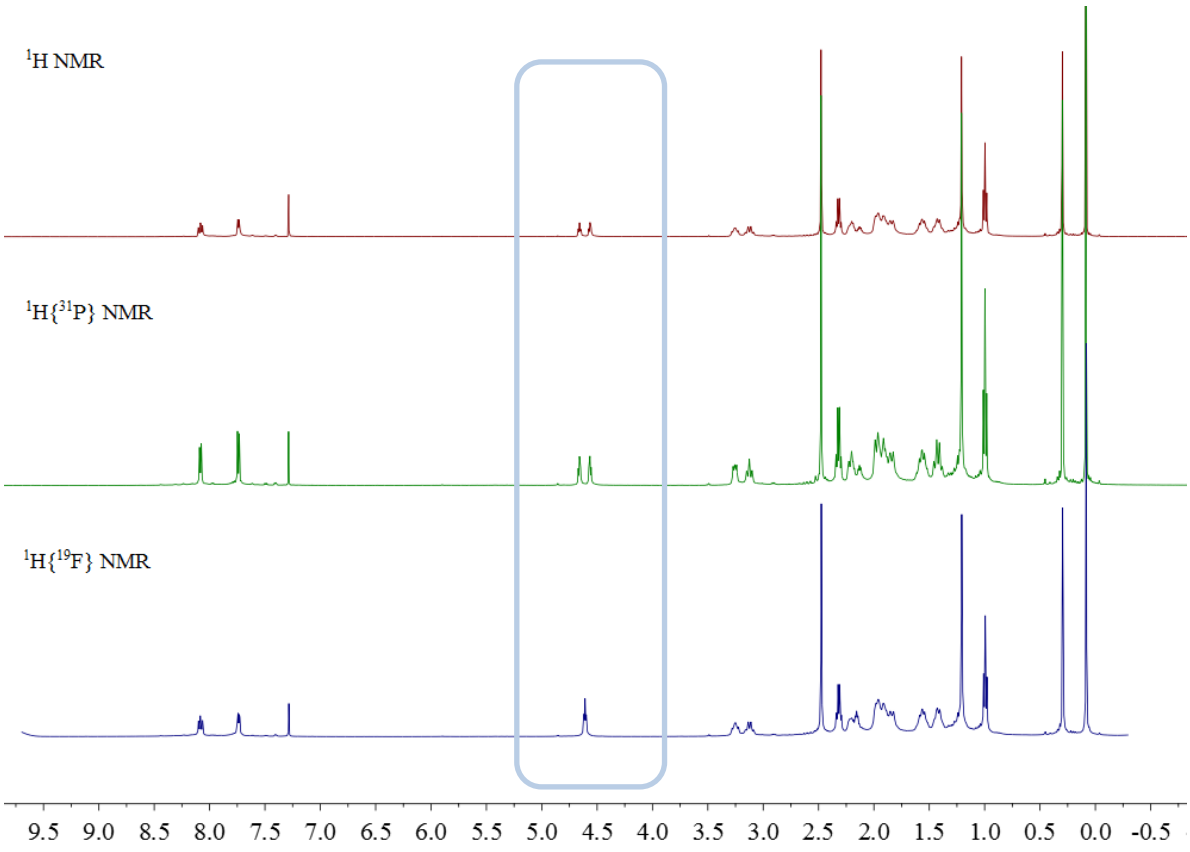

Figure 4.13 NMR studies to deduce the protons within the alkylhalide chain attached to the phosphorus atom.

4.5.1 Photophysical Results

In order to gain an understanding of how the photophysical properties were affected by the addition of the alkyl halide chain, the absorption and emission maxima were recorded, along with the quantum yield to see if any fluorescence quenching was observed.

The photophysical properties of all of the novel phosphonium salts were compared to the parent ligands, shown in Table 4.1.

Table 4.1 Photophysical properties for novel phosphonium salts.

	λ_{abs} (nm)	λ_{em} (nm)	ϕ_F
89a	512	526	0.44
89b	513	527	0.29
93a	516	532	0.24
93b	516	532	0.14
94	515	534	0.29
95	514	533	0.28
96	515	535	0.23
97	512	527	0.36
98	514	532	0.24

Measured in dry, degassed tetrahydrofuran at room temperature, dyes were excited at 485 nm; Fluorescence quantum yields were measured with respect to 4,4-difluoro-8-phenyl-1,3,5,7-tetramethyl-2,6-diethyl-4-bora-3a,4a-diaza-s-indacene **57**.

The majority of the phosphonium salts displayed a slight bathochromic shift (3-4 nm) compared to the phosphine ligands **89a** and **89b**. A decrease in quantum yield of the novel phosphonium salts - **94-97** can be observed compared to the parent compound **89a**. However, they all remain high, concluding that quaternisation of the phosphorus atom does not diminish the fluorescence to an extent that the compounds are no longer fluorescent. As the halogen attached to the alkyl chain gets larger F<Br<I, the quantum yield is marginally decreased, which can possibly be attributed to the heavy atom effect.[35]

Figures 4.14 and 4.15 show the absorption and emission spectra for the novel phosphonium salts – they show similar profiles to the parent compounds, with the absorption maxima observed between 512-516 nm and the fluorescence maxima between 527-535 nm.

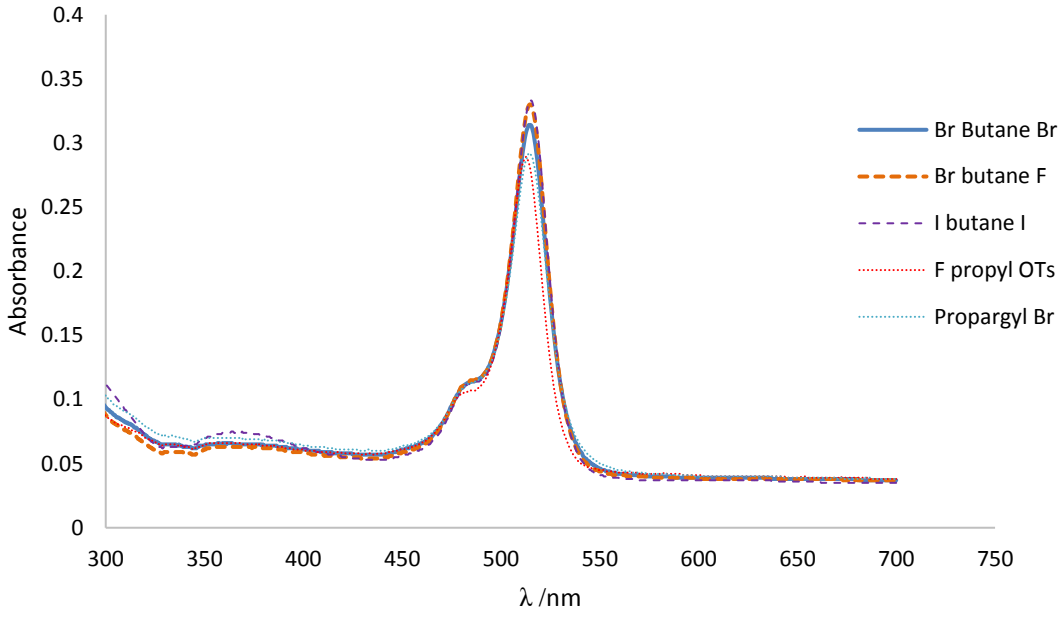

Figure 4.14 Absorption spectra for phosphonium cations 94-98, measured in dry, degassed tetrahydrofuran at room temperature.

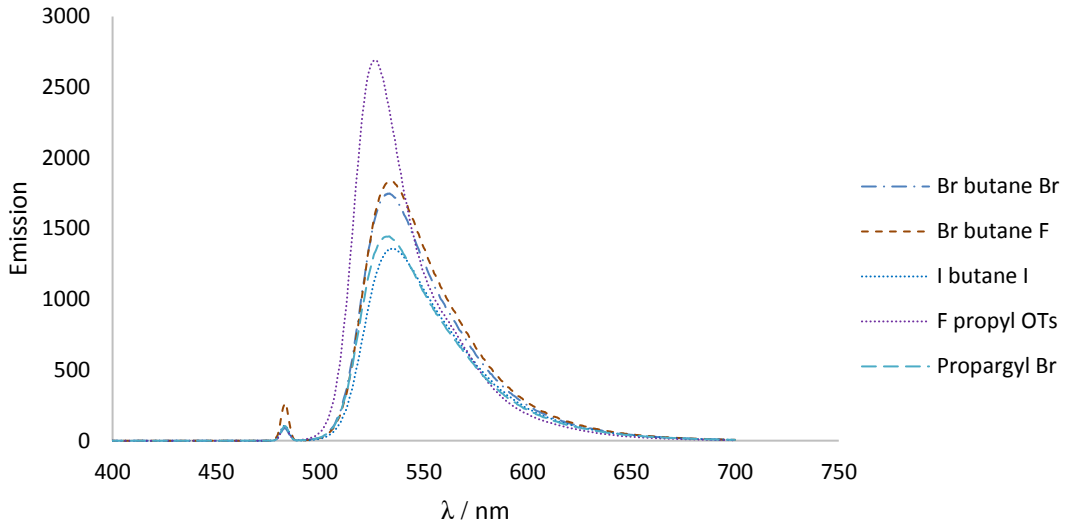

Figure 4.15 Emission spectra for phosphonium cations 94-98, measured in dry, degassed tetrahydrofuran at room temperature.

The photophysical properties have provided us with information to acknowledge that we have successfully made a range of phosphonium salts that are both mitochondria specific and possess important fluorescent properties required for optical imaging.

4.5.2 Flow Cytometry Studies

Flow cytometry studies were carried out for fluoride-substituted compound **94**, which showed improved results relative to the earlier phosphonium salts, **93a** and **93b**. The replacement of the methyl group bound to the phosphorus atom, for the fluorobutyl group, led to an increase in MMP dependent uptake. The addition of CCCP was responsible for a decrease in uptake of 84% for MCF-7 cells and 83% for H9c2 cells, thus validating this approach for the design of MMP-dependent multimodal optical/PET imaging agents.

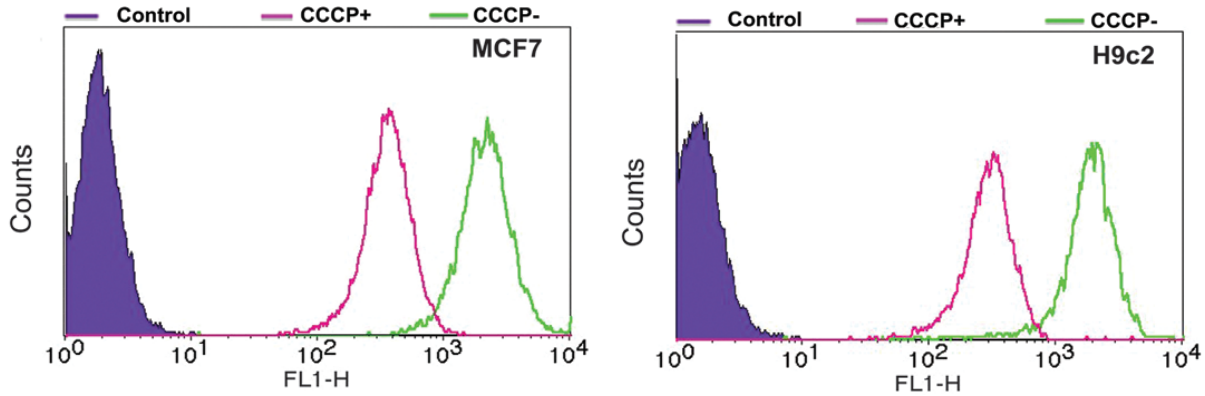

Figure 4.16 Flow cytometry in MCF-7 (left) and H9c2 (right) cells, without (green) and with (pink) CCCP present for compound 94.

4.5.3 Propargyl Derivative for Click Chemistry

A final reaction was attempted where propargyl bromide was reacted with $BodPCy_2$ **89a** in anhydrous toluene and stirred at reflux (110 °C) overnight, which successfully formed novel compound **98**. Analysis by $^{31}P\{^1H\}$ NMR spectroscopy showed a product peak at δ 29.9 ppm, in comparison to the starting material peak at δ 2.8 ppm. The ^1H NMR spectrum also illustrated the additional proton relating to the alkyne group at δ 4.47 ppm. This derivative could theoretically be used in click chemistry where the alkyne is reacted with another compound containing an azide to introduce a bioactive species such as a protein or oligonucleotide (Fig 4.18). This route would present another method to a cell-specific imaging agent and will be looked at in more detail in the future.

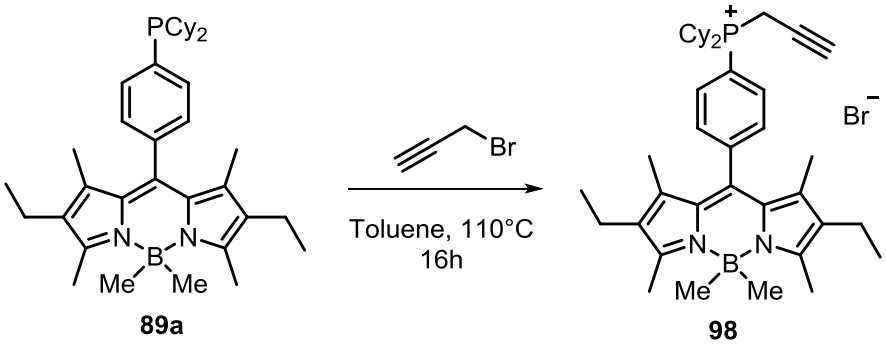

Figure 4.17 A reaction with propargyl bromide introduces an alkyne group which would allow bioconjugation via click chemistry.

An example of click chemistry is shown in Figure 4.18, where copper-catalysed azide-alkyne click chemistry was used for bioconjugation.[136] THPTA (Tris(3-hydroxypropyltriazolyl-methyl)amine] is added to accelerate the reaction by protecting the biomolecule from hydrolysis by Cu(II) by-products and also sacrificially intercepting any radicals or peroxides that are formed. Compound (2) is aminoguanidine and can be added to suppress any unwanted side reactions.

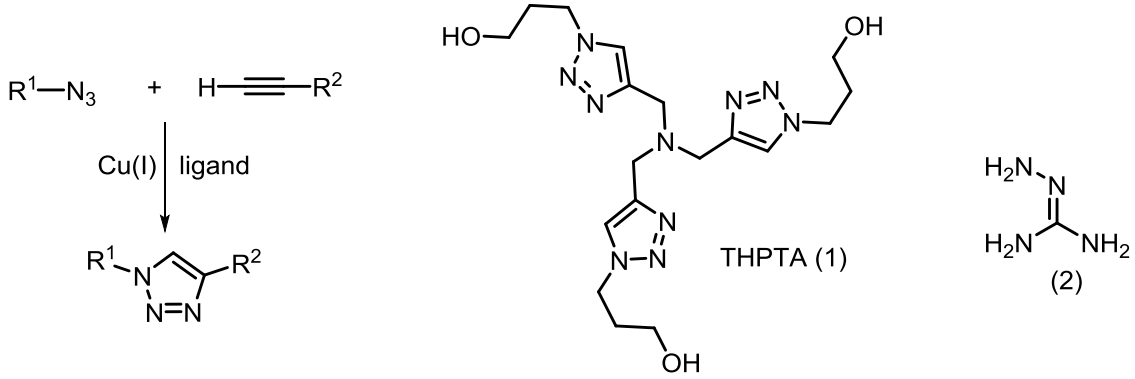

Figure 4.18 A general copper catalysed reaction, and structures of THPTA (1) and aminoguanidine additive 2.

4.6 Applications of Novel Phosphonium Salts in Cell Imaging

Three of the phosphonium salts (**94**, **96** and **98)** were also sent to Dr Amy Reeve, a research fellow at Newcastle University's Wellcome Trust for Mitochondrial Research. The salts were tested in a mouse embryonic stem cell line and compared against Mitotracker Deep Red (MDR) in order to see if they successfully localised within the mitochondria of the cells.

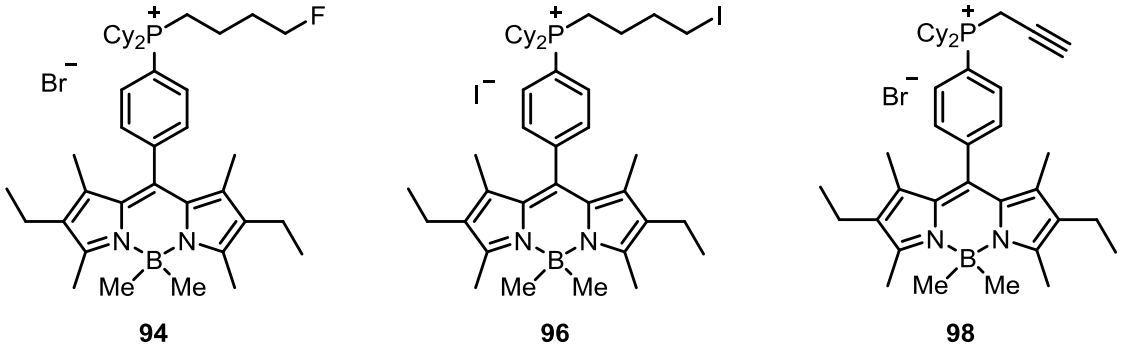

Figure 4.19 Three salts tested in mouse embryonic stem cells at Newcastle University.

The stem cells can be differentiated into neurons and were created to model the effect of a mitochondrial defect on neurons. WT are wild type cells, which are normal cells with no adverse phenotype. Figure 4.20 shows an illustration of the electron transport chain where Complex I and IV play key roles.[137] Complex I and IV deficient cells contain a defect in the mitochondrial complex I or IV. Complex I is a large enzyme which catalyses the first step of the electron transport chain and is responsible for driving ATP production.[138] Complex IV is the last enzyme in the respiratory electron transport chain located in the mitochondrial membrane. It receives an electron from four cytochrome c molecules which are transferred to an oxygen molecule, which helps convert molecular oxygen into two molecules of water.[139]

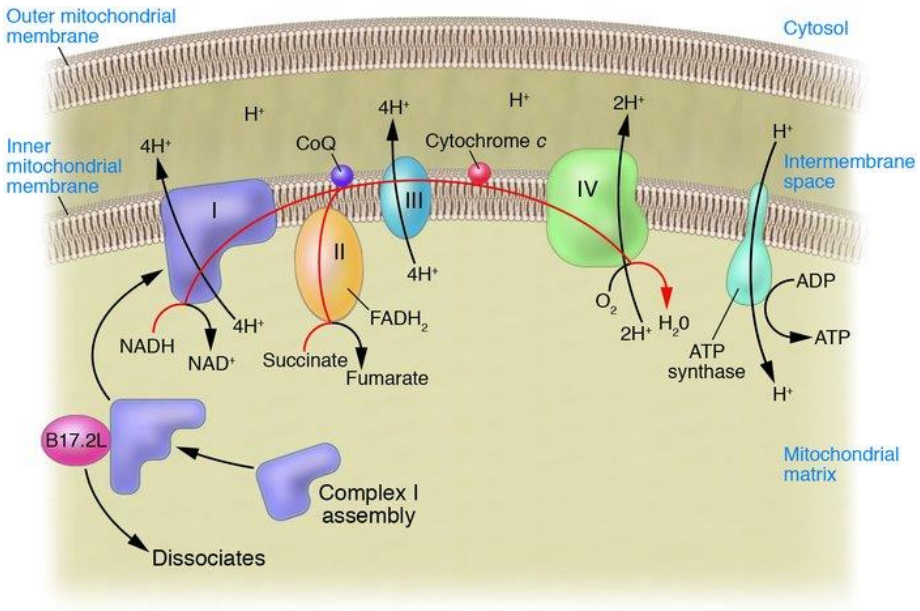

Figure 4.20 Representative diagram of the electron transport chain from the Journal of Clinical Investigation.[137]

The images below in Figure 4.21 show compounds **94**, **96** and **98** in the three cell types described above. The top right image of each group of images, shows the fluorescent detection at 488 nm excitation, bottom right shows a light microscopy image, the red image is MDR, used as a reference, and top left shows an overlay of all three images.

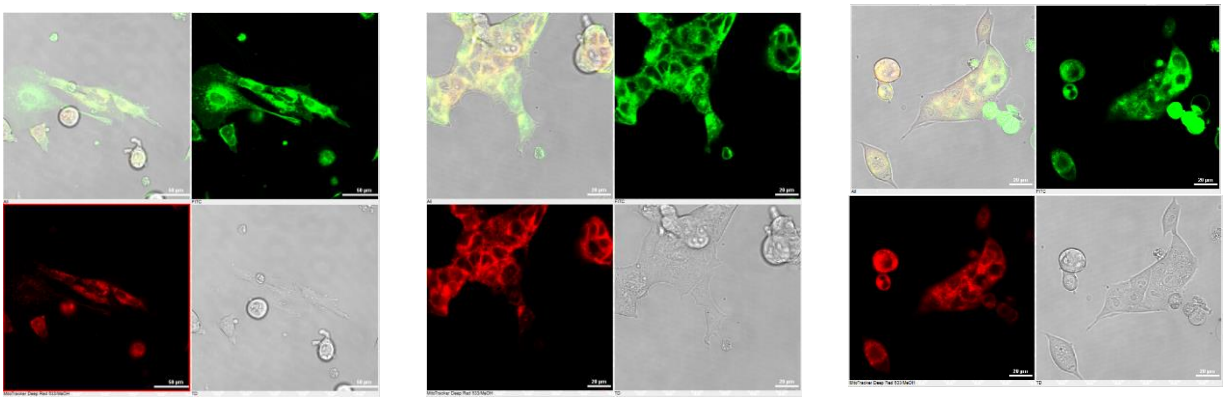

Figure 4.21 Compound 94 in WT cells (left), Complex I-deficient cells (middle) and Complex IV-deficient cells (right).

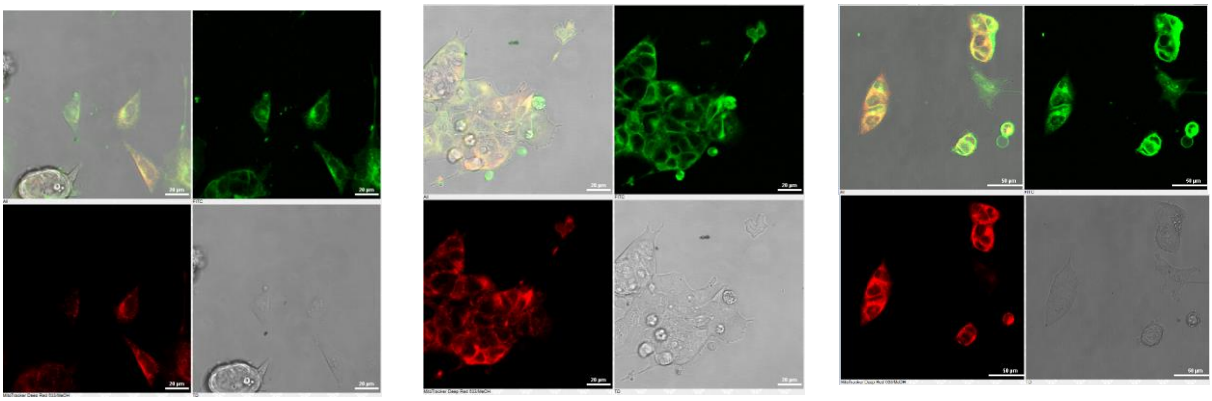

Figure 4.22 Compound 96 in WT cells (left), Complex I-deficient cells (middle) and Complex IV-deficient cells (right).

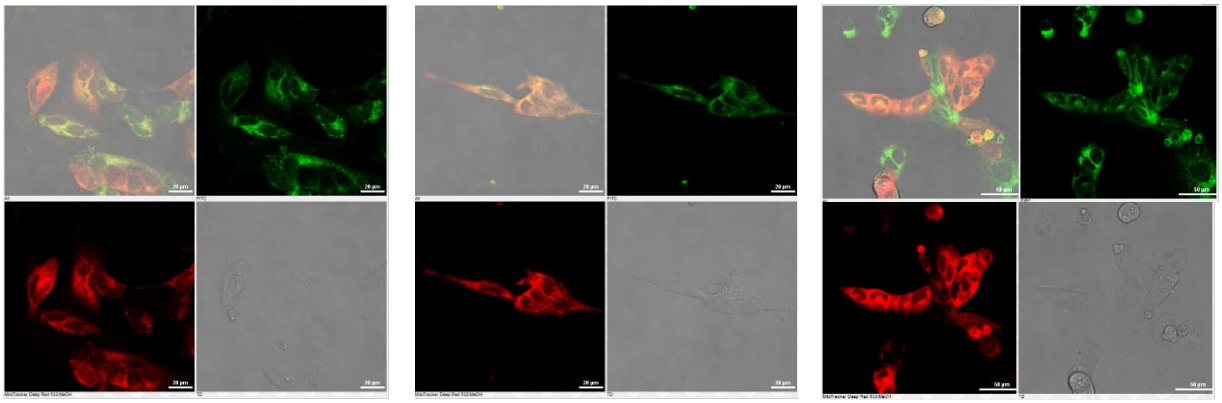

Figure 4.23 Compound 98 in WT cells (left), Complex I-deficient cells (middle) and Complex IV-deficient cells (right).

All three of the phosphonium salts were found to localise in the mitochondria, as confirmed by the overlay picture which shows the orange image of the green Bodipy compounds overlapping with the red MDR dye, indicating that they locate in the mitochondria as predicted.

4.7 Summary

The synthesis of several novel fluorescent phosphonium salts has been described in this chapter, via the addition of an alkylhalide reagent to a tertiary phosphine. Compounds **93a** and **93b** were formed by the addition of methyl trifluoromethanesulfonate to tertiary phosphines **89a** and **89b** which created fluorescent phosphonium cations that were successfully imaged in human breast cancer cells (MCF-7) and rat cardiomyocytes (H9c2). The second part of this chapter discussed the synthesis of five novel phosphonium salts (**94-98**) that, in the future, have the potential to be multi-modal imaging probes containing (i) a phosphonium cation to introduce organelle specificity, in

this case targeting the mitochondria; (ii) a fluorescent Bodipy core for fluorescent microscopy and (iii) a radiolabel such as ^{18}F to allow for PET scanning.

The synthesis and characterisation of five novel phosphonium salts is described, and compounds **94** and **95** have also been successfully analysed by X-ray crystallography.

The photophysical properties of the novel compounds was recorded which identified that the quaternisation of the phosphorus atom did not have a detrimental effect on the fluorescence. All of the phosphonium salts retain high quantum yields and exhibit strong absorption and emission graphs similar to their parent compounds.

Three of the novel phosphonium salts were tested in a mouse embryonic stem cell line, specifically in wild type cells, and complex I and IV deficient cells, all of which showed uptake of the phosphonium salts into the mitochondria, as highlighted by and compared to MDR.

The final compound, propargyl **98**, can potentially open a route to a new range of compounds to be synthesised via click chemistry, which will allow bioactive species, such as proteins, to bind to the Bodipy phosphonium salts.

This next step is currently underway with the research group of Professor Steve Archibald at Hull University, who are attempting to substitute the halogen for an ^{18}F radiolabel and so generate a multifunctional PET imaging probe.

4.8 Experimental

4.8.1 General Experimental Procedure

All air- and/or water-sensitive reactions were performed under a nitrogen atmosphere using standard Schlenk line techniques. Tetrahydrofuran was dried over sodium/benzophenone and deuterated chloroform was dried over phosphorus pentoxide; these solvents were distilled prior to use. Dimethyl sulfoxide was purchased from Fisher in an anhydrous state and was used as received. All starting materials were purchased from Sigma Aldrich, Alfa Aesar or Fisher and were used as received. Flash chromatography was performed on silica gel (40-63 μm, 60 Å) from Merck, thin-layer chromatography was carried out using Merck aluminium-based plates with silica gel and fluorescent indicator (254 nm). ^{1}H, $^{13}C\{^{1}H\}$, $^{19}F\{^{1}H\}$, $^{31}P\{^{1}H\}$ and $^{11}B\{^{1}H\}$ NMR spectra were recorded on a JEOL ECS-400 (^{1}H 399.78 MHz) or Bruker Avance III 300 (^{1}H 300.13 Hz) spectrometer at room temperature (21 °C); ^{1}H and ^{13}C shifts were relative to tetramethylsilane, ^{31}P shifts were relative to 80% H_3PO_4, ^{11}B relative to $BF_3.Et_2O$ and ^{19}F relative to $CFCl_3$. Infrared spectra were recorded on a Varian 800 FT-IR spectrometer and mass spectrometry was carried out by the EPSRC NMSF, Swansea. DFT calculations were carried out on Spartan 14 using the B3LYP functional with a 6-31G* basis set, details of the xyz coordinates and SCF energies can be found in the appendix.

4.8.2 Preparation of of 8-((4-Dicyclohexylphosphino)phenyl)-4,4-dimethyl-1,3,5,7-tetramethyl-2,6- diethyl-4-bora-3a,4a-diaza-*s*-indacene (89a)

Route 1:
Phosphorus pentachloride (0.283 g, 1.36 mmol) was dissolved in anhydrous toluene (6 mL), primary phosphine **20a** was added (0.25 g, 0.62 mmol) and the mixture was stirred at room temperature for one hour. The orange solution was analysed by $^{31}P\{^{1}H\}$ NMR spectroscopy to show the formation of the dichlorophosphine species at δ 159.7 ppm and the solvent was removed *in vacuo.* The orange solid was dissolved in anhydrous THF (6 mL) and triethylamine (0.38 mL, 1.63 mmol) and dicyclohexylmagnesium chloride (1.24 mL, 1.24 mmol, 1M in THF) were added. The reaction mixture was stirred at room temperature overnight. The solvent was removed *in vacuo* and the orange solid was purified by column chromatography (chloroform:petrol, 1:4) to yield the desired product as an orange solid (0.14 g, 40%)

Route 2:

44a (0.50 g, 1.11 mmol) was dissolved in anhydrous diethyl ether (40 mL) and cooled to – 78 °C. *n*-Butyllithium (0.49 mL, 1.22 mmol, 2.5M in hexane) was added dropwise and the reaction mixture was warmed to room temperature over 45 minutes. The solution was cooled back down to – 78 °C and chlorodicyclohexylphosphine (0.27 mL, 1.22 mmol) was added dropwise. The reaction mixture was stirred overnight at room temperature under nitrogen. The reaction was quenched with water (25 mL) and extracted with diethyl ether (3 x 50 mL). The combined organic phases were washed with water, dried over $MgSO_4$ and filtered. The solvent was removed and the dark orange solid was purified by column chromatography (petrol:chloroform 4:1) to yield an orange crystalline solid (0.39 g, 62 %).

^{1}H NMR (400 MHz, $CDCl_3$) δ 7.47 (m, 2H), 7.21 (d, $^3J_{HH}$ = 8.2 Hz, 2H), 2.37 (s, 6H), 2.23 (q, $^3J_{HH}$ = 7.3 Hz, 4H), 1.90 (s, 6H), 1.90-1.56 (m, 12H), 1.30- 0.78 (m, 10H), 0.90 (t, $^3J_{HH}$ = 7.3 Hz, 6H), 0.21 (s, 6H) ppm; **^{13}C{^{1}H} NMR** (100 MHz, $CDCl_3$) δ 150.6, 140.2, 137.9, 135.0 (d, J_{CP} = 19.2 Hz), 134.7 (d, J_{CP} = 19.2 Hz), 133.8, 132.5, 129.1, 128.3 (d, J_{CP} = 7.7 Hz), 32.1 (d, $^1J_{CP}$ = 12.5 Hz), 29.9 (d, $^2J_{CP}$ = 16.3 Hz), 28.7 (d, $^2J_{CP}$ = 6.7 Hz), 27.4 (d, $^3J_{CP}$ = 12.5 Hz), 27.1 (d, $^3J_{CP}$ = 6.7 Hz), 26.7, 17.6, 14.8, 14.4, 11.9, 10.5 (br) ppm; **^{31}P{^{1}H} NMR** (162 MHz, $CDCl_3$) δ 2.8 ppm; **^{11}B{^{1}H} NMR** (128 MHz, CDCl3) δ −2.1 ppm; **IR** (neat) $\tilde{\nu}$: 2927 (w), 2856 (w), 1551 (s), 1448 (m), 1321 (m), 1171 (s), 1145 (s), 946 (s) cm^{-1}; **HRMS** (AP^+) calcd. for $C_{37}H_{55}B_1N_2P_1$ $[M+H]^+$ requires m/z 568.4227, found *m*/*z* 568.4226.

4.8.3 Preparation of 8-((4-Diphenylphosphino)phenyl)-4,4-dimethyl-1,3,5,7-tetramethyl-2,6-diethyl-4-bora-3a,4a-diaza-*s*-indacene (89b)

Route 1:

Phosphorus pentachloride (0.112 g, 0.54 mmol) was dissolved in anhydrous toluene (6 mL), primary phosphine **20a** was added (0.100 g, 0.25 mmol) and the mixture was stirred at room temperature for one hour. The orange solution was analysed by $^{31}P\{^1H\}$ NMR spectroscopy to show the formation of the dichlorophosphine species at δ 159.7 ppm,the solvent was removed *in vacuo.* The orange solid was dissolved in anhydrous THF (6 mL) and triethylamine (0.15 mL, 1.1 mmol) and phenylmagnesium bromide (0.16 mL, 0.50 mmol, 3.0M in diethyl ether) were added. The reaction mixture was stirred at room temperature overnight. The solvent was removed *in vacuo* and the orange solid was purified by column chromatography (chloroform:petrol, 1:4) to yield the desired product as an orange solid (0.114, 82%).

Route 2:
44a (0.50 g, 1.11 mmol) was dissolved in anhydrous diethyl ether (40 mL) and cooled to -78 °C. *n*-Butyllithium (0.49 mL, 1.22 mmol, 2.5M in hexane) was added dropwise over five minutes and the reaction was warmed to room temperature over 45 minutes. The solution was cooled to -78 °C and chlorodiphenylphosphine (0.22 mL, 1.22 mmol) was added dropwise. The reaction was warmed to room temperature and stirred overnight. The reaction mixture was washed with water and extracted with diethyl ether. The combined fractions were dried over $MgSO_4$ and filtered. The solvent was removed *in vacuo* to yield a red/orange solid which was purified using column chromatography on silica gel (chloroform:hexane 1:4) and gave an orange solid (0.34 g, 56%). **^{1}H NMR** (400 MHz, $CDCl_3$) δ 7.45-7.42 (m, 2H), 7.41-7.35 (m, 10H), 7.34-7.30 (m, 2H), 2.47 (s, 6H), 2.35 (q, $^3J_{HH}$ = 7.3 Hz, 4H), 1.36 (s, 6H), 1.01 (t, $^3J_{HH}$ = 7.3 Hz, 6H), 0.30 (s, 6H) ppm; **^{13}C{^{1}H} NMR** (100 MHz, $CDCl_3$) δ 150.6, 139.8, 137.9, 137.8, 136.7 (d, J_{CP} = 11.5 Hz), 133.8, 133.6, 133.5, 132.4, 132.1, 132.0, 128.8, 128.5 (d, J_{CP} = 6.7 Hz), 17.4, 14.7, 14.5, 11.9, 10.4 (br) ppm; **^{31}P{^{1}H} NMR** (162 MHz, $CDCl_3$) δ −5.5 ppm; **^{11}B{^{1}H} NMR** (128 MHz, $CDCl_3$) δ −1.9 ppm; **IR** (neat) $\tilde{\nu}$: 2924 (w), 2863 (w), 1552 (s), 1455 (m), 1372 (w), 1314 (s), 1170 (s), 1144 (s), 1064 (m), 977 (s) cm^{-1}; **HRMS** (EI^+) exact mass calcd. for $C_{37}H_{43}N_2B_1P_1$ $[M+H]^+$ requires m/z 556.3288, found *m*/*z* 556.3294.

4.8.4 Preparation of [89a.Me][OTf] (93a)

89a (0.21 g, 0.36 mmol) was dissolved in DCM (4 mL) and methyl trifluoromethanesulfonate (0.08 mL, 0.73 mmol) was added. The reaction was stirred at room temperature for two hours, which produced an orange precipitate. The solid was filtered off and washed with petroleum ether (3 x 10 mL) to give the desired product as a fine orange solid. (0.18 g, 68 %).
^{1}H NMR (400 MHz, CD_3CN) δ 7.82 (dd, $^3J_{HH}$ = 8.2 Hz, $^3J_{HP}$ = 11.0 Hz, 2H), 7.67 (dd, $^3J_{HH}$ = 8.2 Hz, $^4J_{HP}$ = 2.6 Hz, 2H), 2.71 (m, 2H), 2.43 (s, 6H), 2.31 (q, $^3J_{HH}$ = 8.2 Hz, 4H), 2.04 (d, $^2J_{HP}$ = 12.4 Hz, 3H), 1.98-1.69 (br, 10H), 1.40 (m, 4H), 1.26-1.07 (br, 6H), 1.20 (s, 6H), 0.93 (t, $^3J_{HH}$ = 8.2 Hz, 6H), 0.30 (s, 6H) ppm; **^{31}P{^{1}H} NMR** (162 MHz, CD_3CN) δ 34.5 ppm; **^{11}B{^{1}H} NMR** (128 MHz, CD_3CN) δ −1.6 ppm. Low solubility precluded the collection of a ^{13}C NMR spectrum. **HRMS** (ESI^+) exact mass calculated for $C_{38}H_{57}N_2B_1P_1$ $[M]^+$ requires m/z 582.4383, found *m*/*z* 582.4382 (0.2 ppm).

4.8.5 Preparation of [89b.Me][OTf] (93b)

89b (0.13 g, 0.22 mmol) was dissolved in DCM (4 mL) and methyl trifluoromethanesulfonate (0.07 mL, 0.45 mmol) was added. The reaction was stirred at room temperature for two hours. After removal of the solvent, purification by column chromatography (chloroform:methanol, 10:0.3, R_f = 0.3) was performed to yield the desired product as an orange solid. (0.35 g, 61 %).
^{1}H NMR (400 MHz, $CDCl_3$) δ 7.75-7.70 (m, 4H), 7.66-7.59 (m, 10H), 3.01 (d, $^2J_{HP}$ = 13.7 Hz, 3H), 2.38 (s, 6H), 2.23 (q, $^3J_{HH}$ = 7.8 Hz, 4H), 1.19 (s, 6H), 0.91 (t, $^3J_{HH}$ = 7.8 Hz, 6H), 0.20 (s, 6H) ppm; **^{13}C{^{1}H} NMR** (100 MHz, $CDCl_3$) δ 151.8, 145.1 (d, J_{CP} = 2.8 Hz), 136.6, 135.3 (d, J_{CP} = 2.9 Hz), 133.4 (d, J_{CP} = 11.5 Hz), 133.1 (d, J_{CP} = 11.5 Hz), 133.0 (d, J_{CP} = 39.3 Hz), 131.3 (d, J_{CP} = 13.4 Hz), 130.6 (d, J_{CP} = 13.4 Hz), 128.2, 119.8, 119.2, 118.3, 117.7 (q, J_{CF} = 249.2 Hz), 17.4, 14.6, 14.4, 12.1, 10.4 (br), 9.34 (d, $^1J_{CP}$ = 57.5 Hz) ppm; **^{31}P{^{1}H} NMR** (162 MHz, $CDCl_3$) δ 22.6 ppm; **^{11}B{^{1}H} NMR** (128 MHz, $CDCl_3$) δ −1.9 ppm; HRMS (ESI^+) exact mass calculated for $C_{38}H_{45}N_2B_1P_1$ $[M]^+$ requires m/z 570.3444, found m/z 570.3443.

4.9 General Procedure for the Synthesis of Phosphonium Salts

Bod-dicyclohexylphosphine **89a** (0.27 mmol) was dissolved in anhydrous toluene (7 mL), the appropriate dihalogenated species (0.27 mmol) was added and the mixture was heated at 110 °C until complete consumption of the starting materials (~16 hours), which was confirmed by $^{31}P\{^1H\}$ NMR spectroscopy. The desired product was crystallised out of solution using a layered mixture of deuterated chloroform and pentane.

4.9.1 Preparation of 8-((4-Dicyclohexylphosphino)(fluorobutyl)phenyl)-4,4-dimethyl-1,3,5,7-tetramethyl-2,6- diethyl-4-bora-3a,4a-diaza-*s*-indacene (94)

^{1}H NMR (300 MHz, $CDCl_3$) δ 8.09 (m, 2H), 7.70 (m, 2H), 4.65 (t, J = 5.2 Hz, 1H), 4.50 (t, J = 5.2 Hz, 1H), 3.20 (m 4H), 2.44 (s, 6H), 2.28 (q, J = 7.6 Hz, 4H), 2.22-1.73 (m, 16H), 1.58-1.32 (m, 10H), 1.17 (s, 6H), 0.96 (t, J = 7.5 Hz, 6H), 0.26 (s, 6H) ppm; **^{13}C{^{1}H} NMR** (176 MHz, $CDCl_3$) δ 151.8, 144.4, 136.9, 133.4 (d, J_{CP} = 7.5 Hz), 133.4, 132.8, 131.3 (d, J_{CP} = 11.4 Hz), 128.4, 83.7, 82.8, 31.2, 30.4 (d, J_{CP} = 43.5 Hz), 26.6 (dd, J_{CP} = 13.0 Hz, J_{CP} = 2.9 Hz), 26.3 (m), 25.6, 19.5, 17.5, 15.9 (d, J_{CP} = 44.4 Hz), 14.8, 14.5, 12.1, 10.4 (br) ppm; **^{31}P{^{1}H} NMR** (121 MHz, $CDCl_3$) δ 32.6 ppm; **^{19}F{^{1}H} NMR** (470 MHz, $CDCl_3$) δ – 221. 3 ppm; **^{11}B{^{1}H} NMR** (96 MHz, $CDCl_3$) δ –0.4 ppm; **HRMS** (ESI^+) calcd. for $C_{41}H_{62}BFN_2P$ $[M+H]^+$ requires *m/z* 643.4729, found *m/z* 643.4719.

4.9.2 Preparation of 8-((4-Dicyclohexylphosphino)(bromobutyl)phenyl)-4,4-dimethyl-1,3,5,7-tetramethyl-2,6- diethyl-4-bora-3a,4a-diaza-*s*-indacene (95)

^{1}H NMR (400 MHz, $CDCl_3$) δ 8.02-7.94 (m, 2H), 7.73-7.63 (m, 2H), 3.57 (t, $^{3}J_{HH}$ = 5.1 Hz, 1H), 3.37 (t, $^{3}J_{HH}$ = 5.1 Hz, 1H), 3.29-3.19 (m, 4H), 2.40 (s, 6H), 2.23 (q, $^{3}J_{HH}$ = 7.3 Hz, 4H), 2.18-1.65 (m, 16H), 1.60-1.32 (m, 10H), 1.12 (s, 6H), 0.91 (t, $^{3}J_{HH}$ = 7.5 Hz, 6H), 0.21 (s, 6H) ppm; **^{13}C{^{1}H} NMR** (100 MHz, $CDCl_3$) δ 151.7, 144.3, 136.8, 133.4, 133.2, 132.6, 131.2, 128.3, 33.8, 32.5, 30.6, 30.0, 26.4, 26.2, 25.5, 19.5, 17.4, 15.6, 14.7, 14.4, 11.9, 10.4 (br) ppm; **^{31}P{^{1}H} NMR** (162 MHz, $CDCl_3$) δ 33.0 ppm; **^{11}B{^{1}H} NMR** (128 MHz, $CDCl_3$) δ –1.1 ppm; **IR** (ATR) $\tilde{\nu}$: 2929, 2857, 1555, 1448, 1323, 1174, 946, 728, 640 cm^{-1}; **HRMS** (ESI^{+}) calcd. for $C_{41}H_{63}BBrN_2P$ $[M\text{-}HBr]^{+}$ requires m/z 705.3915, found *m*/*z* 705.3919.

4.9.3 Preparation of 8-((4-Dicyclohexylphosphino)(iodobutyl)phenyl)-4,4-dimethyl-1,3,5,7-tetramethyl-2,6- diethyl-4-bora-3a,4a-diaza-*s*-indacene (96)

^{1}H NMR (400 MHz, $CDCl_3$) δ 8.00-7.93 (m, 2H), 7.69-7.64 (m, 2H), 3.33 (t, $^{3}J_{HH}$ = 5.6 Hz, 1H), 3.32 (t, $^{3}J_{HH}$ = 5.1 Hz, 1H), 3.16-2.90 (m, 4H), 2.39 (s, 6H), 2.23 (q, $^{3}J_{HH}$ = 7.6 Hz, 4H), 1.96-1.72 (m, 16H), 1.58-1.29 (m, 10H), 1.12 (s, 6H), 0.91 (t, $^{3}J_{HH}$ = 7.5 Hz, 6H), 0.21 (s, 6H) ppm; **^{13}C{^{1}H} NMR** (100 MHz, $CDCl_3$) δ 151.9, 144.6, 135.3, 133.6, 133.5, 132.7, 131.4, 128.3, 33.9, 33.1, 30.7, 30.3, 26.4, 26.2, 25.6, 17.5, 15.8, 14.8, 14.5, 12.2, 10.4 (br) ppm; **^{31}P{^{1}H} NMR** (162 MHz, $CDCl_3$) δ 33.0 ppm; **^{11}B{^{1}H} NMR** (128 MHz, $CDCl_3$) δ –19.3 ppm; **IR** (ATR) $\tilde{\nu}$: 2930, 2857, 1552, 1443, 1320, 1171, 945, 801, 731, 674, 601 cm^{-1}.

4.9.4 Preparation of 8-((4-Dicyclohexylphosphino)(fluoropropyl)phenyl)-4,4-dimethyl-1,3,5,7-tetramethyl-2,6- diethyl-4-bora-3a,4a-diaza-*s*-indacene (97)

^{1}H NMR (400 MHz, $CDCl_3$) δ 7.78-7.67(m, 4H), 7.32-7.25 (m, 4H), 4.47 (t, $^{3}J_{HH}$ = 5.4 Hz, 1H), 4.36 (t, $^{3}J_{HH}$ = 5.4 Hz, 1H), 3.24-3.14 (m, 4H), 2.40 (s, 9H), 2.24 (q, $^{3}J_{HH}$ = 7.6 Hz, 4H), 2.05-1.90 (m, 16H), 1.55-1.46 (m, 10H), 1.19 (s, 6H), 0.91 (t, $^{3}J_{HH}$ = 7.6 Hz, 6H), 0.21 (s, 6H) ppm; **^{31}P{^{1}H} NMR** (162 MHz, $CDCl_3$): δ 32.6 (s) ppm; **^{19}F{^{1}H} NMR** (376 MHz, $CDCl_3$): δ –223.1 ppm; **^{11}B{^{1}H} NMR** (128 MHz, $CDCl_3$): δ –1.0 ppm; **IR** (ATR) $\tilde{\nu}$: 2925, 2851, 1548, 1447, 1359, 1320, 1189, 1173, 1144, 941, 753, 663 cm^{-1}; **HRMS** (ESI+) calcd. for $C_{40}H_{60}BFN_2P$ $[M]^{+}$ requires m/z 629.4573, found *m*/*z* 629.4562.

4.9.5 Preparation of 8-((4-Dicyclohexylphosphino)(propargyl)phenyl)-4,4-dimethyl-1,3,5,7-tetramethyl-2,6- diethyl-4-bora-3a,4a-diaza-*s*-indacene (98)

^{1}H NMR (400 MHz, $CDCl_3$) δ 8.28-8.04 (m, 2H), 7.69-7.53 (m, 2H), 4.59 (t, $^{3}J_{HH}$ = 5.4 Hz, 1H), 4.47 (t, $^{3}J_{HH}$ = 5.4 Hz, 1H), 3.94-3.81 (m, 4H), 2.48-2.35 (m, 11H), 2.20-2.00 (m, 16H), 1.80-1.53 (m, 10H), 1.13 (s, 6H), 0.92 (t, $^{3}J_{HH}$ = 7.5 Hz, 6H), 0.21 (s, 6H) ppm; **^{31}P{^{1}H} NMR** (162 MHz, $CDCl_3$) δ 29.9 ppm; **^{11}B{^{1}H} NMR** (128 MHz, $CDCl_3$): δ–1.0 ppm; **IR** (ATR) $\tilde{\nu}$: 3301 (alkyne CC bond), 2969, 2857, 2209, 1549, 1450, 1320, 1172, 944, 802, 720 cm^{-1}.

Chapter 5: Chiral Fluorescent Catalysts

5 Chiral Fluorescent Catalysts

This chapter explores the development of a route to the first chiral, fluorescent phosphonite based on Bodipy and containing the Binol function. The novel phosphonites were then coordinated to a rhodium centre and were subsequently tested in an asymmetric hydrogenation reaction with the benchmark substrate methyl (Z) β-acetamidocinnamate (MAC) which gave excellent conversion and enantioselectivity.

5.1 Fluorescent Catalysts

There are several advantages for using a fluorescent ligand in catalysis, such as: 1) the ability to monitor low concentrations of a catalytically relevant species, 2) to assess catalyst contamination and 3) to monitor the catalytic pathway of a catalyst by measuring the photophysical properties at different stages of the cycle.

There are few examples of fluorescent catalysts within the literature; Plenio *et al*. tagged *N*-heterocyclic carbenes with a dansyl fluorophore and synthesised the corresponding palladium complexes [(NHC)Pd(allyl)Cl] which were used to follow the course of a Suzuki coupling reaction.[140] NHC groups are used because they can be tightly bound to a metal centre, therefore limiting problems such as the fluorophore dissociating from the transition metal centre. Figure 5.1 shows the fluorescence time curve for the NHC palladium-catalysed Suzuki coupling reaction described. Two notable changes were observed in the fluorescence behaviour of the dansyl group: the addition of the base and the addition of the aryl halide. This corresponds to the formation of catalytically active species from the pre-catalyst, and also during the cross-coupling reaction.

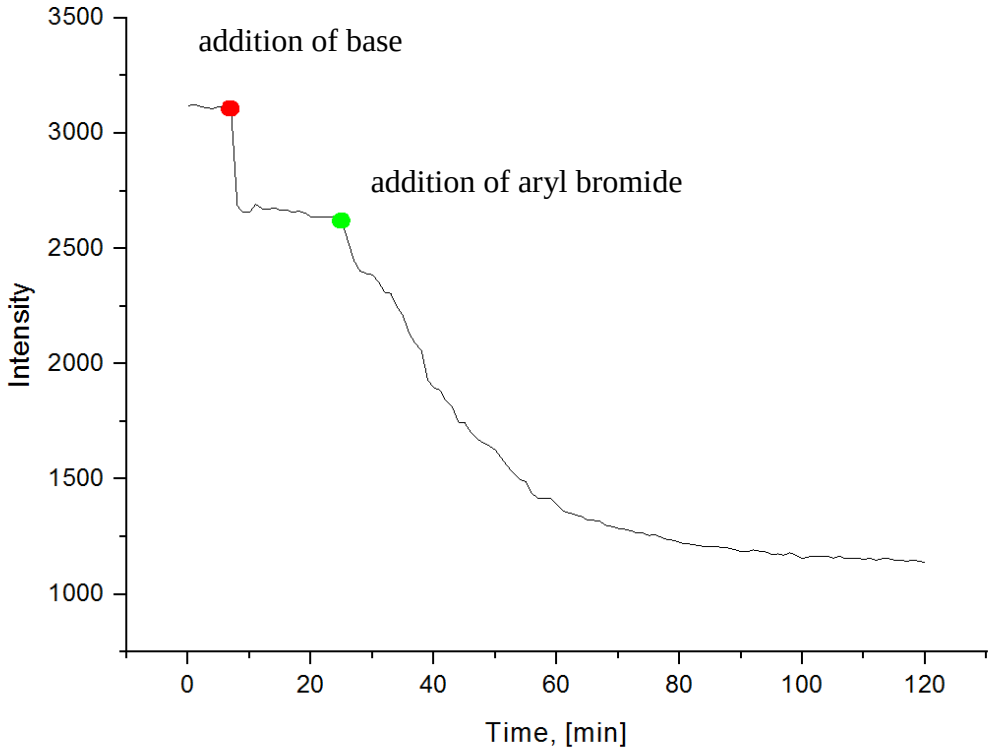

Figure 5.1 Fluorescence time curve for the NHC palladium-catalysed Suzuki coupling.

5.2 Chiral Bodipy Compounds

In 2009, Huszthy and co-workers reported two novel, enantiopure Bodipy-linked azacrown ether chemosensors, **99** and **100**, which are shown in Figure 5.2.[141] The two compounds exhibited prominent off-on fluorescence changes on coordination to metals such as Ca^{2+} and Pb^{2+}. In some cases, more than a 10-fold increase was observed upon complexation.

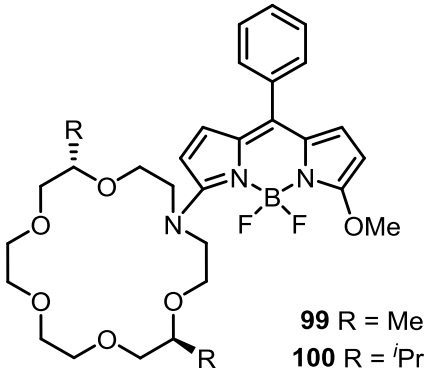

Figure 5.2: Chiral compounds 99 and 100.

In Figure 5.3, compound **101**, synthesised by Ziessel and co-workers, is an example of a resolved Bodipy compound based around an asymmetric boron atom, where the chirality is embedded in the

core structure of the fluorophore.[142] Nabeshima described the efficient synthesis of boron-centred chiral Bodipy **102**, based on the intramolecularly B-O bonded Bodipy.[143] In 2014 Hall *et al*. published a route for the synthesis of axially chiral Bodipy systems, **103** in Figure 5.3 and is currently investigating the interactions between these dyes with chiral analytes in solution and their potential applications in sensing.[144]

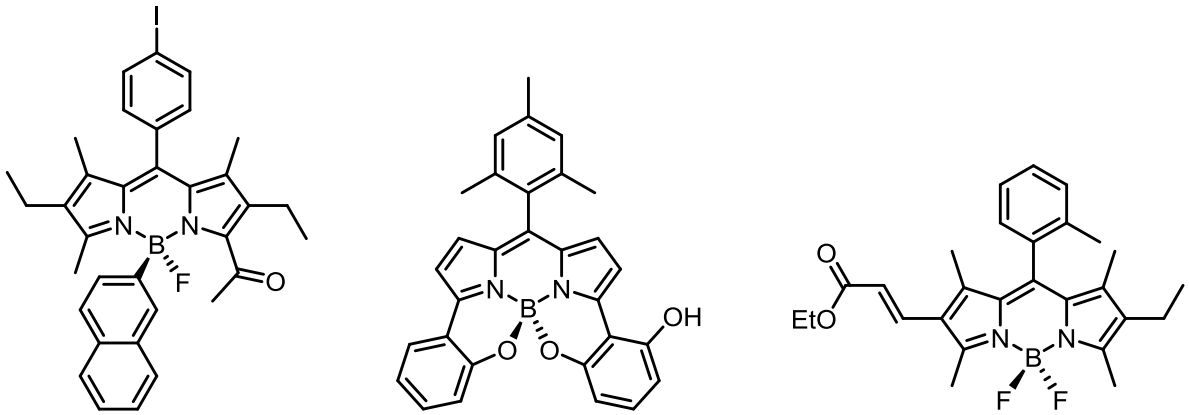

101 **102** **103**

Figure 5.3 Resolved chiral Bodipys containing an asymmetric boron centre (left, 101) and (centre) the Nabeshima compound 102, and (right) Hall's compound 103 an unresolved boron-centred chiral Bodipy.

The ability to make chiral Bodipys opens up the potential development of chiral Bodipy ligands for asymmetric catalysis. The prospect of synthesising a fluorescent catalyst has many positive outcomes, such as the potential to detect low concentrations of catalytically important species due to the sensitivity of the fluorescence method, and the ability to monitor the purity of a product after a catalytic reaction, allowing for verification that there is no contamination i.e. catalyst, remaining in the product.

5.3 Ligand Knowledge Base

The Ligand Knowledge Base (LKB) was developed by Fey and co-workers[145] to collect information on ligands in metal complexes and to predict the effects that the ligands may have, before being synthesised experimentally. A range of monodentate and chelating phosphorus donor ligands, carbon donors and P-N chelating donor ligands have been mapped to create the database with more than 1000 ligands.[146, 147] An example of the factors that have been calculated within this model include Tolman (steric and electronic) parameters, molecular orbital energies and adduct binding energies. The LKB can also be used to identify applications for the ligands, where the assumption is that ligands grouped close to one another may be efficient at the same type of catalytic process.

Principal Component Analysis (PCA) can be used to identify interactions between variables within a dataset. It has been used within the LKB to identify chemically similar ligands which will be clustered together in a 3D scatter graph, i.e. ligands which are clustered together are likely to have similar properties than those ligands further away; an example of a relevant plot is shown in Figure 5.4.[145]

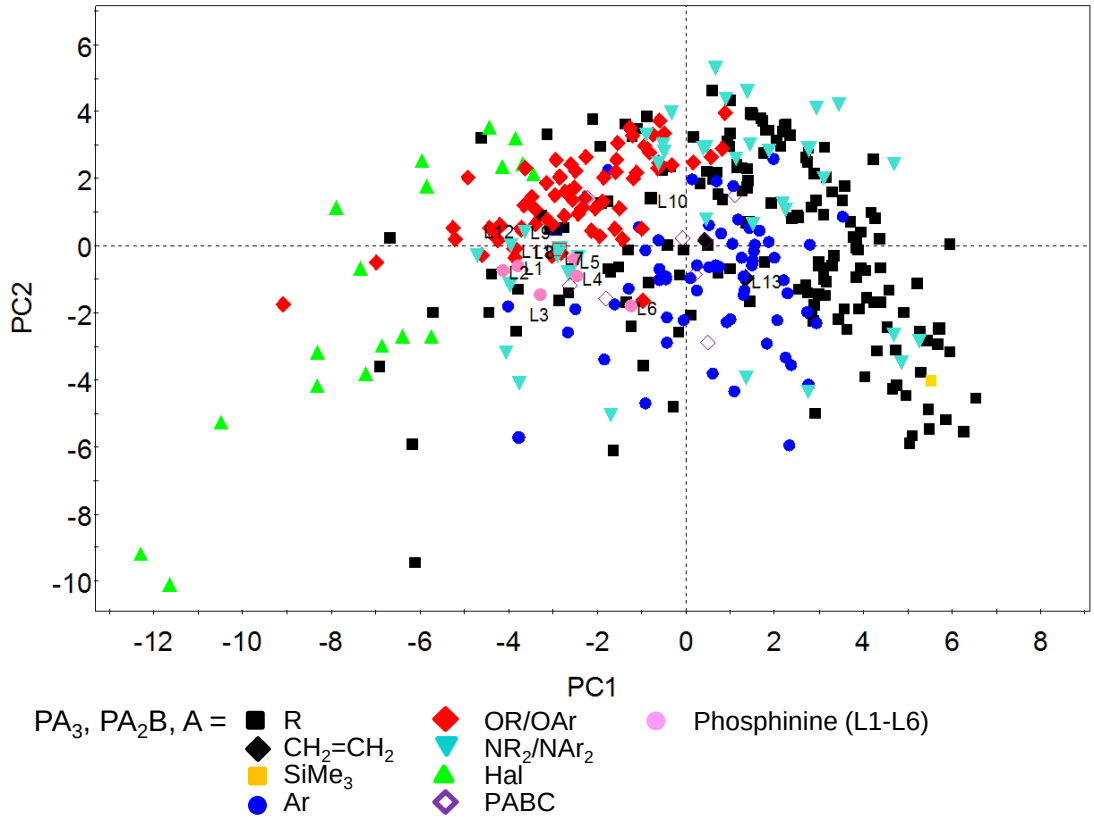

Figure 5.4 An example of a plot representing chemically similar ligands by colour.

Fey modelled a number of MOP ligands reported by the Higham research group, including phosphonites and phosphiranes, and this information has been used to predict the direction of the research of the novel compounds synthesised within this chapter.

5.3.1 Phosphonites

Phosphonites are a class of compound that contain one P-C bond and two P-O bonds. They can be used in homogeneous catalysis and their corresponding transition metal complexes are of interest due to the success of the related phosphines, phosphinites and phosphites in a variety of catalytic reactions.[148] The primary phosphine offers a route to a novel, fluorescent derivative, which will be described in the next section.

5.4 Synthesis of Fluorescent, Chiral Phosphonites 104 and 105

The synthesis of novel fluorescent, chiral phosphonites **104** and **105** is a one-pot, two step reaction starting from primary phosphine **20a**, as shown in Scheme 5.1.

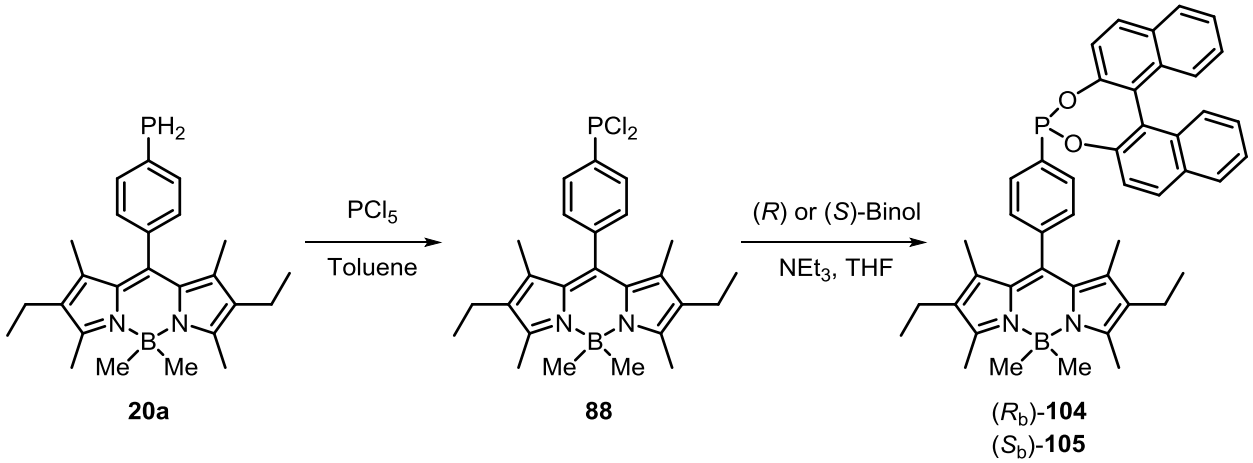

Scheme 5.1 One-pot, two-step synthesis to novel compounds 104 and 105.

Phosphorus pentachloride and primary phosphine **20a** were dissolved in anhydrous toluene and stirred under a nitrogen atmosphere at room temperature. The solution was analysed by $^{31}P\{^{1}H\}$ NMR spectroscopy to show a singlet at δ 159.7 ppm corresponding to the Bodipy dichlorophosphine derivative **88**. The solvent was removed *in vacuo* to remove PCl_3 and the subsequent red solid was dissolved in anhydrous THF. Triethylamine and (*R*) or (*S*)-Binol were added and the solution was stirred for a further 16 hours. The compounds were purified by column chromatography on silica gel to yield the desired products as orange solids. The compounds were analysed by $^{31}P\{^{1}H\}$ NMR spectroscopy and showed single peaks for (R_b)-**104** at δ 181.9 ppm and (S_b)-**105** at δ 181.5 ppm.

5.5 Photophysical Properties

The photophysical properties for (R_b)-**104** and (*S*)-**105** were recorded at room temperature in dry, degassed tetrahydrofuran, which included its absorption and emission spectra and its quantum yield.

Table 5.1 Comparison of the photophysical properties of primary phosphine 20a, (R_b)-104 and (S_b)-105.

	λ_{abs} (nm)	λ_{em} (nm)	Φ_F
20a	512	526	0.33
(R_b)-104	513	529	0.31
(S_b)-105	513	529	0.31
[Rh((S_b)-105)]	512	535	0.27

Measured in dry, degassed tetrahydrofuran at room temperature, dyes were excited at 485 nm; Fluorescence quantum yields were measured with respect to 4,4-difluoro-8-phenyl-1,3,5,7-tetramethyl-2,6-diethyl-4-bora-3a,4a-diaza-s-indacene **57**.

Table 5.1 shows that the addition of the Binol group onto the primary phosphine has no significant effects on the absorption and emission maxima, and only a minimal decrease in the quantum yield. The absorption and emission graph for compound (R_b)-**104** is shown in Figure 5.5. The absorption maxima at 513 nm is due to the S_0-S_1 (π-π^*) electronic transition associated with the Bodipy core. The small Stokes shift of 13 nm is typical of many Bodipy compounds, and shows that there is minimal structural change between the ground state and excited state of the fluorophore.[39]

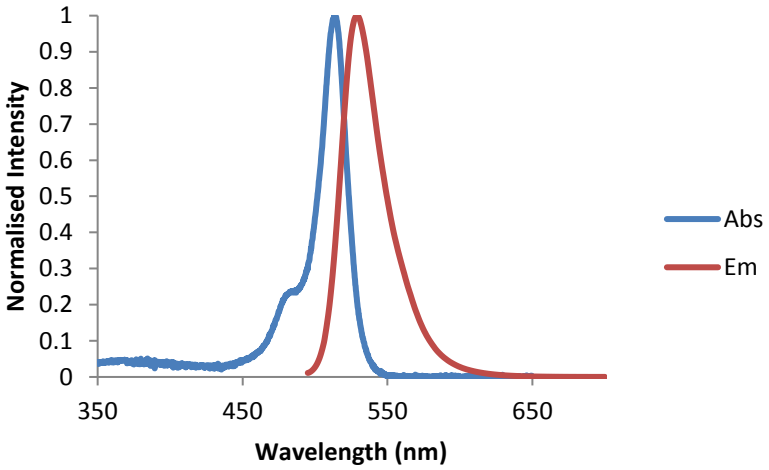

Figure 5.5 Absorption and emission graph for compound (R_b)-104.

5.5.1 Use in Asymmetric Hydrogenation

One equivalent of the novel Bodipy phosphonites (R_b)-**104** and (S_b)-**105** was stirred with the rhodium complex $[Rh(nbd)_2][BF_4]$ in anhydrous dichloromethane for thirty minutes and used immediately *in situ*. The Rh coordinated complex [Rh((R_b)-**104**)] was tested in an asymmetric hydrogenation reaction using a benchmark substrate, methyl (Z)-β-acetamidocinnamate (MAC), shown in Scheme 5.2. The conditions that were initially employed were published by Pringle and co-workers in 2000, when they tested their MOP-based phosphonites in an asymmetric hydrogenation reaction of methyl 2-acetamidoacrylate.[149]

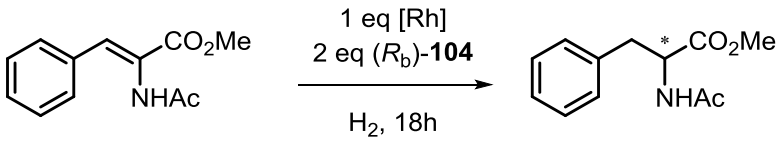

Scheme 5.2 First attempt at asymmetric hydrogenation with (R_b)-104.

The rhodium-catalysed asymmetric hydrogenation reaction studied by Pringle utilised the three phosphonite ligands shown in Figure 5.6, all went to full conversion, but gave a wide range of enantioselectivities, which can be seen in Table 5.2.

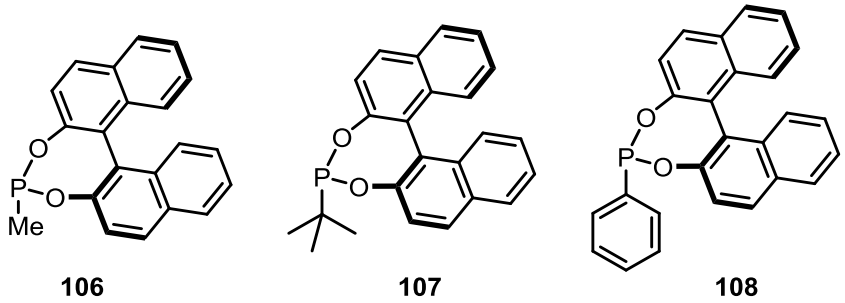

106 **107** **108**

Figure 5.6 Ligands 106, 107 and 108 tested by Pringle and co-workers in an asymmetric hydrogenation reaction of methyl 2-acetamidoacrylate.

Table 5.2 Conversions and enantioselectivities for compounds 106-108 in an asymmetric hydrogenation reaction.[149]

Ligand	Conv.	%*ee*
106	>99	80
107	>99	10
108	>99	63

The Bodipy phosphonite (R_b)-**104** was tested under the same hydrogenation conditions as described above, in order to investigate how its performance compared to those studied by Pringle – Bodipy phosphonite (R_b)-**104** was found to give >99% conversion, but only 36(*S*) % *ee*.

In order to try and increase the enantioselectivity of the reaction, a screening regimen was undertaken to identify the optimum conditions. The reaction time and the Rh complex remained the same, however, the hydrogen pressure was increased from 1.5 bar to 5 bar. This resulted in a >99% conversion and also a >99 (*S*)% *ee*, as shown in the chromatogram in Figure 5.7.

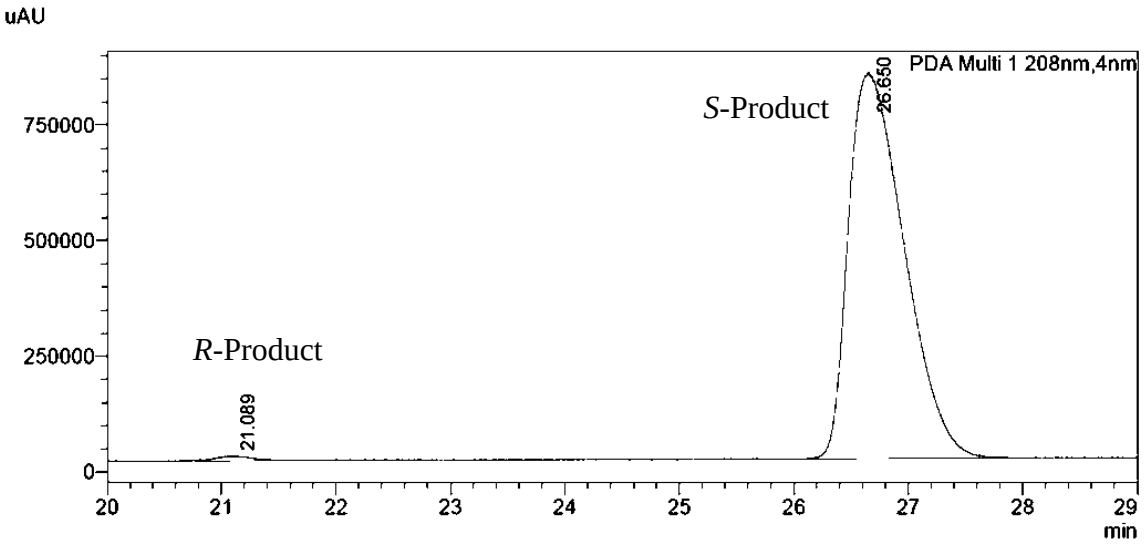

Figure 5.7 HPLC chromatogram showing 99% *ee* for the *S*-product using the novel fluorescent catalyst (R_b)-104.

The product from the asymmetric hydrogenation was subsequently tested for any emissive signal, which would inform us if there was any catalytic amounts of a fluorescent complex still present. The absorption and emission spectra showed no signs of any peaks corresponding to the presence of a Bodipy compound,which confirms that there are no Bodipy-based compounds in the final product. In order to confirm there is no rhodium metal remaining – whereby the rhodium has dissociated from the Bodipy backbone – XPS (X-ray Photoelectron Spectroscopy) could be utilised.

The absorption and emission spectra were recorded for the rhodium complex, [Rh-((S_b)-**105**)] and are shown in Figure 5.8. The maxima appeared to be unaltered compared to (R_b)-**104**, with a λ_{abs} = 512 nm and a λ_{em} = 535 nm. The quantum yield was slightly lower than the ligand (0.27 vs 0.31) which may allow us to compare the two stages (free ligand and metal coordination) of the catalytic cycle by fluorescence.

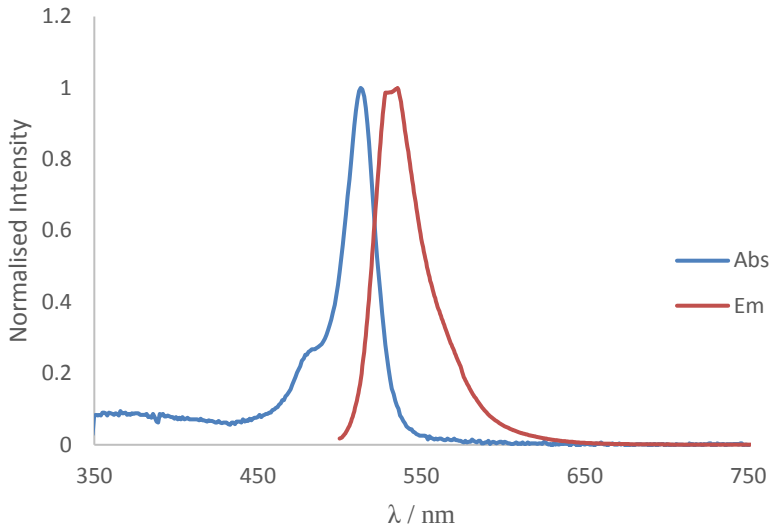

Figure 5.8 Absorption and emission spectra for [Rh-((*S*)-105)] measured in dry, degassed tetrahydrofuran at room temperature.

The asymmetric hydrogenation reaction of methyl (Z)-β-acetamidocinnamate (MAC) using [Rh-((S_b)-**105**)] was attempted however the conversion and enantioselectivity are still pending. Future work for this chapter would involve synthesising the three compounds from Pringles' paper and testing them under the new conditions to see if the enantioselectivities also increase – this will allow a fair comparison.

5.6 Summary

A novel fluorescent, chiral phosphonite ligand has been prepared and used successfully in an asymmetric hydrogenation reaction of MAC to give >99% conversion and >99% selectivity. The synthesis of the fluorescent phosphonite was a one-pot two step reaction that was easily monitored by $^{31}P\{^{1}H\}$ NMR spectroscopy, and formed the products in moderate yields. The ability to purify this class of compound via column chromatography is remarkable without seeing any degradation. The fluorescent catalyst will allow for monitoring of catalytic pathways, and also the detection of any contamination in the final product. Future work will include exploring a range of other benchmark substrates to see how efficient the Bodipy phosphonite catalyst can be in other reactions.

5.7 Experimental

5.7.1 General Procedure

All air- and/or water-sensitive reactions were performed under a nitrogen atmosphere using standard Schlenk line techniques. Tetrahydrofuran was dried over sodium/benzophenone, toluene was dried over sodium, dichloromethane was dried over calcium hydride, and deuterated chloroform was dried over phosphorus pentoxide; all solvents were distilled prior to use. All starting materials were purchased from Sigma Aldrich, Alfa Aesar or Fisher and were used as received. Column chromatography was performed on silica gel (40-63 μm, 60 Å) from Merck, thin-layer chromatography was carried out using Merck aluminium-based plates with silica gel and fluorescent indicator (254 nm). ^{1}H, $^{13}C\{^{1}H\}$, $^{19}F\{^{1}H\}$, $^{31}P\{^{1}H\}$ and $^{11}B\{^{1}H\}$ NMR spectra were recorded on a JEOL ECS-400 (^{1}H 399.78 MHz) or Bruker Avance III 300 (^{1}H 300.13 Hz) spectrometer at room temperature; ^{1}H and ^{13}C chemical shifts were relative to tetramethylsilane, ^{31}P chemical shifts were relative to 80% H_3PO_4, ^{11}B chemical shifts were relative to $BF_3.Et_2O$ and ^{19}F chemical shifts were relative to $CFCl_3$. Infrared spectra were recorded on a Varian 800-FT-IR spectrometer and mass spectrometry was carried out by the EPSRC NMSF, Swansea.

5.7.2 Synthesis of Bodipy Phosphonites (R_b)-104 and (S_b)-105

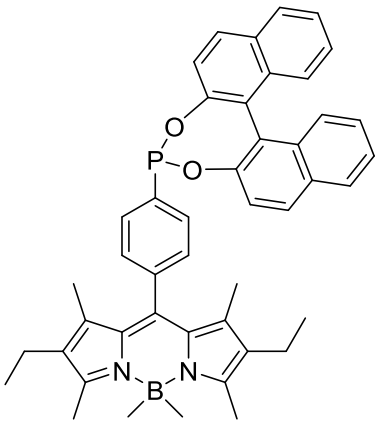

PCl_5 (339 mg, 1.63 mmol) was dissolved in anhydrous toluene (10 mL). **20a** (300 mg, 0.74 mmol) was added and the reaction mixture was stirred under nitrogen for 45 minutes. The volatiles were removed *in vacuo* to give the corresponding dichlorophosphine (^{31}P NMR spectrum in $CDCl_3$ showed a peak at δ = 159.7 ppm as a red solid). THF (10 mL), NEt_3 (0.45 mL, 3.26 mmol) and (*R*)- or (*S*)-BINOL (0.74 mmol) were added and the solution was stirred overnight. The volatiles

were removed *in vacuo* and the crude product was purified by column chromatography (anhydrous toluene) to give the title compound as a red solid: 0.29 g, 55% for (*R*)-**104** and 0.28 g, 52% for (*S*)-**105**)).

^{1}H NMR (700 MHz, $CDCl_3$) δ 8.10 (d, *J* = 8.7 Hz, 1H), 8.01 (d, *J* = 8.2 Hz, 1H), 7.90 (d, *J* = 8.6 Hz, 1H), 7.69 (m, 2H), 7.63 (t, *J* = 7.5 Hz, 2H), 7.52-7.43 (m, 4H), 7.34 (m, 4H), 6.72 (d, *J* = 8.7 Hz, 1H), 2.52 (s, 6H), 2.40 (q, *J* = 7.5 Hz, 4H), 1.34 (s, 6H), 1.07 (t, *J* = 7.5 Hz, 6H), 0.35 (s, 6H) ppm; **^{13}C{^{1}H} NMR** δ 151.0, 149.8, 148.3 (d, *J* = 5.4Hz), 141.3, 139.4, 139.0, 138.8, 138.0, 133.6, 133.1, 132.7, 131.2, 131.0 (d, *J* = 10.2 Hz), 130.9, 129.4, 129.2, 128.8, 128.7 (d, *J* = 6.5 Hz), 128.5 (d, *J* = 22.8 Hz), 128.3, 127.0, 126.5, 126.3, 125.2, 125.1, 122.4, 121..5, 17.6, 14.9, 14.5, 12.3, 10.4 (br) ppm; **^{31}P{^{1}H} NMR** (121 MHz, $CDCl_3$) δ 181.9 ppm; **^{11}B{^{1}H} NMR** (96 MHz, $CDCl_3$) δ – 0.5 ppm.

5.7.3 General Procedure for Rhodium-Catalysed Asymmetric Hydrogenation of Prochiral Alkene MAC

The rhodium source, $[Rh(nbd)_2][BF_4]$ (0.008 mmol, 1.0 mol%) and the ligand (**104**/**105**) (0.009 mmol, 1.1 mol%) were combined in a 45 mL capacity autoclave and dissolved in 4.5 mL of anhydrous DCM, and left to stir for 45 minutes under a nitrogen environment. The substrate (MAC), (0.79 mmol, 1.0 eq) was added, the autoclave was loaded with 5 bar pressure of hydrogen gas. The misture was stirred at room temperature for 18 hours. Conversions were calculated from ^{1}H NMR spectroscopy, where samples were taken from the crude reaction mixture and dissolved in deuterated chloroform. After sample filtration through a plug of silica gel, and again using column chromatography (toluene) in order to remove any traces of colour from the final product, the enantioselectivity was determined using chiral HPLC, using a Phenomenex Lux 5u Cellulose-1 chiral column (250mm x 4.6mm ID). Retention times for product = 21.1 min (*R*) and 26.7 min (*S*) (>99%).

Chapter 6: Synthesis of a Bodipy ‘Switch’

6 Synthesis of a Bodipy 'Switch'

This chapter describes the synthesis of Bodipy compounds with a potential application as a 'switch'. The Bodipy compounds that have previously been described in this thesis have all had an aryl linker separating the Bodipy core and the phosphorus group in the 8-position, illustrated in Figure 6.1. The aryl linker appears to insulate the phosphorus and metal from the Bodipy photophysical properties as evidenced by the calculated molecular orbitals shown in Section 2.4. This chapter details an investigation where the phosphorus is likely to be incorporated in the frontier orbitals of the compounds – thus, rather than being insensitive to the Bodipy (which is a useful attribute for imaging), the phosphorus donor can now act as a reporter to its environment – representing an off/on switch which could be manipulated in sensing applications.

The photophysical properties will be recorded and compared with their analogues containing the aryl linker, to establish the effect that the aryl linker has on the fluorescence quantum yield, absorption and emission maxima and the Stokes' shift.

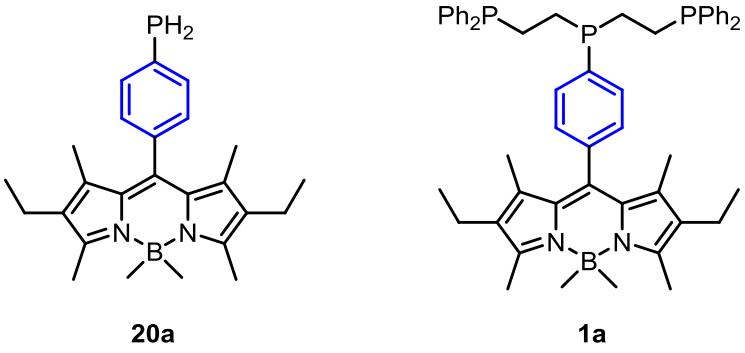

20a **1a**

Figure 6.1 Examples of compounds where the Bodipy core and the phosphorus group are separated by an aryl linker.

6.1 Introduction

There are examples in the literature where metal coordination to fluorescent compounds affects the photophysical properties of the resulting complexes, causing a switching of the fluorescence "off" or "on" upon coordination. Fluorescent transition metal phosphine complexes are usually categorised into either i) LMCT, Ligand-to-Metal Charge Transfer (with phosphines as donors) ii) MLCT, Metal-to-Ligand Charge Transfer (with phosphines as acceptors) or iii) MMCT, Metal-to-Metal Charge Transfer (with phosphines as bridging ligands).[150]

There are examples in the literature of nitrogen donors on a fluorophore that lead to fluorescence quenching via electron transfer processes such as intramolecular and Photoinduced electron Transfer (PeT).[151, 152]

Figure 6.2 shows an example of an acid-responsive fluorescent switch where the presence of a proton increases the fluorescence quantum yield from <0.01 to 0.34, which was synthesised in 2012 by Saito.[153]

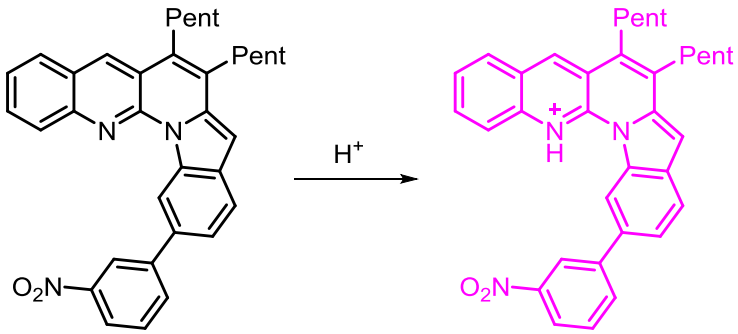

Figure 6.2 Acid-responsive fluorescent compound prepared by Saito and co-workers; the fluorescence was switched on when the amine was protonated, and switched off upon deprotonation.

Figure 6.3 shows an example of a purposely quenched phosphine-fluorophore that is activated upon Staudinger ligation (a reaction between an azide and a phosphine). Bertozzi has published several fluorescent phosphorus-containing compounds which can be used for live-cell imaging.[154]

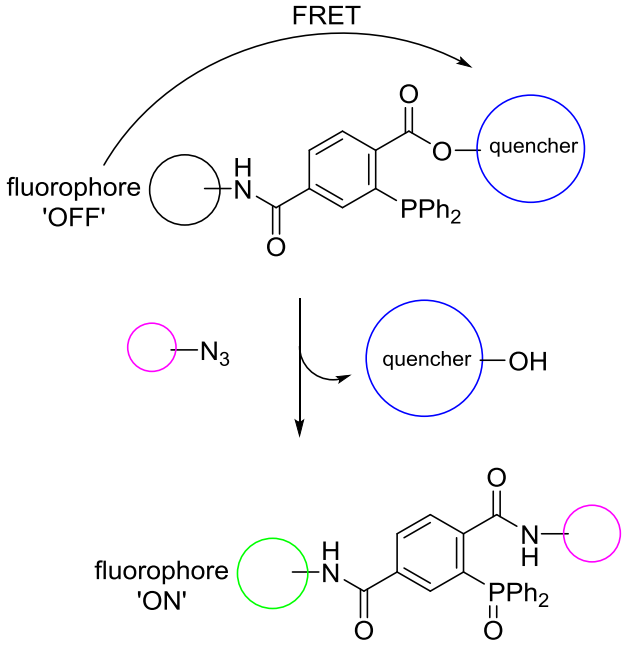

Figure 6.3 Schematic of a FRET-based fluorogenic phosphine for live-cell imaging.

6.1.1 Phosphine Oxides and Oxidative Stress

Oxidative stress refers to the imbalance between Reactive Oxygen Species (ROS) and anti-oxidant defence. There are assays available that measure oxidative stress in cell samples that have fluorescent indicators in them.[155, 156]

Reactive Oxygen Species (ROS) are radicals, ions or molecules that have a single unpaired electron which makes them highly reactive; they can be categorised into two types of ROS: free oxygen radicals, (such as superoxide and organic radicals), and non-radical ROS (such as hydrogen peroxide and singlet oxygen).[157] ROS have been associated with cancer - elevated rates have been detected in almost all cancers, where they are responsible for the promotion of tumour development and progression. High levels of ROS can be found in cancer cells due to several reasons, including increased metabolic activity or mitochondrial dysfunction.[158, 159]

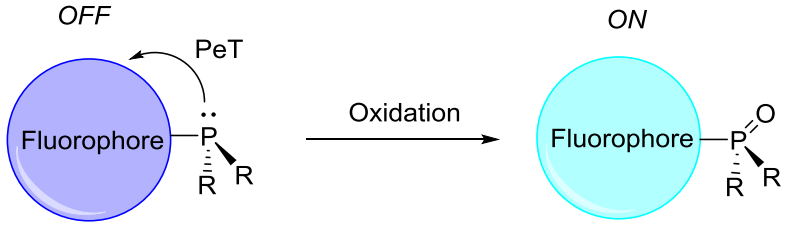

Figure 6.4 Photoinduced electron Transfer mechanism for the oxidation of a phosphine.

There are several known examples of fluorescent phosphines that have been used as sensors for reactive oxygen species (ROS). They can display interesting fluorescence "turn-on" properties due to the oxidation of the phosphine, which deactivates the phosphorus-to-fluorophore Photoinduced electron Transfer (PeT), and results in a reappearance of the fluorophore's emission, illustrated in Figure 6.4.[160]

Figure 6.5 shows four examples of ROS sensors: Akasaka's diphenyl-1-pyrenylphosphine, **109**, showed no fluorescence but the corresponding oxide showed blue fluorescence.[161] Santa synthesised compound **110** as an effective way to detect hydroperoxides, which is important in many different fields including certain cancers and Alzheimer's disease. Compound **111** is weakly fluorescent, but upon oxidation, due to the presence of hydroperoxides, becomes thirty-one times more fluorescent.[162] Imato designed a novel fluorescent probe for monitoring hydrogen peroxide in cellular systems; **112** was developed with Photoinduced electron Transfer (PeT) in mind, with the diphenylphosphine moiety acting as the donor and the 7-hydroxycoumarin as the acceptor. It was rationalised that the formation of the oxide would cancel the PeT process, which in turn would switch the fluorescence on – this was found to be the case.[163]

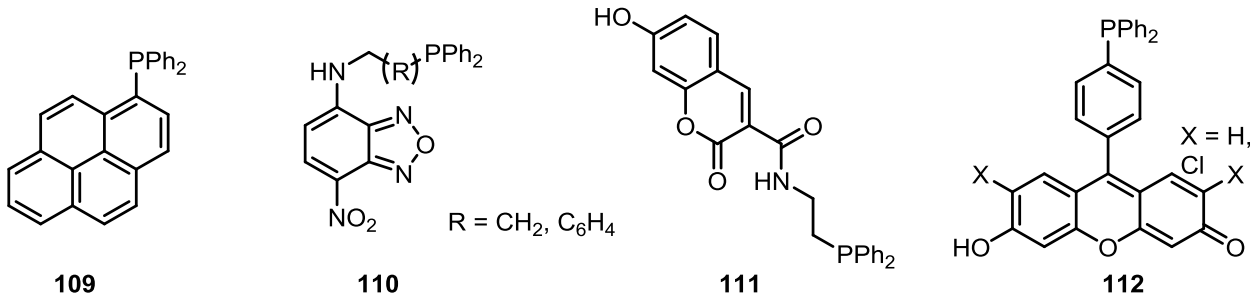

Figure 6.5 Four examples of phosphorus-containing reactive oxygen species sensors.

6.2 Results and Discussion

6.2.1 Novel Phosphine Bodipy Compounds via a Thioether Cleavage Reaction

This research was part of a collaboration with Dr Keith Pannell from the University of Texas, El Paso, whose research group published work showing the rapid reaction between ethylenediamine and 8-thiomethyl Bodipy, as illustrated in Figure 6.6.[164] This reaction could be applicable to a range of diamines, opening up a potentially large range of novel compounds.

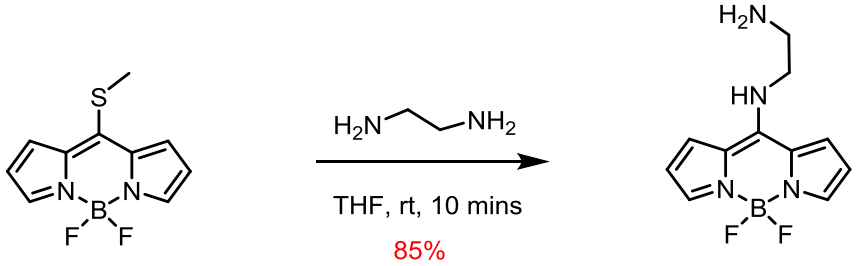

Figure 6.6 The reaction with an ethylenediamine and 8-thiomethyl Bodipy.

This reaction identified a simple way to introduce an amine into the 8-position of the Bodipy core, of interest to our research group was whether phosphorus could be introduced into the same position. However, the corresponding diphosphine analogue of the diamine that Pannell utilised in Figure 6.5 is volatile and can spontaneously ignite in air, therefore the reaction was attempted using a range of more user-friendly primary phosphines, such as **20a**, as shown in Scheme 6.1.

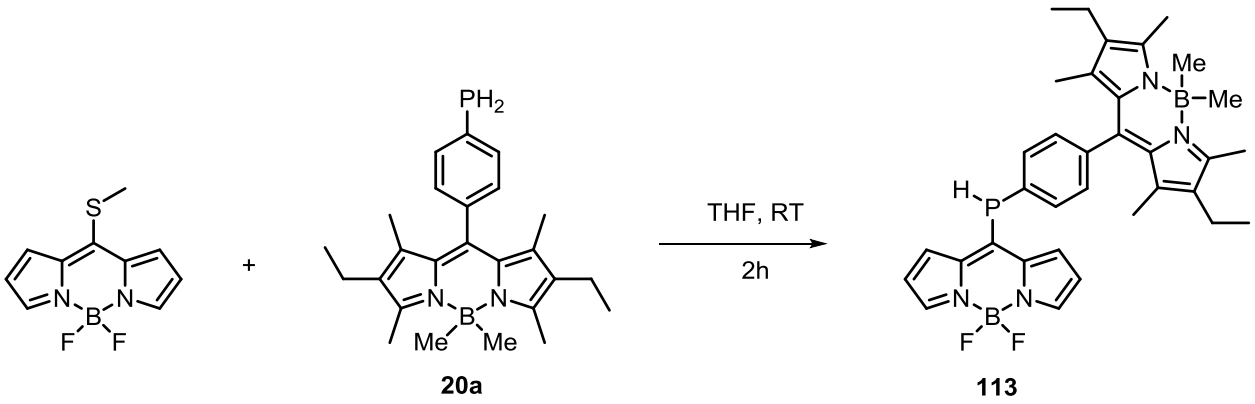

Scheme 6.1 Reaction between 20a and 8-thiomethyl Bodipy to form compound 113.

Compound **20a** and 8-thiomethyl Bodipy were combined in anhydrous THF and stirred for ten minutes; the solution was analysed by $^{31}P\{^{1}H\}$ NMR spectroscopy, which showed two species to be present – a peak at δ –126.2 ppm which corresponded to the primary phosphine starting material **20a**, and a peak at δ –61.0 ppm, which is indicative of a secondary phosphine. Further analysis by ^{31}P-^{1}H NMR spectroscopy revealed that the peak at δ −61.0 ppm was a doublet of triplets, ($^{1}J_{PH}$ = 230.7 Hz, $^{3}J_{PH}$ = 7.4 Hz) which is expected for compound **113**, due to the splitting of the P−H proton, and also the *ortho*-aryl protons from the phenyl ring. After a further two hours of stirring, no more product had formed, so the reaction was stopped and purified by column chromatography to yield **113** in a poor yield of 11%. The reaction was attempted again in anhydrous THF at 76 °C overnight which increased the yield to 40%.

The photophysical properties of di-Bodipy compound **113** were measured which concluded that the absorption and emission maxima had been unaltered, (512 nm and 527 nm respectively), however, the quantum yield had reduced from 0.33 (compound **20a**) to 0.068, indicating that the presence of a phosphorus atom bound directly to the Bodipy core is detrimental to the fluorescence. Figure 6.7 shows the absorption and emission spectra of the di-Bodipy compound **113**.

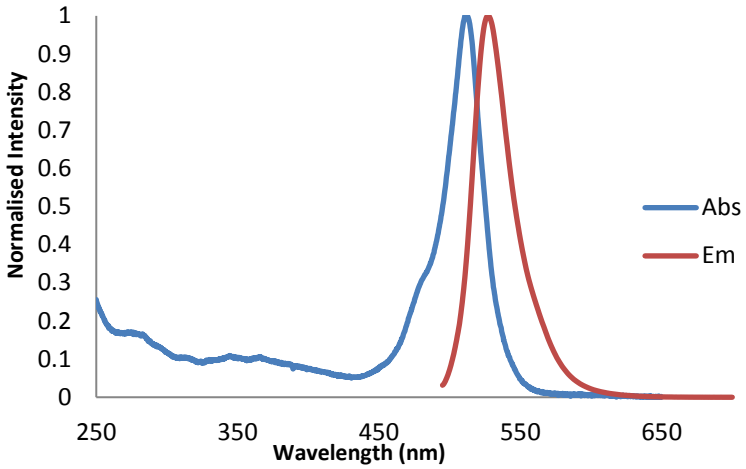

Figure 6.7 Absorption and emission spectra for di-Bodipy 113 measured in dry, degassed tetrahydrofuran at room temperature.

Although the research that has been described above did successfully add a phosphorus atom directly on to the Bodipy core, (and several phosphines could be used using this method, in principle), a new approach was taken. Bodipy compounds with a halogen situated in the 8-position could be substituted with a phosphine, a literature search discovered the following synthesis to form compound **116**.[165, 166]

Compound **116** was synthesised via a three-step synthesis shown in Scheme 6.2. Pyrrole was reacted with thiophosgene in anhydrous diethyl ether at 0 °C to give **114** which was purified through a silica plug. Compound **114** which was then reacted with hydrogen peroxide and potassium hydroxide in aqueous methanol to form **115** which precipitated out as pale yellow needles in a good yield of 80%.

Compound **115** can be converted into the chloro- or bromo-Bodipy structures **116** and **117** respectively. The synthesis of **116** was achieved by heating **115** at reflux with phosphoryl oxychloride in 1,2-dichloroethane for three hours before being cooled and treated with triethylamine and boron trifluoride. Purification by column chromatography yielded **116** as a red crystalline solid and a sample suitable for X-ray crystallographic analysis was obtained by evaporation of deuterated chloroform and is shown in Figure 6.8. Bodipy **117** was synthesised by stirring **115** with phosphoryl oxybromide in 1,2-dichloroethane at room temperature for 72 hours. After purification by column chromatography, compound **117** was isolated as a red solid in a good yield of 80% and was also analysed by X-ray crystallography after evaporation in deuterated chloroform, as shown in Figure 6.8.

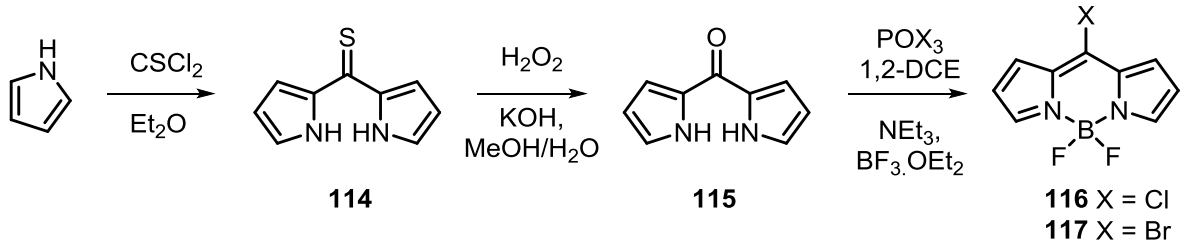

Scheme 6.2 Synthesis of halo-substituted Bodipy compounds 116 and 117.

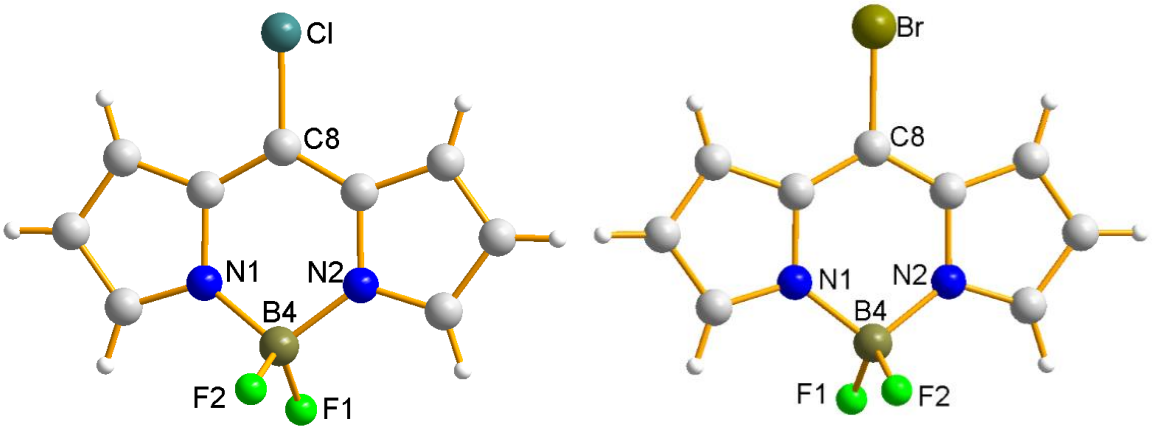

Figure 6.8 Molecular structures of 116 (*l*) and 117 (*r*). Selected bond distances [Å] and angles [°] for 116: Cl1-C8 1.7187(16), B4-F1 1.383(2), B4-F2 1.381(2); F1-B4-F2 109.13(13), F1-B4-N2 110.20(13). Selected bond distances [Å] and angles [°] for 117: Br1-C8 1.8676(19), B4-F1 1.376(3), B4-F2 1.388(3); F1-B4-F2 109.82(18), F1-B4-N2 110.81(18).

The Cl-C bond length of 1.7187(16) Å and the Br-C bond length of 1.8676(19) Å are in agreement with similar structures published within the literature.[167, 168]

6.3 Substitution to give Diphenylphosphino Derivative 118

A method to synthesise phosphine **118** was published by Peña-Cabrera and co-workers in 2013 where they reacted three equivalents of diphenylphosphine with thiomethyl Bodipy, to give **118**, shown in Figure 6.9, however, after several attempts this reaction was not successful.[169]

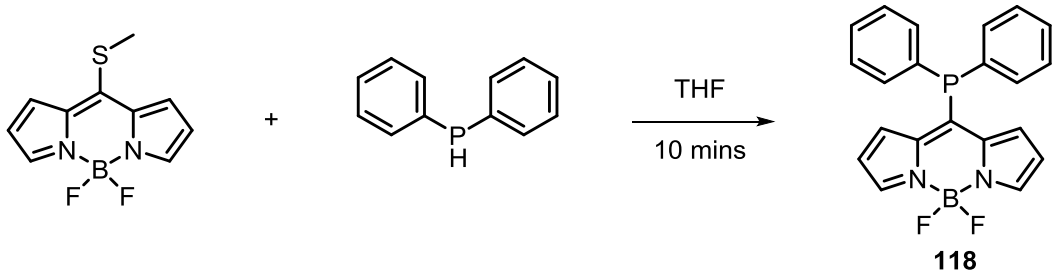

Figure 6.9 A published route for the synthesis of phosphine 118 by Peña-Cabrera.

An alternative method to attach a phosphorus group to the 8-position directly was reacting diphenylphosphine with *n*-butyllithium in anhydrous THF at 0°C, followed by the addition of the

Bodipy **116** in anhydrous tetrahydrofuran to form compound **118**, as detailed in Scheme 6.3. Purification by column chromatography on silica gel gave the desired product and when analysed by $^{11}B\{^{1}H\}$ and $^{19}F\{^{1}H\}$ NMR spectroscopy gave a triplet at δ –0.9 ppm ($^{1}J_{BF}$ = 28.6 Hz) and a quartet (of equal intensity) at δ –145.4 ppm ($^{1}J_{FB}$ = 28.6 Hz) respectively. A sample of **118** suitable for X-ray crystallographic analysis was obtained via slow evaporation of dichloromethane, shown in Figure 6.10. The C-P bond lengths of 1.820(2), 1.824(2) and 1.8530(18) Å are all in accordance with bond lengths associated with tertiary phosphines and are a good comparison to triphenylphosphine.[130]

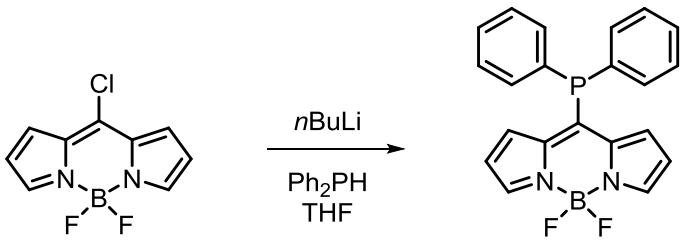

116 **118**

Scheme 6.3 Substitution of the chlorine atom for a diphenylphosphine group to give compound 118.

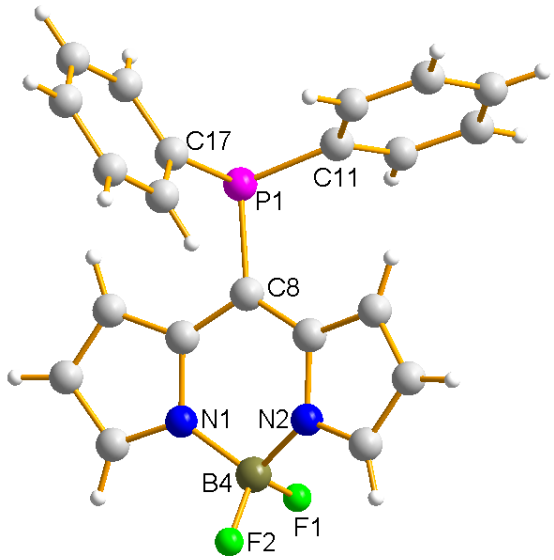

Figure 6.10: Molecular structure of 118. Selected bond distances [Å] and angles [°]: P1-C11 1.820(2), P1-C17 1.824(2), P1-C8 1.8530(18), B4-F1 1.398(2), B4-F2 1.375(2); C17-P1-C11 103.92(9), C17-P1-C8 100.73(8), N1-B4-N2 105.15(15), F1-B4-F2 109.90(16).

The absorption and emission spectra were recorded for phosphine **118** in anhydrous tetrahydrofuran at room temperature which showed a red shift of the maxima and a large decrease in the fluorescence quantum yield (λ_{abs} = 539 nm, λ_{em} = 552 nm, ϕ_F = 0.005). These findings will be discussed in more detail later in the chapter in Section 6.5.

6.3.1 Phosphine Oxide Formation

It may be possible that the oxidation of a phosphine will turn "on" the fluorescence of a compound. If the phosphorus lone pair is coordinated to an oxygen, and no longer engaging in fluorescence quenching via Photoinduced electron Transfer, then the quantum yield may increase.

Compound **118** was converted to phosphine oxide **119** via the addition of hydrogen peroxide in chloroform. The reaction occurred instantly and in a quantitative fashion, which was indicated by a colour change (dark red to purple) and analysis by $^{31}P\{^{1}H\}$ NMR spectroscopy showed a downfield shift from δ −7.7 to δ 25.4 ppm.. It was also evident that oxidation of the phosphine induced fluorescence and increased the quantum yield from 0.005 to 0.13, which means compound **118** could be used as an imaging probe for the detection of oxidative stress. The photophysical properties of compounds **118** and **119** can be found in Table 6.1.

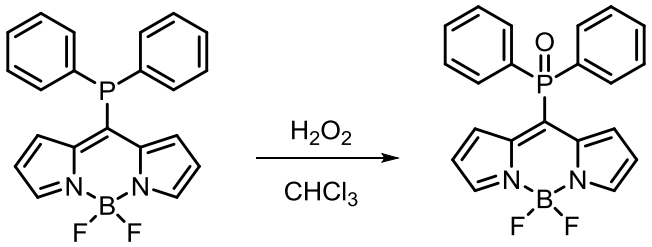

118 **119**

Scheme 6.4 Phosphine 118 was immediately oxidised to phosphine oxide 119.

6.3.2 Gold Coordination

Following the successful production of the phosphine **118** and phosphine oxide **119**, the next step was to study the coordination chemistry of **118**. The coordination of a transition metal may also turn "on" the fluorescence of a compound, in the same way as the oxidation of phosphines has shown to do, detailed by the examples of ROS sensors in Figure 6.5.

The investigation into the use of gold complexes in medicine has been extensively researched, including research towards therapeutics for cancer, rheumatoid arthritis, bronchial asthma, AIDS and malaria.[170, 171] It is known that gold targets the thiol-containing proteins in the body, which have been found to cause or contribute to many human diseases if they malfunction.[172] Gold has many potential therapeutic properties including anticancer and anti-inflammatory effects,[170] some gold complexes have been compared to the successful chemotherapy drug Cisplatin, since gold(III) is isoelectronic with platinum(II) and some tetracoordinate gold (III) complexes can adopt the same square planar geometry.[173]

In 1985 Auranofin, shown in Figure 6.11, was discovered by Sutton and was subsequently approved to treat rheumatoid arthritis.[174] Since then, Auranofin has also demonstrated anticancer properties, specifically for ovarian cancer and bactericidal activity towards tuberculosis.[175, 176]

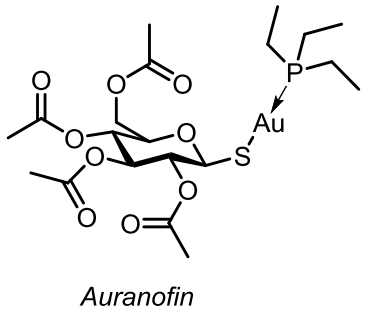

Auranofin

Figure 6.11 Structure of Auranofin which has shown several applications (see text) in medicine.

There are examples in the literature where the coordination of a transition metal - such as gold or silver, has switched "on" the fluorescence of a compound.[177, 178] This is due to the transition metal coordinating through the phosphorus lone pair, thus preventing the lone pair from engaging in PeT quenching.

Therefore, phosphine **118** was coordinated to gold to give the metal complex **120**, shown in Scheme 6.5. Compound **118** and [AuCl(tht)] (tht = tetrahydrothiophene) were combined in anhydrous dichloromethane and stirred at room temperature for one hour under a nitrogen environment. The solvent was evaporated and the solid was washed with hexane to remove excess traces of tetrahydrothiophene. The solid was analysed by $^{31}P\{^{1}H\}$ NMR spectroscopy which revealed that the starting material peak (δ −7.7 ppm) was no longer present and a new peak had appeared at δ 27.9 ppm. This downfield shift suggests that the gold had successfully coordinated to the phosphine. The photophysical properties of this compound will be discussed in Section 6.5.

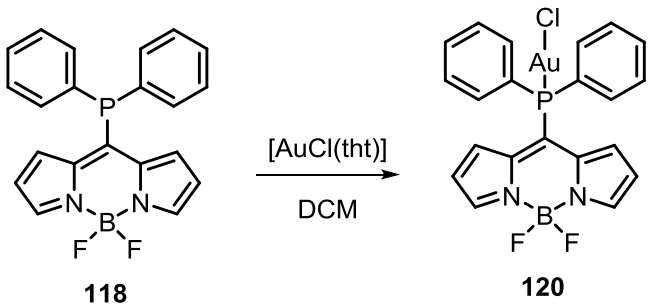

118 **120**

Scheme 6.5 Phosphine 118 was successfully coordinated to a gold complex to form complex 120.

6.3.3 Synthesis of a Switch Containing a Substituted Pyrrole Backbone

A related synthesis was then attempted using a substituted pyrrole, shown in Scheme 6.6. It would be interesting to note the differences in photophysical properties between the two final products

and whether the methyl and ethyl groups on the Bodipy core cause any changes in the fluorescence quantum yield or absorption/emission maxima. The synthesis of dipyrrylketone was outlined by Plater *et al*.[166] The dipyrrylthioketone was synthesised via the addition of thiophosgene and 3-ethyl-2,4-dimethylpyrrole in anhydrous diethyl ether under a nitrogen atmosphere, in a darkened flask. Compound **121** was purified by column chromatography to yield a red solid, in a low yield of 13%. Low yields have been attributed to this reaction due to the tendency of the pyrrole units to polymerise, which was minimised by darkening the flask with foil. The next step saw compound **121** reacted with hydrogen peroxide and potassium hydroxide in an aqueous methanol solution to form **122** which was purified by sublimation, and gave the product as a yellow solid in a high yield of 80%.

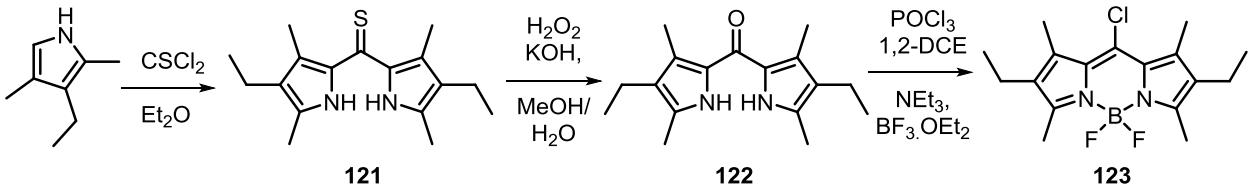

121 122 123

Scheme 6.6 Synthesis of substituted chloro Bodipy 123.

The synthesis of chloro Bodipy **123** was performed following the procedure of Leen and coworkers.[165] Compound **122** was heated to reflux with phosphorus oxychloride in 1,2-dichloroethane, the reaction mixture was cooled, triethylamine and boron trifluoride were both added dropwise and the mixture was stirred at room temperature for two hours. After purification by column chromatography, **123** was produced in a moderate yield of 59%. A sample suitable for analysis by X-ray crystallography was obtained by slow evaporation of dichloromethane:methanol:*n*-pentane (1:1:1 ratio), shown in Figure 6.12 and is a novel structure. The C-Cl bond length of 1.7252(0) Å was representative of other similar compounds published in the literature.[167]

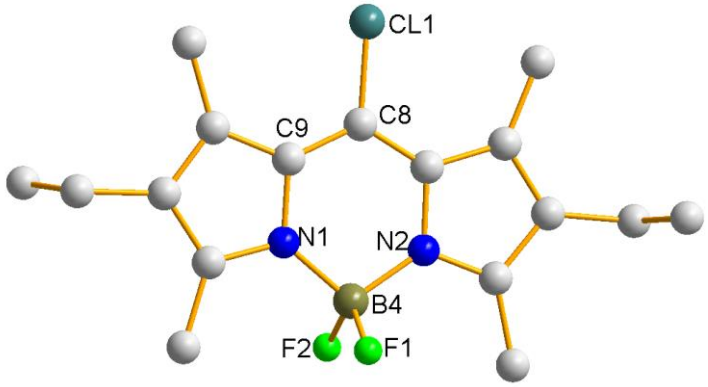

Figure 6.12 Molecular structure of 123. Hydrogens atoms omitted for clarity. Selected bond distances [Å] and angles [°]: C8-Cl1 1.7252(0), B4-F1 1.3881(0), B4-F2 1.3929(0), B4-N1 1.546(0), B4-N2 1.540(0); C9-C8-Cl1 118.168(1), F1-B4-F2 109.042, N1-B4-N2 106.906(2).

6.3.4 Synthesis of Substituted Bodipy Switch Phosphine 124

The final step in the preparation of the novel phosphine compound **124** was the substitution of the chlorine group for a dicyclohexylphosphine which was achieved in the same way as described for phosphine **118**, and is shown in Scheme 6.7. *n*-Butyllithium and dicyclohexylphosphine were combined in anhydrous THF, and added dropwise to a solution of **123** in anhydrous tetrahydrofuran at 0°C; there was an instant colour change from bright pink to dark purple. Analysis by $^{31}P\{^{1}H\}$ NMR spectroscopy at this stage revealed that there was still a large percentage of the dicyclohexylphosphine starting material present (δ –27.2 ppm) and a small second peak at δ –2.9 ppm, which indicated the formation of the desired product. The reaction was stirred for two days, and the $^{31}P\{^{1}H\}$ NMR spectrum showed that the product peak at δ –2.9 ppm had increased by tenfold. Purification by column chromatography yielded the novel phosphine as a dark purple solid. The $^{11}B\{^{1}H\}$ NMR spectrum showed a triplet (δ 0.5 ppm, $^{1}J_{BF}$ = 32.8 Hz) and the $^{19}F\{^{1}H\}$ NMR spectrum showed a quartet (of equal intensity) at (δ –145.6 ppm, $^{1}J_{BF}$ = 32.3 Hz) confirming that no reagents had reacted with the BF_2 group.

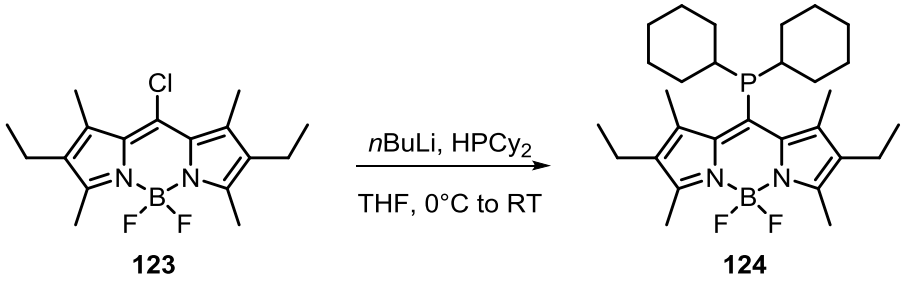

123 **124**

Scheme 6.7 The chloro-substituted Bodipy 123 was reacted with lithium dicyclohexylphosphide to form phosphine 124.

The absorption and emission spectra were recorded in anhydrous THF at room temperature. Interestingly the absorption showed two peaks, one at 528 nm and the other at 567 nm. This may indicate the presence of two species, as the standard Bodipy curve would be assumed for compound **124**, just as compound 118 displayed. The emission maxima showed only one peak with a maxima at 539 nm.

6.4 Spartan Calculations

DFT calculations were ran for the 'switch' Bodipy phosphine compounds **118** and **124**, to establish their electronic properties.

The compounds were performed with both fluorine and methyl groups on the boron atom to see the effect of changing the substituent had, and also because in the future the fluorine atoms may be changed for methyl groups, using previously described methods (Section 2.1)

The HOMO for **118** was situated on the Bodipy core and the LUMO had a slight incorporation of the phosphorus atom. When compared to compound **89b**, with the aryl spacer between the Bodipy core and diphenylphosphine moiety, the HOMO and LUMO are both situated more on the Bodipy core. This indicates that the HOMO and LUMO orbitals are involved in the fluorescence process for 'switch' compound such as **118**, but not necessarily for spacer compounds such as **89b**.

SPACER COMPOUND SWITCH COMPOUND

LUMO – 2.3 eV LUMO – 2.8 eV

HOMO –5.4 eV HOMO –5.8 eV

Figure 6.13 HOMO (bottom) and LUMO (top) orbital distributions for spacer compound 89b (left) and "switch" compound 118 (right).

The HOMO-LUMO gap for the spacer ligand shows an energy difference of 3.1 eV and the 'switch' compounds shows a HOMO-LUMO gap of 3.0 eV. The HOMO of the spacer compound **89b** is not incorporated onto the phosphorus atom until HOMO (-2).

6.5 Photophysical Studies

It was important to determine the influence that the aryl linker plays in the Bodipy compounds, and to establish whether the fluorescence would be quenched when the phosphorus atom was attached directly to the 8-position of the Bodipy core in the new 'switch' phosphines. Chapter 4 details the photophysical properties of the aryl spacer compounds, here they are compared with the 'switch' phosphines **118** and **124**.

Table 6.1 Photophysical properties of the key compounds synthesised within this chapter.

	λ_{abs} (nm)[a]	λ_{em} (nm)[a]	$\Phi^{a,b}$
113	512	527	0.068
Bod-PCy_2 spacer **89a**	512	526	0.44
Bod-PPh2 spacer **89b**	513	527	0.29
Bod-PPh_2 switch **118**	539	552	0.005
Bod-PPh_2(O) switch **119**	557	585	0.13
Bod-PPh_2AuCl switch **120**	545	561	0.15
BodPCy_2 switch **124**	528, 567	539	0.008

[a] Measured in dry, degassed tetrahydrofuran at room temperature, dyes were excited at 485 nm; [b] Fluorescence quantum yields were measured with respect to 4,4-difluoro-8-phenyl-1,3,5,7-tetramethyl-2,6-diethyl-4-bora-3a,4a-diaza-s-indacene **57**.

Table 6.1 concludes that the addition of a phosphorus atom directly bound at the 8-position of the Bodipy core significantly reduces the fluorescence quantum yield compared to the analogues where an aryl linker separates the phosphorus group from the Bodipy core – which is known to occur because the phosphorus lone pair can engage in PeT.

Compound **113** showed a decrease in quantum yield from 0.33 to 0.068 when primary phosphine **20a** was reacted with 8-thiomethyl Bodipy and resulted in a direct bond between the phosphorus atom and a Bodipy core. The absorption and emission spectra of compound **113** can be seen in Figure 6.14.

The coordination of an oxide or metal to the phosphorus increases the fluorescence quantum yield – indicating the successful synthesis of an Off-On switch. The 'switch' phosphine complexes **118** and **124** showed a bathochromic shift of more than 25 nm when compared to their spacer analogues **89a** and **89b** and also a decrease in quantum yield. Figure 6.15 shows the absorption and emission spectra for compound 124. The absorption spectra shows two maxima which is not expected for this compound – as there is only the Bodipy core that would create a peak, this may be due to an impurity within the compound rather than observing two separate absorption wavelengths. This will be re-made and retested in the future.

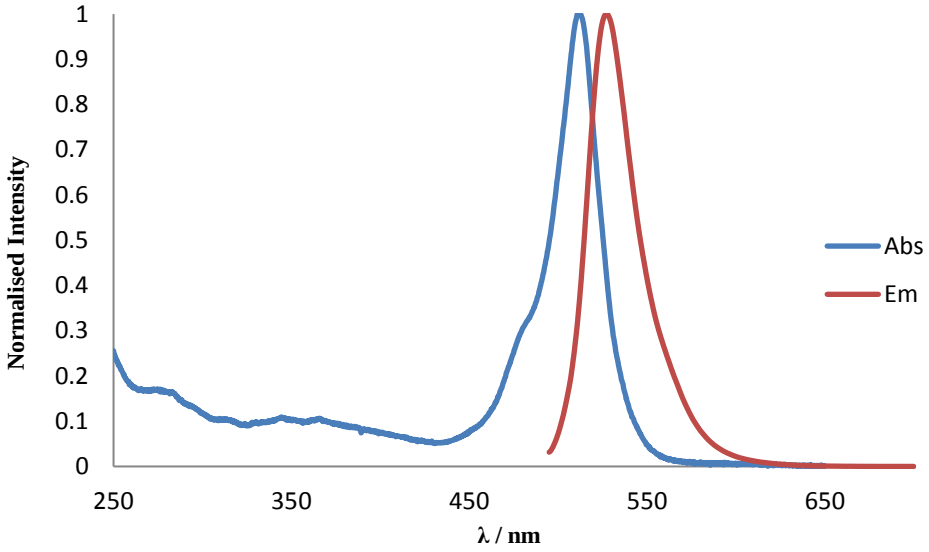

Figure 6.14 Absorption and emission spectra for compound 113.

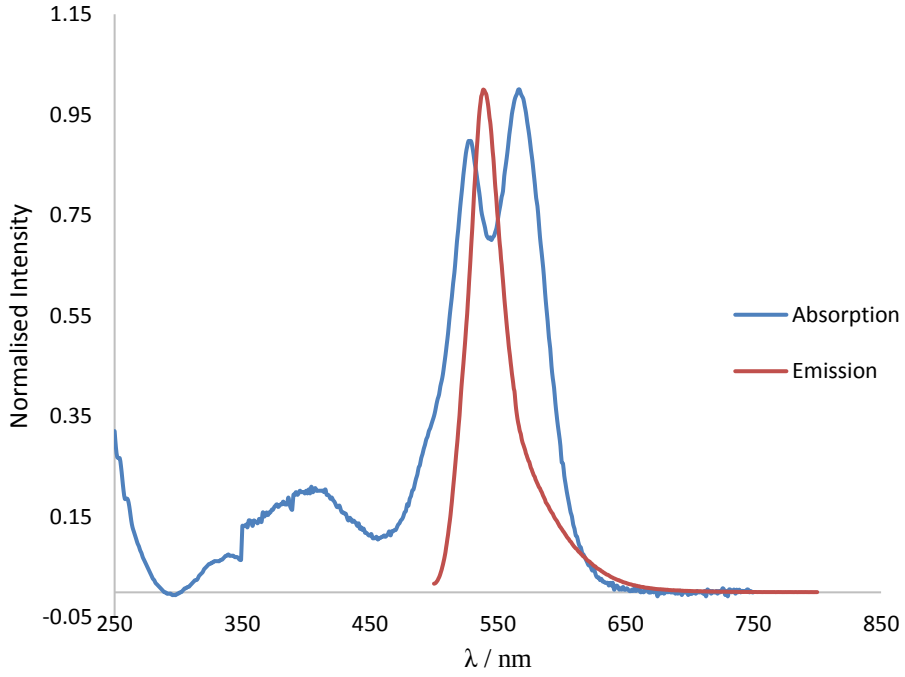

Figure 6.15 Absorption and emission spectra for novel phosphine 124.

6.6 Summary

This chapter has described the synthesis of Bodipy compounds that have potential applications as fluorescence switches; the substitution of a halogen in the 8-position of the Bodipy core, for a phosphorus atom, resulted in significant fluorescence quenching in both cases (compounds **118**

and **124**). The formation of the phosphine oxide appeared to increase the fluorescence quantum yield, which may mean these compounds have potential as ROS sensors.

The coordination of the phosphine compound **118** with a gold complex caused a significant increase in the fluorescence quantum yield from 0.005 to 0.15 – which has been observed previously with other phosphorus-gold complexes within the literature. Plenio described the reactions between gold complexes and phenyl acetylenes, which would enable gold-catalysed reactions to be monitored by fluorescence microscopy.[174]

6.7 Experimental

6.7.1 General Procedure

All air- and/or water-sensitive reactions were performed under a nitrogen atmosphere using standard Schlenk line techniques. Tetrahydrofuran was dried over sodium/benzophenone and deuterated chloroform was dried over phosphorus pentoxide; these solvents were distilled prior to use. All starting materials were purchased from Sigma Aldrich, Alfa Aesar or Fisher and were used as received. Column chromatography was performed on silica gel (40-63 μm, 60 Å) from Merck, thin-layer chromatography was carried out using Merck aluminium-based plates with silica gel and fluorescent indicator (254 nm). ^{1}H, $^{13}C\{^{1}H\}$, $^{19}F\{^{1}H\}$, $^{31}P\{^{1}H\}$ and $^{11}B\{^{1}H\}$ NMR spectra were recorded on a JEOL ECS-400 (^{1}H 399.78 MHz) or Bruker Avance III 300 (^{1}H 300.13 Hz) spectrometer at room temperature (21 °C); ^{1}H and ^{13}C shifts were relative to tetramethylsilane, ^{31}P shifts were relative to 80% H_3PO_4, ^{11}B relative to $BF_3.Et_2O$ and ^{19}F relative to $CFCl_3$. Infrared spectra were recorded on a Varian 800 FT-IR spectrometer and mass spectrometry was carried out by the EPSRC NMSF, Swansea. DFT calculations were carried out on Spartan 14 using the B3LYP functional with a 6-31G* basis set, details of the xyz coordinates and SCF energies can be found in the appendix.

6.7.2 Preparation of Di-Bodipy (113)

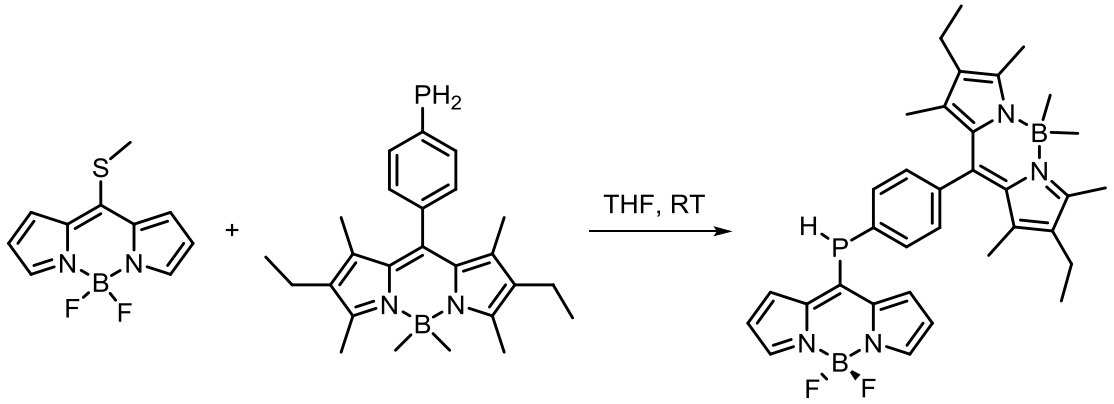

20a (0.085 g, 0.21 mmol) and 8-(thiolmethyl)-4,4-difluoro-4-bora-3a,4a-diaza-*s*-indacene (0.050 g, 0.21 mmol) were dissolved in anhydrous THF (4 mL) and stirred at 75˚C overnight under nitrogen. After removal of the solvent, purification was performed by column chromatography on silica gel (chloroform) to yield an orange solid (0.050 g, 40%). **^{1}H NMR** (500 MHz, $CDCl_3$) δ 7.88 (m, 2H), 7.73 (m, 2H), 7.33 (m, 4H), 6.50 (m, 2H), 5.77 (d, $^{1}J_{HP}$ = 230.7 Hz, 1H), 2.44 (s, 6H), 2.28 (q, $^{3}J_{HH}$ = 7.8 Hz, 4H), 1.18 (s, 6H), 0.97 (t, $^{3}J_{HH}$ = 7.8 Hz, 6H), 0.26 (s, 6H) ppm; **^{13}C{^{1}H} NMR** (126 MHz, $CDCl_3$) δ 151.7, 148.7 (d, J_{CP} = 27.8 Hz), 144.4 139.7, 138.9, 137.3 (d, J_{CP} = 12.5 Hz), 135.5 (d, J_{CP} = 20.2 Hz), 133.4 132.8, 131.9 (d, J_{CP} = 9.6 Hz), 130.6, 129.9 (d, J_{CP} = 7.7 Hz), 128.8, 118.7, 17.5, 14.8, 14.4, 12.1, 10.4 ppm; **^{31}P NMR** (202 MHz, $CDCl_3$) δ −60.0 (dt, $^{1}J_{PH}$ = 230.7 Hz, $^{3}J_{PH}$ = 7.4 Hz) ppm; **^{11}B{^{1}H} NMR** ($CDCl_3$, 128 MHz) δ −0.92 (t, $^{1}J_{BF}$ = 27.96 Hz), −1.8 (s) ppm.

6.7.3 Preparation of 2,2′-Dipyrrylthione (114)

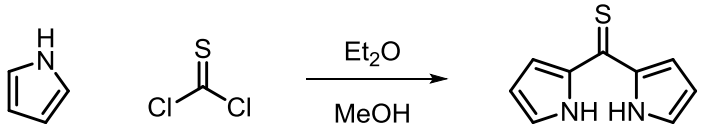

Pyrrole (5.0 g, 74.53 mmol) in anhydrous diethyl ether (15 mL) was added dropwise to a stirred solution of thiophosgene (2.86 mL, 37.27 mmol) in anhydrous diethyl ether (15 mL) at 0 °C under nitrogen. After 30 minutes, methanol (10 mL) was added and the solution was stirred for a further 30 minutes. The solvent was removed under reduced pressure and the residue was dissolved in chloroform and filtered through a short silica plug. The solvent was removed to give a dark purple solid which was purified by column chromatography, (toluene:chloroform, 9:1) to give the desired product as a dark red solid. (2.8 g, 43%).

^{1}H NMR (400 MHz, $CDCl_3$) δ 9.77 (s, 2H), 7.19 (m, 2H), 7.04 (m, 2H), 6.40 (m, 2H) ppm; **^{13}C NMR** (100 MHz, $CDCl_3$) δ 193.4, 138.4, 127.8, 114.9, 112.6 ppm; **HRMS** ($APCI^+$ SOLID) calcd. for $C_9H_9N_2SH$ $[M+H]^+$ requires m/z 177.0481, found m/z 177.0479.

6.7.4 Preparation of 2,2′-Dipyrrylketone (115)

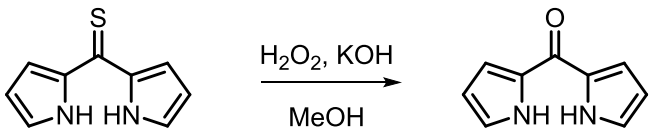

H_2O_2 (10 mL, 37%) was added dropwise to KOH (3.35 g, 59.75 mmol) and **114** (2.34 g, 13.28 mmol) in 95% aqueous MeOH (84 mL) at 0 °C. The mixture was refluxed for five minutes and then cooled and H_2O (134 mL) was added and the solution was chilled in an ice bath. The product was filtered and dried to give the desired compound as pale yellow needles. (1.7 g, 80%).
^{1}H NMR (400 MHz, $CDCl_3$) δ 9.78 (s, 2H), 7.14 (m, 2H), 7.07 (m, 2H), 6.34 (m, 2H) ppm; **^{13}C NMR (100 MHz, $CDCl_3$)** δ 172.9, 130.6, 124.0, 116.1, 111.1 ppm; **HRMS** ($APCI^+$ SOLID) calcd. for $C_9H_9N_2OH$ $[M+H]^+$ requires m/z 161.0709, found m/z 161.0706.

6.7.5 Preparation of 8-Chloro-4,4-difluoro-4-bora-3a,4a-*s*-indacene (116)

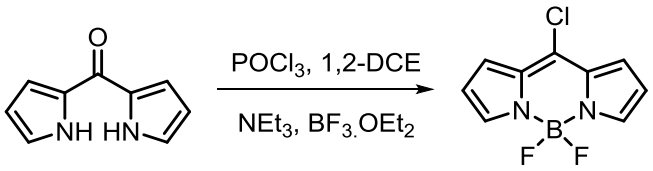

2, 2′-dipyrrylketone **115** (1.0 g, 6.24 mmol) was dissolved in 1, 2-dichloroethane (50 mL). Phosphorus oxychloride (1.16 mL, 12.48 mmol) was added and the reaction mixture was heated to reflux for 3 hours and then cooled on an ice bath. Triethylamine (8.7 mL, 62.4 mmol) was added and the reaction was stirred at 0 ˚C for 5 minutes. Boron trifluoride etherate (8.5 mL, 68.64 mmol) was added dropwise while maintaining the temperature at 0˚C. The reaction was allowed to warm to room temperature and stirred for a further 2 hours. The resulting solution was poured into diethyl ether (200 mL) and washed with water, dried with magnesium sulphate and the solvent removed under reduced pressure. The crude product was purified using column chromatography, (dichloromethane:petrol, 1:1) to give the desired product as a red crystalline solid (0.72 g, 51%).
^{1}H NMR (400 MHz, $CDCl_3$) δ 7.87 (s, 2H), 7.40 (d, J = 4.2 Hz, 2H), 6.56 (d, J = 4.2 Hz, 2H) ppm; **^{13}C NMR** (100 MHz, $CDCl_3$) δ 145.1, 141.2, 134.1, 129.4, 119.2 ppm; **^{11}B NMR** (128 MHz,

$CDCl_3$) δ – 0.9 (t, $^1J_{FB}$ = 27.8 Hz, 1B) ppm; **^{19}F NMR** (282 MHz, $CDCl_3$) δ –145.5 (q (equal intensity), $^1J_{FB}$ = 27.8 Hz, 2F) ppm; **HRMS** ($APCI^+$ SOLID) calcd. for $C_9H_6N_2BClF_2$ $[M]^+$ requires m/z 226.0390, found m/z 226.0388.

6.7.6 Preparation of 8-Bromo-4,4-difluoro-4-bora-3a,4a-*s*-indacene (117)

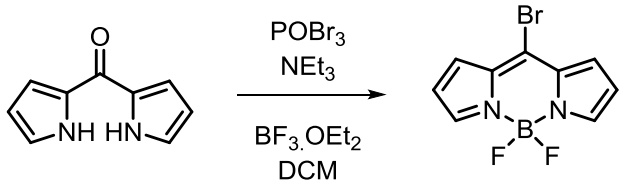

Compound **116** (0.50 g, 3.12 mmol) was dissolved in anhydrous DCM (30 mL). $POBr_3$ (1.96 g, 6.87 mmol) was added and the reaction was stirred at RT for 72 h. The mixture was cooled to 0°C and NEt_3 (4.33 mL, 31.2 mmol) was added dropwise, followed by $BF_3.OEt_2$ (4.23 mL, 34.3 mmol) dropwise. The reaction mixture was warmed to room temperature and stirred for a further two hours. The resulting solution was poured into diethyl ether (200 mL) and washed with water (3 x 50 mL), dried with magnesium sulphate and the solvent removed under reduced pressure. The crude product was purified using column chromatography, (dichloromethane:petrol, 1:1) to give the desired product as a red crystalline solid (0.35 g, 42%). **^{1}H NMR** (300 MHz, $CDCl_3$) δ 7.92 (s, 2H), 7.35 (d, *J* = 4.6 Hz, 2H), 6.54 (d, *J* = 4.6 Hz, 2H) ppm; **^{13}C{^{1}H} NMR** (100 MHz, $CDCl_3$) δ 145.2, 135.8, 133.0, 131.5, 119.3 (d, *J* = 8.6 Hz) ppm; **^{11}B{^{1}H} NMR** (96 MHz, $CDCl_3$) δ 0.1 (t, J_{BF} = 28.8 Hz, 1B) ppm; **^{19}F{^{1}H} NMR** (282 MHz, $CDCl_3$) δ 145.2 (q (equal intensity), $^1J_{FB}$ = 28.8 Hz, 2F) ppm.

6.7.7 Preparation of 8-(Diphenylphosphino)-4,4-difluoro-4-bora-3a,4a-*s*-indacene (118)

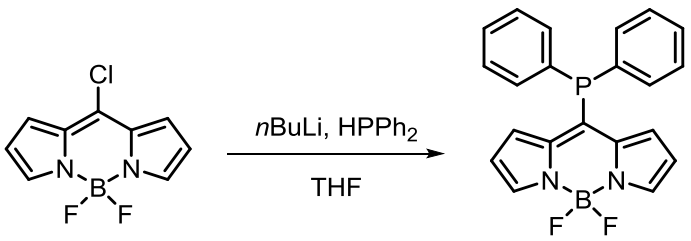

Diphenylphosphine (0.2 mL, 1.14 mmol) and *n*-butyllithium (0.44 mL, 1.14 mmol) were combined in THF (2 mL) at 0 ˚C under nitrogen and added dropwise to a separate flask containing 8-chloro-4, 4-difluoro-4-bora-3a,4a-diaza-*s*-indacene **116** (0.25 g, 1.14 mmol) in THF (5 mL), also at 0 ˚C. The mixture was stirred at room temperature overnight and purified by column chromatography (dichloromethane:petrol 1:1) to give a red solid (0.022 g, 5%).

^{1}H NMR (400 MHz, $CDCl_3$) δ 7.80 (s, 2H), 7.50-7.35 (m, 10H), 6.87 (d, *J* = 4.4 Hz, 2H), 6.32 (d, *J* = 4.4 Hz, 2H) ppm; **^{13}C{^{1}H} NMR** (100 MHz, $CDCl_3$) δ 143.9, 138.4 (d, *J* = 16.5 Hz), 134.4 (d, *J* = 9.5 Hz), 133.9, 133.7, 131.8 (d, *J* = 11.7 Hz), 130.1, 129.3 (d, *J* = 9.0 Hz), 118.6 ppm; **^{31}P{^{1}H} NMR** (162 MHz, $CDCl_3$) δ – 7.1 ppm; **^{11}B{^{1}H} NMR** (128 MHz, $CDCl_3$) δ – 0.9 (t, $^{1}J_{FB}$ = 28.6 Hz, 1B) ppm; **^{19}F{^{1}H} NMR** (282 MHz, $CDCl_3$) δ –145.4 (q (equal intensity), $^{1}J_{FB}$ = 28.6 Hz, 2F) ppm. **HRMS** ($APCI^+$ SOLID + NH_4OAc) calcd. for $C_{21}H_{16}BF_2N_2PH$ $[M+H]^+$ requires m/z 376.1221, found m/z 376.1221.

6.7.8 Preparation of [AuCl(118)] (120)

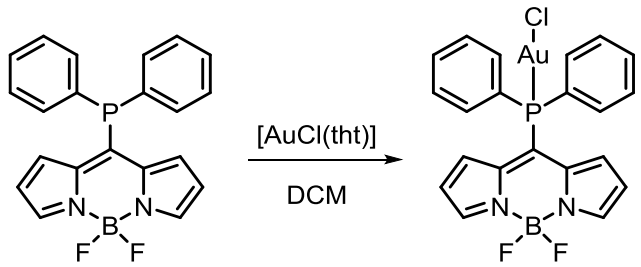

Compound **118** (0.022 g, 0.06 mmol) and [AuCl(tht)] (0.019 g, 0.06 mmol) were dissolved in anhydrous dichloromethane (3 mL) and stirred under nitrogen for one hour. The solvent was removed *in vacuo* and the solid was washed three times with anhydrous hexane (3 x 5mL) to remove the tetrahydrothiophene. The solid was then purified by column chromatography (dichloromethane:hexane, 2:1) to give the product as a purple solid (32 mg, 88%).

^{1}H NMR (400 MHz, $CDCl_3$) δ 7.83 (m, 5H), 7.62 (m, 2H), 7.53 (m, 5H), 6.60 (d, *J* = 4.1 Hz, 2H), 6.32 (d, *J* = 4.1 Hz, 2H) ppm; **^{13}C{^{1}H} NMR** (100 MHz, $CDCl_3$) δ 146.5, 135.0 (d, *J* = 16.5 Hz), 134.4 (d, *J* = 9.5 Hz), 133.4, 133.7, 130.7 (d, *J* = 12.2 Hz), 130.1, 129.3 (d, *J* = 9.0 Hz), 120.0 ppm; **^{31}P{^{1}H} NMR** (162 MHz, $CDCl_3$) δ 28.5 ppm; **^{1}B{1H}NMR** (128 MHz, $CDCl_3$) δ – 1.1 (t, $^{1}J_{FB}$ = 27.8 Hz, 1B) ppm; **^{19}F{^{1}H} NMR** (282 MHz, $CDCl_3$) δ -145.1 (q (equal intensity), $^{1}J_{FB}$ = 28.6 Hz, 2F) ppm.

6.7.9 Preparation of Bis-(4-Ethyl-3,5-dimethyl-1*H*-pyrrol-2-yl)methanthione (121)

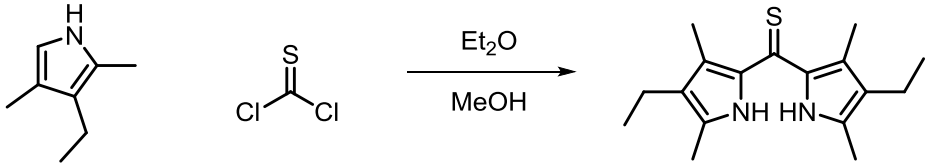

A solution of $CSCl_2$ (1.53 mL, 20.0 mmol) in anhydrous toluene (20 mL) was added dropwise to a solution of 3-ethyl-2,4-dimethylpyrrole (5.67 mL, 42.0 mmol) in anhydrous Et_2O (60 mL) at 0 °C under nitrogen in a darkened flask. The dark purple reaction mixture was stirred at RT for one hour. MeOH (60 mL) was added and the solution was stirred for 30 mins. The solvent was removed and the dark purple residue was purified by column chromatography using silica gel (toluene: chloroform, 4:1) to give an orange red solid (0.89 g, 16%). **^{1}H NMR** (300 MHz, $CDCl_3$) δ 9.09 (br s, 2H), 2.41 (q, *J* = 7.5 Hz, 4H), 2.22 (s, 6H), 2.04 (s, 6H), 1.09 (t, *J* = 7.5 Hz, 6H) ppm; **^{13}C{^{1}H} NMR** (100 MHz, $CDCl_3$) δ 189.6, 129.0, 128.2, 126.7, 125.5, 17.5, 15.0, 11.7, 10.9 ppm.

6.7.10 Preparation of Bis(4-Ethyl-3,5-dimethyl-1*H*-pyrrol-2-yl)methanone (122)

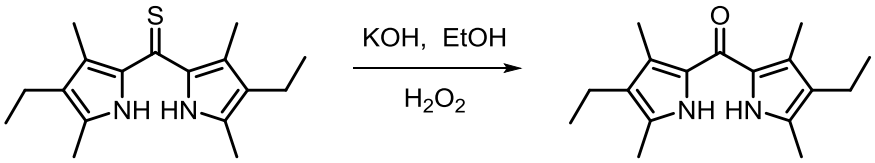

121 (0.23 g, 0.80 mmol) was dissolved in EtOH (100 mL) and KOH (1.00 g, 17.82 mmol) was added and the mixture was cooled to 0 °C. A solution of 5%-hydrogen peroxide (10 mL, 22.38 mmol) was added dropwise and the formation of a white precipitate was observed. The reaction mixture was refluxed for five mins. When cooled to RT, water (150 mL) was added to the solution and the product was extracted with chloroform (3 x 50 mL). The organic phases were washed with water and brine and afterwards dried over Na_2SO_4 and filtered. The solvent was removed *in vacuo*, and the brown residue was purified by sublimation to yield a yellow solid (174 mg, 80%). **^{1}H NMR** (300 MHz, $CDCl_3$) δ 2.39 (q, $^3J_{HH}$ = 7.5 Hz, 4H), 2.22 (s, 6H), 2.13 (s, 6H), 1.06 (t, *J* = 7.5 Hz, 6H) ppm; **IR** (neat) $\tilde{\nu}$: 3240, 2966, 2947, 1676, 1437, 1376, 1093, 1060, 965, 796 cm^{-1}; **HRMS** (ESI$^+$) calcd. for $C_{17}H_{24}N_2O$ $[M+H]^+$ requires m/z 273.1961, found m/z 273.1965.

6.7.11 Preparation of 8-Chloro-4,4-difluoro-1,3,5,7-tetramethyl-2,6-diethyl-4-bora-3a,4a-diaza-*s*-indacene (123)

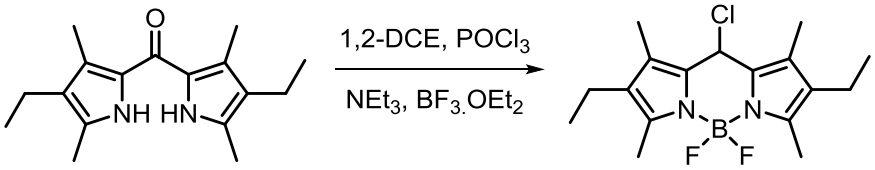

122 (0.28 g, 0.97 mmol) was dissolved in 1,2-dichloroethane (10 mL). Phosphorus oxychloride (0.18 mL, 1.94 mmol) was added and the reaction mixture was stirred at reflux (86 °C) under nitrogen for three hours. The brown solution was cooled to 0 °C and NEt_3 (1.34 mL, 9.70 mmol) was added and the mixture was stirred for five mins. $BF_3.OEt_2$ (1.35 mL, 10.67 mmol) was added dropwise, maintaining the temperature at 0 °C, the reaction mixture was warmed to RT and stirred under nitrogen for two hours. The solution was poured into diethyl ether (40 mL) and washed with water (2 x 40 mL), dried over $MgSO_4$ and filtered. The solvent was removed *in vacuo*. The purple residue was purified by column chromatography on silica gel (DCM: petroleum ether 1:1) to yield an orange solid (0.19 g, 59 %).

^{1}H NMR (300 MHz, $CDCl_3$) δ 2.50 (s, 6H), 2.41 (q, $^3J_{HH}$ = 7.7 Hz, 4H), 2.39 (s, 6H), 1.05 (t, $^3J_{HH}$ = 7.7 Hz, 6H) ppm; **^{13}C{^{1}H} NMR** (100 MHz, $CDCl_3$) δ 152.6, 137.1, 134.1, 132.2, 128.2, 16.1, 13.7, 12.7, 11.4 ppm; **^{19}F{^{1}H} NMR** (376 MHz, $CDCl_3$) δ –145.5 (q, (equal intensity), $^1J_{FB}$ = 32.6 Hz) ppm; **^{11}B{^{1}H} NMR** (128 MHz, $CDCl_3$) δ 0.6 (t, $^1J_{BF}$ = 32.6 Hz) ppm; **IR** (neat) $\tilde{\nu}$: 2983, 2886, 1557, 1473, 1393, 1309, 1195, 1041, 969, 807 cm^{-1}; **HRMS** ($APCI^+$) calcd. for $C_{17}H_{22}BClF_2N_2$ $[M\text{-}HF+H]^+$ requires m/z 319.1552, found m/z 319.1546.

6.7.12 Preparation of 8-(dicyclohexylphosphino)-4,4-difluoro-1,3,5,7-tetramethyl-2,6-diethyl-4-bora-3a,4a-diaza-s-indacene (124)

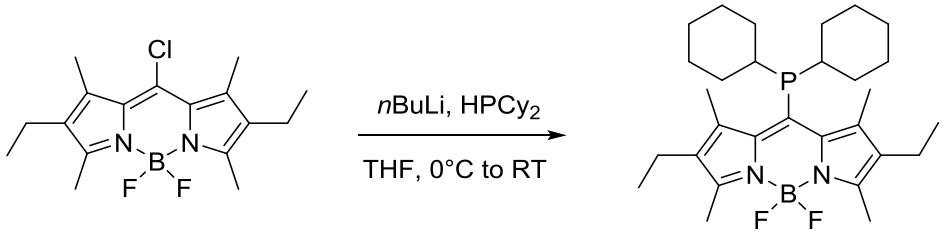

n-Butyllithium (0.08 mL, 0.21 mmol, 2.5M in hexane) was added to dicyclohexylphosphine (0.05 mL, 0.21mmol) in anhydrous THF (2 mL) at 0 °C. In a separate flask **123** (70 mg, 0.21 mmol)

was dissolved in anhydrous THF (2 mL). The lithium dicyclohexylphoshide was added dropwise to the solution of **123** at 0 °C. There was an instant colour change from bright pink to dark purple, the reaction mixture was left to stir at room temperature for thirty minutes and analysed by $^{31}P\{^{1}H\}$ NMR spectroscopy. Purification by column chromatography on silica gel (DCM:petrol, 1:1) afforded the desired product as a purple solid (10 mg, 10%).

^{1}H NMR (300 MHz, $CDCl_3$) δ 2.49 (s, 6H), 2.38 (q, $^{3}J_{HH}$ = 7.6 Hz, 4H), 1.88-1.62 (m, 20H), 1.23 (m, 6H), 1.04 (t, $^{3}J_{HH}$ = 7.8 Hz, 6H) ppm; **^{31}P{^{1}H} NMR** (121 MHz, $CDCl_3$) δ –2.9 ppm; **^{19}F{^{1}H} NMR** (376 MHz, $CDCl_3$) δ –145.6 (q, (equal intensity), $^{1}J_{FB}$ = 32.3 Hz) ppm; **^{11}B{^{1}H} NMR** (128 MHz, $CDCl_3$) δ 0.5 (t, J_{BF} = 32.8) ppm.

7 Conclusion and Future Work

The research generated in this thesis has shown the versatility of a primary phosphine. The main focus of the thesis was the synthesis of a multi-functional imaging agent which was successful and opens up a range of new research topics.

The successful synthesis of novel primary phosphines – described in Chapter 2 – is a starting point for a library of phosphines and transition metal complexes for a range of applications – such as a medicinal imaging probe or an Off-On switch due to metal coordination. Further research into the coordination chemistry of primary phosphines would allow more in depth conclusions to be drawn regarding why some metals quench fluorescence of Bodipy ligands – whereas other metals do not.

The development of multi-functional imaging probes is being widely researched – this is because one can gain more information about the fate of the pharmaceutical within the cell, including its mode of action, by combining several imaging techniques within one probe. The next step in this research would be the addition of a radionuclide, such as ^{18}F, into the Bodipy system to allow *in vivo* imaging along with *in vitro* imaging. The range of phosphonium salts that were synthesised within this thesis showed positive cell imaging, therefore the incorporation of a second imaging technique such as SPECT or PET imaging, would allow us to gather further information.

The introduction of a novel, chiral fluorescent catalyst was also described in this thesis. There are several advantages to using a fluorescent catalyst, which include the ability to detect minute traces of the catalyst in the final product – this is an extremely important safety aspect – especially within the pharmaceutical industry. The fluorescent catalyst synthesised in this research was the first delve into this topic, therefore future work would include testing the fluorescent catalysts in a range of reactions to see how their conversion and enantioselectivities compare to other catalysts.

The final chapter was the development of a Bodipy "switch" which had its fluorescence turned "on" on the addition of a transition metal or oxidation. There are examples of these types of switches in the literature, however we discussed the importance of the phosphorus being attached to the Bodipy core and the role it played in fluorescence. Future work could include the coordination of other transition metals to the phosphorus to see the effect on fluorescence. Other work could be to look at how we could use these compounds as ROS sensors and to develop them further.

8 References

1. O. I. Kolodiazhnyi, *Asymmetric Synthesis in Organophosphorus Chemistry: Synthetic Methods, Catalysis and Applications*, WILEY-VCH, 2016.
2. D. M. Schropp and J. Kovacic, *J. Vet. Emerg. Crit. Care*, 2007, **17**, 127-134.
3. F. H. Westheimer, in *Phosphorus Chemistry*, American Chemical Society, Editon edn., 1992, vol. 486, pp. 1-17.
4. S. O. Obare, C. De, W. Guo, T. L. Haywood, T. A. Samuels, C. P. Adams, N. O. Masika, D. H. Murray, G. A. Anderson, K. Campbell and K. Fletcher, *Sensors*, 2010, **10**, 7018.
5. A. Marklund, B. Andersson and P. Haglund, *Environ. Sci. Technol.*, 2005, **39**, 7423-7429.
6. A. J. De Koning, *Nature*, 1966, **210**, 113-113.
7. T. O. Rogers and J. Birnbaum, *Antimicrob. Agents Chemother.*, 1974, **5**, 121-132.
8. L. D. Quin, 2000.
9. C. A. Tolman, *Chem. Rev.*, 1977, **77**, 313-348.
10. C. A. Tolman, *J. Am. Chem. Soc.*, 1970, **92**, 2956-2965.
11. D. G. Gusev, *Organometallics*, 2009, **28**, 763-770.
12. L. H. Davies, B. B. Kasten, P. D. Benny, R. L. Arrowsmith, H. Ge, S. I. Pascu, S. W. Botchway, W. Clegg, R. W. Harrington and L. J. Higham, *Chem. Commun.*, 2014, **50**, 15503-15505.
13. S. L. Pimlott and A. Sutherland, *Chem. Soc. Rev.*, 2011, **40**, 149-162.
14. S. Liu and D. S. Edwards, *Chem. Rev.*, 1999, **99**, 2235-2268.
15. S. Liu, D. Li, Z. Zhang, G. K. Surya Prakash, P. S. Conti and Z. Li, *Chem. Commun.*, 2014, **50**, 7371-7373.
16. K. Chansaenpak, H. Wang, M. Wang, B. Giglio, X. Ma, H. Yuan, S. Hu, Z. Wu and Z. Li, *Chem. Eur. J.*, 2016, **22**, 12122-12129.
17. D.-Y. Kim and J.-J. Min, *J. Nucl. Med. Mol. Imaging*, 2016, **50**, 185-195.
18. I. Kostova, *Curr. Med. Chem.*, 2006, **13**, 1085-1107.
19. W. H. Ang, A. Casini, G. Sava and P. J. Dyson, *J. Organomet. Chem.*, 2011, **696**, 989-998.
20. C. S. Allardyce, P. J. Dyson, D. J. Ellis and S. L. Heath, *Chem. Commun.*, 2001, 1396-1397.
21. S. Tasan, O. Zava, B. Bertrand, C. Bernhard, C. Goze, M. Picquet, P. Le Gendre, P. Harvey, F. Denat, A. Casini and E. Bodio, *Dalton Trans.*, 2013, **42**, 6102-6109.
22. M. Brynda, *Coord. Chem. Rev.*, 2005, **249**, 2013-2034.
23. J. T. Fleming and L. J. Higham, *Coord. Chem. Rev.*, 2015, **297–298**, 127-145.
24. E. Lippert, *Angew. Chem.*, 1960, **72**, 602-602.
25. R. A. Bartlett, M. M. Olmstead, P. P. Power and G. A. Sigel, *Inorg. Chem.*, 1987, **26**, 1941-1946.
26. M. Yoshifuji, K. Shibayama, N. Inamoto, T. Matsushita and K. Nishimoto, *J. Am. Chem. Soc.*, 1983, **105**, 2495-2497.
27. K. G. Katti, H.; Smith, C. J.; Berning, D. E.;, *Acc. Chem. Res*, 1999, **32**, 9-17.
28. N. J. Goodwin, W. Henderson, B. K. Nicholson, J. Fawcett and D. R. Russell, *J. Chem. Soc., Dalton Trans.*, 1999, 1785-1794.
29. R. M. Hiney, A. Ficks, H. Muller-Bunz, D. G. Gilheany and L. J. Higham, in *Organometallic Chemistry: Volume 37*, The Royal Society of Chemistry, Editon edn., 2011, vol. 37, pp. 27-45.
30. B. Stewart, A. Harriman and L. J. Higham, *Organometallics*, 2011, **30**, 5338-5343.
31. S. Yasui, S. Tojo and T. Majima, *J. Org. Chem.*, 2005, **70**, 1276-1280.

32. Z. B. Alfassi, P. Neta and B. Beaver, *J. Phys. Chem. A*, 1997, **101**, 2153-2158.
33. S. Yasui, S. Tojo and T. Majima, *Org. Biomol. Chem.*, 2006, **4**, 2969-2973.
34. L. H. Davies, B. Stewart, R. W. Harrington, W. Clegg and L. J. Higham, *Angew. Chem. Int. Ed.*, 2012, **51**, 4921-4924.
35. B. Valeur, *Molecular Fluorescence, Principles and Applications*, WILEY-VCH, Germany, 2002.
36. J. R. Lakowicz, *Principles of Fluorescence Spectroscopy, 3rd Ed., Springer, New York*, 2006.
37. B. Valeur and I. Leray, *Coord. Chem. Rev.*, 2000, **205**, 3-40.
38. Invitrogen, *The Molecular Probes Handbook: A Guide to Fluorescent Probes and Labeling Technologies* 11th ed. edn., Life Technologies Corporation, United States of America, 2010.
39. A. Loudet and K. Burgess, *Chem. Rev.*, 2007, **107**, 4891-4932.
40. G. Ulrich, R. Ziessel and A. Harriman, *Angew. Chem. Int. Ed.*, 2008, **47**, 1184-1201.
41. E. V. de Wael, J. A. Pardoen, J. A. van Koeveringe and J. Lugtenburg, *Recl. Trav. Chim. Pays-Bas*, 1977, **96**, 306-309.
42. H. L. Kee, C. Kirmaier, L. Yu, P. Thamyongkit, W. J. Youngblood, M. E. Calder, L. Ramos, B. C. Noll, D. F. Bocian, W. R. Scheidt, R. R. Birge, J. S. Lindsey and D. Holten, *J. Phys. Chem. B*, 2005, **109**, 20433-20443.
43. Z. Dost, S. Atilgan and E. U. Akkaya, *Tetrahedron*, 2006, **62**, 8484-8488.
44. H. Kobayashi, M. Ogawa, R. Alford, P. L. Choyke and Y. Urano, *Chem. Rev.*, 2010, **110**, 2620-2640.
45. M. Monici, *Biotechnology Annual Review*, 2005, **11**, 227-256.
46. Y.-H. Yu, A. B. Descalzo, Z. Shen, H. Röhr, Q. Liu, Y.-W. Wang, M. Spieles, Y.-Z. Li, K. Rurack and X.-Z. You, *Chem. Asian J.*, 2006, **1**, 176-187.
47. G. Ulrich, C. Goze, M. Guardigli, A. Roda and R. Ziessel, *Angew. Chem. Int. Ed.*, 2005, **44**, 3694-3698.
48. R. Ziessel, C. Goze and G. Ulrich, *Synthesis*, 2007, **2007**, 936-949.
49. D. Aigner, S. A. Freunberger, M. Wilkening, R. Saf, S. M. Borisov and I. Klimant, *Anal. Chem.*, 2014, **86**, 9293-9300.
50. T. Kowalczyk, Z. Lin and T. V. Voorhis, *J. Phys. Chem. A*, 2010, **114**, 10427-10434.
51. **B. Valeur**, *Molecular Fluorescence: Principles and Applications.*, Wiley-VCH, Weinheim, 2001.
52. K. Rurack, M. Kollmannsberger and J. Daub, *New J. Chem.*, 2001, **25**, 289-292.
53. K. Rurack, M. Kollmannsberger and J. Daub, *Angew. Chem., Int. Ed.*, 2001, **40**, 385-387.
54. A. C. Benniston, S. Clift and A. Harriman, *J. Mol. Struct.*, 2011, **985**, 346-354.
55. X. Qi, E. J. Jun, L. Xu, S.-J. Kim, J. S. Joong Hong, Y. J. Yoon and J. Yoon, *J. Org. Chem.*, 2006, **71**, 2881-2884.
56. A. Nano, P. Retailleau, J. P. Hagon, A. Harriman and R. Ziessel, *PCCP*, 2014, **16**, 10187-10198.
57. S. Fedeli, P. Paoli, A. Brandi, L. Venturini, G. Giambastiani, G. Tuci and S. Cicchi, *Chem. Eur. J.*, 2015, **21**, 15349-15353.
58. P. J. Barnard and S. J. Berners-Price, *Coord. Chem. Rev.*, 2007, **251**, 1889-1902.
59. S. S. Jurisson, J. J. Benedict, R. C. Elder and E. Deutsch, *Inorg. Chem.*, 1983, **22**, 1332-1338.

60. L. Maffioli, L. Florimonte, L. Pagani, I. Butti and I. Roca, in *Breast Cancer: Nuclear Medicine in Diagnosis and Therapeutic Options*, eds. E. Bombardieri, L. Gianni and G. Bonadonna, Springer Berlin Heidelberg, Berlin, Heidelberg, Editon edn., 2008, pp. 227-238.
61. A. Faucon, R. Lenk, J. Hemez, E. Gautron, D. Jacquemin, J.-Y. Le Questel, J. Graton, A. Brosseau and E. Ishow, *PCCP*, 2013, **15**, 12748-12756.
62. S. Çubuk, M. Fırlak, N. Taşci, E. K. Yetimoğlu and M. V. Kahraman, *Sensors and Actuators B: Chemical*, 2016, **224**, 640-647.
63. C. Fan, C. Duan, Y. Wei, D. Ding, H. Xu and W. Huang, *Chem. Mater.*, 2015, **27**, 5131-5140.
64. X.-D. Jiang, J. Zhao, D. Xi, H. Yu, J. Guan, S. Li, C.-L. Sun and L.-J. Xiao, *Chem. Eur. J.*, 2015, **21**, 6079-6082.
65. F. L. Laughlin, N. Deligonul, A. L. Rheingold, J. A. Golen, B. J. Laughlin, R. C. Smith and J. D. Protasiewicz, *Organometallics*, 2013, **32**, 7116-7121.
66. F.-M. Lu and Z. Yuan, *Quantitative Imaging in Medicine and Surgery*, 2015, **5**, 433-447.
67. J. D. Kelly, A. M. Forster, B. Higley, C. M. Archer, F. S. Booker, L. R. Canning, K. W. Chiu, B. Edwards, H. K. Gill, M. McPartlin, K. R. Nagle, I. A. Latham, R. D. Pickett, A. E. Storey and P. M. Webbon, *J. Nucl. Med.*, 1993, **34**, 222-227.
68. K. Schwochau, *Technetium: Chemistry and Radiopharmaceutical Applications*, John Wiley & Sons, 2008.
69. P. W. Miller, N. J. Long, R. Vilar and A. D. Gee, *Angew. Chem. Int. Ed.*, 2008, **47**, 8998-9033.
70. W. Zhang, K. F. Koehler, B. Harris, P. Skolnick and J. M. Cook, *J. Med. Chem.*, 1994, **37**, 745-757.
71. N. Hail, *Apoptosis*, 2005, **10**, 687-705.
72. G. Kroemer, *Oncogene*, 0000, **25**, 4630-4632.
73. D. C. Wallace, *Science*, 1999, **283**, 1482.
74. C. Xi, S. David and Y. Shi Du, *Curr. Alzheimer Res.*, 2006, **3**, 515-520.
75. H. E. Moon and S. H. Paek, *Exp. Neurobio.*, 2015, **24**, 103-116.
76. L. A. Nguyen, H. He and C. Pham-Huy, *Int. J. Biomed. Sci. : IJBS*, 2006, **2**, 85-100.
77. J. Gal, *Chirality*, 2012, **24**, 959-976.
78. T. J. Leitereg, D. G. Guadagni, J. Harris, T. R. Mon and R. Teranishi, *J. Agric. Food. Chem.*, 1971, **19**, 785-787.
79. J. Hyttel, K. P. Bøgesø, J. Perregaard and C. Sánchez, *J. Neural Transmission*, 1992, **88**, 157-160.
80. J. Peisach and W. E. Blumberg, *Mol. Pharmacol.*, 1969, **5**, 200-209.
81. A. Miyashita, A. Yasuda, H. Takaya, K. Toriumi, T. Ito, T. Souchi and R. Noyori, *J. Am. Chem. Soc.*, 1980, **102**, 7932-7934.
82. J. F. Young, J. A. Osborn, F. H. Jardine and G. Wilkinson, *Chem. Commun. (London)*, 1965, 131-132.
83. M. J. Burk, *J. Am. Chem. Soc.*, 1991, **113**, 8518-8519.
84. H. B. Kagan and P. Dang Tuan, *J. Am. Chem. Soc.*, 1972, **94**, 6429-6433.
85. L. J. Higham, in *Phosphorus Compounds: Advanced Tools in Catalysis and Materials Science*, Springer, Editon edn., 2011.
86. R. M. Hiney, L. J. Higham, H. Müller-Bunz and D. G. Gilheany, *Angew. Chem. Int. Ed.*, 2006, **45**, 7248-7251.
87. L. H. Davies, J. F. Wallis, M. R. Probert and L. J. Higham, *Synthesis*, 2014, **46**, 2622-2628.

88. C. Goze, G. Ulrich, L. J. Mallon, B. D. Allen, A. Harriman and R. Ziessel, *J. Am. Chem. Soc.*, 2006, **128**, 10231-10239.
89. B. Saha and T. V. RajanBabu, *J. Org. Chem.*, 2007, **72**, 2357-2363.
90. T. Bura, P. Retailleau and R. Ziessel, *Angew. Chem. Int. Ed.*, 2010, **49**, 6659-6663.
91. J. Suk, K. M. Omer, T. Bura, R. Ziessel and A. J. Bard, *J. Phys. Chem. C*, 2011, **115**, 15361-15368.
92. G. Ulrich, C. Goze, S. Goeb, P. Retailleau and R. Ziessel, *New J. Chem.*, 2006, **30**, 982-986.
93. L. Bonardi, G. Ulrich and R. Ziessel, *Org. Lett.*, 2008, **10**, 2183-2186.
94. W. Henderson and S. R. Alley, *J. Organomet. Chem.*, 2002, **656**, 120-128.
95. J. R. F. Pritzwald-Stegmann, P. Lonnecke and E. Hey-Hawkins, *Dalton Trans.*, 2016, **45**, 2208-2217.
96. R. Sommer, P. Lönnecke, P. K. Baker and E. Hey-Hawkins, *Inorg. Chem. Commun.*, 2002, **5**, 115-118.
97. R. Sommer, P. Lönnecke, J. Reinhold, P. K. Baker and E. Hey-Hawkins, *Organometallics*, 2005, **24**, 5256-5266.
98. H. C. E. McFarlene, W. McFarlane and D. S. Rycroft, *J. Chem. Soc., Dalton Trans.*, 1976, 1616-1622.
99. A. Rabiee Kenaree, E. R. Sauve, P. J. Ragogna and J. B. Gilroy, *Dalton Trans.*, 2016, **45**, 2859-2867.
100. L. H. Davies, J. F. Wallis, R. W. Harrington, P. G. Waddell and L. J. Higham, *J. Coord. Chem.*, 2016, **69**, 2069-2080.
101. M. S. Davies, R. K. Pierens and M. J. Aroney, *J. Organomet. Chem.*, 1993, **458**, 141-146.
102. J. R. Goerlich, A. Fischer, P. G. Jones and R. Schmutzler, *Polyhedron*, 1993, **12**, 2279-2289.
103. S. Page, *Educ. Chem.*, 2012, **49**.
104. M. J. Clarke, F. Zhu and D. R. Frasca, *Chem. Rev.*, 1999, **99**, 2511-2534.
105. E. Antonarakis and A. Emadi, *Cancer Chemother. Pharmacol.*, 2010, **66**, 1-9.
106. A. E. W. Ledger, C. E. Ellul, M. F. Mahon, J. M. J. Williams and M. K. Whittlesey, *Chem. Eur. J.*, 2011, **17**, 8704-8713.
107. E. Stulz, M. Maue, S. M. Scott, B. E. Mann and J. K. M. Sanders, *New J. Chem.*, 2004, **28**, 1066-1072.
108. E. Bustelo, M. Jiménez-Tenorio, M. C. Puerta and P. Valerga, *Organometallics*, 1999, **18**, 950-951.
109. M. P. de Araujo, A. T. de Figueiredo, A. L. Bogado, G. Von Poelhsitz, J. Ellena, E. E. Castellano, C. L. Donnici, J. V. Comasseto and A. A. Batista, *Organometallics*, 2005, **24**, 6159-6168.
110. J. F. Van der Maelen Uría, S. García-Granda, J. A. Cabeza and I. Del Río, *Acta Crystallographica Section C*, 1994, **50**, 1064-1065.
111. Y. S. Sohn, A. W. Schlueter, D. N. Hendrickson and H. B. Gray, *Inorg. Chem.*, 1974, **13**, 301-304.
112. Z. Li, T.-P. Lin, S. Liu, C.-W. Huang, T. W. Hudnall, F. P. Gabbai and P. S. Conti, *Chem. Commun.*, 2011, **47**, 9324-9326.
113. S. J. Dougan, A. Habtemariam, S. E. McHale, S. Parsons and P. J. Sadler, *Proceedings of the National Academy of Sciences*, 2008, **105**, 11628-11633.

114. S. Nigam, B. P. Burke, L. H. Davies, J. Domarkas, J. F. Wallis, P. G. Waddell, J. S. Waby, D. M. Benoit, A.-M. Seymour, C. Cawthorne, L. J. Higham and S. J. Archibald, *Chem. Commun.*, 2016, **52**, 7114-7117.
115. V. J. A. Jameson, H. M. Cochemé, A. Logan, L. R. Hanton, R. A. J. Smith and M. P. Murphy, *Tetrahedron*, 2015, **71**, 8444-8453.
116. E. J. Lesnefsky and C. L. Hoppel, *Arch. Biochem. Biophys.*, 2003, **420**, 287-297.
117. S. Fulda, L. Galluzzi and G. Kroemer, *Nat Rev Drug Discov*, 2010, **9**, 447-464.
118. C. Lan Bo, *Ann. Rev. Cell Bio.*, 1988, **4**, 155-181.
119. G. F. Kelso, C. M. Porteous, C. V. Coulter, G. Hughes, W. K. Porteous, E. C. Ledgerwood, R. A. J. Smith and M. P. Murphy, *J. Biol. Chem.*, 2001, **276**, 4588-4596.
120. R. A. J. Smith, C. M. Porteous, C. V. Coulter and M. P. Murphy, *Eur. J. Biochem.*, 1999, **263**, 709-716.
121. M. Millard, D. Pathania, Y. Shabaik, L. Taheri, J. Deng and N. Neamati, *PLOS ONE*, 2010, **5**, e13131.
122. I. Y. Strobykina, M. G. Belenok, M. N. Semenova, V. V. Semenov, V. M. Babaev, I. K. Rizvanov, V. F. Mironov and V. E. Kataev, *J. Nat. Prod.*, 2015, **78**, 1300-1308.
123. R. J. van Vuuren, M. H. Visagie, A. E. Theron and A. M. Joubert, *Cancer Chemother Pharmacol*, 2015, **76**, 1101-1112.
124. C. Dumontet and M. A. Jordan, *Nat Rev Drug Discov*, 2010, **9**, 790-803.
125. I. Madar, H. Ravert, B. Nelkin, M. Abro, M. Pomper, R. Dannals and J. J. Frost, *European J. Nucl. Med. Molec. Imaging*, 2007, **34**, 2057-2065.
126. I. Madar, H. T. Ravert, Y. Du, J. Hilton, L. Volokh, R. F. Dannals, J. J. Frost and J. M. Hare, *J. Nucl. Med.*, 2006, **47**, 1359-1366.
127. Z. Cheng, M. Subbarayan, X. Chen and S. S. Gambhir, *J. Labelled Compd. Radiopharm.*, 2005, **48**, 131-137.
128. D.-Y. Kim, H.-J. Kim, K.-H. Yu and J.-J. Min, *Bioorg. Med. Chem. Lett.*, 2012, **22**, 319-322.
129. D.-Y. Kim, H.-J. Kim, K.-H. Yu and J.-J. Min, *Bioconjugate Chem.*, 2012, **23**, 431-437.
130. B. J. Dunne and A. G. Orpen, *Acta Crystallographica Section C*, 1991, **47**, 345-347.
131. M. P. Murphy, *Biochimica et Biophysica Acta (BBA) - Bioenergetics*, 2008, **1777**, 1028-1031.
132. M. L. R. Lim, T. Minamikawa and P. Nagley, *FEBS Lett.*, 2001, **503**, 69-74.
133. H. Steen, J. G. Maring and D. K. F. Meijer, *Biochem. Pharmacol.*, 1993, **45**, 809-818.
134. D. S. Ross, *New England Journal of Medicine*, 2011, **364**, 542-550.
135. A. G. Sharpe, in *Carbon-Fluorine Compounds: Chemistry, Biochemistry & Biological Activities*, ed. C. F. Symposia, John Wiley & Sons, The Netherlands, Editon edn., 1972, pp. 33-50.
136. S. I. Presolski, V. P. Hong and M. G. Finn, *Curr. protocols in chemical biology*, 2011, **3**, 153-162.
137. R. L. Nussbaum, *J. Clin. Invest.*, 2005, **115**, 2689-2691.
138. M. Mimaki, X. Wang, M. McKenzie, D. R. Thorburn and M. T. Ryan, *Biochimica et Biophysica Acta (BBA) - Bioenergetics*, 2012, **1817**, 851-862.
139. Y. Li, J.-S. Park, J.-H. Deng and Y. Bai, *J. Bioenerg. Biomembranes*, 2006, **38**, 283-291.
140. V. Sashuk, D. Schoeps and H. Plenio, *Chem. Commun.*, 2009, 770-772.
141. I. Móczár, P. Huszthy, Z. Maidics, M. Kádár and T. Klára, *Tetrahedron*, 2009, **65**, 8250-8258.
142. A. Haefele, C. Zedde, P. Retailleau, G. Ulrich and R. Ziessel, *Org. Lett.*, 2010, **12**, 1672-1675.

143. C. Ikeda, T. Maruyama and T. Nabeshima, *Tetrahedron Lett.*, 2009, **50**, 3349-3351.
144. R. I. Lerrick, T. P. L. Winstanley, K. Haggerty, C. Wills, W. Clegg, R. W. Harrington, P. Bultinck, W. Herrebout, A. C. Benniston and M. J. Hall, *Chem. Commun.*, 2014, **50**, 4714-4716.
145. N. Fey, S. Papadouli, P. G. Pringle, A. Ficks, J. T. Fleming, L. J. Higham, J. F. Wallis, D. Carmichael, N. Mézailles and C. Müller, *Phosphorus, Sulfur, and Silicon and the Related Elements*, 2015, **190**, 706-714.
146. J. Jover, N. Fey, J. N. Harvey, G. C. Lloyd-Jones, A. G. Orpen, G. J. J. Owen-Smith, P. Murray, D. R. J. Hose, R. Osborne and M. Purdie, *Organometallics*, 2010, **29**, 6245-6258.
147. J. Jover, N. Fey, J. N. Harvey, G. C. Lloyd-Jones, A. G. Orpen, G. J. J. Owen-Smith, P. Murray, D. R. J. Hose, R. Osborne and M. Purdie, *Organometallics*, 2012, **31**, 5302-5306.
148. W. C. Corbin, K. M. Mai, J. L. Freeman, S. D. Hastings and G. M. Gray, *Inorg. Chim. Acta*, 2013, **407**, 223-230.
149. C. Claver, E. Fernandez, A. Gillon, K. Heslop, D. J. Hyett, A. Martorell, A. G. Orpen and P. G. Pringle, *Chem. Commun.*, 2000, 961-962.
150. P. I. P. Elliott, *Annual Reports Section "A" (Inorganic Chemistry)*, 2012, **108**, 389-407.
151. S. Doose, H. Neuweiler and M. Sauer, *ChemPhysChem*, 2009, **10**, 1389-1398.
152. F. Pina, J. C. Lima, C. Lodeiro, J. Seixas de Melo, P. Díaz, M. T. Albelda and E. García-España, *The Journal of Physical Chemistry A*, 2002, **106**, 8207-8212.
153. K. Tateno, R. Ogawa, R. Sakamoto, M. Tsuchiya, T. Otani and T. Saito, *Org. Lett.*, 2014, **16**, 3212-3215.
154. M. J. Hangauer and C. R. Bertozzi, *Angew. Chem. Int. Ed.*, 2008, **47**, 2394-2397.
155. B. Kalyanaraman, V. Darley-Usmar, K. J. A. Davies, P. A. Dennery, H. J. Forman, M. B. Grisham, G. E. Mann, K. Moore, L. J. Roberts and H. Ischiropoulos, *Free Radical Biol. Med.*, 2012, **52**, 1-6.
156. R. Lee, M. Margaritis, K. M. Channon and C. Antoniades, *Curr. Med. Chem.*, 2012, **19**, 2504-2520.
157. G.-Y. Liou and P. Storz, *Free Radical Res.*, 2010, **44**, 479-496.
158. P. Storz, *Frontiers in bioscience : a journal and virtual library*, 2005, **10**, 1881-1896.
159. T. P. Szatrowski and C. F. Nathan, *Cancer Res*, 1991, **51**, 794-798.
160. A. M. Christianson and F. P. Gabbaï, *Inorg. Chem.*, 2016, **55**, 5828-5835.
161. K. Akasaka, T. Suzuki, H. Ohrui and H. Meguro, *Anal. Lett.*, 1987, **20**, 731-745.
162. M. Onoda, S. Uchiyama, A. Endo, H. Tokuyama, T. Santa and K. Imai, *Org. Lett.*, 2003, **5**, 1459-1461.
163. N. Soh, O. Sakawaki, K. Makihara, Y. Odo, T. Fukaminato, T. Kawai, M. Irie and T. Imato, *Biorg. Med. Chem.*, 2005, **13**, 1131-1139.
164. R. I. Roacho, A. Metta-Magaña, M. M. Portillo, E. Peña-Cabrera and K. H. Pannell, *The J. Org. Chem.*, 2013, **78**, 4245-4250.
165. V. Leen, P. Yuan, L. Wang, N. Boens and W. Dehaen, *Org. Lett.*, 2012, **14**, 6150-6153.
166. M. J. Plater, S. Aiken and G. Bourhill, *Tetrahedron*, 2002, **58**, 2405-2413.
167. R. Misra, B. Dhokale, T. Jadhav and S. M. Mobin, *New J. Chem.*, 2014, **38**, 3579-3585.
168. N. Zhao, S. Xuan, B. Byrd, F. R. Fronczek, K. M. Smith and M. G. H. Vicente, *Org. Biomolec. Chem.*, 2016, **14**, 6184-6188.

169. I. Esnal, I. Valois-Escamilla, C. F. A. Gómez-Durán, A. Urías-Benavides, M. L. Betancourt-Mendiola, I. López-Arbeloa, J. Bañuelos, I. García-Moreno, A. Costela and E. Peña-Cabrera, *ChemPhysChem*, 2013, **14**, 4134-4142.
170. S. J. Berners-Price and A. Filipovska, *Metallomics*, 2011, **3**, 863-873.
171. E. A. Pacheco, E. R. T. Tiekink and M. W. Whitehouse, in *Gold Chemistry*, Wiley-VCH Verlag GmbH & Co. KGaA, Editon edn., 2009, pp. 283-319.
172. P. J. Sadler, *Pure Appl. Chem.*, 1998, **70**, 863-871.
173. V. Milacic, D. Fregona and Q. P. Dou, *Histology and histopathology*, 2008, **23**, 101-108.
174. B. Sutton, *Gold Bull*, 1986, **19**, 15-16.
175. M. B. Harbut, C. Vilchèze, X. Luo, M. E. Hensler, H. Guo, B. Yang, A. K. Chatterjee, V. Nizet, W. R. Jacobs, P. G. Schultz and F. Wang, *Proc. Nat. Acad. Sci.*, 2015, **112**, 4453-4458.
176. S. H. Park, J. H. Lee, J. S. Berek and M. C. Hu, *Int. J. Oncol.*, 2014, **45**, 1691-1698.
177. H.-C. Su, O. Fadhel, C.-J. Yang, T.-Y. Cho, C. Fave, M. Hissler, C.-C. Wu and R. Réau, *J. Am. Chem. Soc.*, 2006, **128**, 983-995.
178. R. Vasiuta and H. Plenio, *Chem. Eur. J.*, 2016, **22**, 6353-6360.

9 Appendix

X-ray Crystallographic data, DFT Calculations and Fluorescence Spectra

9.1 Ruthenium Complexes Absorption and Emission Spectra

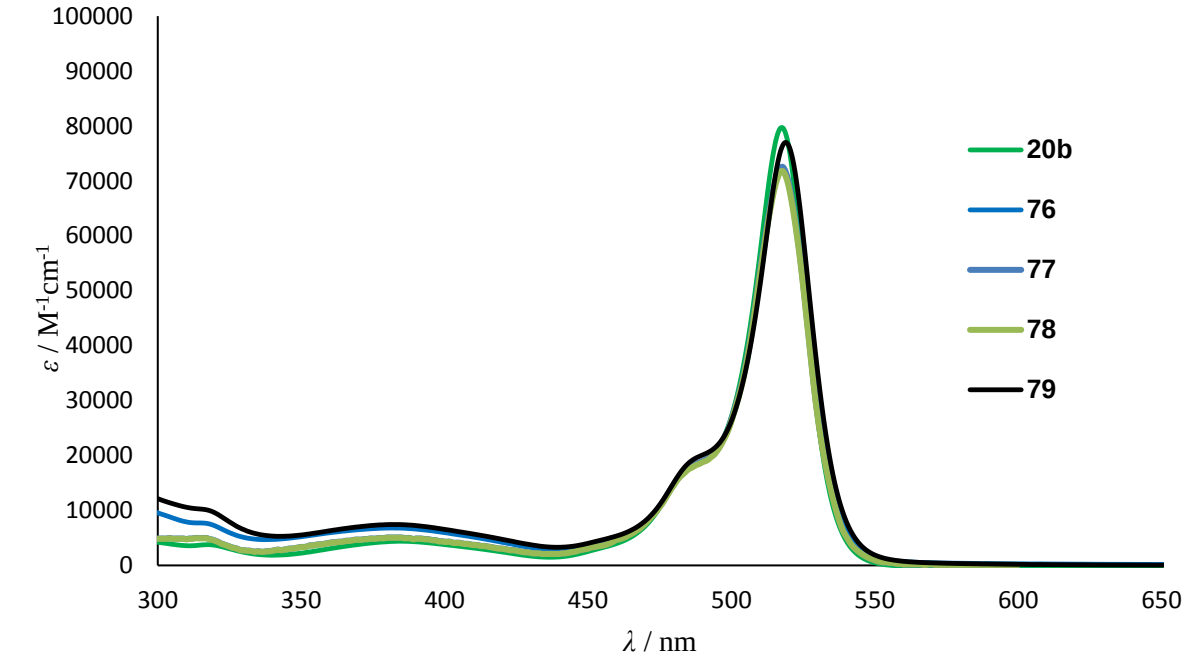

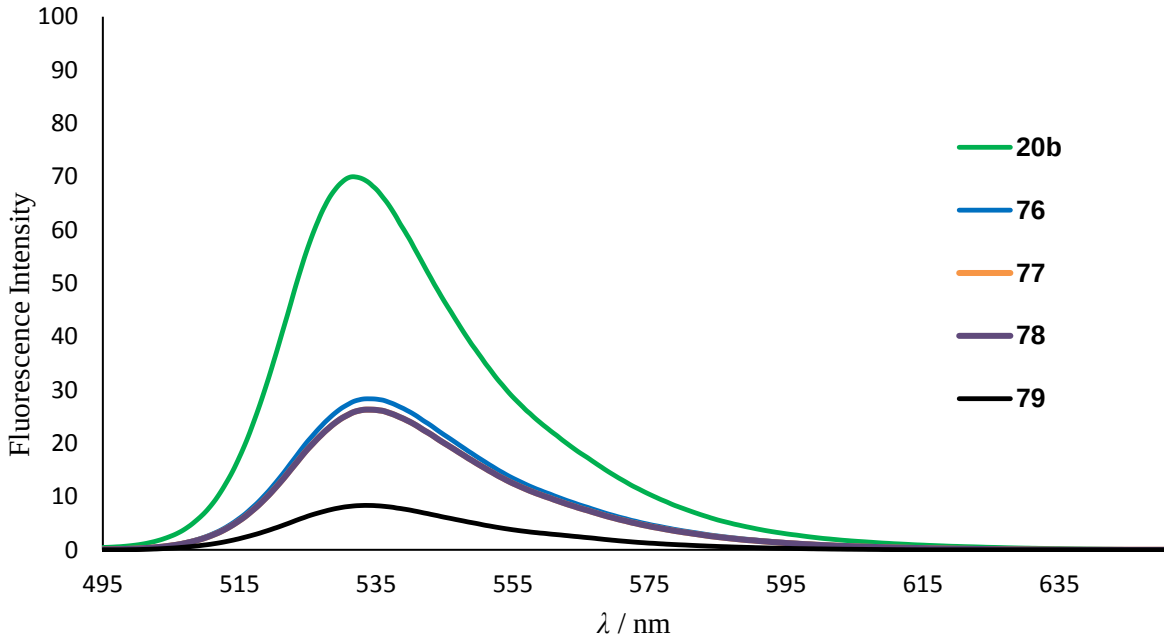

9.2 X-Ray Data

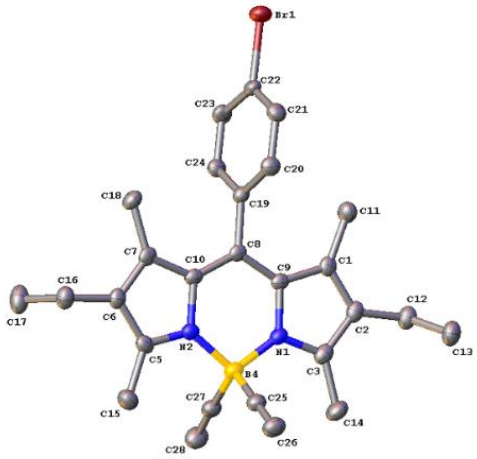

Table 1 Crystal data and structure refinement for 48.

Identification code	ljh140121_fa
Empirical formula	$C_{27}H_{28}BN_2Br$
Formula weight	471.23
Temperature/K	150.01(10)
Crystal system	monoclinic
Space group	$P2_1/c$
a/Å	7.8811(2)
b/Å	21.5815(5)
c/Å	14.0378(3)
α/°	90
β/°	103.154(2)
γ/°	90
Volume/Å^3	2324.97(10)
Z	4
ρ_{calc}g/cm^3	1.346
μ/mm^{-1}	1.785
F(000)	976.0
Crystal size/mm^3	0.22 × 0.13 × 0.04
Radiation	MoKα (λ = 0.71073)
2Θ range for data collection/°	6.514 to 55.556
Index ranges	$-9 \le h \le 9$, $-28 \le k \le 27$, $-17 \le l \le 17$
Reflections collected	18566
Independent reflections	4862 [R_{int} = 0.0540, R_{sigma} = 0.0514]
Data/restraints/parameters	4862/261/286
Goodness-of-fit on F^2	1.024
Final R indexes [I>=2σ (I)]	R_1 = 0.0454, wR_2 = 0.0934
Final R indexes [all data]	R_1 = 0.0692, wR_2 = 0.1032
Largest diff. peak/hole / e Å^{-3}	0.71/-0.46

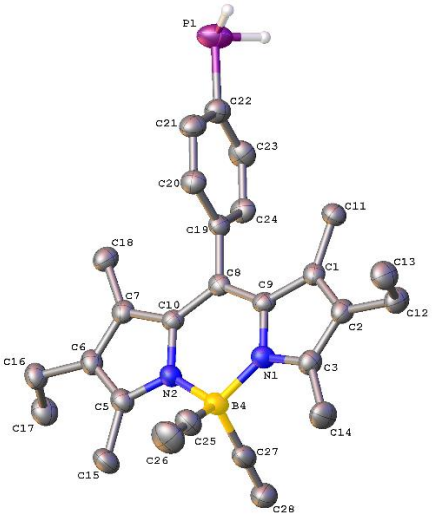

Table 1 Crystal data and structure refinement for 50

Identification code	ljh160005_off
Empirical formula	$C_{27}H_{30}BN_2P$
Formula weight	424.31
Temperature/K	100.0(2)
Crystal system	triclinic
Space group	P-1
a/Å	8.1644(9)
b/Å	11.0902(13)
c/Å	13.8384(16)
α/°	94.936(6)
β/°	102.715(6)
γ/°	90.169(7)
Volume/Å^3	1217.4(2)
Z	2
ρ_{calc}g/cm^3	1.157
μ/mm^{-1}	0.120
F(000)	452.0
Crystal size/mm^3	0.06 × 0.02 × 0.01
Radiation	Synchrotron (λ = 0.6889)
2Θ range for data collection/°	2.936 to 48.416
Index ranges	$-9 \le h \le 9$, $-13 \le k \le 13$, $-16 \le l \le 16$
Reflections collected	9867
Independent reflections	4289 [R_{int} = 0.0678, R_{sigma} = 0.1936]
Data/restraints/parameters	4289/0/292
Goodness-of-fit on F^2	1.034
Final R indexes [I>=2σ (I)]	R_1 = 0.0807, wR_2 = 0.2175
Final R indexes [all data]	R_1 = 0.1042, wR_2 = 0.2428
Largest diff. peak/hole / e Å^{-3}	0.46/-0.22

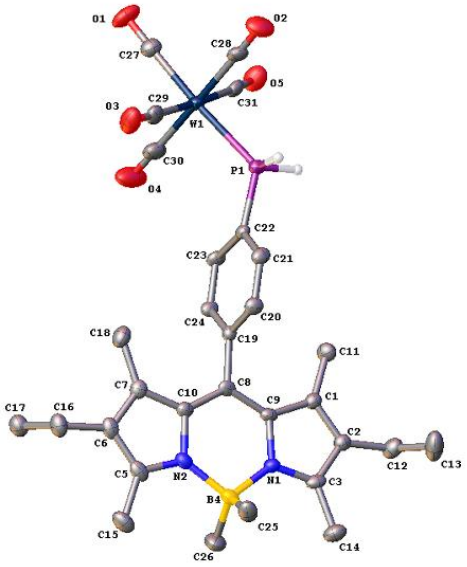

Table 1 Crystal data and structure refinement for 62.

Identification code	ljh140120_fa
Empirical formula	$C_{30}H_{34}BN_2O_5PW$
Formula weight	728.22
Temperature/K	150.01(10)
Crystal system	monoclinic
Space group	$P2_1/c$
a/Å	11.97683(14)
b/Å	17.7954(2)
c/Å	28.5950(3)
α/°	90
β/°	96.6311(11)
γ/°	90
Volume/Å^3	6053.75(13)
Z	8
ρ_{calc}g/cm^3	1.598
μ/mm^{-1}	3.910
F(000)	2896.0
Crystal size/mm^3	0.21 × 0.11 × 0.04
Radiation	MoKα (λ = 0.71073)
2Θ range for data collection/°	6.572 to 55.494
Index ranges	$-15 \le h \le 15$, $-21 \le k \le 22$, $-37 \le l \le 37$
Reflections collected	92956
Independent reflections	13134 [R_{int} = 0.0636, R_{sigma} = 0.0450]
Data/restraints/parameters	13134/8/773
Goodness-of-fit on F^2	1.041
Final R indexes [I>=2σ (I)]	R_1 = 0.0339, wR_2 = 0.0557
Final R indexes [all data]	R_1 = 0.0554, wR_2 = 0.0616
Largest diff. peak/hole / e Å^{-3}	0.55/-0.68

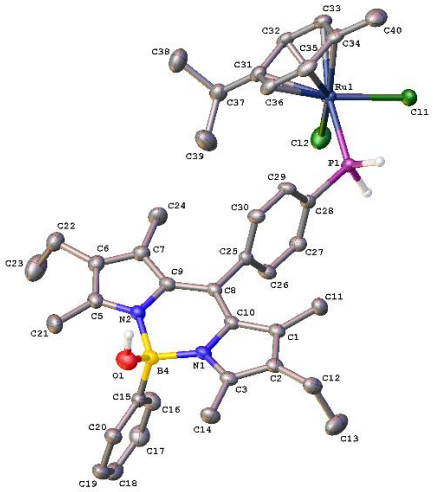

Table 1 : Crystal data and structure refinement for 77a

Identification code	ljh150128_fa
Empirical formula	$C_{43}H_{52}BCl_{14}N_2OPRu$
Formula weight	1252.01
Temperature/K	150.0(2)
Crystal system	triclinic
Space group	P-1
a/Å	10.79639(19)
b/Å	14.7361(3)
c/Å	17.4860(3)
α/°	98.0988(14)
β/°	98.0661(14)
γ/°	94.0622(14)
Volume/Å^3	2715.30(8)
Z	2
ρ_{calc}g/cm^3	1.531
μ/mm^{-1}	1.042
F(000)	1268.0
Crystal size/mm^3	0.21 × 0.17 × 0.09
Radiation	MoKα (λ = 0.71073)
2Θ range for data collection/°	5.884 to 52.744
Index ranges	-13 ≤ h ≤ 13, -18 ≤ k ≤ 18, -21 ≤ l ≤ 21
Reflections collected	83800
Independent reflections	11092 [R_{int} = 0.0515, R_{sigma} = 0.0323]
Data/restraints/parameters	11092/163/757
Goodness-of-fit on F^2	1.019
Final R indexes [I>=2σ (I)]	R_1 = 0.0343, wR_2 = 0.0756
Final R indexes [all data]	R_1 = 0.0463, wR_2 = 0.0814
Largest diff. peak/hole / e Å^{-3}	0.64/-0.49

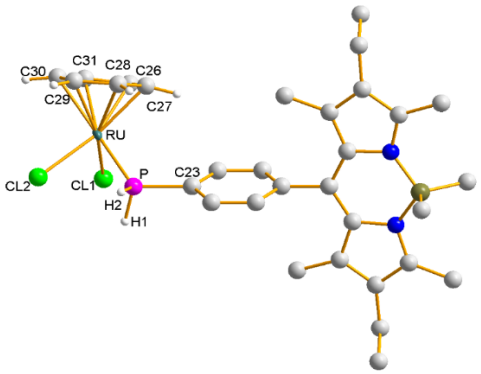

Table 1. Crystal data and structure refinement for 72.

Identification code	ljh120090	
Chemical formula (moiety)	$C_{32}H_{41}BCl_5N_2PRu$	
Chemical formula (total)	$C_{32}H_{41}BCl_5N_2PRu$	
Formula weight	773.77	
Temperature	150(2) K	
Radiation, wavelength	MoKα, 0.71073 Å	
Crystal system, space group	triclinic, $P\bar{1}$	
Unit cell parameters	a = 7.9866(4) Å	α = 87.067(5)°
	b = 8.3564(5) Å	β = 89.842(4)°
	c = 25.8377(15) Å	γ = 85.109(4)°
Cell volume	1715.86(17) $Å^3$	
Z	2	
Calculated density	1.498 g/cm^3	
Absorption coefficient μ	0.918 mm^{-1}	
F(000)	792	
Crystal colour and size	red, 0.40 × 0.30 × 0.02 mm^3	
Reflections for cell refinement	4680 (θ range 3.0 to 28.5°)	
Data collection method	Xcalibur, Atlas, Gemini ultra thick-slice ω scans	
θ range for data collection	3.0 to 25.0°	
Index ranges	h –9 to 9, k –9 to 9, l –30 to 29	
Completeness to θ = 25.0°	99.7 %	
Reflections collected	13069	
Independent reflections	6020 (R_{int} = 0.0439)	
Reflections with $F^2>2\sigma$	5190	
Absorption correction	semi-empirical from equivalents	
Min. and max. transmission	0.7102 and 0.9819	
Structure solution	direct methods	
Refinement method	Full-matrix least-squares on F^2	
Weighting parameters a, b	0.0383, 11.1421	
Data / restraints / parameters	6020 / 0 / 395	
Final R indices [$F^2>2\sigma$]	R1 = 0.0600, wR2 = 0.1340	
R indices (all data)	R1 = 0.0697, wR2 = 0.1402	
Goodness-of-fit on F^2	1.100	
Largest and mean shift/su	0.000 and 0.000	
Largest diff. peak and hole	2.09 and –1.34 e $Å^{-3}$	

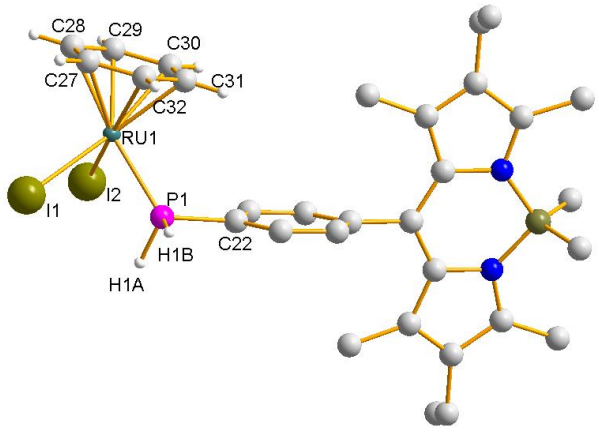

Table 1 : Crystal data and structure refinement for 74.

Identification code	ljh160004
Empirical formula	$C_{32}H_{41}BCl_3I_2N_2PRu$
Formula weight	956.67
Temperature/K	150.0(2)
Crystal system	monoclinic
Space group	C2/c
a/Å	31.8575(6)
b/Å	11.46036(19)
c/Å	21.1225(4)
α/°	90
β/°	108.281(2)
γ/°	90
Volume/Å^3	7322.6(2)
Z	8
ρ_{calc}g/cm^3	1.736
μ/mm^{-1}	2.402
F(000)	3744.0
Crystal size/mm^3	0.23 × 0.18 × 0.04
Radiation	MoKα (λ = 0.71073)
2Θ range for data collection/°	5.864 to 57.512
Index ranges	-42 ≤ h ≤ 42, -14 ≤ k ≤ 14, -28 ≤ l ≤ 28
Reflections collected	57008
Independent reflections	8566 [R_{int} = 0.0397, R_{sigma} = 0.0287]
Data/restraints/parameters	8566/405/393
Goodness-of-fit on F^2	1.010
Final R indexes [I>=2σ (I)]	R_1 = 0.0267, wR_2 = 0.0488
Final R indexes [all data]	R_1 = 0.0393, wR_2 = 0.0523
Largest diff. peak/hole / e Å^{-3}	0.80/-0.71

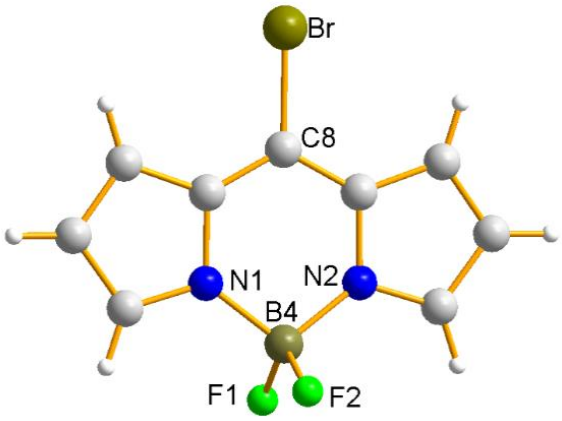

Table 1: Crystal data and structure refinement for 117.

Identification code	**117**
Empirical formula	$C_9H_6BBrF_2N_2$
Formula weight	270.88
Temperature/K	150.0(2)
Crystal system	monoclinic
Space group	$P2_1/c$
a/Å	9.9262(2)
b/Å	13.7437(3)
c/Å	13.8989(3)
α/°	90
β/°	94.0077(19)
γ/°	90
Volume/Å^3	1891.49(7)
Z	8
ρ_{calc}g/cm^3	1.902
μ/mm^{-1}	4.338
F(000)	1056.0
Crystal size/mm^3	0.2 × 0.13 × 0.07
Radiation	MoKα (λ = 0.71073)
2Θ range for data collection/°	5.876 to 57.654
Index ranges	$-13 \leq h \leq 13$, $-18 \leq k \leq 18$, $-18 \leq l \leq 18$
Reflections collected	30425
Independent reflections	4583 [R_{int} = 0.0376, R_{sigma} = 0.0277]
Data/restraints/parameters	4583/0/271
Goodness-of-fit on F^2	1.045
Final R indexes [I>=2σ (I)]	R_1 = 0.0281, wR_2 = 0.0552
Final R indexes [all data]	R_1 = 0.0423, wR_2 = 0.0594
Largest diff. peak/hole / e Å^{-3}	0.54/-0.42

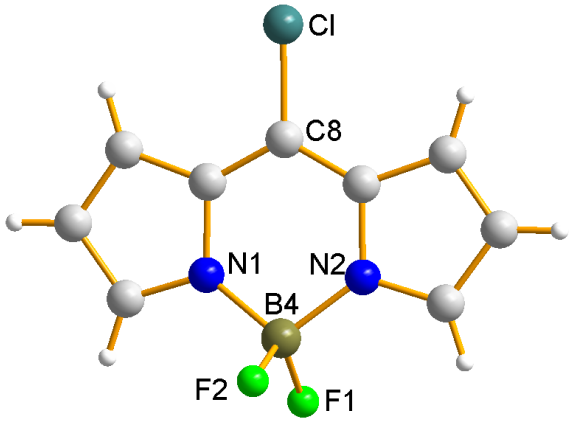

Table 1 Crystal data and structure refinement for 116.

Identification code	**116**
Empirical formula	$C_{18}H_{12}B_2N_4F_4Cl_2$
Formula weight	452.84
Temperature/K	150.01(10)
Crystal system	triclinic
Space group	P-1
a/Å	7.6468(2)
b/Å	7.8865(2)
c/Å	15.7750(4)
α/°	98.274(2)
β/°	100.467(2)
γ/°	95.487(2)
Volume/Å^3	918.49(4)
Z	2
ρ_{calc}g/cm^3	1.637
μ/mm^{-1}	3.674
F(000)	456.0
Crystal size/mm^3	0.23 × 0.13 × 0.1
Radiation	CuKα (λ = 1.54184)
2Θ range for data collection/°	5.776 to 133.476
Index ranges	$-9 \le h \le 9$, $-9 \le k \le 9$, $-18 \le l \le 18$
Reflections collected	19418
Independent reflections	3245 [R_{int} = 0.0295, R_{sigma} = 0.0173]
Data/restraints/parameters	3245/0/271
Goodness-of-fit on F^2	1.041
Final R indexes [I>=2σ (I)]	R_1 = 0.0278, wR_2 = 0.0699
Final R indexes [all data]	R_1 = 0.0329, wR_2 = 0.0740
Largest diff. peak/hole / e Å^{-3}	0.24/-0.22

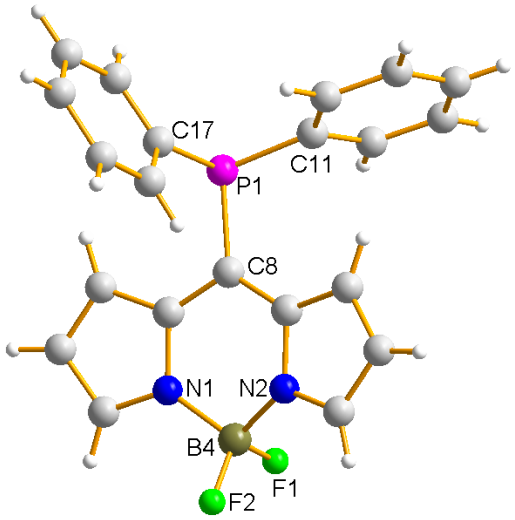

Table 1: Crystal data and structure refinement for 118.

Identification code	**118**
Empirical formula	$C_{21}H_{16}BF_2N_2P$
Formula weight	376.14
Temperature/K	150.0(2)
Crystal system	triclinic
Space group	P-1
a/Å	6.0142(3)
b/Å	11.6841(4)
c/Å	13.6286(6)
α/°	100.451(3)
β/°	101.823(4)
γ/°	98.472(3)
Volume/Å^3	904.73(6)
Z	2
ρ_{calc}g/cm^3	1.381
μ/mm^{-1}	1.583
F(000)	388.0
Crystal size/mm^3	0.18 × 0.13 × 0.06
Radiation	CuKα (λ = 1.54184)
2Θ range for data collection/°	6.79 to 133.802
Index ranges	$-7 \leq h \leq 7$, $-13 \leq k \leq 13$, $-16 \leq l \leq 16$
Reflections collected	24557
Independent reflections	3199 [R_{int} = 0.0563, R_{sigma} = 0.0292]
Data/restraints/parameters	3199/0/244
Goodness-of-fit on F^2	1.041
Final R indexes [I>=2σ (I)]	R_1 = 0.0363, wR_2 = 0.0914
Final R indexes [all data]	R_1 = 0.0477, wR_2 = 0.0990
Largest diff. peak/hole / e Å^{-3}	0.89/-0.24

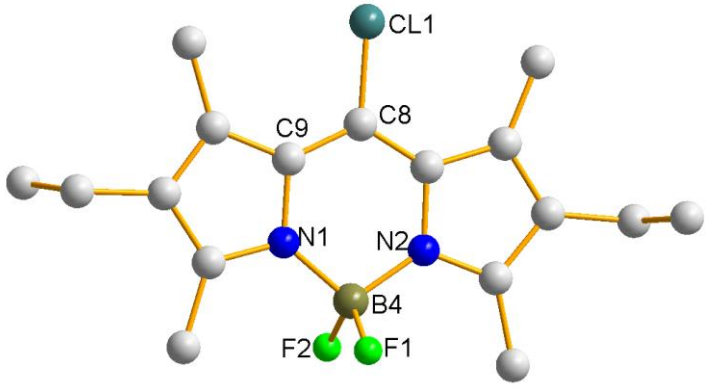

Table 1: Crystal data and structure refinement for 123

Identification code	**123**
Empirical formula	$C_{17}H_{22}BClF_2N_2$
Formula weight	338.62
Temperature/K	150.0(2)
Crystal system	monoclinic
Space group	$P2_1$
a/Å	8.65495(12)
b/Å	24.3479(4)
c/Å	12.5065(2)
α/°	90
β/°	107.7316(17)
γ/°	90
Volume/Å^3	2510.29(7)
Z	6
ρ_{calc}g/cm^3	1.344
μ/mm^{-1}	2.191
F(000)	1068.0
Crystal size/mm^3	0.29 × 0.08 × 0.04
Radiation	CuKα (λ = 1.54184)
2Θ range for data collection/°	7.262 to 133.92
Index ranges	$-10 \leq h \leq 9$, $-28 \leq k \leq 28$, $-14 \leq l \leq 14$
Reflections collected	35530
Independent reflections	8857 [R_{int} = 0.0505, R_{sigma} = 0.0404]
Data/restraints/parameters	8857/1/640
Goodness-of-fit on F^2	1.038
Final R indexes [I>=2σ (I)]	R_1 = 0.0443, wR_2 = 0.1171
Final R indexes [all data]	R_1 = 0.0501, wR_2 = 0.1220
Largest diff. peak/hole / e Å^{-3}	0.34/-0.28
Flack parameter	0.024(10)

9.3 DFT Calculations for Ruthenium complexes

[$RuCl_2(C_6H_6)$(**20b**)]

HOMO

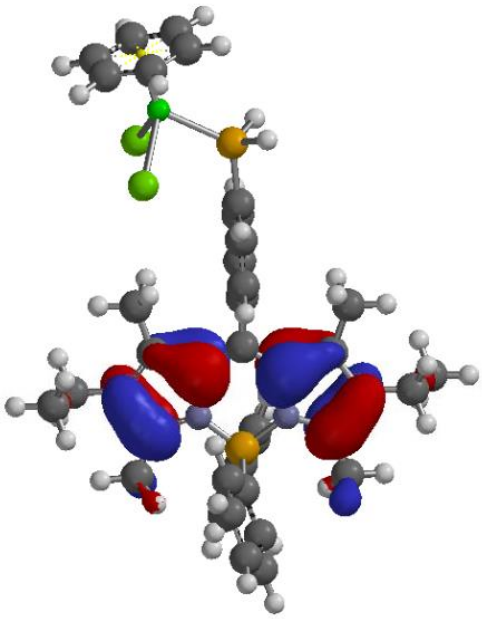

LUMO

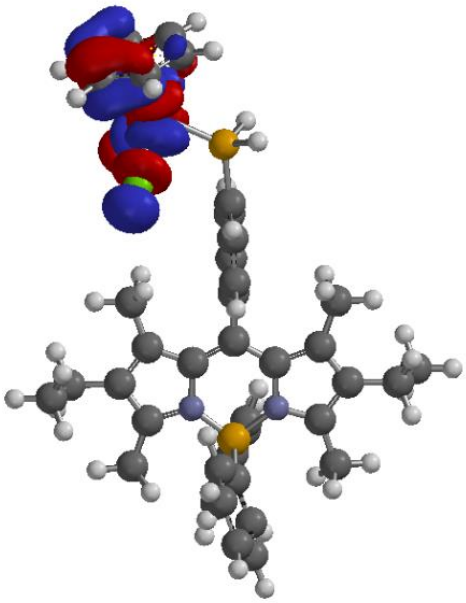

[$RuCl_2$(*p*-cymene)(**20b**)]

HOMO

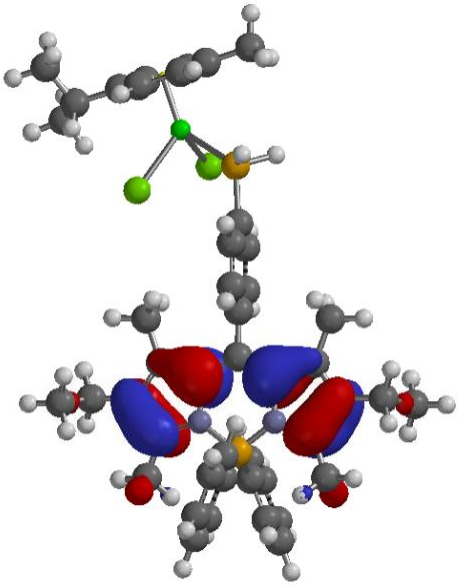

LUMO

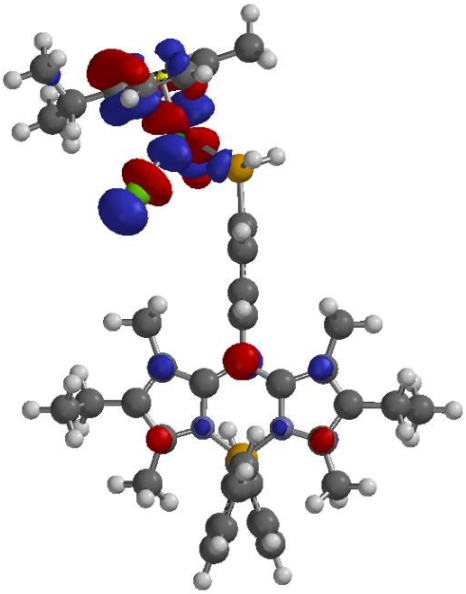

[$RuI_2(C_6H_6)$(**20b**)]

HOMO

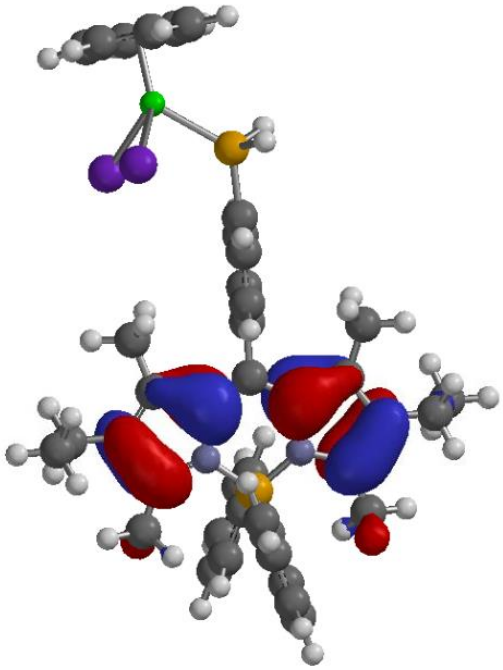

LUMO

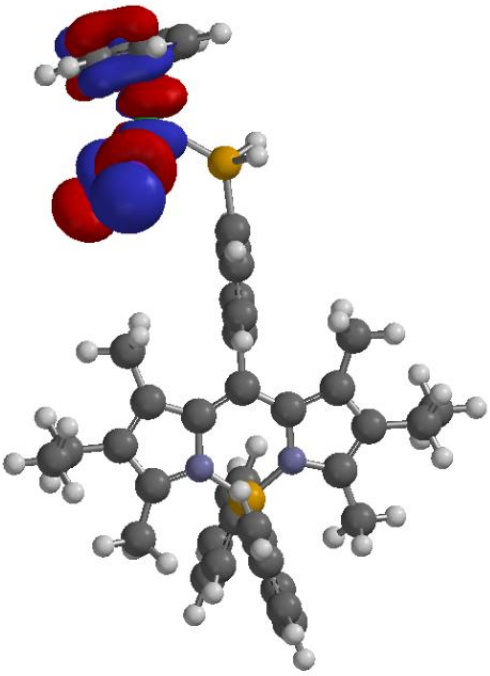

[RuI_2(*p*-cymene)(**20b**)]

HOMO

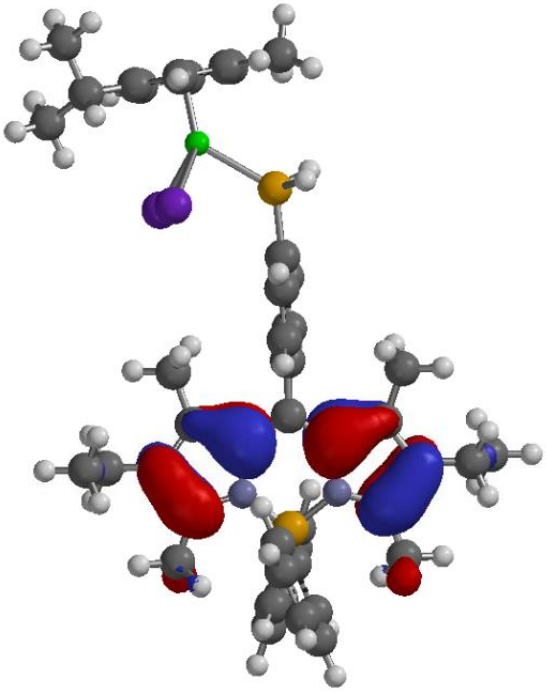

LUMO

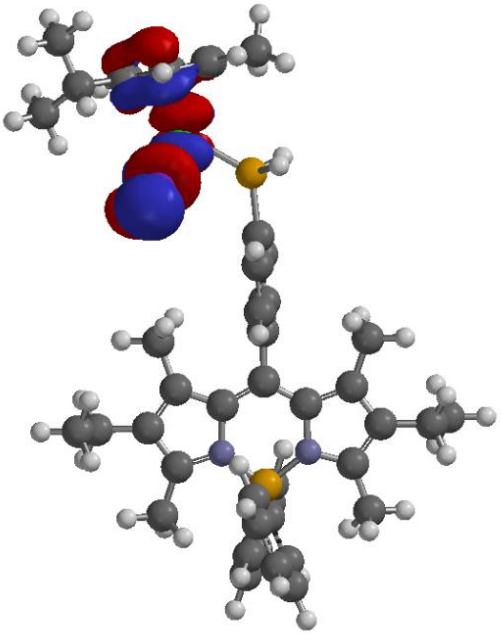

9.4 DFT Calculated SCF Energies and xyz Coordinates

Compound 7

SCF model:
A restricted hybrid HF-DFT SCF calculation will be performed using Pulay DIIS + Geometric Direct Minimization

Optimization:

Step	Energy	Max Grad.	Max Dist.
1	-574.189038	0.008755	0.095361
2	-574.190071	0.002673	0.028560
3	-574.190148	0.001438	0.004271
4	-574.190158	0.000454	0.004450
5	-574.190160	0.000146	0.000978

<step 2>
Job type: Frequency calculation.
Method: RB3LYP
Basis set: 6-31G(D)

Reason for exit: Successful completion
Quantum Calculation CPU Time : 1:52.31
Quantum Calculation Wall Time: 4:32.75

SPARTAN '14 Properties Program: (Linux/P4E) build 14.117
Use of molecular symmetry enabled

Cartesian Coordinates (Angstroms)

Atom	X	Y	Z
1 C C1	-0.4910216	-0.0099078	0.0000000
2 C C4	2.3234382	-0.0025751	0.0000000
3 C C2	0.2248423	-0.0023819	-1.2060028
4 C C6	0.2248423	-0.0023819	1.2060028
5 C C5	1.6203405	-0.0017650	1.2057560
6 C C3	1.6203405	-0.0017650	-1.2057560
7 H H2	-0.3074857	-0.0038685	-2.1545745
8 H H6	-0.3074857	-0.0038685	2.1545745
9 H H5	2.1580372	-0.0046284	2.1504921
10 H H3	2.1580372	-0.0046284	-2.1504921
11 H H4	3.4100405	-0.0038702	0.0000000
12 P P1	-2.3375240	0.1191064	0.0000000
13 H H7	-2.5924881	-0.8205358	-1.0386115
14 H H1	-2.5924881	-0.8205358	1.0386115

Compound 11

SCF model:
A restricted hybrid HF-DFT SCF calculation will be performed using Pulay DIIS + Geometric Direct Minimization

Optimization:

Step	Energy	Max Grad.	Max Dist.
1	-2194.135319	0.013984	0.094978
2	-2194.140063	0.003594	0.101284
3	-2194.140618	0.002832	0.068133
4	-2194.140797	0.002515	0.051595
5	-2194.140892	0.003243	0.034545
6	-2194.140951	0.003630	0.027960
7	-2194.140989	0.003237	0.018523
8	-2194.141010	0.002434	0.035726
9	-2194.141034	0.001352	0.082614
10	-2194.140918	0.003357	0.069141
11	-2194.141070	0.001398	0.019928
12	-2194.141103	0.001226	0.069463
13	-2194.141083	0.001973	0.019469
14	-2194.141133	0.000924	0.034466
15	-2194.141151	0.001167	0.013228
16	-2194.141146	0.000863	0.011389
17	-2194.141141	0.000806	0.007439
18	-2194.141140	0.000730	0.021146
19	-2194.141139	0.000321	0.022916
20	-2194.141122	0.000441	0.010783
21	-2194.141132	0.000523	0.021721
22	-2194.141139	0.000572	0.017631
23	-2194.141147	0.000473	0.045784
24	-2194.141169	0.000405	0.018685
25	-2194.141177	0.000345	0.011530
26	-2194.141178	0.000174	0.007818
27	-2194.141182	0.000214	0.001852
28	-2194.141181	0.000068	0.000697

<step 2>
Job type: Frequency calculation.
Method: RB3LYP
Basis set: 6-31G(D)

Reason for exit: Successful completion
Quantum Calculation CPU Time : 16:18.98
Quantum Calculation Wall Time: 22:38.32

SPARTAN '14 Properties Program: (Linux/P4E) build 14.117
Use of molecular symmetry disabled

Cartesian Coordinates (Angstroms)

Atom	X	Y	Z
1 S S1	-0.5160464	-2.4325983	-0.3893369
2 C C1	-2.2400869	-2.2361931	0.2406812
3 H H3	-2.2335358	-1.5754812	1.1140145
4 H H4	-2.6478856	-3.2031188	0.5468095
5 C C2	0.4101122	-2.4167552	1.2083947
6 H H5	0.3096526	-3.3782811	1.7190852
7 H H6	0.0014581	-1.6336966	1.8567859
8 S S2	-3.3821158	-1.6138315	-1.0399532
9 S S3	2.2007359	-2.1747120	0.9718362
10 C C3	-2.8168888	0.1277566	-1.2145610

11	H	H1	-3.2235335	0.4534951	-2.1783791
12	C	C4	2.2421057	-0.4124947	0.4407126
13	H	H2	1.8322513	0.2100378	1.2452413
14	H	H9	1.6037633	-0.3004402	-0.4410487
15	C	C6	3.6796725	0.0086210	0.1186643
16	H	H10	4.0876592	-0.6467994	-0.6606418
17	H	H13	4.3091114	-0.1265478	1.0077060
18	C	C7	-3.2795384	1.0629528	-0.0906917
19	H	H15	-2.9151204	0.6928834	0.8765467
20	H	H16	-4.3745633	1.0451797	-0.0349483
21	C	C8	3.7417224	1.4717200	-0.3474498
22	H	H17	3.3318083	2.1358945	0.4215174
23	H	H18	3.1256190	1.5984190	-1.2468712
24	P	P2	5.4944086	1.9846319	-0.8169797
25	H	H20	5.2360661	3.3798156	-0.9486618
26	H	H14	6.0020923	2.1186148	0.5086269
27	H	H21	-1.7254098	0.1181920	-1.3078108
28	C	C5	-2.7895402	2.5025241	-0.2980254
29	H	H7	-1.6933190	2.5312944	-0.3557944
30	H	H11	-3.1484936	2.8949906	-1.2587261
31	P	P1	-3.2831180	3.7616279	1.0077507
32	H	H12	-4.6578565	3.3952476	1.1002738
33	H	H8	-2.9156547	2.9858841	2.1476223

Compound 13b

SCF model:
A restricted hybrid HF-DFT SCF calculation will be performed using Pulay DIIS + Geometric Direct Minimization

Optimization:

Step	Energy	Max Grad.	Max Dist.
1	-2071.226192	0.034064	0.174916
2	-2071.242372	0.025703	0.179473
3	-2071.254182	0.019905	0.167683
4	-2071.262385	0.013276	0.150109
5	-2071.267118	0.006963	0.240195
6	-2071.269089	0.003662	0.249205
7	-2071.270186	0.002116	0.244319
8	-2071.270945	0.001376	0.254639
9	-2071.271400	0.000855	0.120628
10	-2071.271293	0.002673	0.263177
11	-2071.271717	0.000364	0.166758
12	-2071.271681	0.000721	0.211799
13	-2071.271696	0.000666	0.096465
14	-2071.271727	0.000507	0.084564
15	-2071.271770	0.000164	0.121425
16	-2071.271786	0.000196	0.214420
17	-2071.271805	0.000312	0.213024
18	-2071.271820	0.000436	0.086736
19	-2071.271824	0.000187	0.055432
20	-2071.271825	0.000072	0.002541
21	-2071.271825	0.000033	0.002365

<step 2>
Job type: Frequency calculation.
Method: RB3LYP
Basis set: 6-31G(D)

Reason for exit: Successful completion
Quantum Calculation CPU Time : 28:30.66
Quantum Calculation Wall Time: 34:44.87

SPARTAN '14 Properties Program: (Linux/P4E) build 14.117
Use of molecular symmetry disabled

Cartesian Coordinates (Angstroms)

Atom	X	Y	Z
1 H H1	-2.6276950	-0.9116923	2.2557413
2 C C1	-2.4976289	-1.0303106	1.1878360
3 C C5	-1.5240932	-1.8559303	0.5476725
4 H H2	-4.0635614	0.3280678	0.3334127
5 H H5	-0.7885047	-2.4757638	1.0440463
6 C C4	-1.6818638	-1.7105769	-0.8636712
7 H H4	-1.0882233	-2.2009749	-1.6244823
8 C C3	-2.7523033	-0.7947933	-1.0958815
9 H H3	-3.1099445	-0.4661047	-2.0630736
10 C C2	-3.2570807	-0.3756499	0.1718186
11 Fe Fe1	-1.2649621	0.1112913	0.0020790
12 H H6	0.3332212	0.8933199	2.1928750
13 C C6	0.0881330	1.1291324	1.1642430
14 C C7	-0.9495131	2.0070100	0.7290886
15 H H8	-1.6313525	2.5529331	1.3684447
16 C C8	-0.9444858	2.0159286	-0.6982898
17 H H9	-1.6232088	2.5688796	-1.3349259
18 C C9	0.0960330	1.1431868	-1.1386143
19 H H10	0.3455327	0.9205252	-2.1690216
20 C C10	0.7413150	0.5855785	0.0118072
21 C C11	1.9323365	-0.3348611	0.0145897
22 H H7	1.9118492	-0.9527768	0.9217995
23 H H12	1.8731012	-1.0277237	-0.8342280
24 C C12	3.2633445	0.4421274	-0.0486801
25 H H11	3.3283689	1.1454119	0.7877864
26 H H13	3.2963713	1.0349731	-0.9706998
27 P P1	4.7455012	-0.7200617	-0.0843136
28 H H14	5.7529136	0.2671075	0.1200474
29 H H15	4.7124679	-1.0938777	1.2914157

Compound 14

SCF model:
A restricted hybrid HF-DFT SCF calculation will be performed using Pulay DIIS + Geometric Direct Minimization

Optimization:

Step	Energy	Max Grad.	Max Dist.
1	-1114.886255	0.103422	0.131742
2	-1114.930260	0.040780	0.082890
3	-1114.940681	0.008905	0.138901
4	-1114.941679	0.003971	0.121749
5	-1114.941919	0.002148	0.037916
6	-1114.941995	0.001128	0.034490

7	-1114.942015	0.000356	0.011367
8	-1114.942016	0.000222	0.002916

<step 2>
Job type: Frequency calculation.
Method: RB3LYP
Basis set: 6-31G(D)

Reason for exit: Successful completion
Quantum Calculation CPU Time : 2:01:15.97
Quantum Calculation Wall Time: 2:08:10.40

SPARTAN '14 Properties Program: (Linux/P4E) build 14.117
Use of molecular symmetry disabled

Cartesian Coordinates (Angstroms)

Atom		X	Y	Z
1	C C1	-1.1197282	-1.8242515	-0.3076223
2	C C6	-0.7989651	-0.5747595	0.2111300
3	C C3	-3.3950876	-1.0918194	-0.7787366
4	C C5	-1.7917644	0.4616351	0.2436847
5	C C2	-2.4335434	-2.0709248	-0.7975500
6	C C4	-3.1065074	0.1974381	-0.2619887
7	C C10	-1.5208565	1.7577131	0.7656628
8	H H2	-2.6762751	-3.0511107	-1.1999161
9	H H7	-5.0781172	1.0105030	-0.6176129
10	H H3	-4.3915242	-1.2937839	-1.1651538
11	C C9	-2.4916799	2.7349722	0.7809671
12	H H10	-0.5319134	1.9677973	1.1596006
13	H H9	-2.2622168	3.7174055	1.1851992
14	C C8	-3.7873283	2.4699679	0.2778696
15	H H8	-4.5446742	3.2490451	0.2968888
16	C C7	-4.0845938	1.2260464	-0.2308774
17	C C11	0.5747394	-0.3098752	0.7537429
18	C C12	3.1165968	0.1020073	1.8235633
19	C C13	1.5846002	0.2678457	-0.0522199
20	C C14	0.8510689	-0.6620092	2.0798932
21	C C15	2.1213181	-0.4553858	2.6178939
22	C C16	2.8664126	0.4677811	0.4934773
23	H H6	0.0629105	-1.0992633	2.6868297
24	H H5	2.3306967	-0.7344061	3.6471001
25	H H12	4.1128227	0.2578165	2.2330634
26	C C17	1.2842273	0.6236140	-1.5010760
27	H H4	0.2966643	1.0920993	-1.5710599
28	H H13	1.2051385	-0.3086161	-2.0815194
29	C C22	2.3387438	1.5297076	-2.1492121
30	H H15	2.2277634	2.5567709	-1.7732449
31	H H16	2.1701166	1.5715234	-3.2320596
32	C C21	3.7503791	1.0302510	-1.8322358
33	H H14	4.5062618	1.6295872	-2.3541217
34	H H17	3.8608773	-0.0031928	-2.1901632
35	C C20	3.9917999	1.0870428	-0.3205786
36	H H18	4.1092315	2.1400554	-0.0204226
37	H H19	4.9388651	0.5965492	-0.0616741

38	P	P1	0.0776925	-3.2380515	-0.2356711
39	H	H11	-0.3865093	-3.8954483	-1.4106835
40	H	H1	1.1855055	-2.6345422	-0.8907099

Compound 16

SCF model:
A restricted hybrid HF-DFT SCF calculation will be performed using Pulay DIIS + Geometric Direct Minimization

Optimization:

Step	Energy	Max Grad.	Max Dist.
1	-1036.296258	0.009785	0.113623
2	-1036.297762	0.007653	0.032495
3	-1036.298117	0.001902	0.028350
4	-1036.298150	0.000605	0.024999
5	-1036.298165	0.000402	0.064255
6	-1036.298173	0.000221	0.042445
7	-1036.298177	0.000218	0.001576
8	-1036.298178	0.000079	0.001601

<step 2>
Job type: Frequency calculation.
Method: RB3LYP
Basis set: 6-31G(D)

Reason for exit: Successful completion
Quantum Calculation CPU Time : 1:13:20.38
Quantum Calculation Wall Time: 1:20:12.35

SPARTAN '14 Properties Program: (Linux/P4E) build 14.117
Use of molecular symmetry enabled

Cartesian Coordinates (Angstroms)

Atom	X	Y	Z
1 P P1	0.0000000	0.0000000	1.2094814
2 C C1	1.6704982	0.0000000	0.4046425
3 C C4	4.2771492	0.0866398	-0.6541261
4 C C2	1.9974724	-0.7244846	-0.7516521
5 C C6	2.6757496	0.7591314	1.0273392
6 C C5	3.9652988	0.8104588	0.4986603
7 C C3	3.2917304	-0.6826209	-1.2746749
8 H H2	1.2402226	-1.3267303	-1.2443972
9 H H6	2.4448069	1.3103499	1.9361750
10 H H5	4.7285340	1.4065767	0.9922815
11 H H4	3.5287348	-1.2519696	-2.1700573
12 H H7	5.2839322	0.1171726	-1.0625423
13 C C7	-0.8352491	1.4466939	0.4046425
14 C C8	-2.2136069	3.6608000	-0.6541261
15 C C9	-1.9953019	1.9377014	1.0273392
16 C C10	-0.3713142	2.0921042	-0.7516521
17 C C11	-1.0546981	3.1920326	-1.2746749
18 C C12	-2.6845273	3.0288201	0.4986603
19 H H1	-2.3571997	1.4620899	1.9361750

20	H	H8	0.5288709	1.7374294	-1.2443972
21	H	H9	-0.6801299	3.6819588	-2.1700573
22	H	H10	-3.5823981	3.3917422	0.9922815
23	H	H11	-2.7434405	4.5174332	-1.0625423
24	C	C13	-0.8352491	-1.4466939	0.4046425
25	C	C14	-2.0635423	-3.7474398	-0.6541261
26	C	C15	-0.6804477	-2.6968329	1.0273392
27	C	C16	-1.6261584	-1.3676196	-0.7516521
28	C	C17	-2.2370323	-2.5094117	-1.2746749
29	C	C18	-1.2807715	-3.8392789	0.4986603
30	H	H3	-0.0876071	-2.7724398	1.9361750
31	H	H12	-1.7690935	-0.4106991	-1.2443972
32	H	H13	-2.8486049	-2.4299892	-2.1700573
33	H	H14	-1.1461358	-4.7983188	0.9922815
34	H	H15	-2.5404917	-4.6346058	-1.0625423

Compound 20a

SCF model:
An unrestricted hybrid HF-DFT SCF calculation will be performed using Pulay DIIS + Geometric Direct Minimization

Optimization:

Step	Energy	Max Grad.	Max Dist.
1	-1448.661177	0.045391	0.107217
2	-1448.686800	0.019297	0.124654
3	-1448.695008	0.012760	0.134780
4	-1448.697393	0.007965	0.084840
5	-1448.697764	0.006275	0.127698
6	-1448.698552	0.005565	0.116493
7	-1448.696398	0.012981	0.097583
8	-1448.699132	0.001929	0.092061
9	-1448.698897	0.004149	0.070322
10	-1448.699475	0.000980	0.104806
11	-1448.699569	0.001009	0.082493
12	-1448.699625	0.000496	0.097110
13	-1448.699666	0.001094	0.125736
14	-1448.699680	0.001674	0.044573
15	-1448.699701	0.000872	0.019639
16	-1448.699710	0.000229	0.016580
17	-1448.699712	0.000160	0.008637
18	-1448.699714	0.000205	0.019147
19	-1448.699716	0.000229	0.017860
20	-1448.699718	0.000190	0.033595
21	-1448.699722	0.000330	0.070221
22	-1448.699726	0.000547	0.009299
23	-1448.699732	0.000457	0.084571
24	-1448.699740	0.000483	0.046397
25	-1448.699741	0.000502	0.030891
26	-1448.699747	0.000228	0.021044
27	-1448.699749	0.000145	0.011857
28	-1448.699748	0.000067	0.002432

<step 2>
Job type: Frequency calculation.
Method: UB3LYP
Basis set: 6-31G(D)

Reason for exit: Successful completion
Quantum Calculation CPU Time : 4:36:29.73
Quantum Calculation Wall Time: 4:48:59.34

SPARTAN '14 Properties Program: (Linux/P4E) build 14.117
Use of molecular symmetry disabled

Cartesian Coordinates (Angstroms)

	Atom	X	Y	Z
1	C C1	0.2126187	0.0094061	0.0082378
2	C C2	-0.5021445	1.2159978	-0.0863430
3	C C3	-0.4616294	-1.2196653	0.1110544
4	N N1	-1.8685265	-1.2810303	0.1431118
5	N N2	-1.9108701	1.2334717	-0.1016438
6	B B1	-2.8799222	-0.0439593	-0.0202732
7	C C4	-0.0126650	2.5873044	-0.2048176
8	C C5	-1.1275127	3.3810992	-0.3076717
9	C C6	-2.2905954	2.5038337	-0.2420311
10	C C7	0.0717123	-2.5751438	0.2269918
11	C C8	-1.0169379	-3.4037269	0.3380488
12	C C9	-2.2075772	-2.5621953	0.2849796
13	C C10	-3.8119576	0.0740203	1.3196941
14	H H6	-3.9268131	1.1080371	1.6653923
15	H H8	-3.3912265	-0.4735536	2.1734098
16	H H11	-4.8311180	-0.3038995	1.1694797
17	C C11	-3.6327218	-0.2087235	-1.4522540
18	H H9	-4.3234333	0.6146381	-1.6679524
19	H H12	-4.2402224	-1.1207047	-1.4978103
20	H H13	-2.9255308	-0.2570868	-2.2917909
21	C C12	1.7078391	0.0322793	0.0018644
22	C C13	4.5338089	0.0682934	-0.0053885
23	C C14	2.4164017	-0.0507732	-1.2039633
24	C C15	2.4202559	0.1299486	1.2036748
25	C C16	3.8146067	0.1460139	1.1974715
26	C C17	3.8104579	-0.0368430	-1.2041853
27	H H1	1.8787458	-0.1270685	-2.1459132
28	H H14	1.8860587	0.1965550	2.1482822
29	H H15	4.3428827	0.2251920	2.1441313
30	H H16	4.3356960	-0.1069160	-2.1533751
31	C C18	1.5045896	-3.0164972	0.2218694
32	H H5	2.0121083	-2.7339875	-0.7052676
33	H H18	1.5634797	-4.1028008	0.3180339
34	H H19	2.0748383	-2.5725151	1.0429134
35	C C19	-1.0521643	-4.8999455	0.4533719
36	H H10	-0.1348700	-5.2519480	0.9357070
37	H H21	-1.8742851	-5.1976625	1.1151569
38	C C20	-1.2139101	-5.6095200	-0.9087810
39	H H20	-0.3755220	-5.3791755	-1.5739663
40	H H22	-2.1369467	-5.3078772	-1.4153494
41	H H23	-1.2485716	-6.6937566	-0.7652200
42	C C21	-3.5964729	-3.0839695	0.3830500
43	H H4	-3.8337178	-3.6770805	-0.5102336
44	H H24	-4.3431202	-2.3021670	0.4896073

45	H	H25	-3.6734632	-3.7669061	1.2372225
46	C	C22	-3.6942758	2.9848528	-0.3564829
47	H	H7	-3.8528540	3.4080760	-1.3577328
48	H	H26	-3.8701810	3.7986493	0.3564868
49	H	H27	-4.4324509	2.2052052	-0.1923667
50	C	C23	-1.2120675	4.8742185	-0.4381425
51	H	H3	-2.0692889	5.1351824	-1.0702688
52	H	H28	-0.3266085	5.2458823	-0.9637664
53	C	C24	-1.3386794	5.6022745	0.9171880
54	H	H29	-2.2270941	5.2801880	1.4713689
55	H	H30	-1.4166577	6.6818966	0.7564301
56	H	H31	-0.4649881	5.4141783	1.5496169
57	C	C25	1.4054959	3.0737482	-0.2090294
58	H	H2	1.9895121	2.6339287	-1.0224377
59	H	H32	1.9220549	2.8234679	0.7227389
60	H	H33	1.4294086	4.1596447	-0.3238579
61	P	P1	6.3824662	-0.0571769	-0.0063582
62	H	H34	6.6234866	0.8730501	-1.0538763
63	H	H17	6.6202357	0.8839695	1.0312334

Compound 20b

SCF model:
A restricted hybrid HF-DFT SCF calculation will be performed using Pulay DIIS + Geometric Direct Minimization

Optimization:

Step	Energy	Max Grad.	Max Dist.
1	-1832.341060	0.084650	0.080392
2	-1832.387373	0.036741	0.094028
3	-1832.402006	0.012576	0.110190
4	-1832.402660	0.009174	0.110671
5	-1832.403838	0.007157	0.117453
6	-1832.403784	0.004598	0.083597
7	-1832.403809	0.009366	0.042199
8	-1832.404513	0.003013	0.053608
9	-1832.404599	0.001434	0.036582
10	-1832.404625	0.001137	0.052823
11	-1832.404652	0.000804	0.083886
12	-1832.404667	0.000373	0.061877
13	-1832.404670	0.000367	0.021603
14	-1832.404676	0.000192	0.013701
15	-1832.404679	0.000125	0.035046
16	-1832.404680	0.000098	0.027843

<step 2>
Job type: Frequency calculation.
Method: RB3LYP
Basis set: 6-31G(D)

Reason for exit: Successful completion
Quantum Calculation CPU Time : 8:48:05.60
Quantum Calculation Wall Time: 9:05:17.09

SPARTAN '14 Properties Program: (Linux/P4E) build 14.117
Use of molecular symmetry disabled

Cartesian Coordinates (Angstroms)

Atom	X	Y	Z
1 C C1	1.2293775	0.0156057	-0.0981443
2 C C2	0.5331961	1.2334358	-0.0688623
3 C C3	0.5632451	-1.2186987	-0.1282575
4 N N1	-0.8693735	1.2565906	-0.0936634
5 N N2	-0.8385076	-1.2757703	-0.1095620
6 B B1	-1.8234799	-0.0211651	-0.0980285
7 C C4	1.0695094	-2.5617615	-0.1465661
8 C C5	-0.0410054	-3.4017836	-0.1302737
9 C C6	-1.1967631	-2.5766518	-0.1011542
10 C C7	1.0070397	2.5883570	-0.0441919
11 C C8	-0.1229866	3.4016979	-0.0715779
12 C C9	-1.2589369	2.5482696	-0.0999533
13 C C12	2.4964143	-3.0330553	-0.1757029
14 H H3	3.0488828	-2.7427430	0.7243305
15 H H14	3.0521493	-2.6278230	-1.0268888
16 H H15	2.5328455	-4.1239116	-0.2446516
17 C C13	-2.6116488	-3.0580532	-0.0760103
18 H H10	-3.2227680	-2.4747179	0.6170660
19 H H16	-2.6494720	-4.1058101	0.2324788
20 H H17	-3.0761393	-2.9806293	-1.0661984
21 C C14	2.4235200	3.0880474	0.0082022
22 H H5	2.4391845	4.1808867	0.0384652
23 H H18	3.0116745	2.7721335	-0.8594787
24 H H19	2.9556362	2.7271257	0.8942076
25 C C15	-0.1769826	4.9060901	-0.0427949
26 H H20	-0.9764462	5.2602300	-0.7064532
27 H H21	0.7497620	5.3184215	-0.4580954
28 C C16	-2.6842990	2.9960581	-0.1270915
29 H H7	-3.1426463	2.9222942	0.8662081
30 H H22	-3.2856350	2.3905866	-0.8094707
31 H H23	-2.7458911	4.0396661	-0.4475203
32 C C17	-0.4013223	5.4889820	1.3652969
33 H H2	-0.4466112	6.5840416	1.3341863
34 H H24	0.4099220	5.2002438	2.0429840
35 H H25	-1.3387465	5.1232565	1.7986605
36 C C18	-0.0501231	-4.9078721	-0.1043094
37 H H8	0.7878862	-5.2941009	-0.6971408
38 H H26	-0.9542638	-5.2819716	-0.5991341
39 C C19	0.0290085	-5.4949270	1.3179269
40 H H27	0.9469377	-5.1726333	1.8220134
41 H H28	0.0196888	-6.5910793	1.2938591
42 H H29	-0.8165197	-5.1605895	1.9298122
43 C C20	2.7243013	0.0328026	-0.0943249
44 C C21	5.5527567	0.0765970	-0.0866406
45 C C22	3.4420292	0.0830200	-1.2958073
46 C C23	3.4366794	-0.0004377	1.1106912
47 C C24	4.8311002	0.0186915	1.1143023
48 C C25	4.8363436	0.1008274	-1.2920968
49 H H1	2.9042202	0.1103730	-2.2399647
50 H H30	2.8951162	-0.0361559	2.0524548
51 H H31	5.3569042	-0.0051342	2.0660165
52 H H32	5.3663404	0.1402921	-2.2409652
53 P P1	7.4004800	-0.0302508	-0.0872672

54	H	H33	7.6444789	0.9606297	-1.0794275
55	H	H34	7.6382716	0.8598068	0.9974926
56	C	C10	-2.6472645	-0.0307115	1.3226073
57	C	C11	-3.9157867	-0.0058742	3.8766828
58	C	C26	-1.9867008	-0.4605910	2.4917438
59	C	C27	-3.9701883	0.4178804	1.4928928
60	C	C28	-4.5987755	0.4303263	2.7424987
61	C	C29	-2.5989472	-0.4509058	3.7449781
62	H	H4	-0.9616619	-0.8175826	2.4193142
63	H	H6	-4.5313530	0.7730869	0.6340878
64	H	H9	-5.6253248	0.7809178	2.8256352
65	H	H11	-2.0488738	-0.7927675	4.6191640
66	H	H12	-4.4014294	0.0008774	4.8494989
67	C	C30	-2.6614887	-0.0322918	-1.5099460
68	C	C31	-3.9531426	-0.0873381	-4.0513909
69	C	C32	-3.9787714	-0.5017962	-1.6656003
70	C	C33	-2.0178824	0.4017339	-2.6869844
71	C	C34	-2.6416676	0.3774031	-3.9342437
72	C	C35	-4.6189398	-0.5289916	-2.9090937
73	H	H13	-4.5253273	-0.8632776	-0.8000628
74	H	H35	-0.9975978	0.7740394	-2.6254802
75	H	H36	-2.1049371	0.7228935	-4.8152578
76	H	H37	-5.6406098	-0.8958931	-2.9812627
77	H	H38	-4.4476652	-0.1056462	-5.0195804

Compound 50

SCF model:
A restricted hybrid HF-DFT SCF calculation will be performed using Pulay DIIS + Geometric Direct Minimization

Optimization:

Step	Energy	Max Grad.	Max Dist.
1	-1522.538368	0.075780	0.121793
2	-1522.587541	0.040976	0.096591
3	-1522.604882	0.019659	0.100315
4	-1522.608710	0.004961	0.136597
5	-1522.609544	0.003772	0.138859
6	-1522.609852	0.004574	0.135528
7	-1522.610083	0.002984	0.061678
8	-1522.610279	0.003392	0.055371
9	-1522.610393	0.002128	0.070279
10	-1522.610427	0.003376	0.029700
11	-1522.610550	0.000695	0.070661
12	-1522.610597	0.000731	0.143277
13	-1522.610650	0.000756	0.046470
14	-1522.610660	0.000670	0.015963
15	-1522.610674	0.000447	0.016790
16	-1522.610679	0.000248	0.012518
17	-1522.610680	0.000163	0.006773
18	-1522.610681	0.000143	0.007437

<step 2>
Job type: Frequency calculation.
Method: RB3LYP
Basis set: 6-31G(D)

Reason for exit: Successful completion

Quantum Calculation CPU Time : 8:03:12.07
Quantum Calculation Wall Time: 10:49:58.33

SPARTAN '14 Properties Program: (Linux/P4E) build 14.117
Use of molecular symmetry disabled

Cartesian Coordinates (Angstroms)

	Atom	X	Y	Z
1	C C1	4.7240350	0.0281065	0.0085872
2	C C4	1.8954784	0.0208104	-0.0056752
3	C C2	3.9981016	0.1252022	1.2051201
4	C C6	4.0112044	-0.0594284	-1.1953999
5	C C5	2.6160522	-0.0619658	-1.2027892
6	C C3	2.6041372	0.1137410	1.1991608
7	H H2	4.5211756	0.2053021	2.1554829
8	H H6	4.5439153	-0.1343438	-2.1403587
9	H H5	2.0807920	-0.1377058	-2.1457154
10	H H3	2.0584834	0.1787435	2.1368632
11	P P1	6.5700473	0.1613709	0.0275453
12	H H1	6.8263804	-0.8698946	0.9754660
13	H H7	6.8237177	-0.6765156	-1.0933170
14	C C7	0.4004680	0.0068396	-0.0084495
15	N N2	-1.6963871	1.2369710	-0.1423970
16	N N1	-1.6702579	-1.2657541	0.1430236
17	B B1	-2.6258069	-0.0234182	0.0070492
18	C C11	-0.2708820	-1.2204203	0.1133437
19	C C12	-0.2958290	1.2198218	-0.1267161
20	C C9	-3.5005438	0.1266008	1.3271912
21	C C13	-3.5157557	-0.1900015	-1.3014134
22	C C8	0.2155895	-2.5649279	0.2339828
23	C C10	-0.9060908	-3.3874280	0.3440787
24	C C14	-2.0519683	-2.5510586	0.2818391
25	C C15	0.1626533	2.5736692	-0.2556097
26	C C16	-2.1046392	2.5140442	-0.2782612
27	C C17	-0.9761706	3.3731833	-0.3550649
28	C C18	1.6386690	-3.0475265	0.2331744
29	H H9	2.2212845	-2.6301545	1.0610195
30	H H11	2.1640834	-2.7749367	-0.6880772
31	H H12	1.6707803	-4.1369289	0.3210423
32	C C19	-0.9398943	-4.8879440	0.4653284
33	H H13	-1.7577481	-5.1855987	1.1336835
34	H H16	-0.0227725	-5.2419687	0.9501553
35	C C20	-1.1065474	-5.6102129	-0.8852559
36	H H17	-2.0345558	-5.3062759	-1.3819146
37	H H18	-1.1343840	-6.6977255	-0.7483187
38	H H19	-0.2777318	-5.3725701	-1.5615853
39	C C21	-3.4839108	-2.9699810	0.3556376
40	H H20	-4.0008181	-2.4480234	1.1678255
41	H H21	-3.5636932	-4.0470978	0.5188900
42	H H22	-4.0128234	-2.7117758	-0.5683321
43	C C22	-3.5452093	2.9061902	-0.3360523
44	H H14	-3.6457451	3.9798487	-0.5095220
45	H H23	-4.0566422	2.6485149	0.5979802
46	H H24	-4.0635099	2.3663268	-1.1354241

47	C	C23	-1.0433299	4.8724232	-0.4795180
48	H	H25	-1.8692680	5.1493589	-1.1469532
49	H	H26	-0.1356324	5.2464053	-0.9668769
50	C	C24	-1.2240148	5.5938577	0.8697147
51	H	H10	-1.2812116	6.6797942	0.7296388
52	H	H27	-0.3864398	5.3803196	1.5432239
53	H	H28	-2.1416088	5.2670426	1.3712661
54	C	C25	1.5761509	3.0824178	-0.2777530
55	H	H4	1.5875036	4.1735161	-0.3480574
56	H	H29	2.1463012	2.6899971	-1.1264312
57	H	H30	2.1287349	2.8041497	0.6254255
58	C	C26	-4.1807759	-0.3232186	-2.3087105
59	H	H8	-4.7643376	-0.4383669	-3.1947034
60	C	C27	-4.1552856	0.2481381	2.3426528
61	H	H15	-4.7295446	0.3529772	3.2359562

Compound 56

DFT calculations gave this output with one imaginary number present.

SCF model:
A restricted hybrid HF-DFT SCF calculation will be performed using Pulay DIIS + Geometric Direct Minimization

Optimization:

Step	Energy	Max Grad.	Max Dist.
1	-1984.670941	0.088065	0.083099
2	-1984.720223	0.039837	0.093848
3	-1984.738577	0.017017	0.141107
4	-1984.743603	0.006297	0.109065
5	-1984.744183	0.002830	0.133487
6	-1984.744467	0.004253	0.097999
7	-1984.744499	0.002962	0.042669
8	-1984.744772	0.003502	0.040958
9	-1984.744908	0.001734	0.065923
10	-1984.744778	0.002798	0.020862
11	-1984.745028	0.001479	0.069408
12	-1984.745092	0.001319	0.141264
13	-1984.745228	0.001025	0.150374
14	-1984.744576	0.005866	0.092635
15	-1984.745397	0.001095	0.134468
16	-1984.745493	0.001028	0.137906
17	-1984.745593	0.000745	0.156801
18	-1984.745680	0.000917	0.036117
19	-1984.745716	0.000665	0.049603
20	-1984.745744	0.000303	0.040080
21	-1984.745748	0.000271	0.019854
22	-1984.745752	0.000267	0.014854
23	-1984.745761	0.000195	0.037945
24	-1984.745767	0.000185	0.025549
25	-1984.745770	0.000161	0.017095
26	-1984.745768	0.000133	0.011041
27	-1984.745768	0.000117	0.015232

<step 2>
Job type: Frequency calculation.

Method: RB3LYP
Basis set: 6-31G(D)

Reason for exit: Successful completion
Quantum Calculation CPU Time : 5:28:27.80
Quantum Calculation Wall Time: 5:47:22.10

SPARTAN '14 Properties Program: (Linux/P4E) build 14.117
Use of molecular symmetry disabled

Cartesian Coordinates (Angstroms)

Atom	X	Y	Z
1 C C1	6.2351684	0.0823468	0.0206511
2 C C4	3.4079367	0.0826736	-0.0152106
3 C C2	5.5192606	1.2255655	-0.3656426
4 C C6	5.5112943	-1.0579220	0.3992709
5 C C5	4.1165940	-1.0564093	0.3868282
6 C C3	4.1250221	1.2234155	-0.3956636
7 H H2	6.0550774	2.1307947	-0.6418626
8 H H6	6.0367558	-1.9582204	0.7067454
9 H H5	3.5698262	-1.9460405	0.6881311
10 H H3	3.5874314	2.1162339	-0.7040856
11 P P1	8.0849756	0.1780841	0.0537437
12 H H1	8.3442001	-0.3564326	-1.2435234
13 H H7	8.3201797	-1.0655955	0.7026948
14 C C7	1.9127785	0.0799574	-0.0228631
15 C C8	1.2357522	-0.3045273	-1.1908005
16 C C9	1.2238966	0.4587881	1.1402975
17 C C10	1.7169013	-0.7154119	-2.4792665
18 C C11	0.5907496	-0.9719069	-3.2621559
19 C C12	1.6891935	0.8993166	2.4246451
20 C C13	0.5538958	1.1424183	3.1982901
21 C C14	-0.5786198	0.8561961	2.3902300
22 C C15	-0.5512122	-0.7266399	-2.4545382
23 N N1	-0.1638158	-0.3268522	-1.2271072
24 N N2	-0.1760277	0.4502465	1.1698304
25 B B1	-1.1142694	0.0130580	-0.0183849
26 C C16	3.1376882	-0.8618198	-2.9447053
27 H H8	3.1642275	-1.1701958	-3.9935529
28 H H11	3.6865823	-1.6138883	-2.3672317
29 H H16	3.7026042	0.0721731	-2.8597979
30 C C17	0.5523707	-1.4590932	-4.6868493
31 H H17	1.4220819	-1.0763266	-5.2341078
32 H H18	-0.3220881	-1.0368243	-5.1968584
33 C C18	0.5151862	-2.9939964	-4.8080157
34 H H12	0.4832223	-3.3054461	-5.8587125
35 H H19	-0.3654113	-3.4064338	-4.3028525
36 H H20	1.4002668	-3.4441468	-4.3448239
37 C C19	-1.9855690	-0.8690713	-2.8468169
38 H H4	-2.0724205	-1.2346665	-3.8724665
39 H H21	-2.5092491	0.0893489	-2.7648666
40 H H22	-2.5040051	-1.5651561	-2.1784748
41 C C20	-2.0174292	0.9754483	2.7744467
42 H H15	-2.5781615	0.0888148	2.4646568

43	H	H23	-2.4839130	1.8343905	2.2782856
44	H	H24	-2.1187058	1.1019936	3.8551605
45	C	C21	0.4970680	1.6537592	4.6132318
46	H	H25	1.3859894	1.3248091	5.1645907
47	H	H26	-0.3546920	1.1998194	5.1352847
48	C	C22	0.3835265	3.1868890	4.7083669
49	H	H14	-0.5170766	3.5477375	4.1989723
50	H	H27	1.2456423	3.6728670	4.2379785
51	H	H28	0.3359879	3.5126807	5.7541224
52	C	C23	3.1040643	1.0856935	2.8948564
53	H	H10	3.6811649	0.1562912	2.8507011
54	H	H29	3.1155485	1.4374097	3.9299497
55	H	H30	3.6470278	1.8204068	2.2912359
56	C	C24	-1.9227037	-1.2916390	0.3984165
57	C	C25	-2.0721251	1.2172330	-0.4071031
58	C	C26	-2.5301378	-2.2997559	0.7190025
59	C	C41	-2.8081288	2.1448304	-0.6987596
60	C	C28	-3.2361464	-3.4846294	1.0935952
61	C	C29	-4.6296568	-5.8178884	1.8303385
62	C	C30	-3.6544980	-4.4122816	0.1189021
63	C	C31	-3.5295909	-3.7517362	2.4456700
64	C	C32	-4.2191552	-4.9066068	2.8062745
65	C	C33	-4.3433754	-5.5652781	0.4866682
66	H	H13	-3.4314032	-4.2158994	-0.9256316
67	H	H31	-3.2095706	-3.0438172	3.2043728
68	H	H32	-4.4374801	-5.0961888	3.8541781
69	H	H33	-4.6585682	-6.2693836	-0.2791815
70	H	H34	-5.1678542	-6.7180282	2.1149590
71	C	C34	-3.6761802	3.2292791	-1.0357564
72	C	C35	-5.3883019	5.3634660	-1.6942983
73	C	C36	-3.1631635	4.4182902	-1.5910632
74	C	C37	-5.0649080	3.1310216	-0.8174079
75	C	C38	-5.9088674	4.1895228	-1.1441892
76	C	C39	-4.0133010	5.4724213	-1.9161013
77	H	H9	-2.0938427	4.5003022	-1.7616129
78	H	H35	-5.4667790	2.2169549	-0.3906598
79	H	H36	-6.9778060	4.0977922	-0.9693119
80	H	H37	-3.6010092	6.3826306	-2.3439607
81	H	H38	-6.0498249	6.1874143	-1.9483906

Compound 62

SCF model:
A restricted hybrid HF-DFT SCF calculation will be performed using Pulay DIIS + Geometric Direct Minimization

Optimization:

Step	Energy	Max Grad.	Max Dist.
1	-2082.657370	0.141888	0.183009
2	-2082.698069	0.068375	0.156671
3	-2082.709614	0.034956	0.162986
4	-2082.720080	0.006889	0.105379
5	-2082.717932	0.008977	0.142702
6	-2082.719139	0.014366	0.135617
7	-2082.718734	0.010187	0.126554
8	-2082.718919	0.013731	0.209240
9	-2082.719652	0.009090	0.161183

10	-2082.718213	0.010233	0.187062
11	-2082.718798	0.020135	0.129909
12	-2082.718573	0.011845	0.170860
13	-2082.718329	0.016314	0.100095
14	-2082.718779	0.012269	0.092686
15	-2082.718086	0.017223	0.089774
16	-2082.719613	0.005047	0.134724
17	-2082.718932	0.010824	0.088930
18	-2082.720022	0.004589	0.189450
19	-2082.718913	0.009004	0.155545
20	-2082.719911	0.004195	0.203904
21	-2082.719473	0.005525	0.222392
22	-2082.720109	0.003457	0.144034
23	-2082.718263	0.007960	0.049791
24	-2082.720509	0.003757	0.038422
25	-2082.719736	0.005780	0.029030
26	-2082.720667	0.001183	0.011033
27	-2082.720650	0.001352	0.008421
28	-2082.720685	0.000636	0.004922
29	-2082.720680	0.000861	0.004700
30	-2082.720688	0.000616	0.006125
31	-2082.720688	0.000610	0.007623
32	-2082.720691	0.000575	0.011843
33	-2082.720701	0.000453	0.002606
34	-2082.720701	0.000373	0.002055
35	-2082.720695	0.000338	0.009743
36	-2082.720693	0.000254	0.008121
37	-2082.720687	0.000240	0.012695
38	-2082.720680	0.000272	0.008970
39	-2082.720677	0.000335	0.014876
40	-2082.720660	0.000486	0.004974
41	-2082.720661	0.000411	0.009644
42	-2082.720663	0.000407	0.013623
43	-2082.720662	0.000428	0.011681
44	-2082.720664	0.000387	0.013201
45	-2082.720665	0.000258	0.010208
46	-2082.720667	0.000138	0.013068
47	-2082.720668	0.000118	0.006517
48	-2082.720669	0.000084	0.007987

<step 2>
Job type: Frequency calculation.
Method: RB3LYP
Basis set: LACVP

<step 3>
Job type: Single point.
Method: RB3LYP
Basis set: LACVP
SCF total energy: -2082.7206655 hartrees

NMR shifts (ppm)

	Atom	Isotropic	Rel. Shift
1	Mo1	8419.4055	
2	C1	68.0052	115.90
3	O1	-410.6897	

4	C2	-152.1336	336.04
5	O2	101.3284	
6	C3	-1325.9604	1509.87
7	O3	-1539.6879	
8	C4	321.9722	-138.06
9	O4	-159.5212	
10	C6	-1091.7013	1275.61
11	O6	-1325.5055	
12	P1	15444.1783	-15155.11
13	H2	-291.5959	323.57
14	H3	-313.5921	345.57
15	C5	-2040.4661	2224.38
16	C7	-1849.3235	2033.23
17	C8	-1678.1996	1862.11
18	C9	-1785.9921	1969.90
19	C10	-1274.4341	1458.34
20	C11	-1145.9068	1329.82
21	H1	-1221.2870	1253.26
22	H6	-1410.1342	1442.11
23	H5	-965.3293	997.31
24	H4	-889.8410	921.82
25	C12	-671.1409	855.05
26	C14	-1081.1360	1265.05
27	N3	-1284.0716	1130.84
28	B1	427.6348	
29	C13	-1300.9861	1484.90
30	N1	-1847.8648	1694.64
31	C16	-323.3806	507.29
32	C15	-1359.0529	1542.96
33	C17	-687.9162	871.83
34	C18	-543.0410	726.95
35	C19	-1410.4828	1594.39
36	C20	-955.3970	1139.31
37	C21	191.0823	-7.17
38	H9	-303.4020	335.38
39	H10	-522.7143	554.69
40	H14	-547.6233	579.60
41	C22	578.6502	-394.74
42	H15	18.3186	13.66
43	H17	106.4110	-74.43
44	H18	103.4239	-71.45
45	C23	551.0717	-367.16
46	H16	-11.2539	43.23
47	H19	-99.1373	131.12
48	H20	5.9843	25.99
49	C24	151.1677	32.74
50	H8	-1109.1349	1141.11
51	H21	-1063.1126	1095.09
52	H22	-783.7909	815.77
53	C25	489.8627	-305.95
54	H13	58.9417	-26.96
55	H23	-102.5404	134.52
56	C26	472.5285	-288.62
57	H24	24.7870	7.19
58	H25	113.1294	-81.15
59	H26	-127.5525	159.53
60	C27	414.2626	-230.35
61	H7	-378.8584	410.84

62	H28	-123.9051	155.88
63	C28	383.5684	-199.66
64	H27	-44.0526	76.03
65	H29	-321.9638	353.94
66	H30	-102.9955	134.97
67	C29	219.8138	-35.90
68	H11	-30.6220	62.60
69	H31	-307.3803	339.36
70	H32	-62.5150	94.49
71	C30	64.3491	119.56
72	H12	33.4410	-1.46
73	H33	-190.1407	222.12
74	H34	-136.9543	168.93

Reason for exit: Successful completion
Quantum Calculation CPU Time : 7:59:49.33
Quantum Calculation Wall Time: 8:45:01.87

SPARTAN '10 Properties Program: (Linux/P4E) build 1.1.0
Use of molecular symmetry disabled

Cartesian Coordinates (Angstroms)

Atom	X	Y	Z
1 Mo Mo1	-5.0965766	-0.1044159	0.0717571
2 C C1	-6.0480407	-0.4891471	-1.7056120
3 O O1	-6.5863830	-0.7124232	-2.7236828
4 C C2	-6.4004656	1.3642737	0.4756980
5 O O2	-7.1631886	2.2276729	0.7128805
6 C C3	-3.8528881	1.2332168	-0.8694695
7 O O3	-3.1365089	1.9974546	-1.3985168
8 C C4	-6.3061827	-1.4640243	1.0220855
9 O O4	-6.9947914	-2.2403083	1.5692402
10 C C6	-4.1139037	0.2470030	1.8395203
11 O O6	-3.5460080	0.4420416	2.8483562
12 P P1	-3.3587692	-1.9893680	-0.4492393
13 H H2	-3.4039477	-2.6071714	-1.7425379
14 H H3	-3.3988322	-3.1799264	0.3520407
15 C C5	-1.5355380	-1.5462952	-0.3502858
16 C C7	1.1274045	-0.6516915	-0.1717396
17 C C8	-0.8258585	-1.2106314	-1.5116660
18 C C9	-0.9098619	-1.4431195	0.9007511
19 C C10	0.4137475	-1.0021334	0.9858073
20 C C11	0.4968880	-0.7664684	-1.4206026
21 H H1	-1.2970764	-1.2870260	-2.4869628
22 H H6	-1.4480185	-1.6891196	1.8110168
23 H H5	0.8946256	-0.9193470	1.9549423
24 H H4	1.0417853	-0.5032605	-2.3211838
25 C C12	2.5354830	-0.1520672	-0.0795942
26 C C14	3.5906117	-1.0758329	-0.1486995
27 N N3	4.9334048	-0.6401743	-0.0837853
28 B B1	5.4162185	0.8742638	0.0898074
29 C C13	2.7543341	1.2251671	0.0653208
30 N N1	4.0708575	1.7377636	0.1405951
31 C C16	3.5927811	-2.5110243	-0.2824526
32 C C15	4.9337394	-2.9087592	-0.2982614

33	C	C17	5.7340264	-1.7324974	-0.1712204
34	C	C18	1.8361531	2.3355018	0.1548857
35	C	C19	2.6173721	3.4873755	0.2832466
36	C	C20	3.9886570	3.0853042	0.2664674
37	C	C21	2.4209073	-3.4476995	-0.3776540
38	H	H9	2.7697000	-4.4781640	-0.4883774
39	H	H10	1.7730975	-3.2252962	-1.2326983
40	H	H14	1.7871141	-3.4114549	0.5157567
41	C	C22	7.2295145	-1.7014306	-0.1147636
42	H	H15	7.5921380	-1.9257730	0.8977755
43	H	H17	7.6351596	-0.7314356	-0.3991252
44	H	H18	7.6523568	-2.4601460	-0.7821312
45	C	C23	5.1653642	4.0002600	0.4034600
46	H	H16	6.0498696	3.6138225	-0.1030629
47	H	H19	5.4304511	4.1496814	1.4589197
48	H	H20	4.9332810	4.9842114	-0.0151283
49	C	C24	0.3326470	2.3248472	0.1238546
50	H	H8	-0.0972595	1.6996117	0.9139654
51	H	H21	-0.0698938	1.9548820	-0.8259851
52	H	H22	-0.0535420	3.3384983	0.2609569
53	C	C25	5.4735623	-4.3124367	-0.3763523
54	H	H13	6.4224924	-4.3152759	-0.9289963
55	H	H23	4.7903688	-4.9438068	-0.9584375
56	C	C26	5.6997957	-4.9625930	1.0085271
57	H	H24	6.4194356	-4.3857222	1.6008452
58	H	H25	6.0850949	-5.9839980	0.9056320
59	H	H26	4.7625262	-5.0039594	1.5746894
60	C	C27	2.1415042	4.9134151	0.3812456
61	H	H7	1.1966951	4.9549035	0.9376923
62	H	H28	2.8571937	5.5009642	0.9703904
63	C	C28	1.9439347	5.5911455	-0.9946039
64	H	H27	1.6159515	6.6307574	-0.8775896
65	H	H29	1.1901632	5.0587978	-1.5856339
66	H	H30	2.8773376	5.5890351	-1.5692979
67	C	C29	6.1784198	1.0105333	1.5267581
68	H	H11	7.0909948	0.4023727	1.5663318
69	H	H31	5.5350130	0.6877170	2.3581590
70	H	H32	6.4872276	2.0427737	1.7357849
71	C	C30	6.2987723	1.3251065	-1.2290961
72	H	H12	7.2775654	1.7496394	-0.9609917
73	H	H33	5.7743401	2.0774713	-1.8342907
74	H	H34	6.4911701	0.4799965	-1.9039285

Compound 63

SCF model:
A restricted hybrid HF-DFT SCF calculation will be performed using Pulay DIIS + Geometric Direct Minimization

Optimization:

Step	Energy	Max Grad.	Max Dist.
1	-2082.959197	0.153644	0.145815
2	-2082.993670	0.085776	0.157609
3	-2083.010900	0.041164	0.184526
4	-2083.021348	0.013161	0.116261
5	-2083.021735	0.007532	0.170643
6	-2083.019940	0.009314	0.148073
7	-2083.021525	0.009645	0.187129

8	-2083.021052	0.011416	0.136711
9	-2083.021263	0.008014	0.171228
10	-2083.021593	0.007026	0.129189
11	-2083.020979	0.008332	0.134717
12	-2083.021192	0.009792	0.128342
13	-2083.021020	0.008973	0.097162
14	-2083.021087	0.009631	0.114479
15	-2083.022315	0.004685	0.171523
16	-2083.021773	0.007276	0.161521
17	-2083.021684	0.009428	0.115004
18	-2083.021630	0.009875	0.138943
19	-2083.021939	0.006500	0.177909
20	-2083.022062	0.008318	0.136064
21	-2083.021299	0.007917	0.173851
22	-2083.022532	0.007459	0.199813
23	-2083.021887	0.006868	0.218015
24	-2083.022024	0.008741	0.222237
25	-2083.022313	0.010041	0.197070
26	-2083.021657	0.013122	0.080219
27	-2083.023297	0.003735	0.029230
28	-2083.023183	0.006281	0.017837
29	-2083.023566	0.001991	0.122416
30	-2083.023053	0.004275	0.106169
31	-2083.023593	0.001575	0.152224
32	-2083.023419	0.002630	0.128197
33	-2083.023617	0.001646	0.007615
34	-2083.023618	0.001282	0.006616
35	-2083.023650	0.000990	0.007709
36	-2083.023683	0.000839	0.010010
37	-2083.023703	0.000815	0.007075
38	-2083.023710	0.000884	0.004879
39	-2083.023715	0.000867	0.002521
40	-2083.023716	0.000863	0.023344
41	-2083.023728	0.000837	0.016883
42	-2083.023729	0.000831	0.019465
43	-2083.023719	0.000768	0.016101
44	-2083.023719	0.000748	0.026082
45	-2083.023720	0.000685	0.025098
46	-2083.023722	0.000618	0.015851
47	-2083.023723	0.000519	0.005170
48	-2083.023726	0.000620	0.010442
49	-2083.023724	0.000626	0.016241
50	-2083.023724	0.000625	0.013656
51	-2083.023725	0.000607	0.009051
52	-2083.023726	0.000579	0.007672
53	-2083.023727	0.000526	0.010507
54	-2083.023731	0.000448	0.012584
55	-2083.023734	0.000319	0.012895
56	-2083.023736	0.000217	0.007767
57	-2083.023737	0.000126	0.003183
58	-2083.023739	0.000090	0.004553
59	-2083.023739	0.000080	0.003568

<step 2>
Job type: Frequency calculation.
Method: RB3LYP
Basis set: LACVP

<step 3>
Job type: Single point.
Method: RB3LYP
Basis set: LACVP
SCF total energy: -2083.0237375 hartrees

NMR shifts (ppm)

	Atom	Isotropic	Rel. Shift
1	W6	14043.4999	
2	C1	-198.1844	382.09
3	O1	-1018.7592	
4	C2	-1417.5045	1601.41
5	O2	-507.8757	
6	C3	-2507.1960	2691.11
7	O3	-2698.0522	
8	C4	90.6203	93.29
9	O4	-692.1275	
10	C6	-2191.8722	2375.78
11	O6	-2260.1012	
12	P1	33877.7030	-33588.64
13	H2	-803.7200	835.70
14	H3	-848.1294	880.11
15	C5	-4132.0126	4315.92
16	C7	-4099.8788	4283.79
17	C8	-3527.1759	3711.09
18	C9	-3796.0969	3980.01
19	C10	-2802.6318	2986.54
20	C11	-2552.1642	2736.07
21	H1	-2587.6486	2619.63
22	H6	-3027.6553	3059.63
23	H5	-2095.3864	2127.36
24	H4	-1914.5692	1946.55
25	C12	-1105.5347	1289.44
26	C14	-2288.4758	2472.38
27	N3	-2814.6390	2661.41
28	B1	952.8619	
29	C13	-2770.7075	2954.62
30	N1	-4146.3686	3993.14
31	C16	-519.4867	703.40
32	C15	-2983.2929	3167.20
33	C17	-1524.3143	1708.22
34	C18	-941.0584	1124.97
35	C19	-2996.7738	3180.68
36	C20	-2125.3152	2309.22
37	C21	165.8151	18.09
38	H9	-675.7768	707.75
39	H10	-1127.8348	1159.81
40	H14	-1192.5567	1224.53
41	C22	1121.7654	-937.86
42	H15	80.2402	-48.26
43	H17	299.7507	-267.77
44	H18	278.5374	-246.56
45	C23	1047.7243	-863.82
46	H16	37.7049	-5.73
47	H19	-188.4227	220.40
48	H20	52.2565	-20.28

49	C24	67.2709	116.64
50	H8	-2408.4386	2440.42
51	H21	-2300.0418	2332.02
52	H22	-1733.7469	1765.72
53	C25	886.1329	-702.22
54	H13	155.8102	-123.83
55	H23	-221.5373	253.52
56	C26	841.1156	-657.21
57	H24	68.9455	-36.97
58	H25	241.8527	-209.87
59	H26	-292.6684	324.65
60	C27	688.2962	-504.39
61	H7	-847.4214	879.40
62	H28	-267.3086	299.29
63	C28	623.6776	-439.77
64	H27	-119.3346	151.31
65	H29	-719.7538	751.73
66	H30	-211.5752	243.55
67	C29	316.8213	-132.91
68	H11	-26.8682	58.85
69	H31	-661.6710	693.65
70	H32	-97.3144	129.29
71	C30	-21.5431	205.45
72	H12	131.0857	-99.11
73	H33	-359.6399	391.62
74	H34	-263.6398	295.62

Reason for exit: Successful completion
Quantum Calculation CPU Time : 8:54:54.91
Quantum Calculation Wall Time: 9:45:52.34

SPARTAN '10 Properties Program: (Linux/P4E) build 1.1.0
Use of molecular symmetry disabled

Cartesian Coordinates (Angstroms)

Atom		X	Y	Z
1	W W6	-4.6339777	-0.0816560	0.0667050
2	C C1	-5.6186026	-0.4480173	-1.6849303
3	O O1	-6.1790018	-0.6640158	-2.6950800
4	C C2	-5.9254651	1.3805218	0.5120669
5	O O2	-6.6843909	2.2424727	0.7748546
6	C C3	-3.4067218	1.2496485	-0.8838256
7	O O3	-2.6904972	2.0106004	-1.4226717
8	C C4	-5.8126153	-1.4490293	1.0233269
9	O O4	-6.4833040	-2.2401457	1.5761201
10	C C6	-3.6183334	0.2485032	1.8080016
11	O O6	-3.0280939	0.4329992	2.8086412
12	P P1	-2.9225053	-1.9535721	-0.5094434
13	H H2	-2.9813950	-2.5268186	-1.8212204
14	H H3	-2.9794292	-3.1633987	0.2594080
15	C C5	-1.0989087	-1.5208703	-0.3985961
16	C C7	1.5661578	-0.6428675	-0.1984942
17	C C8	-0.3804248	-1.1859825	-1.5544874
18	C C9	-0.4822176	-1.4268304	0.8576234
19	C C10	0.8430430	-0.9938780	0.9531095

20	C	C11	0.9441362	-0.7497298	-1.4523191
21	H	H1	-0.8459111	-1.2550759	-2.5330078
22	H	H6	-1.0285726	-1.6716168	1.7630941
23	H	H5	1.3176725	-0.9170163	1.9257265
24	H	H4	1.4967116	-0.4856812	-2.3479081
25	C	C12	2.9755590	-0.1496887	-0.0938586
26	C	C14	4.0270840	-1.0782063	-0.1531985
27	N	N3	5.3710055	-0.6487040	-0.0734192
28	B	B1	5.8588483	0.8633505	0.1067235
29	C	C13	3.1986312	1.2264583	0.0537776
30	N	N1	4.5166803	1.7332814	0.1406240
31	C	C16	4.0242455	-2.5131292	-0.2896526
32	C	C15	5.3635195	-2.9168544	-0.2923606
33	C	C17	6.1676248	-1.7443313	-0.1544842
34	C	C18	2.2843485	2.3406736	0.1366977
35	C	C19	3.0695038	3.4889693	0.2722051
36	C	C20	4.4391753	3.0810058	0.2669842
37	C	C21	2.8489706	-3.4440413	-0.3985243
38	H	H9	3.1938520	-4.4759758	-0.5076756
39	H	H10	2.2107216	-3.2170723	-1.2596210
40	H	H14	2.2065961	-3.4065351	0.4886907
41	C	C22	7.6623114	-1.7190103	-0.0810132
42	H	H15	8.0124021	-1.9345264	0.9378288
43	H	H17	8.0751430	-0.7533287	-0.3700669
44	H	H18	8.0894020	-2.4860369	-0.7358875
45	C	C23	5.6179607	3.9912738	0.4172913
46	H	H16	6.5115282	3.5923242	-0.0624641
47	H	H19	5.8587771	4.1550912	1.4765099
48	H	H20	5.4013813	4.9704975	-0.0207185
49	C	C24	0.7810320	2.3366627	0.0946842
50	H	H8	0.3427193	1.7087934	0.8779900
51	H	H21	0.3831772	1.9745899	-0.8602340
52	H	H22	0.3982406	3.3511192	0.2352256
53	C	C25	5.8982951	-4.3225183	-0.3691251
54	H	H13	6.8491415	-4.3286606	-0.9185751
55	H	H23	5.2148084	-4.9509388	-0.9539928
56	C	C26	6.1173774	-4.9743161	1.0160883
57	H	H24	6.8367710	-4.4001652	1.6113179
58	H	H25	6.4997389	-5.9968776	0.9138581
59	H	H26	5.1779648	-5.0130477	1.5788885
60	C	C27	2.5992368	4.9169152	0.3687611
61	H	H7	1.6524782	4.9620704	0.9216726
62	H	H28	3.3152223	5.5011581	0.9608094
63	C	C28	2.4095942	5.5961483	-1.0074470
64	H	H27	2.0854118	6.6369875	-0.8909209
65	H	H29	1.6557882	5.0673332	-1.6015797
66	H	H30	3.3450782	5.5907290	-1.5787598
67	C	C29	6.6021864	0.9966744	1.5536264
68	H	H11	7.5124066	0.3858385	1.6049879
69	H	H31	5.9470682	0.6763487	2.3767670
70	H	H32	6.9111312	2.0281545	1.7661700
71	C	C30	6.7619242	1.3098610	-1.1998066
72	H	H12	7.7533041	1.6959071	-0.9195685
73	H	H33	6.2669337	2.0916418	-1.7921732
74	H	H34	6.9281556	0.4721461	-1.8907738

Compound 72

SCF model:
A restricted hybrid HF-DFT SCF calculation will be performed using Pulay DIIS + Geometric Direct Minimization

Optimization:

Step	Energy	Max Grad.	Max Dist.
1	-2695.161839	0.009544	0.117609
2	-2695.164844	0.004953	0.111197
3	-2695.165414	0.002405	0.168308
4	-2695.165379	0.002766	0.199388
5	-2695.165381	0.002761	0.205077
6	-2695.165494	0.001472	0.215469
7	-2695.165493	0.003027	0.062129
8	-2695.165580	0.002335	0.035588
9	-2695.165483	0.003560	0.046262
10	-2695.165680	0.001235	0.026862
11	-2695.165666	0.001011	0.009743
12	-2695.165697	0.000984	0.020359
13	-2695.165698	0.001014	0.013806
14	-2695.165710	0.000674	0.024150
15	-2695.165718	0.000526	0.032265
16	-2695.165725	0.000582	0.043861
17	-2695.165731	0.000746	0.046229
18	-2695.165746	0.001108	0.093047
19	-2695.165773	0.001124	0.055308
20	-2695.165770	0.001634	0.091000
21	-2695.165845	0.000702	0.061908
22	-2695.165836	0.001073	0.032315
23	-2695.165856	0.000722	0.047558
24	-2695.165856	0.000995	0.053988
25	-2695.165885	0.000848	0.134306
26	-2695.165933	0.000584	0.046338
27	-2695.165952	0.000377	0.033629
28	-2695.165965	0.000336	0.107460
29	-2695.166005	0.000522	0.098112
30	-2695.166052	0.000663	0.063519
31	-2695.166047	0.000413	0.039382
32	-2695.166057	0.000421	0.037409
33	-2695.166049	0.000360	0.065822
34	-2695.166036	0.000512	0.063074
35	-2695.166045	0.000342	0.024381
36	-2695.166053	0.000212	0.062140
37	-2695.166055	0.000323	0.027206
38	-2695.166061	0.000121	0.008959
39	-2695.166063	0.000127	0.005009
40	-2695.166063	0.000087	0.003633

<step 2>
Job type: Frequency calculation.
Method: RB3LYP
Basis set: LACVP

<step 3>
Job type: Single point.
Method: RB3LYP
Basis set: LACVP
SCF total energy: -2695.1660780 hartrees

NMR shifts (ppm)

	Atom	Isotropic	Rel. Shift
1	P1	12682.8298	-12393.76
2	C5	-2550.1743	2734.08
3	C7	-2218.6969	2402.61
4	C8	-2172.4572	2356.37
5	C9	-2445.4301	2629.34
6	C10	-1655.9949	1839.90
7	C11	-1467.2983	1651.21
8	H1	-1700.8342	1732.81
9	H6	-2166.1128	2198.09
10	H5	-1295.2051	1327.18
11	H4	-1172.9536	1204.93
12	C12	-814.4740	998.38
13	C14	-1254.7199	1438.63
14	N3	-1476.7786	1323.55
15	B1	321.6575	
16	C13	-1466.6474	1650.56
17	N1	-1954.1849	1800.96
18	C16	-449.9013	633.81
19	C15	-1486.1974	1670.11
20	C17	-835.3949	1019.30
21	C18	-705.0623	888.97
22	C19	-1548.7712	1732.68
23	C20	-1068.5998	1252.51
24	C21	-32.4768	216.39
25	H9	-521.8602	553.84
26	H10	-780.5122	812.49
27	H14	-831.1695	863.15
28	C22	477.5585	-293.65
29	H15	-82.6972	114.68
30	H17	-20.7759	52.75
31	H18	23.1089	8.87
32	C23	432.3689	-248.46
33	H16	-63.5184	95.50
34	H19	-174.8137	206.79
35	H20	-93.4725	125.45
36	C24	-210.5634	394.47
37	H8	-1387.1100	1419.09
38	H21	-1397.5149	1429.49
39	H22	-1024.0724	1056.05
40	C25	357.3270	-173.42
41	H13	-54.7927	86.77
42	H23	-247.4154	279.39
43	C26	359.3444	-175.44
44	H24	-68.2679	100.25
45	H25	10.5343	21.44
46	H26	-258.5914	290.57
47	C27	251.6040	-67.69
48	H7	-525.3469	557.32
49	H28	-231.2347	263.21
50	C28	231.0932	-47.18
51	H27	-158.6514	190.63
52	H29	-478.1787	510.16
53	H30	-221.1128	253.09
54	C29	115.0003	68.91

55	H11	-113.6808	145.66
56	H31	-414.8524	446.83
57	H32	-145.2487	177.23
58	C30	-17.9678	201.88
59	H12	-46.6441	78.62
60	H33	-233.8721	265.85
61	H34	-307.7051	339.68
62	H3	-1263.8526	1295.83
63	H2	-1459.2332	1491.21
64	Ru1	13961.7223	
65	H36	-193.8679	225.85
66	C1	-424.4532	608.36
67	C4	-548.4599	732.37
68	C6	-685.5335	869.44
69	C2	-466.3784	650.29
70	C3	-608.3799	792.29
71	C31	-587.7517	771.66
72	H38	-378.2887	410.27
73	H39	450.1376	-418.16
74	H40	800.3774	-768.40
75	H41	132.8648	-100.89
76	H42	679.0347	-647.06
77	Cl1	9934.5672	
78	Cl2	10752.3146	

Reason for exit: Successful completion
Quantum Calculation CPU Time : 8:30:28.04
Quantum Calculation Wall Time: 9:15:50.59

SPARTAN '10 Properties Program: (Linux/P4E) build 1.1.0
Use of molecular symmetry disabled

Cartesian Coordinates (Angstroms)

Atom		X	Y	Z
1	P P1	3.2558824	1.6842855	-0.4164921
2	C C5	1.4456391	1.2403769	-0.2993663
3	C C7	-1.2606124	0.5061295	-0.1423553
4	C C8	0.7079352	1.0260558	-1.4707116
5	C C9	0.8375946	1.0808420	0.9531337
6	C C10	-0.5110402	0.7220486	1.0252932
7	C C11	-0.6379378	0.6594095	-1.3907025
8	H H1	1.1760837	1.1315285	-2.4441908
9	H H6	1.4157363	1.2016324	1.8618062
10	H H5	-0.9833368	0.5970440	1.9940776
11	H H4	-1.2081101	0.4900210	-2.2981428
12	C C12	-2.7032252	0.1138964	-0.0652587
13	C C14	-3.6851112	1.1167279	-0.1480955
14	N N3	-5.0589106	0.7865808	-0.1159479
15	B B1	-5.6592818	-0.6877278	0.0521075
16	C C13	-3.0300125	-1.2407236	0.0746585
17	N N1	-4.3840510	-1.6514368	0.1403435
18	C C16	-3.5714745	2.5457442	-0.2789835
19	C C15	-4.8774585	3.0473897	-0.3361147
20	C C17	-5.7696608	1.9386483	-0.2320747
21	C C18	-2.1977061	-2.4167704	0.1744022

22	C	C19	-3.0648535	-3.5038541	0.3069820
23	C	C20	-4.4016124	-3.0004467	0.2804316
24	C	C21	-2.3294919	3.3909962	-0.3364157
25	H	H9	-2.5947264	4.4515742	-0.3668696
26	H	H10	-1.7176603	3.1791280	-1.2207947
27	H	H14	-1.6838884	3.2384343	0.5352332
28	C	C22	-7.2636558	2.0192382	-0.2331518
29	H	H15	-7.6626917	2.0836186	0.7874332
30	H	H17	-7.7223098	1.1520703	-0.7095116
31	H	H18	-7.5928330	2.9162450	-0.7664443
32	C	C23	-5.6346981	-3.8375530	0.4287954
33	H	H16	-6.5326078	-3.3163923	0.1039195
34	H	H19	-5.7817635	-4.1326367	1.4770427
35	H	H20	-5.5447020	-4.7607395	-0.1543653
36	C	C24	-0.6979063	-2.5189214	0.1508153
37	H	H8	-0.2254281	-2.0072558	0.9959894
38	H	H21	-0.2576804	-2.0870145	-0.7536675
39	H	H22	-0.3888160	-3.5665810	0.1924971
40	C	C25	-5.2960944	4.4905009	-0.4376759
41	H	H13	-6.2222909	4.5701291	-1.0224349
42	H	H23	-4.5432156	5.0575180	-0.9998174
43	C	C26	-5.5128999	5.1680377	0.9352744
44	H	H24	-6.2976427	4.6570924	1.5051274
45	H	H25	-5.8072801	6.2177153	0.8152948
46	H	H26	-4.5948332	5.1343599	1.5326337
47	C	C27	-2.7004989	-4.9608037	0.4233805
48	H	H7	-1.7661736	-5.0671711	0.9886384
49	H	H28	-3.4658173	-5.4849900	1.0107041
50	C	C28	-2.5423988	-5.6677809	-0.9429744
51	H	H27	-2.2967979	-6.7283136	-0.8108320
52	H	H29	-1.7433977	-5.2020531	-1.5306809
53	H	H30	-3.4665616	-5.6011468	-1.5289494
54	C	C29	-6.4691163	-0.7568185	1.4684665
55	H	H11	-7.3516851	-0.1043849	1.4693136
56	H	H31	-5.8320439	-0.4481803	2.3101222
57	H	H32	-6.8350115	-1.7667080	1.6947963
58	C	C30	-6.5320617	-1.0724367	-1.2904909
59	H	H12	-7.6177615	-1.0182401	-1.1233143
60	H	H33	-6.3214991	-2.0889098	-1.6474258
61	H	H34	-6.2953952	-0.4030090	-2.1298577
62	H	H3	3.3355447	2.8616320	0.3946580
63	H	H2	3.2882417	2.2817474	-1.7208477
64	Ru	Ru1	5.0203015	0.1264890	0.0380469
65	H	H36	6.2573788	1.2985219	-2.5203275
66	C	C1	6.5020137	0.7767555	-1.6034555
67	C	C4	7.0896969	-0.6049052	0.8246020
68	C	C6	6.4796873	-0.6374244	-1.5643388
69	C	C2	6.8014846	1.5223469	-0.4077989
70	C	C3	7.0700685	0.8356553	0.7992916
71	C	C31	6.7993006	-1.3326589	-0.3431625
72	H	H38	6.1800614	-1.2027818	-2.4361911
73	H	H39	6.7867108	2.6049852	-0.4252343
74	H	H40	7.2192378	1.3867301	1.7179808
75	H	H41	6.7172138	-2.4107164	-0.3085842
76	H	H42	7.2364434	-1.1181890	1.7655023
77	Cl	Cl1	3.3981711	-1.6248236	-0.5614325
78	Cl	Cl2	4.0808632	0.2582534	2.3245692

Compound 76

SCF model:
A restricted hybrid HF-DFT SCF calculation will be performed using Pulay DIIS + Geometric Direct Minimization

Optimization:

Step	Energy	Max Grad.	Max Dist.
1	-3078.532687	0.020494	0.112574
2	-3078.543024	0.017267	0.129583
3	-3078.551666	0.011639	0.144750
4	-3078.555631	0.003249	0.102459
5	-3078.555005	0.007292	0.054350
6	-3078.556434	0.002931	0.172630
7	-3078.556112	0.003553	0.220106
8	-3078.556363	0.003619	0.165741
9	-3078.554849	0.008738	0.061439
10	-3078.556556	0.002858	0.243547
11	-3078.556409	0.002873	0.222284
12	-3078.556492	0.002990	0.114120
13	-3078.556404	0.002443	0.102237
14	-3078.556604	0.002904	0.019882
15	-3078.556610	0.002847	0.025999
16	-3078.556643	0.002869	0.121793
17	-3078.556689	0.001846	0.096711
18	-3078.556712	0.001917	0.035022
19	-3078.556764	0.001650	0.017697
20	-3078.556781	0.001383	0.032435
21	-3078.556809	0.000737	0.062414
22	-3078.556837	0.000546	0.044578
23	-3078.556831	0.000489	0.032690
24	-3078.556842	0.000678	0.021981
25	-3078.556846	0.000425	0.029525
26	-3078.556850	0.000289	0.035859
27	-3078.556858	0.000246	0.061727
28	-3078.556873	0.000365	0.157474
29	-3078.556842	0.001115	0.145253
30	-3078.556834	0.001582	0.093488
31	-3078.556857	0.001743	0.041037
32	-3078.556890	0.001433	0.057288
33	-3078.556914	0.001485	0.117144
34	-3078.556921	0.001198	0.052476
35	-3078.556941	0.001073	0.024328
36	-3078.556944	0.000911	0.027769
37	-3078.556946	0.000436	0.018722
38	-3078.556943	0.000388	0.031612
39	-3078.556951	0.000540	0.039453
40	-3078.556953	0.000602	0.027594
41	-3078.556964	0.000676	0.023213
42	-3078.556960	0.000707	0.015501
43	-3078.556963	0.000691	0.024802
44	-3078.556965	0.000636	0.019807
45	-3078.556970	0.000403	0.008687
46	-3078.556971	0.000276	0.014597
47	-3078.556976	0.000294	0.012511
48	-3078.556979	0.000149	0.008756
49	-3078.556984	0.000113	0.006259
50	-3078.556984	0.000057	0.001841

<step 2>
Job type: Frequency calculation.
Method: RB3LYP
Basis set: LACVP

<step 3>
Job type: Single point.
Method: RB3LYP
Basis set: LACVP
SCF total energy: -3078.5568266 hartrees

NMR shifts (ppm)

	Atom	Isotropic	Rel. Shift
1	P1	14603.3325	-14314.27
2	C5	-3095.3932	3279.30
3	C7	-2318.7099	2502.62
4	C8	-2779.3692	2963.28
5	C9	-2719.1192	2903.03
6	C10	-1729.1975	1913.11
7	C11	-1760.6113	1944.52
8	H1	-2208.2148	2240.19
9	H6	-2077.6103	2109.59
10	H5	-1389.8209	1421.80
11	H4	-1430.5615	1462.54
12	C12	-1547.3524	1731.26
13	C14	-1562.0724	1745.98
14	N3	-1669.5158	1516.29
15	B1	-278.6435	
16	C13	-1847.9187	2031.83
17	N1	-2210.6357	2057.41
18	C16	-886.9526	1070.86
19	C15	-1634.0555	1817.96
20	C17	-953.6050	1137.51
21	C18	-1295.0547	1478.96
22	C19	-1820.2226	2004.13
23	C20	-1257.8636	1441.77
24	C21	-70.2398	254.15
25	H9	-557.8365	589.81
26	H10	-898.9458	930.92
27	H14	-884.8964	916.87
28	C22	308.6868	-124.78
29	H15	-230.0260	262.00
30	H17	-245.2763	277.25
31	H18	-110.3540	142.33
32	C23	234.8905	-50.98
33	H16	-375.2932	407.27
34	H19	-395.9141	427.89
35	H20	-284.1261	316.10
36	C24	-356.9261	540.84
37	H8	-1683.2183	1715.20
38	H21	-1760.8970	1792.87
39	H22	-1258.1821	1290.16
40	C25	306.9883	-123.08
41	H13	-160.7943	192.77
42	H23	-314.0458	346.02

43	C26	290.0275	-106.12
44	H24	-166.1475	198.13
45	H25	-45.2231	77.20
46	H26	-303.9154	335.89
47	C27	115.7716	68.14
48	H7	-675.3803	707.36
49	H28	-392.4881	424.47
50	C28	104.7915	79.12
51	H27	-288.4423	320.42
52	H29	-650.0293	682.01
53	H30	-391.6636	423.64
54	H3	-1310.2182	1342.20
55	H2	-1415.1940	1447.17
56	Ru1	13258.3616	
57	H36	509.0195	-477.04
58	C1	-312.4789	496.39
59	C4	-718.0876	902.00
60	C6	-784.5777	968.49
61	C2	-415.1534	599.06
62	C3	-446.2433	630.15
63	C31	-352.1510	536.06
64	H38	166.1655	-134.19
65	H39	676.8896	-644.91
66	H40	573.2198	-541.24
67	H41	254.5995	-222.62
68	H42	320.3520	-288.37
69	Cl2	11303.4746	
70	Cl1	10074.4936	
71	C29	-781.1595	965.07
72	C30	-411.9738	595.88
73	C32	-229.5322	413.44
74	C33	-351.0824	534.99
75	C34	-452.6135	636.52
76	C35	-361.4804	545.39
77	H11	-637.0270	669.00
78	H12	-288.4152	320.39
79	H31	-212.4015	244.38
80	H32	-414.9919	446.97
81	H33	-265.2153	297.19
82	C36	-691.5534	875.46
83	C37	-403.0748	586.98
84	C38	-317.5945	501.50
85	C39	-206.1301	390.04
86	C40	-353.6092	537.52
87	C41	-430.2699	614.18
88	H34	-297.4405	329.42
89	H35	-577.1306	609.11
90	H37	-373.8390	405.82
91	H43	-217.6125	249.59
92	H44	-250.9019	282.88

Reason for exit: Successful completion
Quantum Calculation CPU Time : 5:29:43.91
Quantum Calculation Wall Time: 6:04:00.29

Use of molecular symmetry disabled

Cartesian Coordinates (Angstroms)

	Atom	X	Y	Z
1	P P1	4.5208376	1.7574321	-0.1308409
2	C C5	2.6802429	1.4586424	-0.1157618
3	C C7	-0.0581476	0.8455364	-0.0656841
4	C C8	2.0212265	1.1046538	-1.3006621
5	C C9	1.9729462	1.5170527	1.0918631
6	C C10	0.6085353	1.2150029	1.1125469
7	C C11	0.6579274	0.8035173	-1.2730558
8	H H1	2.5687914	1.0272841	-2.2325579
9	H H6	2.4838014	1.7610172	2.0162805
10	H H5	0.0629143	1.2457547	2.0498590
11	H H4	0.1513845	0.5141337	-2.1878594
12	C C12	-1.5065260	0.4710410	-0.0346738
13	C C14	-2.4771063	1.4592491	-0.2675158
14	N N3	-3.8547628	1.1401790	-0.2418809
15	B B1	-4.4705724	-0.3138845	0.0055527
16	C C13	-1.8520486	-0.8613171	0.2234759
17	N N1	-3.2106089	-1.2635469	0.2509834
18	C C16	-2.3506208	2.8697062	-0.5178910
19	C C15	-3.6511811	3.3749477	-0.6374166
20	C C17	-4.5549013	2.2882013	-0.4569497
21	C C18	-1.0349588	-2.0248463	0.4701178
22	C C19	-1.9143220	-3.0987415	0.6405563
23	C C20	-3.2436362	-2.6015269	0.4936863
24	C C21	-1.0975145	3.6924518	-0.6277402
25	H H9	-1.3450581	4.7342986	-0.8500534
26	H H10	-0.4311265	3.3332715	-1.4190040
27	H H14	-0.5145889	3.6840110	0.3002027
28	C C22	-6.0453586	2.3710118	-0.4976121
29	H H15	-6.4971576	1.8090868	0.3241835
30	H H17	-6.4453059	1.9579840	-1.4310588
31	H H18	-6.3708398	3.4112916	-0.4227943
32	C C23	-4.4951085	-3.4095993	0.5878590
33	H H16	-5.1791828	-3.1877134	-0.2362961
34	H H19	-5.0346936	-3.2039985	1.5194669
35	H H20	-4.2606380	-4.4761011	0.5600699
36	C C24	0.4626070	-2.1293974	0.5383026
37	H H8	0.8925204	-1.5238063	1.3428594
38	H H21	0.9517869	-1.8057346	-0.3858950
39	H H22	0.7642265	-3.1649131	0.7150947
40	C C25	-4.0553747	4.8080500	-0.8658664
41	H H13	-4.9822076	4.8443263	-1.4522400
42	H H23	-3.2990518	5.3139710	-1.4790724
43	C C26	-4.2552534	5.6055018	0.4439997
44	H H24	-5.0342674	5.1482265	1.0647886
45	H H25	-4.5478203	6.6415934	0.2349567
46	H H26	-3.3305852	5.6215061	1.0320667
47	C C27	-1.5493653	-4.5399563	0.8837460
48	H H7	-0.6406397	-4.5936205	1.4955947
49	H H28	-2.3341194	-5.0285134	1.4750469
50	C C28	-1.3246183	-5.3402393	-0.4205018
51	H H27	-1.0665744	-6.3836557	-0.2031995
52	H H29	-0.5107056	-4.9004191	-1.0077307

53	H	H30	-2.2264864	-5.3323572	-1.0434527
54	H	H3	4.6607751	2.7207812	0.9187225
55	H	H2	4.6657578	2.6138538	-1.2739143
56	Ru	Ru1	6.1149175	-0.0353596	0.0102919
57	H	H36	7.8750291	2.0266165	-1.4146110
58	C	C1	7.9146467	1.1061275	-0.8449704
59	C	C4	7.9481647	-1.3236146	0.6530282
60	C	C6	7.8401589	-0.1404786	-1.5128961
61	C	C2	8.0113461	1.1546674	0.5906824
62	C	C3	7.9905365	-0.0517359	1.3288097
63	C	C31	7.8668587	-1.3616474	-0.7524258
64	H	H38	7.7110894	-0.1805105	-2.5857821
65	H	H39	8.0471014	2.1070334	1.1038373
66	H	H40	7.9606450	-0.0247315	2.4096908
67	H	H41	7.7275453	-2.3051028	-1.2631425
68	H	H42	7.8804368	-2.2348392	1.2313910
69	Cl	Cl2	4.7591779	-0.6322717	1.9924249
70	Cl	Cl1	4.5680897	-1.2474368	-1.4808209
71	C	C29	-5.2099225	-0.7926502	-1.3791253
72	C	C30	-6.3539050	-1.5679473	-3.8802738
73	C	C32	-4.4187824	-1.2768979	-2.4473825
74	C	C33	-6.5981861	-0.7045262	-1.6240446
75	C	C34	-7.1648001	-1.0863325	-2.8487312
76	C	C35	-4.9721404	-1.6588085	-3.6737587
77	H	H11	-3.3441549	-1.3618850	-2.3122243
78	H	H12	-7.2575836	-0.3283872	-0.8497161
79	H	H31	-8.2391591	-1.0073141	-2.9924532
80	H	H32	-4.3268831	-2.0281559	-4.4664435
81	H	H33	-6.7894197	-1.8672953	-4.8291200
82	C	C36	-5.3496905	-0.2675130	1.3918435
83	C	C37	-6.7174717	-0.1747269	3.8977798
84	C	C38	-6.5247143	-1.0138865	1.6273514
85	C	C39	-4.8843976	0.5207783	2.4705628
86	C	C40	-5.5486525	0.5707055	3.7000573
87	C	C41	-7.2016298	-0.9697604	2.8548972
88	H	H34	-6.9214188	-1.6485946	0.8429263
89	H	H35	-3.9835345	1.1138032	2.3404181
90	H	H37	-5.1565428	1.1900638	4.5024233
91	H	H43	-8.1054999	-1.5571860	2.9931124
92	H	H44	-7.2397512	-0.1368585	4.8492941

Compound 77

SCF model:
A restricted hybrid HF-DFT SCF calculation will be performed using Pulay DIIS + Geometric Direct Minimization

Optimization:

Step	Energy	Max Grad.	Max Dist.
1	-3235.689785	0.035424	0.072915
2	-3235.724364	0.022450	0.100216
3	-3235.744794	0.016800	0.119159
4	-3235.758268	0.012161	0.131955
5	-3235.767351	0.009548	0.147267
6	-3235.773844	0.008414	0.163086
7	-3235.778172	0.007300	0.180209
8	-3235.781008	0.006088	0.181664
9	-3235.782957	0.004921	0.186672

10	-3235.784471	0.003431	0.175595
11	-3235.785766	0.002969	0.131227
12	-3235.786453	0.002080	0.089128
13	-3235.786774	0.001862	0.097714
14	-3235.787152	0.001330	0.093547
15	-3235.787445	0.001482	0.098708
16	-3235.787669	0.001697	0.104491
17	-3235.787868	0.001843	0.102197
18	-3235.788046	0.001800	0.092134
19	-3235.788120	0.001479	0.040849
20	-3235.788163	0.001101	0.029738
21	-3235.788197	0.000855	0.030660
22	-3235.788213	0.000571	0.054153
23	-3235.788221	0.000498	0.069308
24	-3235.788236	0.000578	0.159800
25	-3235.788265	0.001232	0.174302
26	-3235.788279	0.002393	0.164259
27	-3235.788312	0.003021	0.066180
28	-3235.788376	0.002951	0.060007
29	-3235.788420	0.002910	0.040758
30	-3235.788513	0.002385	0.107301
31	-3235.788526	0.002266	0.058698
32	-3235.788601	0.001958	0.036971
33	-3235.788652	0.001591	0.017813
34	-3235.788680	0.001318	0.039287
35	-3235.788735	0.001098	0.016998
36	-3235.788763	0.001050	0.027377
37	-3235.788774	0.000982	0.013432
38	-3235.788790	0.000922	0.009785
39	-3235.788793	0.000820	0.013315
40	-3235.788796	0.000753	0.013420
41	-3235.788807	0.000626	0.016310
42	-3235.788823	0.000533	0.022430
43	-3235.788826	0.000620	0.009378
44	-3235.788826	0.000542	0.008070
45	-3235.788829	0.000358	0.003967
46	-3235.788831	0.000316	0.002780
47	-3235.788832	0.000227	0.005307
48	-3235.788830	0.000111	0.004176
49	-3235.788832	0.000083	0.005856
50	-3235.788826	0.000080	0.004322
51	-3235.788828	0.000054	0.003027
52	-3235.788830	0.000064	0.001696
53	-3235.788827	0.000067	0.001860
54	-3235.788827	0.000047	0.000825

<step 2>
Job type: Frequency calculation.
Method: RB3LYP
Basis set: LACVP

<step 3>
Job type: Single point.
Method: RB3LYP
Basis set: LACVP
SCF total energy: -3235.7886815 hartrees

NMR shifts (ppm)

	Atom	Isotropic	Rel. Shift
1	P1	13794.4933	-13505.43
2	C5	-3155.7271	3339.64
3	C7	-2423.6356	2607.54
4	C8	-2573.6424	2757.55
5	C9	-3012.6332	3196.54
6	C10	-1951.2919	2135.20
7	C11	-1682.7595	1866.67
8	H1	-1969.1425	2001.12
9	H6	-2723.2304	2755.21
10	H5	-1580.9557	1612.93
11	H4	-1372.7426	1404.72
12	C12	-1336.6246	1520.53
13	C14	-1543.8094	1727.72
14	N3	-1726.1948	1572.97
15	B1	-248.3501	
16	C13	-1829.3776	2013.29
17	N1	-2341.2521	2188.02
18	C16	-769.5133	953.42
19	C15	-1674.1018	1858.01
20	C17	-992.4422	1176.35
21	C18	-1142.5950	1326.50
22	C19	-1795.3756	1979.28
23	C20	-1314.3393	1498.25
24	C21	-137.3181	321.23
25	H9	-607.2298	639.21
26	H10	-896.6230	928.60
27	H14	-987.3716	1019.35
28	C22	322.7059	-138.80
29	H15	-223.2431	255.22
30	H17	-188.9873	220.97
31	H18	-82.4143	114.39
32	C23	220.8661	-36.96
33	H16	-371.2128	403.19
34	H19	-294.4926	326.47
35	H20	-390.4738	422.45
36	C24	-455.2093	639.12
37	H8	-1763.0155	1794.99
38	H21	-1731.9297	1763.91
39	H22	-1310.1498	1342.13
40	C25	277.8774	-93.97
41	H13	-143.6451	175.62
42	H23	-319.6397	351.62
43	C26	280.9396	-97.03
44	H24	-165.0730	197.05
45	H25	-50.5435	82.52
46	H26	-339.5412	371.52
47	C27	50.3204	133.59
48	H7	-769.8620	801.84
49	H28	-460.7988	492.78
50	C28	97.2054	86.70
51	H27	-299.0599	331.04
52	H29	-612.9988	644.98
53	H30	-349.1217	381.10
54	H2	-1716.6687	1748.65
55	H3	-1593.1295	1625.11

56	Ru1	13821.3167	
57	C1	-646.8396	830.75
58	C4	-726.0208	909.93
59	C6	-947.0480	1130.96
60	C2	-1205.5661	1389.48
61	C3	-1192.1782	1376.09
62	C31	-1445.6449	1629.55
63	H38	-101.7229	133.70
64	H39	741.0982	-709.12
65	H40	235.3959	-203.42
66	H41	-702.4593	734.44
67	Cl1	9211.1520	
68	Cl2	8625.1906	
69	C32	2505.2331	-2321.32
70	H35	519.1370	-487.16
71	H36	1683.4423	-1651.46
72	H37	588.9146	-556.94
73	C33	1129.0795	-945.17
74	H44	-1020.0893	1052.07
75	C34	427.1695	-243.26
76	H42	603.0200	-571.04
77	H45	-63.9808	95.96
78	H46	-1120.8652	1152.84
79	C35	2094.2926	-1910.38
80	H43	1866.8814	-1834.90
81	H47	1291.3321	-1259.35
82	H48	973.3747	-941.40
83	C29	-637.4275	821.34
84	C30	-405.0194	588.93
85	C36	-162.0892	346.00
86	C37	-288.8658	472.78
87	C38	-433.1602	617.07
88	C39	-341.4443	525.35
89	H11	-549.5394	581.52
90	H12	-273.1358	305.11
91	H31	-209.4921	241.47
92	H32	-368.6989	400.68
93	H33	-247.6167	279.59
94	C40	-760.4888	944.40
95	C41	-427.9040	611.81
96	C42	-358.6516	542.56
97	C43	-214.7560	398.67
98	C44	-365.7770	549.69
99	C45	-472.6930	656.60
100	H34	-272.2688	304.25
101	H49	-648.2712	680.25
102	H50	-436.6364	468.61
103	H51	-210.0613	242.04
104	H52	-277.5874	309.57

Reason for exit: Successful completion
Quantum Calculation CPU Time : 21:49:11.57
Quantum Calculation Wall Time: 22:53:18.92

SPARTAN '14 Properties Program: (Linux/P4E) build 14.117
Use of molecular symmetry disabled

Cartesian Coordinates (Angstroms)

	Atom		X	Y	Z
1	P	P1	3.8466224	1.9271759	-0.6152922
2	C	C5	2.0220018	1.5409400	-0.4922282
3	C	C7	-0.6910920	0.8373434	-0.3116698
4	C	C8	1.2793674	1.3044465	-1.6564300
5	C	C9	1.4120461	1.4291729	0.7645161
6	C	C10	0.0611689	1.0844206	0.8480200
7	C	C11	-0.0711710	0.9552751	-1.5651545
8	H	H1	1.7481365	1.3755880	-2.6328717
9	H	H6	1.9958063	1.5641716	1.6671541
10	H	H5	-0.4106627	0.9892429	1.8204172
11	H	H4	-0.6428265	0.7632894	-2.4672625
12	C	C12	-2.1299284	0.4400583	-0.2064935
13	C	C14	-3.1221898	1.4279831	-0.3216037
14	N	N3	-4.4930982	1.0885253	-0.2498326
15	B	B1	-5.0762059	-0.3683307	0.0511284
16	C	C13	-2.4474079	-0.9066076	0.0108761
17	N	N1	-3.7958130	-1.3148754	0.1620181
18	C	C16	-3.0252512	2.8466221	-0.5369331
19	C	C15	-4.3366194	3.3321230	-0.6145848
20	C	C17	-5.2179039	2.2271747	-0.4310097
21	C	C18	-1.6083575	-2.0715297	0.1526923
22	C	C19	-2.4634905	-3.1488220	0.4070775
23	C	C20	-3.8015088	-2.6524889	0.4058711
24	C	C21	-1.7906651	3.6969788	-0.6494378
25	H	H9	-2.0626565	4.7554528	-0.6855868
26	H	H10	-1.2081209	3.4742282	-1.5510598
27	H	H14	-1.1158943	3.5575013	0.2012814
28	C	C22	-6.7092515	2.2863136	-0.4232554
29	H	H15	-7.1006394	2.2789044	0.6008037
30	H	H17	-7.1472337	1.4321585	-0.9447786
31	H	H18	-7.0547436	3.2025793	-0.9095016
32	C	C23	-5.0337926	-3.4606924	0.6409540
33	H	H16	-5.7479892	-2.9276390	1.2730179
34	H	H19	-4.7793656	-4.4055645	1.1281831
35	H	H20	-5.5443723	-3.6937158	-0.3010252
36	C	C24	-0.1118353	-2.1732176	0.0520968
37	H	H8	0.4030847	-1.6835231	0.8859831
38	H	H21	0.2815105	-1.7171097	-0.8607766
39	H	H22	0.1981072	-3.2211486	0.0509489
40	C	C25	-4.7684182	4.7618448	-0.8079714
41	H	H13	-5.6921464	4.7938820	-1.4008113
42	H	H23	-4.0182660	5.2990368	-1.4018536
43	C	C26	-5.0007524	5.5209025	0.5187918
44	H	H24	-5.7715586	5.0274949	1.1219210
45	H	H25	-5.3224392	6.5525304	0.3310451
46	H	H26	-4.0824661	5.5513950	1.1163597
47	C	C27	-2.0791760	-4.5902504	0.6118342
48	H	H7	-1.0647382	-4.6464831	1.0238597
49	H	H28	-2.7321312	-5.0439272	1.3696560
50	C	C28	-2.1486526	-5.4365038	-0.6798232
51	H	H27	-1.8733382	-6.4794924	-0.4821468
52	H	H29	-1.4663731	-5.0408735	-1.4408052
53	H	H30	-3.1598351	-5.4248046	-1.1029426

54	H	H2	3.9232680	2.3569408	-1.9828955
55	H	H3	3.9467142	3.1964408	0.0437365
56	Ru	Ru1	5.5490417	0.3899663	0.0906949
57	C	C1	7.4044460	1.7525761	-0.2263449
58	C	C4	7.3121449	-1.1627845	-0.1998372
59	C	C6	7.1280334	1.0024951	-1.4291532
60	C	C2	7.5512455	1.0119185	0.9732219
61	C	C3	7.5363164	-0.4289047	0.9834595
62	C	C31	7.0659280	-0.4122172	-1.4132473
63	H	H38	6.9406857	1.5348560	-2.3550941
64	H	H39	7.6489616	1.5366345	1.9150802
65	H	H40	7.6147653	-0.9368468	1.9337963
66	H	H41	6.7993086	-0.9454142	-2.3168642
67	Cl	Cl1	4.5024700	0.7471527	2.3185796
68	Cl	Cl2	3.9215829	-1.3841568	-0.4723558
69	C	C32	7.5065934	3.2550897	-0.2468668
70	H	H35	6.9219018	3.6872388	-1.0657441
71	H	H36	8.5499808	3.5655136	-0.3901711
72	H	H37	7.1553516	3.6905133	0.6934203
73	C	C33	7.2323078	-2.6792138	-0.2482282
74	H	H44	6.3601508	-2.9161393	-0.8729496
75	C	C34	7.0030807	-3.3362076	1.1230211
76	H	H42	7.8613734	-3.1946774	1.7920031
77	H	H45	6.8662438	-4.4148139	0.9923646
78	H	H46	6.1040079	-2.9388702	1.6042848
79	C	C35	8.5000411	-3.2452790	-0.9384942
80	H	H43	9.3965613	-3.0373190	-0.3417016
81	H	H47	8.6475193	-2.8147417	-1.9354455
82	H	H48	8.4095253	-4.3313681	-1.0484885
83	C	C29	-5.9518873	-0.8546037	-1.2485842
84	C	C30	-7.3176254	-1.7173830	-3.6044072
85	C	C36	-5.5077300	-0.5002806	-2.5440543
86	C	C37	-7.1036303	-1.6696173	-1.1860243
87	C	C38	-7.7797795	-2.0924521	-2.3395686
88	C	C39	-6.1714527	-0.9188451	-3.7016208
89	H	H11	-4.6239648	0.1237946	-2.6456444
90	H	H12	-7.4842071	-1.9871439	-0.2210577
91	H	H31	-8.6661935	-2.7143557	-2.2465425
92	H	H32	-5.7968018	-0.6221464	-4.6777532
93	H	H33	-7.8393903	-2.0423596	-4.4998035
94	C	C40	-5.8085594	-0.3183187	1.5189998
95	C	C41	-6.9508318	-0.1085043	4.1294265
96	C	C42	-7.1996409	-0.1706974	1.7151075
97	C	C43	-5.0142182	-0.3516027	2.6889488
98	C	C44	-5.5668283	-0.2487572	3.9696833
99	C	C45	-7.7655796	-0.0700308	2.9942349
100	H	H34	-7.8603930	-0.1298117	0.8562187
101	H	H49	-3.9379688	-0.4651981	2.5935230
102	H	H50	-4.9192078	-0.2791530	4.8418650
103	H	H51	-8.8417790	0.0385340	3.0998562
104	H	H52	-7.3848883	-0.0314611	5.1220210

Compound 89b

SCF model:
A restricted hybrid HF-DFT SCF calculation will be performed using Pulay DIIS + Geometric Direct Minimization

Optimization:

Step	Energy	Max Grad.	Max Dist.
1	-1563.003533	0.072354	0.123425
2	-1563.023378	0.018333	0.146282
3	-1563.030515	0.006981	0.105291
4	-1563.032146	0.010443	0.103231
5	-1563.034023	0.007979	0.107680
6	-1563.036446	0.013371	0.130290
7	-1563.040070	0.015602	0.135151
8	-1563.043952	0.012175	0.120573
9	-1563.047723	0.015515	0.108392
10	-1563.052241	0.017529	0.096889
11	-1563.057651	0.017496	0.089995
12	-1563.064298	0.023704	0.111791
13	-1563.071277	0.027273	0.142456
14	-1563.079225	0.025425	0.133879
15	-1563.086933	0.026779	0.104964
16	-1563.095726	0.021000	0.138252
17	-1563.102365	0.017860	0.120165
18	-1563.108382	0.009090	0.143475
19	-1563.112073	0.012233	0.126218
20	-1563.115444	0.009093	0.117595
21	-1563.117811	0.009120	0.110646
22	-1563.119768	0.005136	0.112777
23	-1563.120967	0.002594	0.179317
24	-1563.121452	0.004835	0.126659
25	-1563.121878	0.002034	0.189614
26	-1563.122346	0.002647	0.199220
27	-1563.122921	0.002837	0.196702
28	-1563.123617	0.002682	0.187243
29	-1563.124321	0.003427	0.190160
30	-1563.124945	0.004316	0.179836
31	-1563.125506	0.004985	0.202989
32	-1563.125915	0.005010	0.142030
33	-1563.126373	0.004780	0.190261
34	-1563.126968	0.003829	0.174617
35	-1563.127742	0.001838	0.134005
36	-1563.128047	0.001381	0.038559
37	-1563.128082	0.000668	0.047559
38	-1563.128091	0.000348	0.021633
39	-1563.128099	0.000244	0.007975
40	-1563.128100	0.000192	0.013549
41	-1563.128100	0.000128	0.004744

<step 2>
Job type: Frequency calculation.
Method: RB3LYP
Basis set: 6-31G(D)

Reason for exit: Successful completion
Quantum Calculation CPU Time : 4:45:59.85
Quantum Calculation Wall Time: 5:00:07.29

SPARTAN '14 Properties Program: (Linux/P4E) build 14.117
Use of molecular symmetry disabled

		Cartesian Coordinates (Angstroms)		
	Atom	X	Y	Z
1	B B1	5.7241682	0.1162244	-0.1024369
2	C C1	4.8945804	1.3804917	0.0534014
3	C C2	4.8286862	-1.1570273	-0.5562240
4	C C3	3.4408677	-1.0709841	0.0511168
5	C C4	3.4189977	1.3546254	0.0935824
6	C C5	2.7035643	0.1694667	0.1573287
7	C C6	5.2604989	-2.5369992	-0.1749880
8	C C7	3.1471445	-2.2702432	0.6514722
9	C C8	4.2718960	-3.1691016	0.5106744
10	C C9	7.2921421	0.0116696	0.0337726
11	H H4	7.7514813	-0.5629349	-0.7826344
12	H H7	7.5329602	-0.5420436	0.9546223
13	H H10	7.8009973	0.9801909	0.0982539
14	C C10	4.7767156	-1.0401160	-2.1188759
15	H H2	5.7794618	-1.1439144	-2.5478020
16	H H11	4.3744247	-0.0696750	-2.4252878
17	H H12	4.1435827	-1.8310573	-2.5375146
18	C C11	5.2517872	2.7178560	0.0729847
19	C C12	2.9607872	2.7267135	0.1146732
20	C C13	4.0689094	3.5417967	0.0995972
21	C C22	1.2417815	0.1269116	0.3931645
22	C C23	-1.5609169	0.0221991	0.8371445
23	C C24	0.6322627	0.9427145	1.3644772
24	C C25	0.4228697	-0.7532678	-0.3359161
25	C C26	-0.9541967	-0.7973152	-0.1262592
26	C C27	-0.7395054	0.8818379	1.5866217
27	H H9	1.2491861	1.5964561	1.9727557
28	H H30	0.8721312	-1.3946585	-1.0881870
29	H H31	-1.5594459	-1.4780681	-0.7172470
30	H H32	-1.1789317	1.5023836	2.3642898
31	P P1	-3.3668409	0.0118847	1.2548190
32	C C28	-4.0100017	1.4310621	0.2512350
33	C C29	-5.1271947	3.6074387	-1.1357730
34	C C30	-3.3814258	1.9480639	-0.8923378
35	C C31	-5.1994431	2.0312217	0.6949022
36	C C32	-5.7589628	3.1060043	0.0035468
37	C C33	-3.9364212	3.0287923	-1.5799228
38	H H34	-2.4518531	1.5078571	-1.2415875
39	H H35	-5.6851841	1.6558608	1.5926862
40	H H36	-6.6811848	3.5575066	0.3600137
41	H H37	-3.4375164	3.4194608	-2.4633481
42	H H38	-5.5565807	4.4500708	-1.6714789
43	C C34	-3.9876669	-1.4712936	0.3339356
44	C C35	-4.9242661	-3.8302024	-0.8845234
45	C C36	-4.5059585	-1.4461194	-0.9696255
46	C C37	-3.9597108	-2.6972356	1.0204872
47	C C38	-4.4139425	-3.8684173	0.4146971
48	C C39	-4.9722298	-2.6165776	-1.5720418
49	H H33	-4.5512617	-0.5092881	-1.5166934
50	H H39	-3.5841941	-2.7318714	2.0408585
51	H H40	-4.3800714	-4.8074831	0.9610586
52	H H41	-5.3726446	-2.5782632	-2.5820657
53	H H42	-5.2887334	-4.7393736	-1.3554323
54	H H43	1.9279399	3.0510210	0.1221167

55	H	H44	2.2465135	-2.4892977	1.2151779
56	H	H45	4.3035038	-4.1812167	0.9005533
57	H	H47	6.2089337	-2.9719509	-0.4736543
58	H	H48	6.2673277	3.1007493	0.0512847
59	H	H50	4.0610423	4.6263555	0.1051926

Compound 118

DFT calculations gave this output with one imaginary number present.

SCF model:
A restricted hybrid HF-DFT SCF calculation will be performed using Pulay DIIS + Geometric Direct Minimization

Optimization:

Step	Energy	Max Grad.	Max Dist.
1	-1485.191471	0.212036	0.122805
2	-1485.287424	0.112388	0.107135
3	-1485.339484	0.077166	0.146622
4	-1485.376401	0.043023	0.145001
5	-1485.396738	0.035130	0.138170
6	-1485.410731	0.015462	0.118383
7	-1485.415626	0.016879	0.148972
8	-1485.416572	0.009592	0.210141
9	-1485.417821	0.006758	0.069410
10	-1485.417703	0.007908	0.107220
11	-1485.418173	0.000996	0.046748
12	-1485.418203	0.000434	0.028455
13	-1485.418209	0.000241	0.002640
14	-1485.418210	0.000136	0.002449

<step 2>
Job type: Frequency calculation.
Method: RB3LYP
Basis set: 6-31G(D)

Reason for exit: Successful completion
Quantum Calculation CPU Time : 1:14:49.60
Quantum Calculation Wall Time: 1:19:45.52

SPARTAN '14 Properties Program: (Linux/P4E) build 14.117
Use of molecular symmetry enabled

Cartesian Coordinates (Angstroms)

Atom		X	Y	Z
1	C	C1	0.6309687	0.5665629	0.0000000
2	C	C2	1.3372340	0.4416037	-1.2186858
3	C	C6	1.3372340	0.4416037	1.2186858
4	N	N1	2.6776414	0.0468375	1.2272489
5	N	N2	2.6776414	0.0468375	-1.2272489
6	C	C7	0.9891461	0.7696495	-2.5608764
7	H	H2	0.0296741	1.1335624	-2.8945737
8	C	C8	3.1339685	0.1179275	-2.4839103
9	H	H6	4.1547677	-0.1606618	-2.7089642

10	C	C9	2.1172963	0.5750902	-3.3449723
11	H	H7	2.2138819	0.7464405	-4.4081776
12	C	C10	0.9891461	0.7696495	2.5608764
13	H	H9	0.0296741	1.1335624	2.8945737
14	C	C11	2.1172963	0.5750902	3.3449723
15	C	C12	3.1339685	0.1179275	2.4839103
16	H	H11	4.1547677	-0.1606618	2.7089642
17	H	H14	2.2138819	0.7464405	4.4081776
18	P	P1	-1.1198345	1.1744859	0.0000000
19	C	C13	-1.9235982	0.2951631	1.4208069
20	C	C14	-3.3446964	-0.9042796	3.5260659
21	C	C15	-1.7119960	-1.0544246	1.7468103
22	C	C16	-2.8543395	1.0332826	2.1663874
23	C	C17	-3.5632980	0.4362903	3.2121676
24	C	C18	-2.4155625	-1.6478937	2.7923683
25	H	H1	-0.9834851	-1.6398937	1.1949911
26	H	H5	-3.0230853	2.0807711	1.9290043
27	H	H8	-4.2814212	1.0211869	3.7806365
28	H	H10	-2.2381773	-2.6919385	3.0362078
29	H	H12	-3.8928478	-1.3700315	4.3406741
30	C	C19	-1.9235982	0.2951631	-1.4208069
31	C	C20	-3.3446964	-0.9042796	-3.5260659
32	C	C21	-2.8543395	1.0332826	-2.1663874
33	C	C22	-1.7119960	-1.0544246	-1.7468103
34	C	C23	-2.4155625	-1.6478937	-2.7923683
35	C	C24	-3.5632980	0.4362903	-3.2121676
36	H	H3	-3.0230853	2.0807711	-1.9290043
37	H	H13	-0.9834851	-1.6398937	-1.1949911
38	H	H15	-2.2381773	-2.6919385	-3.0362078
39	H	H16	-4.2814212	1.0211869	-3.7806365
40	H	H17	-3.8928478	-1.3700315	-4.3406741
41	B	B1	3.4478865	-0.5314315	0.0000000
42	F	F1	4.7549731	-0.0854368	0.0000000
43	F	F2	3.3735633	-1.9148978	0.0000000